CHARACTERIZATION OF ACTIVE SPECIES IN MOLYBDENUM- AND COPPER-BASED CATALYSTS BY MEANS OF XAFS AND UV-VIS SPECTROSCOPY

HIROFUMI ARITANI

1996

CHARACTERIZATION OF ACTIVE SPECIES IN MOLYBDENUM- AND COPPER-BASED CATALYSTS BY MEANS OF XAFS AND UV-VIS SPECTROSCOPY

HIROFUMI ARITANI

DIVISION OF MOLECULAR ENGINEERING
GRADUATE SCHOOL OF ENGINEERING
KYOTO UNIVERSITY

1996

Preface

The progress and development of chemical industry has been due to the improvement of the catalytic system and the innovation of new catalytic reactions concerning industrial technologies for a long time. For example, in the history of NH_3 synthesis, Haber found in 1908 that Fe acts as a good catalyst for producing NH_3 from N_2 and H_2, and then, Bosch and Mittasch found the Fe_2O_3·Al_2O_3·K_2O as a more active catalyst in 1909. Their findings and improvement resulted in the industrial use of NH_3 synthesis in 1910s. It was an epoch in modern chemical industry. By the studies in the later years, it was found that the addition of some elements to Fe_2O_3·Al_2O_3·K_2O brings about higher activity for producing NH_3 and longer catalytic lifetime. In short, catalysis chemistry has been developed along innovation of catalysts with higher activity and better selectivity than known ones as well as the elucidation of the mechanism of catalysis.

The characterization of catalytically active center is necessary to study a catalytic system, because the analysis of physicochemical properties often uncovers the behavior of the active species. The structure not only in the surface layer but also in the bulk phase relates to the generation of catalytic activity. In addition, it is widely known that the local structure at a molecular-level strongly affects the activity of active species. The structural analyses of catalysts in the surface layer and bulk phase have been studied so far, and the behavior of the active species has been made clearer. However, the discussion about the active species and reaction mechanism is continuing still now in a number of catalytic systems. When the relationship between the structure of active species and its behavior in catalysis is established, the control of the catalytic reaction will be achieved. Therefore, much efforts to the characterization of catalysts has been made by means of many techniques such as spectroscopy, diffraction, adsorption measurements, electron microscopy, microanalysis, *etc.*

Spectroscopy is one of the most useful technique for structural analyses. In recent years, structural analysis at a molecular-level by means of spectroscopies has been applied widely to elucidating the property of active sites and mechanisms of catalyses. Many spectroscopic techniques, XPS, AES, UPS, IR, UV-VIS, XRF, XAFS, Raman,

EELS, *etc.*, has been adopted and applied to a number of studies, because each spectroscopy can provide a lot of information of the target atoms or species directly. Now the photo-emission in a wide range of energy can be used, and therefore, heterogeneous catalysts including almost any elements can be observed now.

In the study presented in this thesis, the author used mainly two spectroscopic techniques, *i.e.*, XAFS (X-ray absorption fine structure) and UV-VIS spectroscopies, for characterizing the catalytically active species and clarifying the catalytic behavior in the two catalyst systems. The XAFS spectroscopy has been widely applied to catalysis science since 1980s. The definite parameters of local structures, symmetry, valence, *etc.* can be obtained directly by XAFS. By use of information on the basis of XAFS, the local structure of catalytically active species and the structural changes during the reaction can be discussed. On the other hand, UV-VIS spectroscopy, so to speak a classical one, has been applied to the investigation of structures for a long time. Since the energy of photo-emission is below 6.2 eV, the spectral data reflects interatomic or intermolecular electron transition. For example, in a UV-VIS spectrum one can observe a the bands due to *d-d* transition in transitional metal ion, charge transfer between metal ions and its ligands, and vibration of free electrons in a metal micro-particles. Thus, the UV-VIS spectroscopy can be applied to the characterization widely, although it is not available for characterizing some catalysts in which no absorption band exists in UV-VIS region.

In this thesis, the author applied XAFS and UV-VIS to the characterization of catalysis systems. In order to clarify the local structure of active species and the catalytic behavior, structural study of two catalytic systems, *i.e.*, Mo-Mg binary oxides for metathesis of olefins and TiO_2-supported Cu for reduction of NO, has been carried out. This thesis is divided into two parts; In part I, characterization of active molybdenum species in Mo-Mg binary oxide catalysts is described, and in part II, characterization of active copper species in supported Cu catalysts for *de*NO_x reactions is described. In addition, structural study of molybdenum bronzes, which are suitable samples for Mo L-edge XANES, is carried out and it is described in appendix section.

The present thesis is a collection of the studies which were carried out at the

Division of Molecular Engineering, Graduate School of Engineering, Kyoto University from 1994 to 1996 under supervision of Professor Satohiro Yoshida. The author wishes to express his sincerest gratitude to Professor Satohiro Yoshida for his helpful and keen guidance, a lot of fruitful discussions, and hearty encouragement throughout this work. The author is deeply grateful to Professor Takuzo Funabiki for his invaluable instructions, and useful suggestions and discussions. The author makes special acknowledgments to Dr. Tsunehiro Tanaka for a number of continual suggestions and discussions, valuable indications, and helpful advises in the studies. The author is thankful to Professor Sadao Hasegawa for his considerable advises about molybdena catalysts, and many instructions when the author had belonged under his guidance. Grateful acknowledgment is made to Professor Yasuaki Okamoto for many valuable discussions and presentations of the cooperative studies about Cu/TiO_2 and Cu/ZrO_2 catalysts, which are described in chapter 5 and 6. The author thanks Mr. Masataka Kudo for ICP and XRF measurements and helpful discussions. The author is also grateful to Professor Noriyuki Sotani for offering the molybdenum bronze samples and those structural information.

Thanks must be made to Ryoji Kuma and Nobuhiko Akasaka for their collaborations and lively discussions about Cu-based catalysts. The author acknowledges Mr. Takaki Hatsui for helpful advice of XANES. The author also thanks Messrs. Takashi Yamamoto, Atsushi Suzuki and Yoshiumi Kohno for collaborations and assistance of L-edge XANES measurements. The author thanks Mr. Tamio Yamazaki for computional assistance. Hearty thanks are made to Messrs. Hisao Yoshida, Tomoko Yoshida, Sakae Takenaka, Hiroyuki Hirano, and Hiroki Hayashi for their collaborations and lively discussions. The author must express his gratitudes to Mr. Shigehiro Matsuo for the collaborations and helpful assistance in preparing this thesis overnight. Thanks are also made to Mr. Tomomasa Yokomizo and Mr. Tomoyuki Itoh for their assistance. The author is indebted to all the members of the group of catalysis research led by Professor Yoshida.

The author thanks to Mr. Osamu Matsudo, Dr. Yasuhiko Takata, Professor Toyohiko Kinoshita, Professor Masao Kamada, and Professor Nobuhiro Kosugi for technical assistance of XANES measurements and helpful discussion. The acknowledge is made to Professor Masaharu Nomura and staffs of Photon Factory at KEK for making a good condition of beamlines and the assistance of K-edge XAFS

measurements. Thanks are made to Mr. Hideki Gotoh for cooperation of Cu K-edge XAFS. Acknowledgments should be made to Dr. Kohki Ebitani who gave him helpful discussion.

Finally, the author sincerely thanks to his parents, Motonami and Yaeko, and his sister, Hitomi, for their understanding and encouragement.

Hirofumi Aritani

Kyoto

December, 1996

CONTENTS

General Introduction

The characterization of catalytically active species is very important for studying catalysis. It is well known that the structure of solid catalysts in the surface layer or bulk phase has a strong correlation with the catalytic activity. Thus, the importance of the structural study in a molecular-level is widely recognized for characterizing catalytic active species.

For the structural study, spectroscopy is one of the most effective tools. Now, the application of these spectroscopies is used widely, and revelation of distinct active species can be expected in many catalytic systems. In particular, XAFS (X-ray absorption fine structure) study is developed remarkably for the application to catalytic science, because it is a powerful technique for analyses of local structures and electronic states. The XAFS is divided in two regions; XANES (X-ray absorption near-edge structure) and EXAFS (Extended X-ray absorption fine structure). By EXAFS study, the local structure, *i.e.*, interatomic bond lengths and coordination numbers of the atom, can be obtained. XANES spectrum is associated with the excitation process of a core electron to bound and quasi-bound states, and therefore, it reflects the electronic states directly. In the recent studies, XAFS is applied to the characterization of a catalyst not only in a static state but also in a dynamic state, *e.g.*, being recorded *in situ* conditions. UV-VIS spectroscopy has been used so far as a fundamental technique. The UV-VIS spectroscopy measured in a diffuse-reflectance mode can be applied for characterization of catalytic active species in solid catalysts. In fact, many groups have published the studies about the characterization of active species in solid catalysts including transitional metal ions. UV-VIS is a classic technique, however, it is a useful one to determine the environmental coordination and symmetry around a transitional metal.

In this thesis, the author focused his attention on the characterization of two catalytic systems, *i.e.*, binary oxide catalysts including molybdenum for olefin metathesis and supported copper catalysts for NO reduction, and he applied XAFS and UV-VIS spectroscopies to the characterization. The outlines of these spectroscopies are described below.

1. EXAFS

Since the detailed theory of EXAFS is published by many reviews[1-3] and books,[4] the fundamental method or theory is only outlined in this section.

In the theory of EXAFS, the analysis studied by Lee *et al.*[1] is widely accepted. The following equation has been derived on the basis of a single scattering theory for the EXAFS function $\chi(k)$.

$$\chi(k) = \Sigma \frac{N_j}{r_j^2} f_j(k) \exp(-2\sigma_j^2 k^2) S_j(k) \sin[2kr_j + \delta_j(k)] \qquad (1)$$

where N_j is the coordination number of scatterers at the distance of r_j, $f_j(k)$ the backscattering amplitude, $\delta_j(k)$ the scattering phase shift, $S_j(k)$ the damping factor for compensation of the loss by inelastic scattering, and σ_j the Debye-Waller factor which is introduced to estimate the damping of the amplitude by the turbulence in back-scatterers in the jth shell. The wavenumber, k, can be obtained according to the equation;

$$k = \frac{2\pi \sqrt{m\,(E - E_0)}}{h} \qquad (2)$$

where h is a Plank's constant, m the mass of the electron, E the photon energy, and E_0 the threshold (initial) energy for photoionization.

The normalized EXAFS, $\chi(E)$, is obtained by subtracting the background from the total absorption and by dividing the resultant function, $\Delta\mu(E)$, by a smoothed absorption, $\mu_s(E)$. The smoothed absorption is estimated by fitting the empirical formula to background in the region of 30 - 50 eV above the edge. The formula used in this thesis is

$$\mu_s(E) = A / E^{-2.75} \qquad (4)$$

according to the suggestion by McMaster.[5] A is a constant to be determined by least-squares fitting. Then, normalized EXAFS, $\chi(E)$, is obtained as

$$\chi(E) = \Delta\mu(E) / \mu_s(E) \qquad (5)$$

where $\Delta\mu(E)$ is the oscillatory part of EXAFS.

The present method of analysis is proposed and applied to the study of V K-edge EXAFS by Tanaka *et al.*[6]

The normalized EXAFS oscillation is represented as a function of k by assuming

single scattering, as described above. By use of Fourier filtering, an EXAFS function by a single set of near neighbors may be isolated from the total EXAFS function if the peak in the radial structure function is well resolved. The empirical phase and amplitude functions deduced from XAFS data of model compounds may be applied to the analysis of XAFS of unknown samples with the same pair of absorber-scatter by assuming transferability of the phase shift and amplitude. Parham *et al.*[7] suggested that distance calculations may readily be made with an accuracy of ± 0.02 Å. Amplitude transferability is less guaranteed and thus obtained coordination numbers are less accurate, especially in distorted systems such as that expected on dispersed catalysts. In case of molybdena with MoO_6 octahedral units, it is reported that coordination numbers with uncertainty of ± 20% can be expected in systems with a little disorder.[7]

2. XANES

Although there is no complete theoretical analysis methods for XANES spectra, XANES has become popular for characterization in recent years. XANES is associated with the excitation process of a core electron to bound and quasi-bound states, where the bound states are located below the ionization threshold and the quasi-bound states interacting with the continuum are located above and near the threshold.[2] Therefore, XANES contains an information about the electronic states of the absorbing atom and the local structure surrounding that atom, although interpretation of XANES spectra is not straightforward. Since the excitation process involves multi-electron and multi-scattering effects, interpretation of XANES is rather complicated.[8] There are two typical approaches to the XANES analysis, *i.e.*, ab-initio MO theory and multiple scattering theory. The MO theory in condensed systems employs one-electron approximations based on Hartree, Hartree-Fock and local density approximations, applied to molecular systems like a finite cluster of atoms surrounding the absorbing atom. The alternative cluster approach to XANES theory uses a multiple-scattering approach to solve the one-electron Schrödinger equation.

In case that the one-electron picture is valid, an excited electron from a core orbital behaves as an 'active' electron and remaining ones (in which one electron is come out) are in a 'passive' state affected by many electron interactions. However, there are

some difficulties in obtaining one electron functions for the active electron and many electron functions for the passive electrons. Furthermore, if the one electron picture does not hold, interaction between the active and passive electrons must be explicitly taken in account. In this manner, a variety of problem remains about the interpretations given on XANES spectra. In Japan, the studies of the approaches by means of MO and multiple scattering have been established by Kosugi,[8,9] Fujikawa,[10] and other workers.

While, the difference of XANES spectra relates directly to that of local structure and/or valence of absorbing atoms. And therefore, the XANES spectra is used widely in characterization of catalytic active species recently, because it can afford information on the local structure, coordination symmetry, oxidation states, and furthermore, aggregated states of highly dispersed species on supports. Recently, deconvolution method of XANES spectra is applied for characterization of catalysts by Yoshida *et al.* as a new technique.[11]

3. UV-VIS

UV-VIS spectra of solids are originated by the interatomic and/or molecular orbital electron transitions. Absorption frequencies are characteristic of certain arrangements of molecules and their environments.[12] Even pure compounds give rather broad absorption bands, and catalysts exhibits even broader spectra. Hence, the UV-VIS spectra gives the semiquantitative information.

When using the monochromatized incidence photon, Lambart-Beer's theory is applicable in the process of absorption, *i.e.*,

$$A\ (= -\log t = -\log (I/I_0)) = \varepsilon\, c\, l \qquad (5)$$

when A is absorbance, t the transmittance, ε the molar absorption coefficient, c (mol dm^{-3}) the concentration, and l (cm) the length of transmission. It is a fundamental theory for the spectroscopy in a transmission mode.

In case of diffuse reflectance mode, the spectrum (diffuse reflectance spectra, DRS) is usually recorded using an integrated spherical photon-analyzer. If the reflectance is due to the purely diffuse-reflected photons, the Kubelka-Munk theory is applicable. In this theory, absorbance coefficient is represented by the Kubelka-Munk function, *i.e.*,

$$F(R_d) = \frac{(1-R_d)^2}{2R_d} \qquad (6)$$

when R_d is reflectance, and $F(R_d)$ indicates the Kubelka-Munk function, which parallels to molar absorption, ε. The UV-VIS spectrum is shown generally as wavelength (λ) *vs.* Kubelka-Munk function ($F(R_d)$).

References

(1) Lee, P. A.; Citrin, P. H.; Eisenberger, P.; Kincaid, B. M. *Rev. Mod. Phys.* **1981**, *53*, 769.

(2) Bart, J. C. *Adv. Catal.* **1986**, *34*, 203.

(3) Bart, J. C.; Vlaic, G. *Adv. Catal.* **1987**, *35*, 1.

(4) Iwasawa, Y. In *X-ray Absorption Fine Structure for Catalysts and Surfaces*; World Scientific: Danvers, 1996, p 1.

(5) McMaster, Report No. UCRL-50174, 1969 (unpublished).

(6) Tanaka, T.; Yamashita, H.; Tsuchitani, R.; Funabiki, T.; Yoshida, S. *J. Chem. Soc. Faraday Trans. 1* **1988**, *84*, 2987.

(7) Parham, T. G.; Merrill, R. P. *J. Catal.* **1984**, *85*, 295.

(8) Kosugi, N. In *X-ray Absorption Fine Structure for Catalysts and Surfaces*; Y. Iwasawa, Ed.; World Scientific, Co.: Danvers, 1996; Vol. 4; p 60.

(9) Kosugi, N.; Kondoh, H.; Tajima, H.; Kuroda, H. *Chem. Phys.* **1989**, *135*, 149.

(10) Fujikawa, T. In *X-ray Absorption Fine Structure for Catalysts and Surfaces*; Y. Iwasawa, Ed.; World Scientific, Co.: Danvers, 1996; Vol. 4; p 77.

(11) Yoshida, S.; Tanaka, T.; Hanada, T.; Hiraiwa, T.; Kanai, H.; Funabiki, T. *Catal. Lett.* **1992**, *12*, 277.

(12) Massoth, F. E. *Adv. Catal.* **1978**, 265.

Part I

Characterization of Active Molybdenum Species in Mo-Mg Binary Oxides

Introduction of Part 1

Molybdenum is one of the most popular elements for many oxide catalysts. However, a single oxide, MoO_3, is rarely used as a catalyst, because it exhibits a low activity for most of reactions and it sublimates at a relatively low temperature. In general, molybdenum oxides are used in a state of a supported and mixed oxides for catalysts. Since Mo atom is a d^6 metal, the cation is stably present as Mo^{6+}, but Mo^{5+}, Mo^{4+}, or Mo^{2+} are metastable. From the catalytic viewpoint, the redox performance of these ions is important in many catalytic reactions.

In case of MoO_3, each molybdenum atom is surrounded by a distorted octahedron of six oxygen atoms, and every octahedron shares the edges and corners with neighboring octahedra.[1] The octahedral MoO_6 units in many molybdates, such as polymolybdates, molybdic acid, molybdenyl salts, *etc.*, are slightly distorted because of the interaction of neighboring Mo-Mo.[2] Only molybdenum bronze, $A^+_xMoO_y$ (A^+ = proton or alkaline-metal ion), has an axially symmetric octahedron in a layered structure.[3,4] Thus, for structural analysis of MoO_6 octahedra, the molybdenum bronze is one of the suitable reference compounds, as discussed in chapter 3 of this thesis.

MoO_4 tetrahedron unit is found in metal molybdates, in general. The divalent-metal molybdates are the typical samples including MoO_4 tetrahedral unit. The crystal structures of divalent-metal molybdates are summarized by Matsuura *et al.*[5] The structure of metal molybdate of divalent cation changes according to its ionic radii. For example, Mg^{2+} (0.69Å), Ni^{2+} (0.69Å), Co^{2+} (0.72Å), Fe^{2+} (0.74Å), and Mn^{2+} (0.80Å) forms α-$CoMoO_4$ (consists of MoO_4 tetrahedra) or α-$MnMoO_4$ (coexist in tetrahedra and octahedra) structure which have MoO_4 unit. For the metal cations with larger ionic radii than 0.9Å, *i.e.*, Cd^{2+} (0.97Å), Ca^{2+} (0.99Å), and Pb^{2+} (1.20Å), the scheelite type ($CaWO_4$ type) structure including MoO_4 tetrahedra is the most stable.

The difference in the local structure around Mo ions strongly affect the activity and selectivity of the catalysts for a variety of reactions, as described in the following parts.

1. Molybdenum oxide as catalysts

Molybdena in a supported state or mixed with other metal oxides are used as catalysts for isomerization, oxidation, hydrogenation, desulfurization, metathesis, and many other reactions. Of these reactions, well known ones are as follows; (1) hydrodesulfurization over cobalt-molybdate (Co-Mo-O) catalysts, (2) selective oxidation of olefins over bismuth-molybdate (Bi-Mo-O) catalysts, (3) metathesis reactions of olefins over supported molybdena catalysts, *e.g.*, MoO_3/SiO_2, MoO_3/Al_2O_3, and MoO_3/TiO_2. In the following sections, the studies for characterization of the catalytically active Mo species are summarized.

(1) Cobalt-molybdate as a catalyst for hydrodesulfurization

Co-Mo-O/Al_2O_3 catalyst is used industrially for hydrogenation (HYD) and hydrodesulfurization (HDS) of hydrocarbons in petroleum refinery.[6] Massoth *et al.*[7] studied the catalytic activity of molybdena on different oxide supports, and showed that dispersion of Mo is an important key for generation of active sites of HDS and HYD. Nishijima *et al.* also presented the relationship between activity and dispersion of molybdena, and observed two-dimentional polymolybdate structures on TiO_2 or Al_2O_3.[8] They found that these phases are the most favorable for high HYD activity, and they proposed that the phase correlates with HDS activity.

It is clarified definitely that the active species of HDS is co-called Co-Mo-S phase which was found to be present in sulfided Al_2O_3-supported and unsupported Co-Mo catalysts, as reported by Topsøe *et al.*[9,10] They also characterized Co-Mo-S phases by EXAFS, and proposed that Mo atoms in the phase exist as dispersed species of MoS_2-like local structure,[11] which is of a prismatic MoS_6 octahedron.[2] A Co ion is present in the edge of MoS_2,[12] and makes the Mo-S bonds be weaker than those of MoS_2.[13] However, the role of cobalt ions in the reaction is still unclear. The reason why Co-Mo-S phase acts as an active species for HDS is summarized; the formation of active species for HDS relates to highly dispersed Co ions in MoS_2 phases, and the activity relates to the effect of support such as activation of Co-S species.[6] Recently, the

detailed structural study of the Co-Mo-S phase has been reported by means of XAFS, and generation of several types of the phases is proposed.[13] Now, the relationship between several phases and the HDS activity is being studied. As mentioned above, in particular, the study intending to elucidate why the Co-Mo-S species is active for HDS is now in progress.

(2) Bismuth-molybdate as a catalyst for selective oxidation

Selective oxidation of light olefins is widely industrialized as the basic unit process in petrochemistry. For instance, propene is partially oxidized to acrolein over some catalysts in practice. In the many processes, acrolein is only an intermediate to yield acrylic acid, a desired product. In this manner, partially oxidation of olefins is an important reaction in catalysis chemistry, and bismuth-molybdates are studied and was used industrially as a practical ones at the early stage.

Most of binary molybdate catalysts exhibit an activity for oxidation of hydrocarbons. The activity of the reaction relates to the oxygen atoms even in bulk phase. For bismuth-molybdates, the relationship between the catalytic activity and mobility of lattice oxygens has been studied. In 1970, Keulks[14] and Wragg[15] *et al.* demonstrated that lattice oxygen in Bi-Mo-O catalysts participates in the formation of oxygenated compound from propene. Further studies have been revealed the mobility of oxygen during the reactions, and it is suggested that the catalytic activity is directly related to the rate of diffusion of the oxide ion through the lattice.[16] It is noted that lattice oxygens in the bulk phase are definitely diffused during the reaction for Bi-Mo binary oxides, which is confirmed by means of ^{18}O-exchanging method.[16,17]

For a structural viewpoint of Bi-Mo-O binary oxides, it is concluded that a few types of phases, *e.g.*, $Bi_2Mo_3O_{12}$ (α-phase), $Bi_2Mo_2O_6$ (β-phase), Bi_2MoO_6 (γ-phase), *etc.*, are act as an active center for oxidation.[18] The phase produced depends on the both atomic composition and preparation temperature.[19] It is summarized that diffusivity of lattice oxygen is very different from a phase to phase, and the diffusivity affects the activity of selective oxidation. For the local structure around Mo ions, α-phase consists of MoO_4 tetrahedra, and γ-phase consists of MoO_6 octahedra. In β-phase, molybdena exist as a mixture of tetrahedra and octahedra. The coexistence of

these polyhedra induces the generation of oxygen vacancy site and affects the oxidation activity because of the enhancement of lattice oxygen diffusion.[20] It is widely accepted that olefins reduce Mo ions deoxygenatively, and Bi-oxide species play a role for activation of oxygen in gas phase and supply the lattice oxygen by diffusion into the bulk phase.[20] The mechanism of olefin oxidation has been studied up to now.

(3) Metathesis reactions of olefins over supported molybdena catalysts

Olefin metathesis is one of the most intriguing reactions in heterogeneous catalysis. Generally, a high-valent transition-metal oxide exhibits the activity when it is partially reduced by pre-reduction treatment. Supported molybdena are known as metathesis catalysts and many papers on it have been published. However, the reaction mechanism of metathesis is not clarified satisfactory. While, in case of supported molybdena catalysts, the mechanism involving metal carbene (alkylidene) and metallo-cyclobutane is widely accepted.[21,22] This mechanism is proposed in the study of homogeneous alkene metathesis,[23] and it is applied to heterogeneous catalysts such as $Mo(CO)_6/Al_2O_3$.[24]

It is known that molybdena supported on many oxide-supports such as TiO_2, Al_2O_3, SiO_2, ZnO, and ZrO_2 exhibit the metathesis activity after pre-reduction treatment, while MgO, GeO_2, and SnO_2-supported ones are not active, as reported by Tanaka *et al.*[25] They found that the metathesis reaction takes place at room temperature over β-TiO_2-supported molybdena without side reactions such as hydrogen scrambling or isomerization. They proved that the reaction is stereoselective and also of structure-retaining by using deuterared olefins and proposed a mechanism including metallo-cyclobutae intermediated to explain the characteristics of the reaction.[25,26] However, other reaction mechanisms for metathesis are suggested by some workers. It is recently reported that combination reaction of carbenes formed on the surface, is one of the mechanism of metathesis in Mo-metal catalyst, as reported by Tysoe *et al.*[27,28] In case of photocatalysis, Anpo *et al.* suggested that oxo-alkylidene type carbenes should play a role in metathesis.[29] Recently, it is noted that non-transitional metal oxide also exhibits a photo-metathesis reactivity.[30] Thus, it needs further studies for the clarification of the mechanism of olefin metathesis.

So far, several species have been proposed as active species for metathesis reactions over molybdena catalysts. Kazansky *et al.* reported in the study of MoO_3/SiO_2 catalysts that tetrahedral Mo^{4+} monoxo-species, which is formed by photo-reduction of the oxidized catalysts with CO at room temperature, possesses the highest reactivity, and dioxo-species shows a lower reactivity.[31] On the other hand, Zhang *et al.* proposed that Mo^{5+} species is active for metathesis.[32] Kadushin *et al.* suggested that dimeric Mo^{5+} is the effective species. Tanaka *et al.* concluded that carbene species are formed on either Mo^{5+} or Mo^{4+}.[25] Therefore, a discussion about the active species with reduced Mo ions is still in progress.

So far, it is accepted that binary oxides containing molybdenum are not active for metathesis but oxidation of alkenes. Mo-Mg binary oxides, for example, also exhibit an activity for partial oxidation of olefins, *e.g.*, propene oxidation to acrolein.[33] On the contrary, it is found that propene metathesis takes place by Mo-Mg binary oxides with higher Mo loadings pretreated with H_2 at 773K.[34] Thus, the structural analysis of Mo-Mg binary oxides in oxidized and reduced states are important. The author has carried out the studies about the characterization of catalytically active species of Mo-Mg binary oxides, and describes the results in chapte 1 and 2 in this thesis.

(4) Other reactions

Supported molybdena are reported to catalyze other reaction, *e.g.*, NO reduction and/or decomposition over MoO_3/ZrO_2,[35] partial oxidation of methane over MoO_3/SiO_2,[36,37] and so on. The development of catalytic application using molybdena has been continued now.

2. Mo K- and L-edge XAFS for characterizing molybdenum compounds

Application of XAFS to the characterization of molybdenum-containing catalysts were reported in 1980s. A variety of molybdena catalysts used in several reaction systems have been analyzed and clarified the local structures and crystalline phases. In Japan, Iwasawa *et al.* used the Mo K-edge EXAFS for analyses of SiO_2-supported monomer- and dimer- Mo clusters and oxides,[38,39] and then, they explained the

dynamic change of the local structure around Mo ions during the dehydration of ethanol.[40,41] Now, it may be considered that the analyses by them are not guaranteed and the presented mechanisms can not explained the experimental results satisfactorily, however, the usefulness of XAFS study is well recognized for characterization of catalytic species by many workers.

(1) Mo K-edge XAFS

As mentioned above, the structural studies of active molybdena species in representative reactions are reported, and detailed discussions are presented about the catalytic active species.

In the structural study of Co-Mo-O catalysts for HDS and/or HYD, Johnson *et al.* tendered the definite conclusion by Mo K-edge XAFS study.[42,43] For Co-Mo/Al_2O_3 after H_2S(10%)/H_2 treatment above 673K, the Mo K-edge XANES spectra showed the existence of Mo^{4+} ions. They concluded the formation of dispersed MoS_2 species in the lower Mo-loading samples and MoS_xO_y sulfided phase at the plate net dimension in the higher loading ones.[43] Clausen *et al.*[11] reported by the study of Mo K-edge EXAFS for Co-Mo/Al_2O_3 that oxidized and sulfided Mo ions are not greatly influenced by the presence of Co ions. Okamoto *et al.* elucidated that (*1*) for CoS_x-MoS_x/NaY catalysts, the reactivity is maximized at Co/Mo=1; (2) in the active species for HDS and HYD, both Mo-Mo and Co-Mo bonds are present; (*3*) coordinatively unsaturated ions do not exist in Mo but in Co ions.[44] In addition, coordinatively unsaturated Co ion relates to the active species for HDS.[44] In these studies, it is concluded that reduced Mo ions in MoS_2-like structure are formed by sulfurization, and these Mo species are more stabilized by co-existence of Co ions which coordinate to Mo ions during the reaction. Recently, the structural studies of a variety of Co-Mo-S(O) phases are reported and the relationship between each phase and reactivity of HDS and HYD are discussed by many workers. For instance, Bouwens *et al.*[13,45] analyzed the structure of two types of Co-Mo-S phases on Al_2O_3 by means of Mo and Co K-edge XAFS, and explained that all Co ions are stabilized in Co-Mo-S states, and most likely position for Co ions is in front of the square sulfur faces of MoS_6 trigonal prisms along the edge of MoS_2

crystals with two additional S ions or H_2S molecules attached. It has been suggested that the coordination number of Co ions in Co-Mo-S layers relates to the reactivity.

As for Mo binary oxide catalysts for selective oxidation, there have been a few XAFS studies. In general, each distinct phase formed in the binary oxides is thought to exhibit the catalytic activity respectively, and therefore, the identification of phases by XRD has been one of the main themes for these catalysts. However, an amorphous phase can not be observed by XRD, and thus, XPS and XAFS studies are also carried out. XAFS measurement in a transmission mode can afford the structural information of bulk phase in a molecular level for both crystalline and amorphous oxides. In particular, the local structure around Mo^{6+} ions, *e.g.*, MoO_4 tetrahedron or MoO_6 octahedron, is an important information to discuss a catalytic activities. Thus, Antonio *et al.*[46] studied that the local structure around both Bi and Mo ions for three Bi-Mo-O phases, *i.e.*, α- (Bi_2O_3-$nMoO_3$; n=3), β- (n=2), and γ- (n=1) phases by Mo K- and Bi L- edge XAFS, and the difference of these phases are shown clearly. The distorted Mo-O_6 octahedra exist in α- and β-phases, and Mo-O_5 (as an average of total molybdates) exists in γ-phase. In addition, Bi-Bi coordination, which is assigned to that found in Bi_3O_2, indicates that O vacancy is formed by coexistence of reduced Bi ions which have Bi-Bi bonds. It is also concluded that Bi-O_8 coordination exists mainly in α- and β-phases, and Bi-O_6 coordination with elongated Bi-O bonds exists partly in γ-phase.[46]

There are several papers investigating the local structure of supported molybdena by XAFS. The local structure of supported molybdena (2 - 10 wt% as Mo) on typical oxide supports, *i.e.*, SiO_2, Al_2O_3, TiO_2, and MgO are studied by Shimada *et al.*[47] It is concluded that monolayered molybdena on SiO_2 and TiO_2 are present as MoO_6 octahedra, while those on MgO exist as MoO_4 tetrahedra. In case of Al_2O_3-support, a ratio of tetrahedron to octahedron is decreased with increase in Mo loading. These results are consistent with the conclusion by UV-VIS spectroscopy.[48] For TiO_2-supported molybdena, the structure of molybdates and its change by addition of alkaline-ion is studied by Martin *et al.* The MoO_6 octahedra is formed on TiO_2 (in 5.8

wt% Mo), and tetrahedral species is formed by alkaline-ion doping.[49] They concluded that (*1*) Li_2MoO_4 phase is formed by addition of Li (1 wt%) ion; (2) $(Mo_2O_7)^{2-}$ chains exist by addition of Na or K ion; (3) polymolybdates such as $Rb_2Mo_3O_{10}\cdot H_2O$ and $Rb_2Mo_4O_{13}$ are formed by addition of Rb ion.[50] By means of *in situ* EXAFS study, Prins *et al.*[51] concluded the spreading of MoO_3 on γ-Al_2O_3, which is prepared from physical mixture, by addition of water vapor. It is noted that the distances of Mo-O and Mo-Mo changed during the formation of polyanions by water addition, and Mo-O-Al bonds are generated by thermal treatment at 720K.

In these studies mentioned above, XAFS is applied widely to the characterization of catalytically active species of many systems. It is concluded that XANES provides the information of structural symmetry and valence of Mo ions, and EXAFS gives the structural parameters, *i.e.*, bond lengths and coordination numbers. These informations are quite useful for clarification of catalytic active species and determination of local phases.

(2) Mo L-edge XANES

The white lines of Mo L_2- and L_3-edge XANES are due to electronic transitions from a core level, $2p_{1/2}$ or $2p_{3/2}$, to a vacant $4d$ state. Teo and Lee proposed that the contribution of the *p-d* transition to these spectra is about fifty times that of the *p-s* one.[52] Thus, the L-edge XANES straightforwardly reflects the $4d$ field of Mo, and the information is the same as that of the pre-peak of K-edge XANES. In general, the splitting of the white lines reveals the t_{2g}-e_g (for MoO_6 octahedron) or e-t_2 (for MoO_4 tetrahedron) splitting of $4d$ orbitals by the ligand field, and the relative intensity of the two bands depends on the local symmetry of Mo ions.[53-55]

For characterization of molybdate species, Mo L-edge XANES study was started quite recently. Hedman *et al.*[54] were the first presenting the spectra in the study on materials of biological interest. By using the three types of reference Mo^{6+} compounds, they showed that the variable splitting in the Mo $L_{2,3}$-edges reflected the ligand field splitting of $4d$-orbitals definitely.[54] In 1993, Bare *et al.*[55] utilized XANES of MgO-supported molybdena catalysts, and used for the determination of tetrahedral or

octahedral molybdate species including Mo^{6+} ions. It is concluded that isolated MoO_6 octahedron exists mainly in the samples below 15 wt% MoO_3, and MoO_4 tetrahedra due to $MgMoO_4$ phase is found in the samples above 20 wt%. The structure of molybdates in 15 wt% sample changes from octahedra to tetrahedra by addition of water vapor, and the tetrahedra changes to octahedra reversibly by evacuation.[54] In addition, they applied this technique to characterizing molybdate species on various oxide supports. It is revealed that the structures of the hydrated surface molybdena species are controlled by the net surface pH at the zero point charge, and the structures of molybdena are the same as those observed in aqueous solution such as MoO_4^{2-}, $Mo_7O_{24}^{6-}$, and $Mo_8O_{26}^{4-}$.[56] In addition, it is concluded that molybdena supported on Al_2O_3, ZrO_2, TiO_2, and Nb_2O_5 are isolated and tetrahedrally coordinated in low coverages, and polymolybdates are formed on TiO_2 and Nb_2O_5 in high coverages, while coexistence of tetrahedra and octahedra is seen on Al_2O_3 and ZrO_2. SiO_2-supported molybdena are isolated and exist in both tetrahedral and octahedral species.[56]

Therefore, the characterization of Mo and other *4d* transition metal complexes by L-edge XANES spectroscopy is promising for more precise determination of the symmetry around the target atoms than that by K-edge XANES spectroscopy.[57]

3. UV-VIS spectroscopy for characterizing molybdenum compounds

UV-VIS spectra of heterogeneous catalyst sample are often recorded in the diffuse reflectance mode. In case of molybdena catalysts, the informations of environmental coordination or valence of Mo ions are useful. As a problem, detection depth into bulk phase is unclear in this method. But it is suitable for the structural analysis of Mo ions which exist only in the surface layer. The diffuse reflectance UV-VIS spectroscopy has been applied to the structural analysis of supported molybdena catalysts conventionally.

The Mo^{6+} ion has no *d* electron, and the assignment of electron transition from the absorption band is LMCT, $O^{2-} \rightarrow Mo^{6+}$. From the results of many UV-VIS studies, it is

generally accepted that tetrahedrally coordinated Mo^{6+} species absorbs the light of 260 - 290 nm, and octahedrally coordinated one absorbs the light of 300 - 330 nm.[48,58,59] An additional band at 230 - 240 nm is common to both tetrahedral and octahedral configurations.[48] In case of Mo-polyanion samples, it is concluded that Mo dispersion (*e.g.*, Mo cluster size and distance between clusters) and Mo-support interaction exhibit more influence than local symmetry of Mo.[58] For the samples including reduced Mo ions such as Mo^{5+} or Mo^{4+}, the existence of 4*d* electrons leads to strong absorption bands, which is due to *d-d* electron transition, in the visible spectrum. For example, a band centered at 400 nm suggests the existence of octahedrally coordinated Mo^{5+} ions, and bands at 350 and 480 - 500 nm are ascribed to octahedrally coordinated Mo^{4+} ions. Therefore, UV-VIS spectroscopy can be applied widely for the assignment of local structure or crystalline phases around Mo ions.

UV-VIS spectroscopy has been used for characterization of catalytically active species so far. In 1976, Che *et al.* summarized the absorption bands of molybdena on typical oxide-supports.[48] It is concluded that supported molybdates exist as MoO_6 octahedra, except for the case of formation of molybdates such as $MgMoO_4$ or $Al_2(MoO_4)_3$. Kazansky *et al.*[60,61] reported that UV-VIS is utilized the structural analysis of active molybdena species for olefin metathesis, and proposed that Mo^{4+} monoxo-species which is formed by photo-reduction with CO is a precursor of high active species. Then, they suggested that the absorption band at 580 - 600 nm is characteristic of π-compexes of olefins with Mo^{4+} ions, and explained the mechanism including metallo-cyclobutane during the metathesis reaction.[31,62]

Survey of Part 1

As mentioned above, it is concluded that the activity of molybdena relates fundamentally to the local structure of molybdena species, *e.g.*, coordination number of Mo-O and valence of Mo ions. Characterization of these species is necessary to clarify the catalytic performance. On these backgrounds, the structural analyses of molybdena catalysts have been applied. In this thesis, the author chose the Mo-Mg-O system, whose binary oxide exhibits an activity for oxidation of propene[33] and no

activity for olefin metathesis.[25] Recently, it is reported that reduced Mo-Mg-O catalysts with high Mo amount exhibit a metathesis activity.[34] The author has studied the local structure of Mo-Mg-O with various Mo amounts, and obtained a structural information of active species for metathesis by means of Mo *K*-, *L*-edge XAFS and UV-VIS spectroscopy.

In chapter 1, Mo K-edge XAFS is applied to Mo-Mg-O binary oxide catalysts with various Mo amounts in oxidized and reduced states, and structural information in bulk phase is obtained. From these results, the correlation between the structure in the bulk phases and metathesis active species is discussed. In chapter 2, the structure of Mo species in near-surface region is analyzed by Mo L-edge XANES and UV-VIS spectroscopy, and the role of surface Mo species for metathesis active species is discussed. In Mo L-edge XAFS study in this chapter, local symmetry of molybdenum is focused on the discussion, and therefore, molybdenum bronze is one of the suitable compounds because it has an axially symmetric MoO_6 octahedron. Thus, the structure of hydrogen molybdenum bronzes (H_xMoO_3) is elucidated by Mo K-edge XAFS study, and clarified the more detailed structure around Mo ions, as mentioned in the 'appendix' section.

References

(1) Cotton, F.; Wilkinson, G. In *Adv. Inorg. Chem. (4th ed.)*; Interscience: New York, 1980, p 847.

(2) Goodenough, J. B. In *Proc. Climax 4th Int. Conf. Chemistry and Uses of Molybdenum*, Ann Arbor, Michigan, 1982: (H. F. Barry and P. C. H. Mitchell, Eds.; Climax Molybdenum Co., 1982), , p 1.

(3) Sotani, N.; Eda, K.; Kunitomo, M. *J. Chem. Soc. Faraday Trans.* **1990**, *86(9)*, 1583.

(4) Dickens, P. G.; Neild, D. J. In *Proc. Climax 2nd Int. Conf. Chemistry and Uses of Molybdenum*, Oxford, 1976: (P. C. H. Mitchell and A. Seaman, Eds.; Crimax Molybdenum Co., 1976), , p 134.

(5) Matsuura, I. *Shokubai (Catalyst)* **1979**, *21*, 409 (in Japanese).

(6) Okamoto, Y. *Shokubai (Catalyst)* **1996**, *38(1)*, 26 (in Japanese).

(7) Massoth, F. E. *Adv. Catal.* **1978**, 265.

(8) Shimada, H.; Sato, T.; Yoshimura, Y.; Hiraishi, J.; Nishijima, A. *J. Catal.* **1988**, *110*, 275.

(9) Wivel, C.; Candia, R.; Clausen, B. S.; Mørup, S.; Topsøe, H. *J. Catal.* **1981**, *68*, 453.

(10) Topsøe, H.; Clausen, B. S.; Candia, R.; Wivel, C.; Mørup, S. *J. Catal.* **1981**, *68*, 433.

(11) Clausen, B. S.; Topsøe, H.; Candia, R.; Villadsen, J.; Lengeler, B.; Als-Nielsen, J.; Christsen, F. *J. Phys. Chem.* **1981**, *85*, 3868.

(12) Topsøe, N.; Topsøe, H. *J. Catal.* **1983**, *84*, 386.

(13) Bouwens, S. M. A. M.; van Zon, F. B. M.; van Dijk, M. P.; van der Kraan, A. M.; de Beer, V. H. J.; van Veen, J. A. R.; Koningsberger, D. C. *J. Catal.* **1994**, *146*, 375.

(14) Keulks, G. W. *J. Catal.* **1970**, *19*, 232.

(15) Wragg, R. D.; Ashmore, P. R.; Hockey, J. A. *J. Catal.* **1971**, *22*, 49.

(16) Keulks, G. W.; Krenzke, L. D. In *Proc. 6th Int. Congr. Catal.*, London, 1976: (G. C. Bond, P. B. Wells and F. C. Tompkins, Eds.; The Chemical Society, 1976), vol. B, p 20.

(17) Moro-oka, Y.; Ueda, W.; Tanaka, S.; Ikawa, T. In *Proc. 7th Int. Congr. Catal.*, Tokyo, 1980: (T. Seiyama and K. Tanabe, Eds.; Kodansha-Elsevier, 1980), vol. B, p 1086.

(18) Egasira, M.; Matsuo, K.; Kagawa, S.; Seiyama, T. *J. Catal.* **1979**, *58*, 409.

(19) Bleijenberg, A. C. A. M. *J. Catal.* **1965**, *4*, 581.

(20) Moro-oka, Y.; Ueda, W. *Adv. Catal.* **1994**, *40*, 233.

(21) Mol, J. C.; Moulijn, J. A. *Adv. Catal.* **1975**, *24*, 131.

(22) Kazuta, M.; Tanaka, K. *J. Catal.* **1990**, *123*, 164.

(23) Banks, R. L.; Bailey, G. C. *Ind. Eng. Chem., Prod. Res. Develop.* **1964**, *3*, 170.

(24) Brenner, A.; Burwell Jr., R. L. *J. Catal.* **1978**, *52*, 1978.

(25) Tanaka, K.; Miyahara, K.; Tanaka, K. In *Proc. 7th Int. Congr. Catal.*, Tokyo, 1980: (T. Seiyama and K. Tanabe, Eds.; Kodansha-Elsevier, 1980), vol. B, p 1318.

(26) Tanaka, K.; Miyahara, K.; Tanaka, K. *J. Mol. Catal.* **1982**, *15*, 133.

(27) Bartlett, B.; Shneerson, V.; Tysoe, W. T. *Catal. Lett.* **1995**, *32*, 1.

(28) Wang, L. P.; Soto, C.; Tysoe, W. T. *J. Catal.* **1993**, *143*, 92.

(29) Anpo, M.; Kondo, M.; Kubokawa, Y.; Louis, C.; Che, M. *J. Chem. Soc. Faraday Trans. 1* **1988**, *84(8)*, 2771.

(30) Yoshida, H.; Tanaka, T.; Matsuo, S.; Funabiki, T.; Yoshida, S. *J. Chem. Soc., Chem. Commun.* **1995**, 761.

(31) Vikulov, K. A.; Elev, I. V.; Shelimov, B. N.; Kazansky, V. B. *J. Mol. Catal.* **1989**, *55*, 126.

(32) Zhang, B.; Li, Y.; Lin, Q.; Jin, D. *J. Mol. Catal.* **1988**, *46*, 229.

(33) Yun, Y.; Ueda, W.; Moro-oka, M. In *Preprint of the 72nd Annual Meeting of the Catalysis Society of Japan,*, Nishinomiya, 1993: (C. S. Jpn., Eds.; Catal. Soc. Jpn., 1993), , p 470.

(34) Hasegawa, S.; Tanaka, T.; Kudo, M.; Mamada, H.; Hattori, H.; Yoshida, S. *Catal. Lett.* **1992**, *12*, 255.

(35) Tanabe, K.; Ikeda, H.; Iizuka, T.; Hattori, H. *React. Kinet. Catal. Lett.* **1979**, *11*, 149.

(36) Bañares, M. A.; Fierro, J. L. G.; Moffat, J. B. *J. Catal.* **1993**, *142*, 406.

(37) Liu, H. F.; Liu, R. S.; Liew, K. Y.; Johnson, R. E.; Lunsford, J. H. *J. Am. Chem. Soc.* **1984**, *106*, 4117.

(38) Iwasawa, Y.; Nakano, Y.; Ogasawara, S. *J. Chem. Soc., Faraday Trans. 1* **1978**, *74*, 2968.

(39) Iwasawa, Y.; Ogasawara, S.; Sato, Y.; Kuroda, H. In *Proc. Climax 4th Int. Conf. Chemistry and Uses of Molybdenum*, Ann Arber, Michigan, 1982: (H. F. Barry and P. C. H. Mitchell, Eds.; Crimax Molybdenum Co., 1982), , p 283.

(40) Iwasawa, Y.; Yamagishi, M. *J. Catal.* **1983**, *82*, 373.

(41) Iwasawa, Y. *Adv. Catal.* **1987**, *35*, 187.

(42) Chiu, N.-S.; Bauer, S. H.; Johnson, M. F. L. *J. Catal.* **1984**, *89*, 226.

(43) Chiu, N.-S.; Bauer, S. H.; Johnson, M. F. L. *J. Catal.* **1986**, *98*, 32.

(44) Okamoto, Y. *Appl. Surf. Sci.* **1996**, in press.

(45) Bouwens, S. M. A. M.; van Veen, J. A. R.; Koningsberger, D. C.; de Beer, V. H. J.; Prins, R. *J. Phys. Chem.* **1991**, *95*, 123.

(46) Antonio, M. R.; Teller, R. G.; Sandstorm, D. R.; Mehicic, M.; Brazdil, J. F. *J. Phys. Chem.* **1988**, *92*, 2939.

(47) Shimada, H.; Matsubayashi, N.; Sato, T.; Yoshimura, Y.; Nishiyama, A.;

Kosugi, N.; Kuroda, H. *J. Catal.* **1992**, 746.

(48) Che, M.; Figueras, F.; Forisser, M.; McAtter, J.; Perrin, M.; Portefaix, J. L.; Praliaud, H. In *Proc. 6th Int. Congr. Catal.*, London, 1976: (G. C. Bond, P. B. Wells and F. C. Tompkins, Eds.; The Chemical Society, 1976), vol. 1, p 261.

(49) Martin, C.; Martin, I.; Rives, V. *J. Catal.* **1994**, *147*, 465.

(50) Martin, C.; Martin, I.; Rives, V.; Maret, P. *J. Catal.* **1996**, *161*, 87.

(51) Kisfaludi, G.; Leyrer, J.; Knözinger, H.; Prins, R. *J. Catal.* **1991**, *130*, 192.

(52) Teo, B. K.; Lee, P. A. *J. Am. Chem. Soc.* **1979**, *101*, 2815.

(53) Evans, J.; Frederick, W.; Mosselmans, W. *J. Phys. Chem.* **1991**, *95*, 9673.

(54) Hedman, H.; Frank, P.; Gheller, S. F.; Roe, A. L.; Newton, W. E.; Hodgson, K. O. *J. Am. Chem. Soc.* **1988**, *110*, 3798.

(55) Bare, S. R.; Mitchell, G. E.; Maj, J. J.; Vrieland, G. E.; Gland, J. L. *J. Phys. Chem.* **1993**, *97*, 6048.

(56) Hu, H.; Wachs, I. E.; Bare, S. R. *J. Phys. Chem.* **1995**, *99*, 10897.

(57) Yoshida, S.; Tanaka, T. In *X-ray Absorption Fine Structure for Catalysts and Surfaces*; Y. Iwasawa, Ed.; World Scientific, Co.: Danvers, 1996; Vol. 8; p 304.

(58) Fournier, M.; Louis, C.; Che, M.; Chaquin, P.; Masure, D. *J. Catal.* **1989**, *119*, 400.

(59) Prialiaud, H. In *Proc. Climax 3rd Int. Conf. Chemistry and Uses of Molybdenum*, Ann Arbor, Michigan, 1976: (P. C. H. Mitchell and A. Seaman, Eds.; Climax Molybdenum Co., 1976), , p 195.

(60) Shelimov, B. N.; Elev, I. V.; Kazansky, V. B. *J. Catal.* **1986**, *98*, 70.

(61) Elev, I. V.; Shelimov, B. N.; Kazansky, V. A. *J. Catal.* **1988**, *113*, 229.

(62) Kazansky, V. B.; Shelimov, B. N.; Vikulov, K. A. In *Proc. 10th Int. Congr. Catal.*, Budapest, 1992: ; Elsevier, 1992), , p 515.

Chapter 1

Mo K-edge XAFS Study of Mo-Mg Binary Oxides for Characterization of Active Mo Species in the Bulk Phase for Olefin Metathesis

Abstract

The local structure around Mo atoms in Mo-Mg binary oxides has been investigated by X-ray absorption spectroscopy at Mo *K*- and Mg *K*- edges. XANES and EXAFS spectra show that the binary oxides have a tetrahedral MoO_4 unit in the samples with a (Mo/(Mo+Mg)) ratio less than 0.5, and an octahedral MoO_6 unit in the samples with a higher ratio. By H_2-treatment at 773K, a molybdena-rich binary oxide was easily reduced to form MoO_2 phase, which was not detected by XRD but was by EXAFS. It is concluded that the reduced oxide contains low valent Mo ions in the MoO_2 phase and the ions work as an active center for propene metathesis.

Introduction

Supported and mixed molybdenum oxides catalyze a variety of reactions such as oxidation, hydrogenation, and metathesis. From these reactions, the olefin metathesis takes readily place over SiO_2, Al_2O_3, or TiO_2-supported MoO_3 when the sample is pre-reduced.[1-3] On the other hand, MgO-supported MoO_3 does not exhibit a metathesis activity.[4] Characterization studies of MgO-supported MoO_3 catalysts have shown that most Mo ions loaded on MgO are stabilized as MoO_4 tetrahedra, attributed to the formation of magnesium orthomolybdate ($MgMoO_4$) by calcination.[5-7] The formation of such species has also been observed for mechanical mixtures of MoO_3 and MgO calcined at low temperature.[8] In addition, the Mo ions have been found to be present not only in the surface layer of MgO but also in the bulk, indicating that the Mo ions diffuse easily in MgO. Therefore, MgO-supported MoO_3 may be the same as MoO_3-MgO binary metal oxide in nature. This might be the reason why MgO-supported MoO_3 does not exhibit a metathesis activity despite the presence of MoO_4 tetrahedra which are often regarded as a precursor of the active species for olefin metathesis; most of the active species are buried in the bulk. However, it has been reported that Mo-Mg binary oxide exhibits a catalytic activity for partial oxidation, *e.g.*, oxidative dehydrogenation of butane to butene and butadiene,[9] and ethylbenzene to styrene.[10,11] In these studies, the Mo ions were proposed to be responsible for the oxidation. These results strongly suggest that the inactivity of MgO-supported MoO_3 for the olefin metathesis does not result only from the bulk diffusion of Mo ions in MgO but from another reason related to the electronic states and/or the particular structure of molybdate species.

Recently, we have studied the structure and catalytic activity of MoO_3-MgO binary oxides with various Mo contents. In that work, we have found that highly molybdenum-containing MoO_3-MgO (Mo/(Mo+Mg)=0.6-0.7) pretreated with hydrogen at 773K exhibits a high activity for propene metathesis,[12] although MoO_3 itself was almost inactive. This is a very significant finding because MoO_3-MgO was thought to be inactive for the olefin metathesis and the nature of the active species must be

reexamined since it is hardly acceptable that the binary oxide with a high Mo ratio (Mo/(Mo+Mg)=0.6-0.7) has MoO_4 tetrahedra.

There have been a few structural studies on MoO_3-MgO binary oxides so far. A Mo $L_{2,3}$-edge XANES study of the local structure of MgO-supported MoO_3[13] showed that the molybdenum species are stabilized on MgO as MoO_6 octahedra in a sample of low Mo content, and MoO_4 tetrahedra are formed at a relatively higher content of Mo (- 15 wt%).[13,14] This result is inconsistent with the studies by diffuse reflectance UV/VIS spectroscopy[5,15] and Raman spectroscopy,[16] in which it was concluded that tetrahedral molybdate is stabilized onto MgO at low content of Mo ions.

Some of the results mentioned above are inconsistent with each other and hence the local structure of the species on MoO_3-MgO is still unclear. A more detailed structural study is called for. The present paper is devoted to a clarification of the structure of MoO_3-MgO by Mo *K*-edge and Mg *K*-edge XAFS spectroscopy. In the sample, several molybdates and magnesium oxides are present as a mixture, so that the definite structure of these species and parameters such as coordination numbers and bond lengths can not be obtained precisely. Here, we focused the discussion on the structural change by the reduction of the binary oxides which show the olefin metathesis activity.

Experimental

Materials and Preparation Methods. MoO_3-MgO samples, ranging in molybdenum content from 0.1 to 0.9 by atomic ratio (x=Mo/(Mo+Mg)), were prepared by a solution-evaporation method as follows. A given amount of $(NH_4)_6Mo_7O_{24}\cdot 4H_2O$ (Nacalai Tesque) was dissolved in distilled water. Then a given amount of $MgCl_2\cdot 6H_2O$ (Nacalai Tesque) was added slowly to the solution at 353K with stirring to form a slurry. This slurry was kept with stirring for about 8 h to evaporate excess water to form a paste. The obtained paste was dried overnight at 343K and calcined in air at 873K for 3 h. The atomic ratio of molybdenum atoms (x) was determined by ICP (Inductively Coupled Plasma) emission spectroscopy, and is shown in Table 1. The

values determined by ICP are consistent with these in the starting solutions, indicating no sublimation of MoO_3 in the calcination procedure.

Reduction of MoO_3-MgO samples was carried out by evacuating at 773K, followed by treatment with H_2 gas (100 Torr) at 773K for 1 h, trapping resultant water into a liquefied N_2 cold trap. Finally, the samples were evacuated at 773K for 1 h.

X-ray Diffraction. Crystalline phases were analyzed by a Rigaku RINT-1300 powder X-ray diffractometer with monochromatized Cu $K\alpha_1$ radiation (1.5406 Å). Identification of crystalline phases from diffraction patterns was done with the aid of JCPDS files.

X-ray Absorption Measurements and Analyses. The measurement of the Mo *K*-edge XANES and EXAFS spectra of these samples were carried out at the BL-10B station with a Si(311) double crystal (d=1.6375Å) monochromator at the Photon Factory in the National Laboratory for High Energy Physics (KEK-PF) with a ring energy of 2.5 GeV and stored current of 150 - 190 mA in the transmission mode in air at room temperature. Incident X-ray flux and transmitted flux were measured with ionization chambers in which argon and krypton gases are flowing at 1 atm. The spectra were measured with energy steps of *ca.* 0.3 eV at the Mo *K*-edge (20.002 keV).

The measurement of Mg *K*-edge XANES spectra was carried out at the BL-7A station with soft X-ray beamline with a beryl double crystal (d=7.9825Å) monochromator at UVSOR in the Institute for Molecular Science, with a ring energy of 750 MeV and stored current of 80 - 190 mA in the total electron yield mode. Each energy step was *ca.* 0.25 eV at the Mg *K*-edge (1,303 eV). Each sample was mounted on the first dynode of the electron multiplier in an ultra high vacuum system ($<1.0\times 10^{-7}$ Torr), and the spectrum was recorded at room temperature. Incident X-ray flux was measured with gold-mesh transmitting 80 % of X-ray at the same time as an electron yield.

Computational analyses for these spectra were performed with the FACOM M382 computer system at the Data Processing Center of Kyoto University. Each spectrum was normalized to the height of the edge jump after removal of the contribution from absorptions other than the *K*-edge absorption, as described elsewhere.[17] The k^3-weighted EXAFS were obtained from normalized EXAFS spectra, and Fourier-

Table 1 Contents of Mo atom in MoO_3-MgO samples.

Mo ratio (x)[a] corresponded in preparation	Mo ratio[a] of MoO_3-MgO determined by ICP
0.80	0.789
0.70	0.708
0.60	0.632
0.50	0.509
0.30	0.319

a) value of Mo/(Mo+Mg).

Table 2 Crystalline phases of MoO_3-MgO (calcined at 873K) by X-ray diffraction.

x	phases
0.9	MoO_3[b]
0.8	MoO_3 $Mg_2Mo_3O_{11}$
0.7	MoO_3 $Mg_2Mo_3O_{11}$ $(Mg_2Mo_2O_7)$[a]
0.6	MoO_3 $Mg_2Mo_3O_{11}$ $(MgMoO_4)$ $(Mg_2Mo_2O_7)$
0.5	$MgMoO_4$[c]
0.4	α-$MgMoO_4$[d] (MgO)
0.3	α-$MgMoO_4$ MgO
0.1	(α-$MgMoO_4$) MgO

a) Compounds in parentheses are only a minor species.

b) Orthorombic. c) Monoclinic. d) Triclinic.

transformations were performed within the range Δk=3.5-14.5 $Å^{-1}$ without any phase shift correction.

3. Results

(1) X-ray Diffraction.

Fig. 1 shows the X-ray diffraction patterns of the prepared samples of x (Mo/(Mo+Mg)) =0.3, 0.5, 0.7 and 0.8; and MoO_3, and the identified crystalline phases are summarized in Table 2. The diffraction pattern of MoO_3 exhibits peaks at 2θ=12.7, 23.3, 25.7 and 27.3 degrees, which arise from diffraction from (020), (110), (040) and (021) planes of orthorhombic MoO_3, respectively. This MoO_3 phase was observed for the samples of $x>0.6$ (Table 2). In these samples, the $Mg_2Mo_3O_{11}$ phase is present besides MoO_3. It is noteworthy that weak peaks due to a $MgMo_2O_7$ phase were observed in the samples of x=0.6 and 0.7. These samples exhibit activity for metathesis reaction by treatment with H_2.[12] The diffraction patterns for the samples after treatment with H_2 at 773K were also recorded. The pattern did not include diffraction lines due to MoO_3 and $MgMo_2O_7$ and the intensity of the peaks due to $Mg_2Mo_3O_{11}$ was significantly reduced. The results indicate that part of the binary oxides of x=0.6 and 0.7 became X-ray amorphous by H_2 treatment at 773K.

For the samples of $x \leqq 0.5$ which have a low activity for metathesis reaction, only the crystalline phases of MgO and $MgMoO_4$ were detected by XRD. These phases did not disappear by the H_2 treatment, indicating that MgO and $MgMoO_4$ are substantially stable after treatment with H_2.

(2) Near-edge Spectra (XANES) of Oxidized Samples.

Fig. 2 shows the normalized Mo *K*-edge XANES of reference compounds. The spectrum of $MgMoO_4$ which has a tetrahedral MoO_4 T_d-structure exhibited a peak centered at 19,995 eV (pre-peak), which is attributed to 1*s*-4*d* transition,[18] and broad bands (resonance peaks) above 20,010eV. The pre-peak is presumably caused by mixing of the 2*p* orbitals of oxygen with the 5*p* and 4*d* orbitals of molybdenum,[19] and

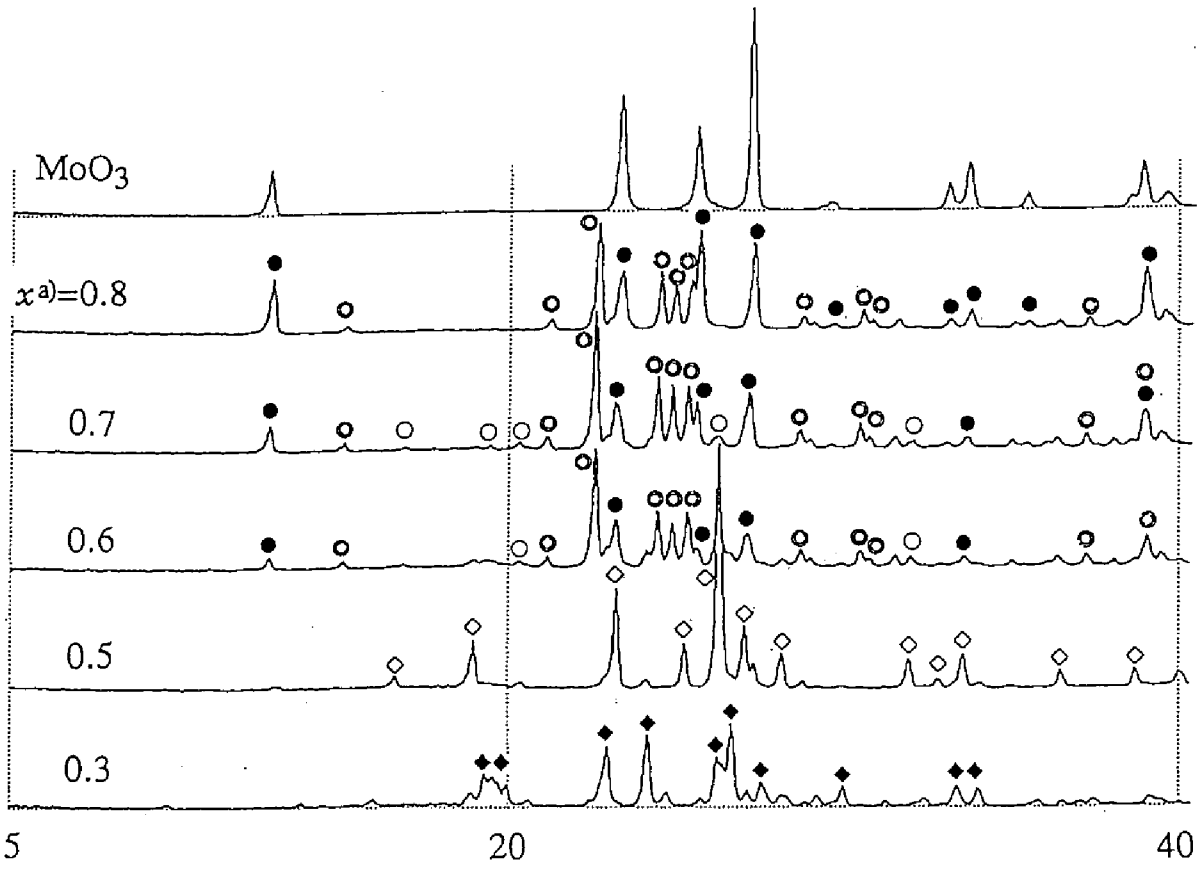

Fig. 1 X-ray diffraction patterns of MoO_3-MgO.

● MoO_3 (orthorhombic)
○ $MgMo_2O_7$
◎ $Mg_2Mo_3O_{11}$
◇ $MgMoO_4$ (monoclinic)
◆ α-$MgMoO_4$ (triclinic)

a) value of Mo/(Mo+Mg).

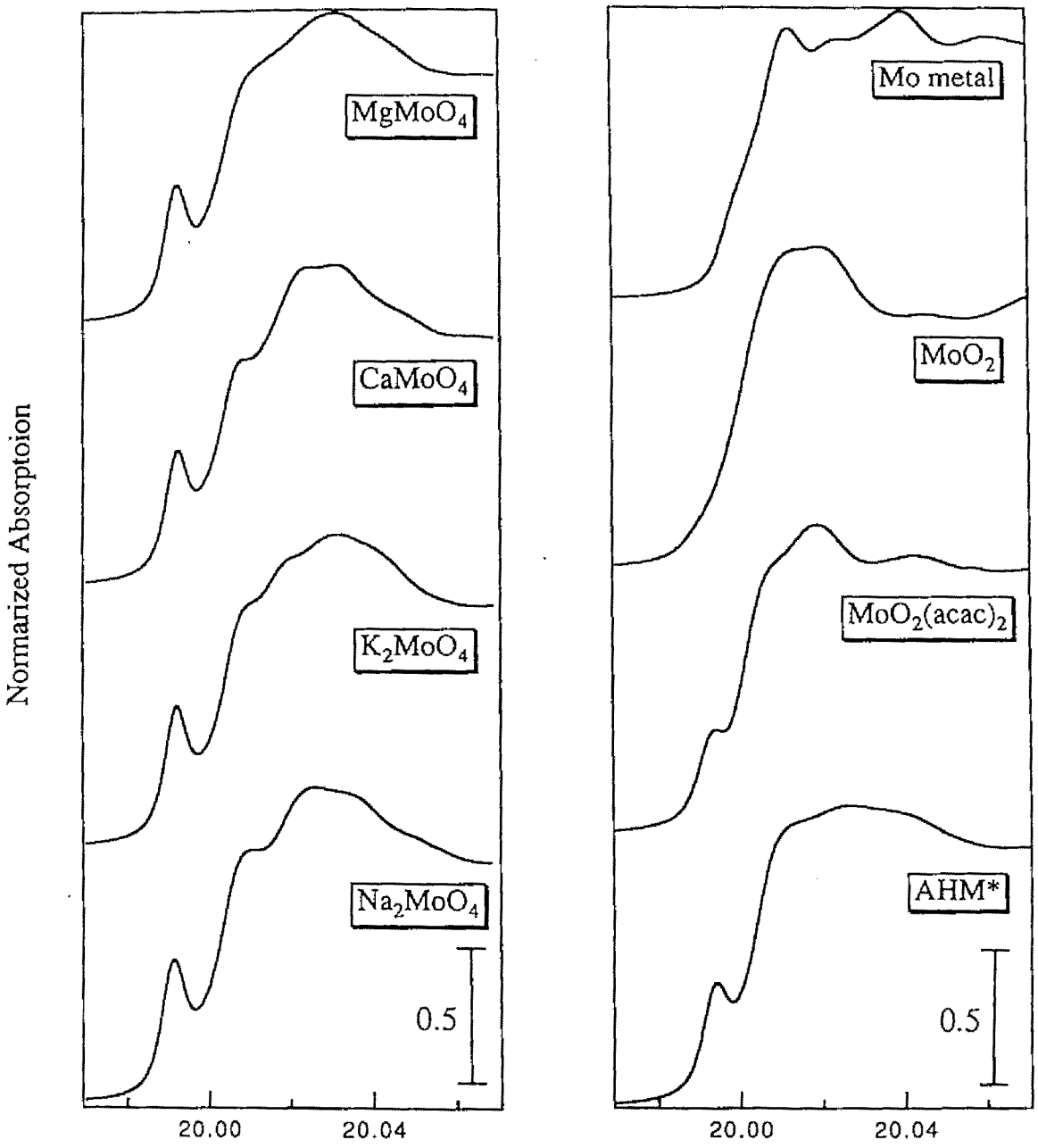

Fig. 2 Mo *K*-edge XANES spectra of reference compounds. (*AHM=ammonium heptamolybdate)

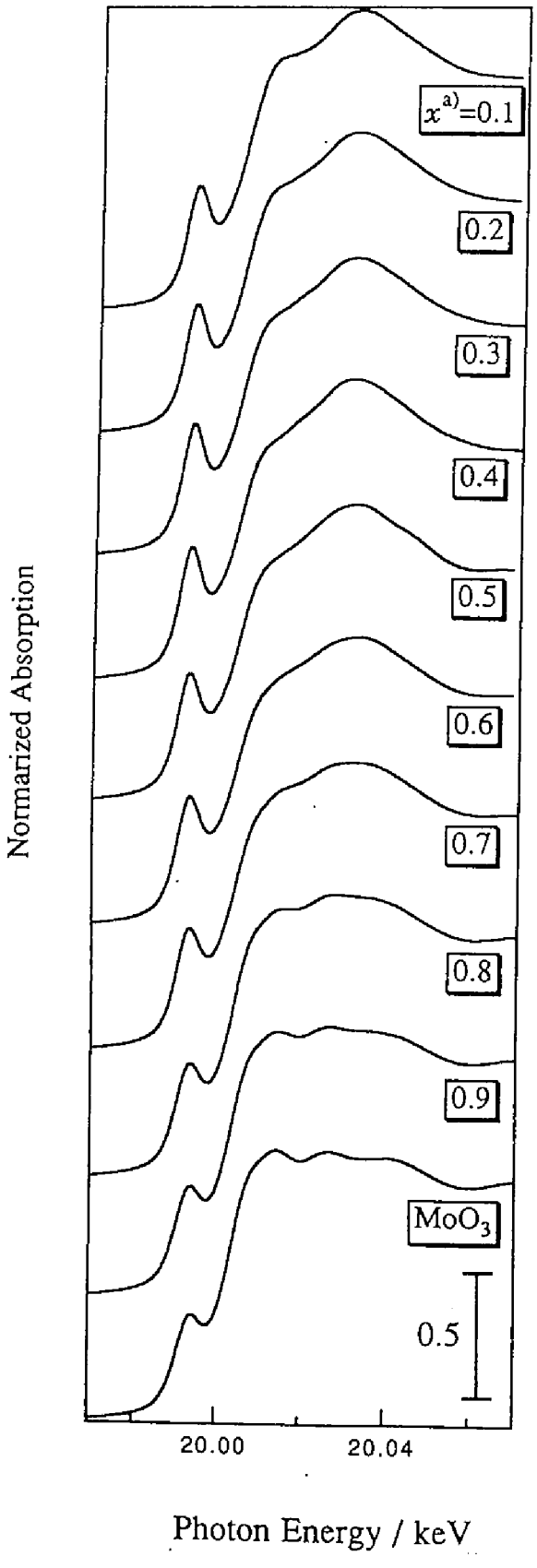

Fig. 3 Mo *K*-edge XANES spectra of MoO_3-MgO calcined at 873K.
a) the ratio of Mo/(Mo+Mg).

the probability of this transition is much higher than that of 1*s*-4*d* allowed quadrupole transition.[20] Such mixing does not occur for a regular octahedral MoO_6 structure. For a distorted octahedra, however, the *d*-*p* mixing can occur although to a smaller extent than in the case of T_d structure. For the samples of $MoO_2(acac)_2$, ammonium-heptamolybdate and MoO_3 (shown in Fig. 3) which have a distorted MoO_6 octahedron,[21] the pre-peaks are also found, and the relative intensity (peak height) is smaller than that of $MgMoO_4$. In the case of the reference compounds with T_d-symmetric MoO_4, such as Na_2MoO_4, K_2MoO_4 and $CaMoO_4$, the XANES pre-peak is similar to that of $MgMoO_4$.

The XANES spectra of the prepared samples calcined at 873K are shown in Fig. 3. For the samples of $x \leqq 0.5$, the XANES spectra resemble each other, and are almost identical to that of $MgMoO_4$. XANES spectra of the samples with higher x are more similar to that of MoO_3 with an increase in x. These results suggest that the local structure around a Mo ion in the Mo-Mg binary oxides is MoO_4 tetrahedral, and that a MoO_6 octahedron is generated at $x > 0.5$.

In order to obtain information about the local structure around the Mg atoms, measurements of Mg *K*-edge XANES spectra were also carried out. These are shown in Fig. 4. For bulk MgO with a symmetric MgO_6 O_h-structure, a sharp peak at 1309.9 eV is seen. This peak is not a so-called pre-edge peak, but due to a 1*s*-3*p* transition as reported by Yoshida *et al*,[22] although the definite assignment of the peak has not been established. Therefore, when Mg ions are located at a highly symmetrical center, the 3*p* orbitals of Mg are degenerated resulting in a sharp and narrow XANES peak. For the Mo-Mg oxide samples, it is evident that the spectra can be classified into two types. For x below 0.3, the spectra are similar to that of MgO, while for $x > 0.3$, the spectra resemble each other and that of $MgMoO_4$. The spectrum of the x=0.3 sample has an intermediate feature between those of MgO and $MgMoO_4$. In fact, the spectrum can be almost reproduced by superposition of the spectrum of MgO multiplied by 0.7 and that of $MgMoO_4$ by 0.3. In the case of $MgMoO_4$, Mg ions are surrounded by eight oxygen atoms, while, in case of MgO, Mg ions are located at the center of regular octahedra of oxygen ions.[21] Therefore, the Mg ions in MoO_3-MgO are

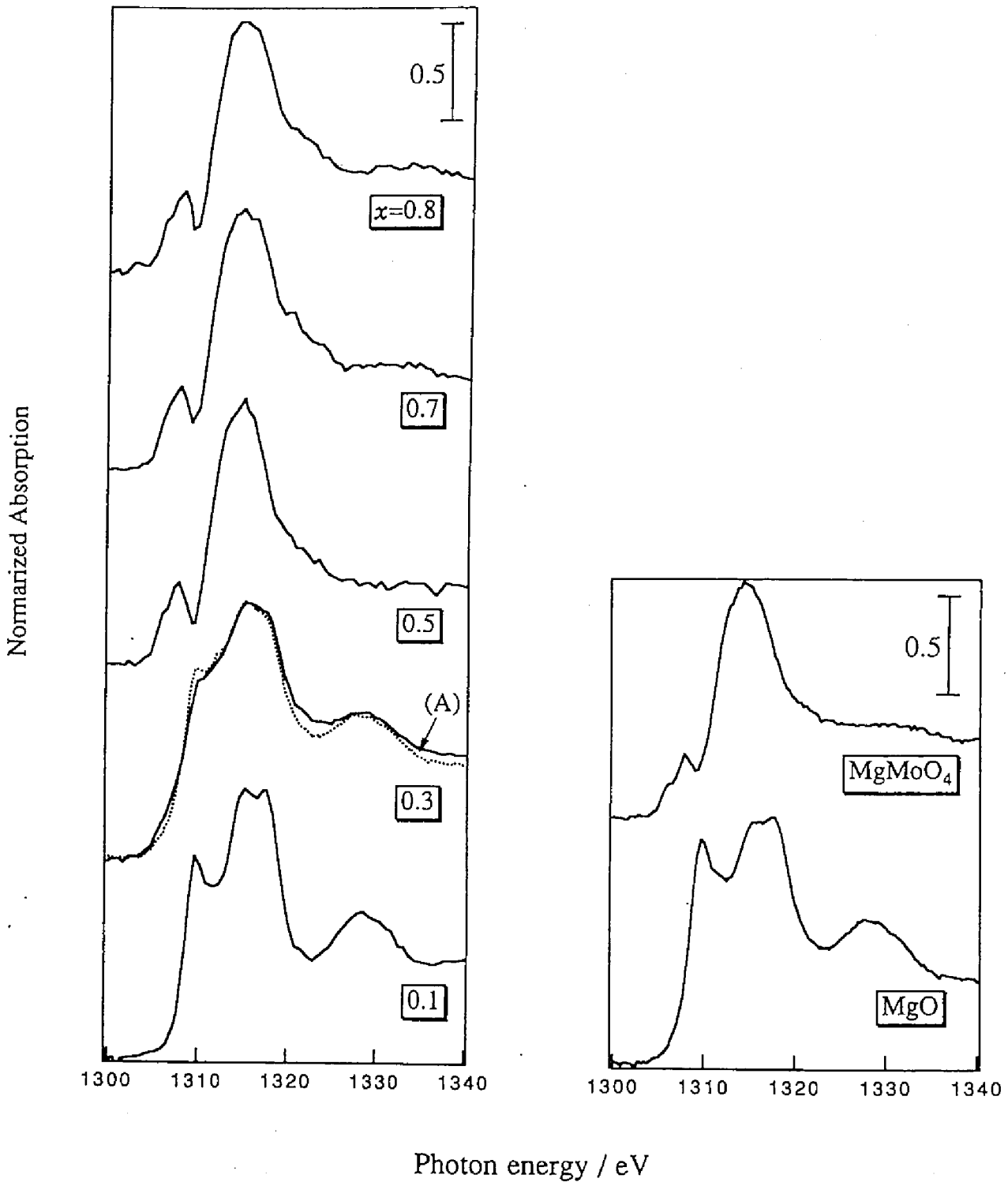

Fig. 4 Mg *K*-edge XANES spectra of MoO_3-MgO.
A dotted line (A) is a superposition of XANES spectra of ($MgO \times 0.7 + MgMoO_4 \times 0.3$).

present in either a MgO_6 or a MgO_8 structure.

(3) Near-edge Spectra of Reduced Samples.

In Fig. 2, the Mo *K*-edge XANES spectrum of MoO_2 is shown. In this sample, Mo^{4+} ions are octahedrally coordinated.[21] A striking feature is the lack of the pre-peak found in the case of Mo^{6+} compounds. It is presumably not only due to the symmetry around Mo ions but also the valence of Mo ions.

Mo *K*-edge XANES spectra of MoO_3-MgO treated with H_2 at 773K are shown in Fig. 5. It is noted that the pre-peak became smaller or almost disappeared following H_2-treatment over the whole range of x. The pre-peak remained after reduction for the samples of x=0.1, 0.3, 0.9 and 1.0. In the cases of x=0.1 and 0.3, the pre-peak revealed the presence of Mo^{6+} ions or lower valent Mo ions (Mo^{5+} or Mo^{4+}, possibly) in MoO_4 tetrahedra. Referring to the XRD result that a $MgMoO_4$ phase exists in these samples, molybdenum ions are expected to be hexavalent mainly. On the other hand, the samples of x=0.9 and 1.0 have a MoO_3 phase. These results strongly suggest that MoO_3 and $MgMoO_4$ is inactive for metathesis reaction. In the cases of the samples with intermediate Mo ratios, x=0.5 - 0.8, the total features are similar to those of MoO_2. The metathesis reactions take place over the samples only in this region of x. One may conjecture that a MoO_2-like species is the active center, but bulk MoO_2 itself is almost inert for the reaction.[23]

(4) EXAFS Spectra of Oxidized Samples.

The oscillatory part of absorption beyond the Mo edge was extracted from the total absorption of the Mo *K*-edge by the method reported by Boland *et al.*[24] The k^3-weighted EXAFS oscillation spectra of oxidized MoO_3-MgO are shown in Fig. 6, and the spectra of reference compounds are depicted in Fig. 7. As shown in Fig. 6, it is evident that all spectra for $x \leqq 0.5$ are almost identical and consist of almost a single sine wave which is the same as that of $MgMoO_4$. In particular, the EXAFS spectrum of x=0.3 is very similar to that of $MgMoO_4$. This is consistent with the results of XRD and XANES. On the other hand, at higher Mo contents ($x > 0.5$), each oscillation

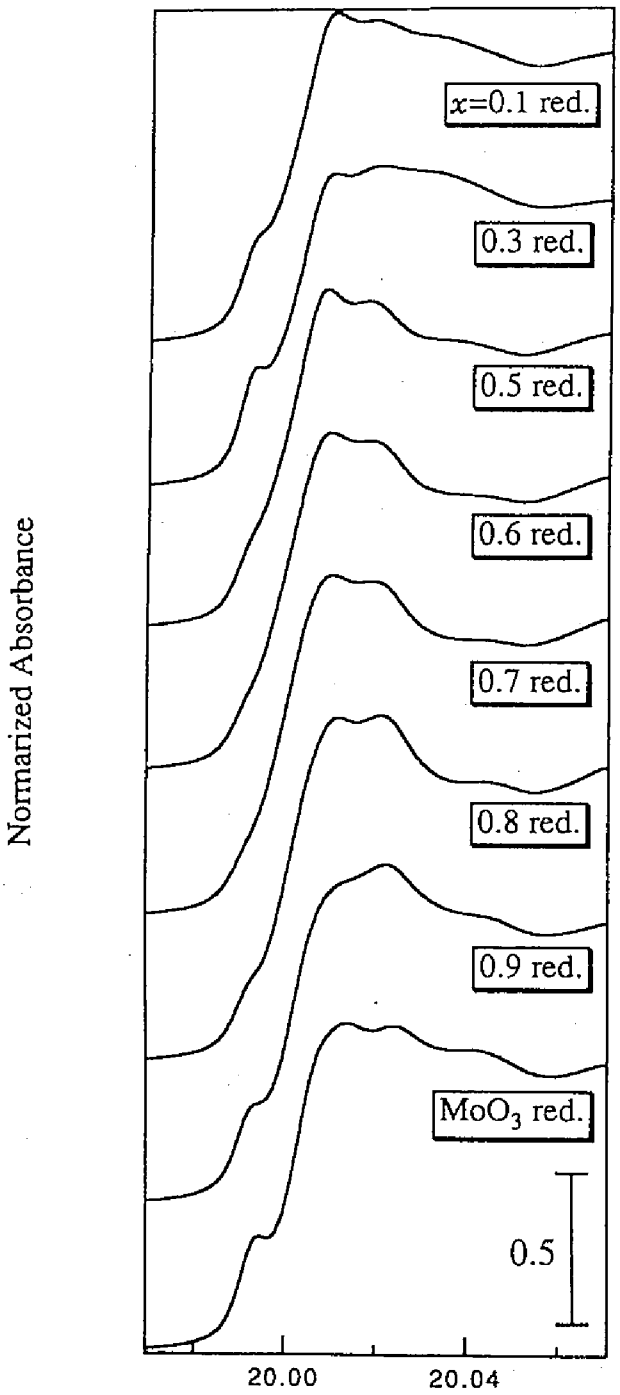

Fig. 5 Mo *K*-edge XANES spectra of H_2-treated MoO_3-MgO at 773K.

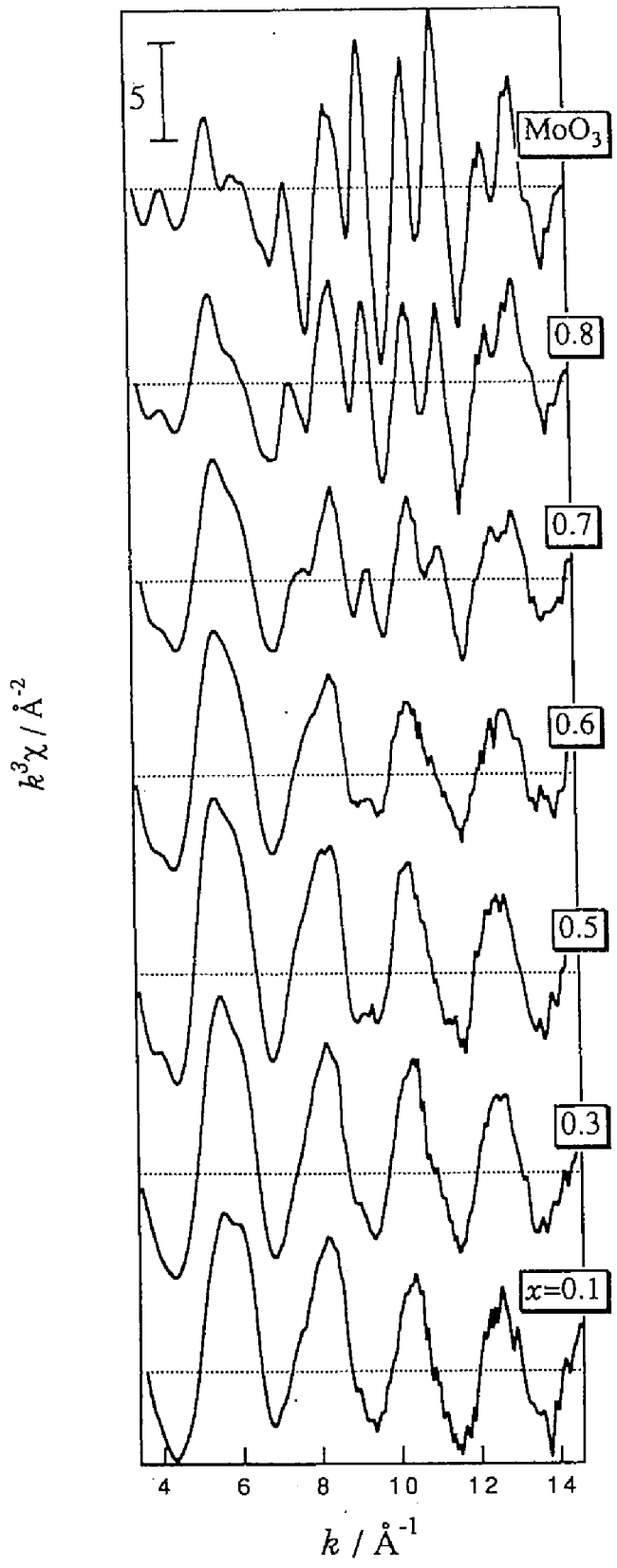

Fig. 6 k^3-weighted EXAFS spectra of MoO_3-MgO calcined at 873K.

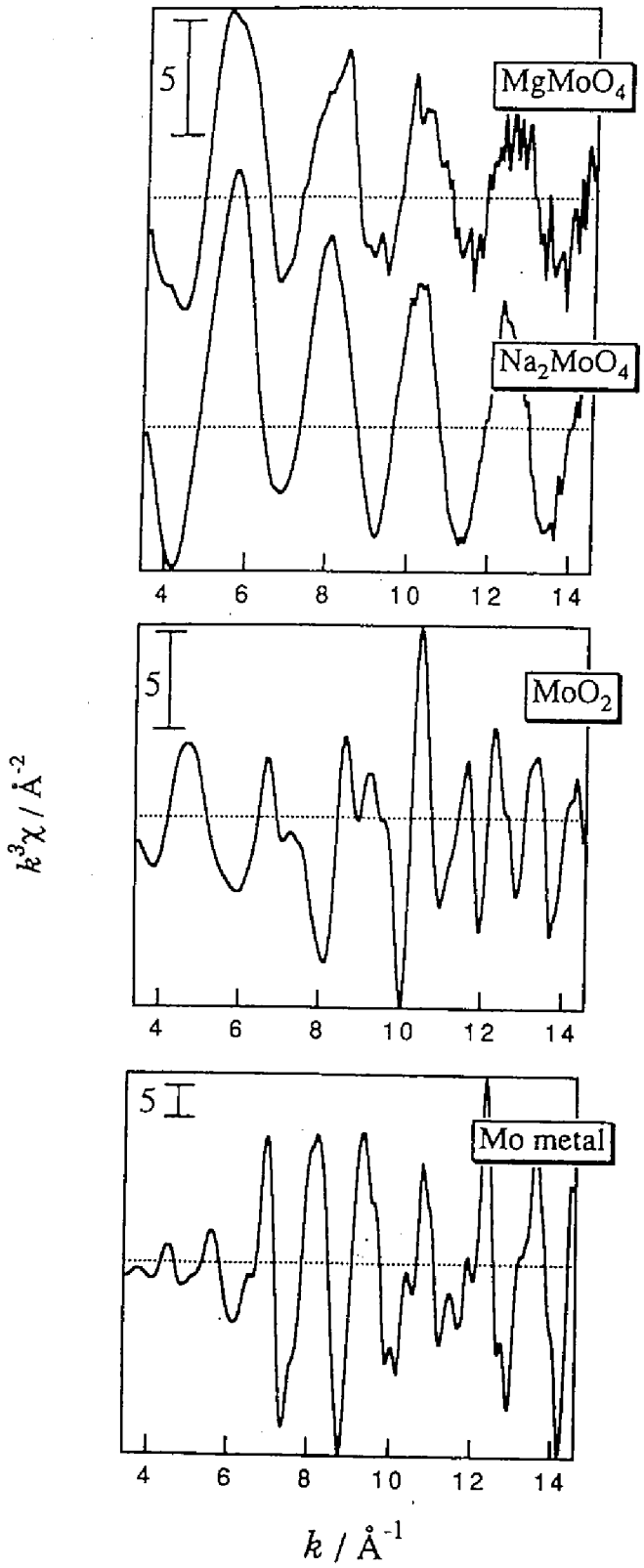

Fig. 7 k^3-weighted EXAFS spectra of reference compounds.

spectrum contains several components. The oscillation part above 9.3 $Å^{-1}$ is more intense with increasing Mo ratio, and the oscillation has a higher frequency. This feature is similar to that of MoO_3 EXAFS. The high frequency at high k values shows the presence of heavier atoms at longer distance than that of the nearest oxygens. In the case of MoO_3, this is clear. These suggest that the spectra shown in Fig. 6 can be composed of two kinds of oscillations, those of $MgMoO_4$ and MoO_3.

We have attempted to simulate the spectra by superposition of the spectrum of $MgMoO_4$ and MoO_3. The results are shown in Fig. 8. For $x \leqq 0.5$, each oscillation can be fitted to that of $MgMoO_4$. The EXAFS spectra for $x > 0.5$ can be fitted as shown in the caption, indicating that the main components of these samples are $MgMoO_4$ and MoO_3. The discrepancy between the experimental and simulated spectra may be due to the presence of other components, such as $Mg_2Mo_3O_{11}$ and/or $MgMo_2O_7$ detected by X-ray diffraction. Therefore, $MgMoO_4$ phase is formed in the samples of $x \leqq 0.5$, and MoO_3-like structure is generated with the phase in the samples of $x > 0.5$.

The characteristics mentioned above become more clear by Fourier-transformation of the EXAFS oscillation. Fig. 9 shows the radial structure functions of unreduced MoO_3-MgO obtained by Fourier transformation of EXAFS within the range Δk= 3.5 - 14.5 $Å^{-1}$. For the samples of $x \leqq 0.5$, only a single peak is seen at 1.4 Å, which is assigned to Mo-O scattering, like that of $MgMoO_4$ shown in Fig. 10. By increasing the Mo content, an Mo-O peak at *ca.* 1.8 Å grows accompanied by an increase in the peak height at 3.2 Å probably due to Mo-Mo scattering. The latter is poorly characterized in $MgMoO_4$ and at a lower content of MoO_3-MgO. This change parallels with that of XANES; the Mo ions in MoO_3-MgO are stabilized as $MgMoO_4$ in the samples $x \leqq 0.5$, and octahedral MoO_3-like structures are generated at higher contents of $x > 0.5$.

(5) EXAFS Spectra of Reduced Samples.

Fig. 11 shows the EXAFS of H_2-treated MoO_3-MgO samples. All EXAFS spectra change very much by H_2 treatment. For $x \leqq 0.5$, a high frequency component appears in addition to the low frequency one found in the case of $MgMoO_4$. However, in the

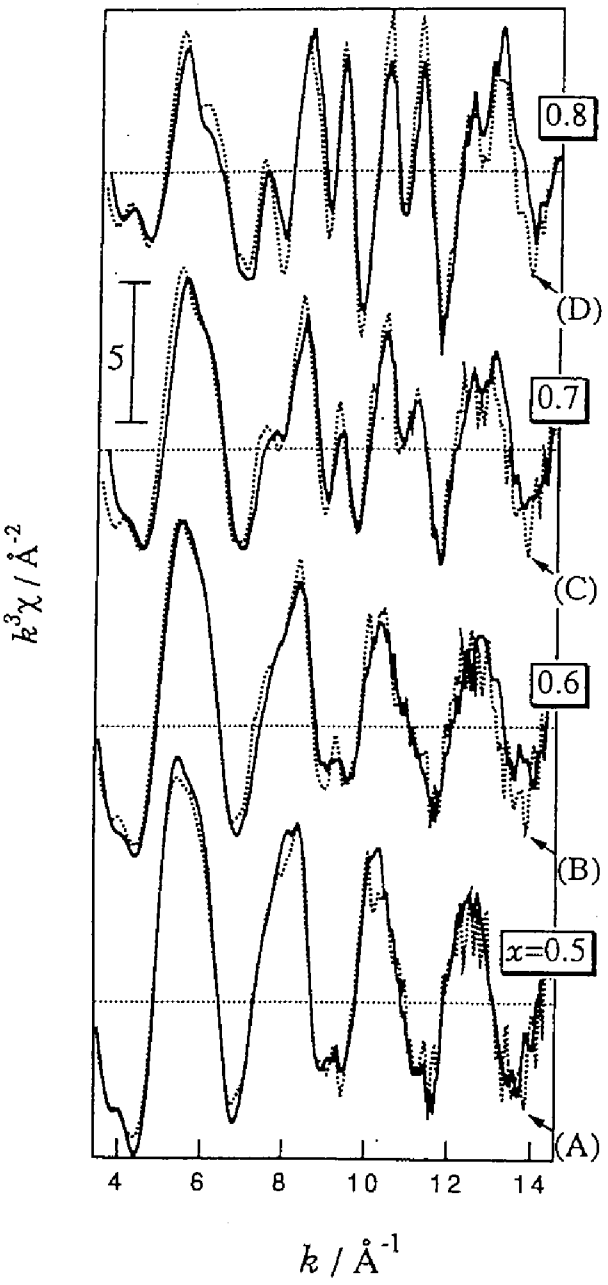

Fig. 8 EXAFS oscillations of MoO_3-MgO (x=0.5-0.8) and superposed EXAFS oscillation of MoO_3 and $MgMoO_4$ (dotted lines). Superpositions of each intensities are as follows:

(A) $MgMoO_4$.
(B) $MgMoO_4 \times 0.85 + MoO_3 \times 0.15$.
(C) $MgMoO_4 \times 0.63 + MoO_3 \times 0.37$.
(D) $MgMoO_4 \times 0.31 + MoO_3 \times 0.69$.

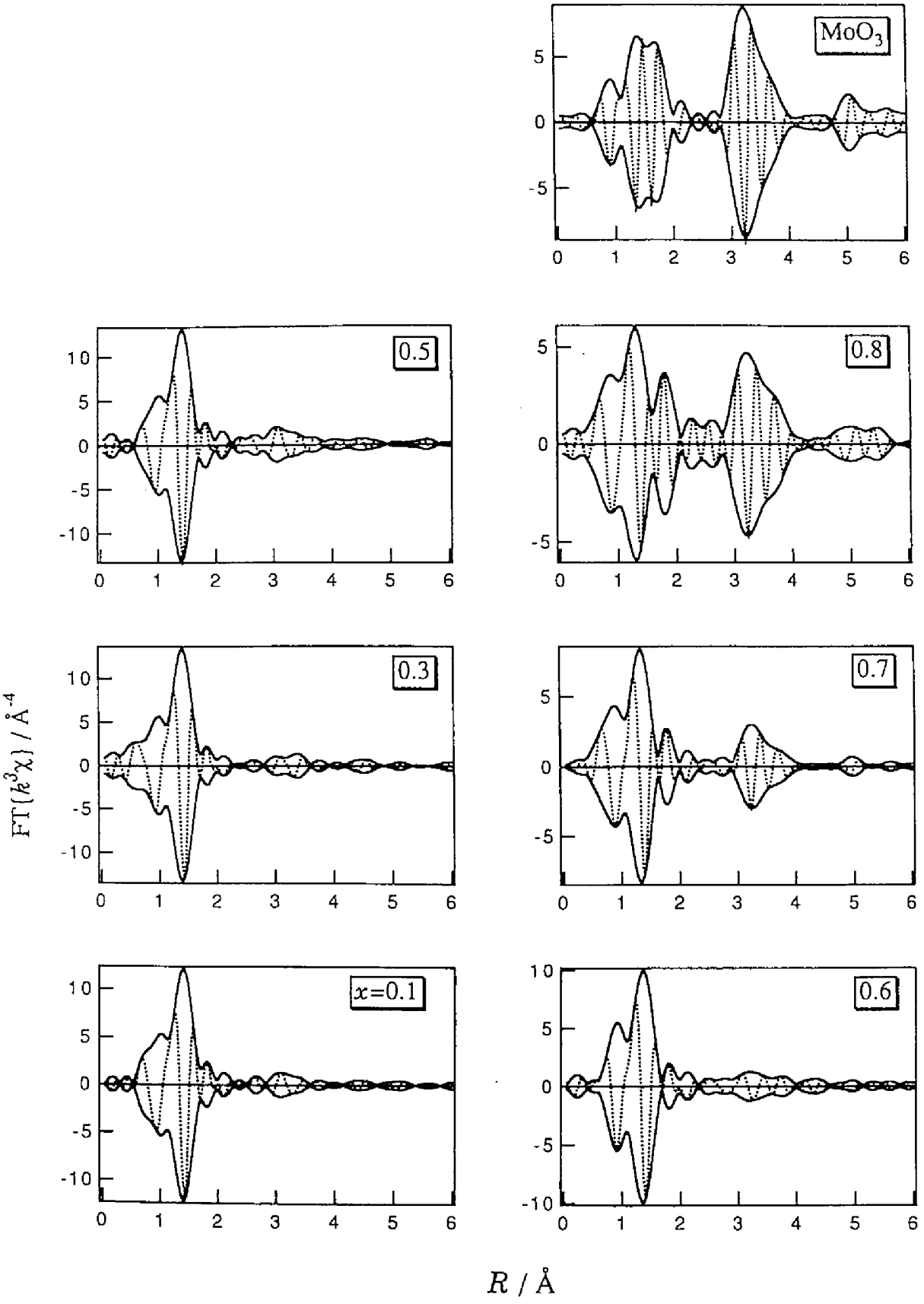

Fig. 9 Fourier transformed EXAFS of MoO_3-MgO calcined at 873K.

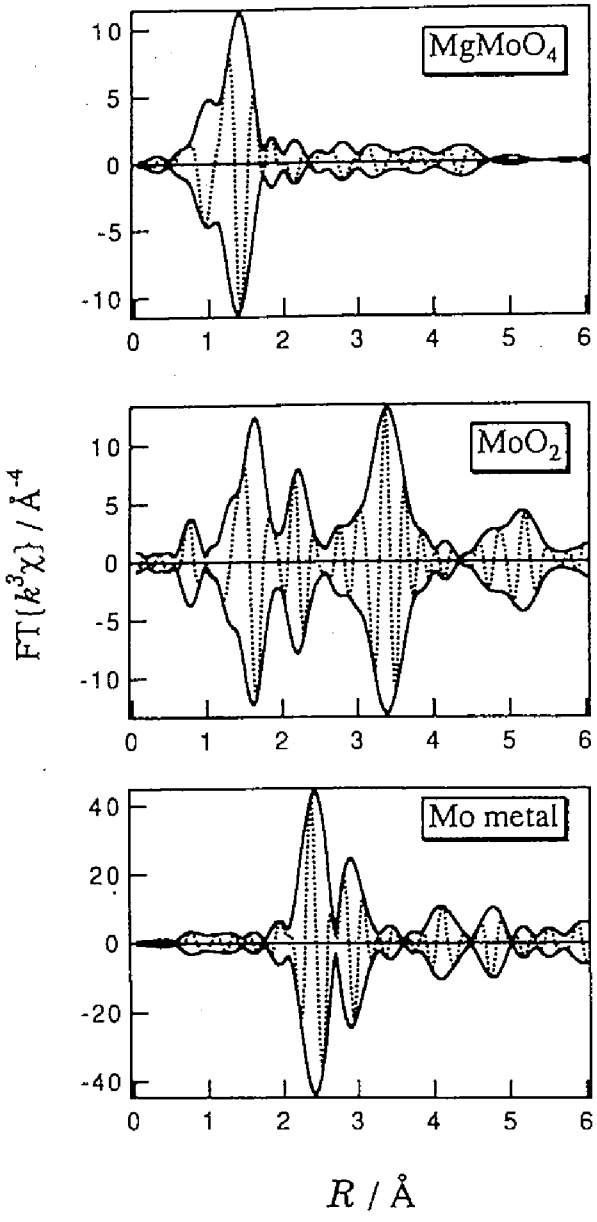

Fig. 10 Fourier transformed EXAFS of reference compounds.

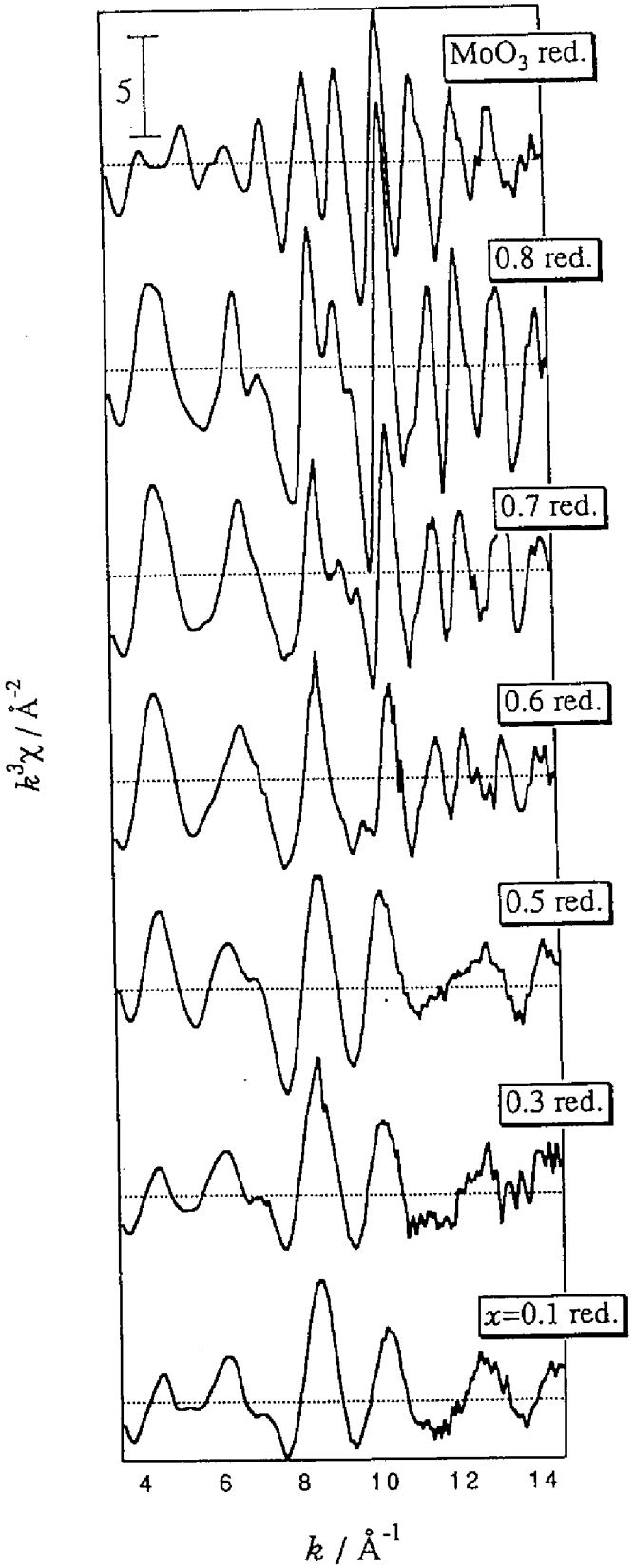

Fig. 11 k^3-weighted EXAFS spectra of H_2-treated MoO_3-MgO at 773K.

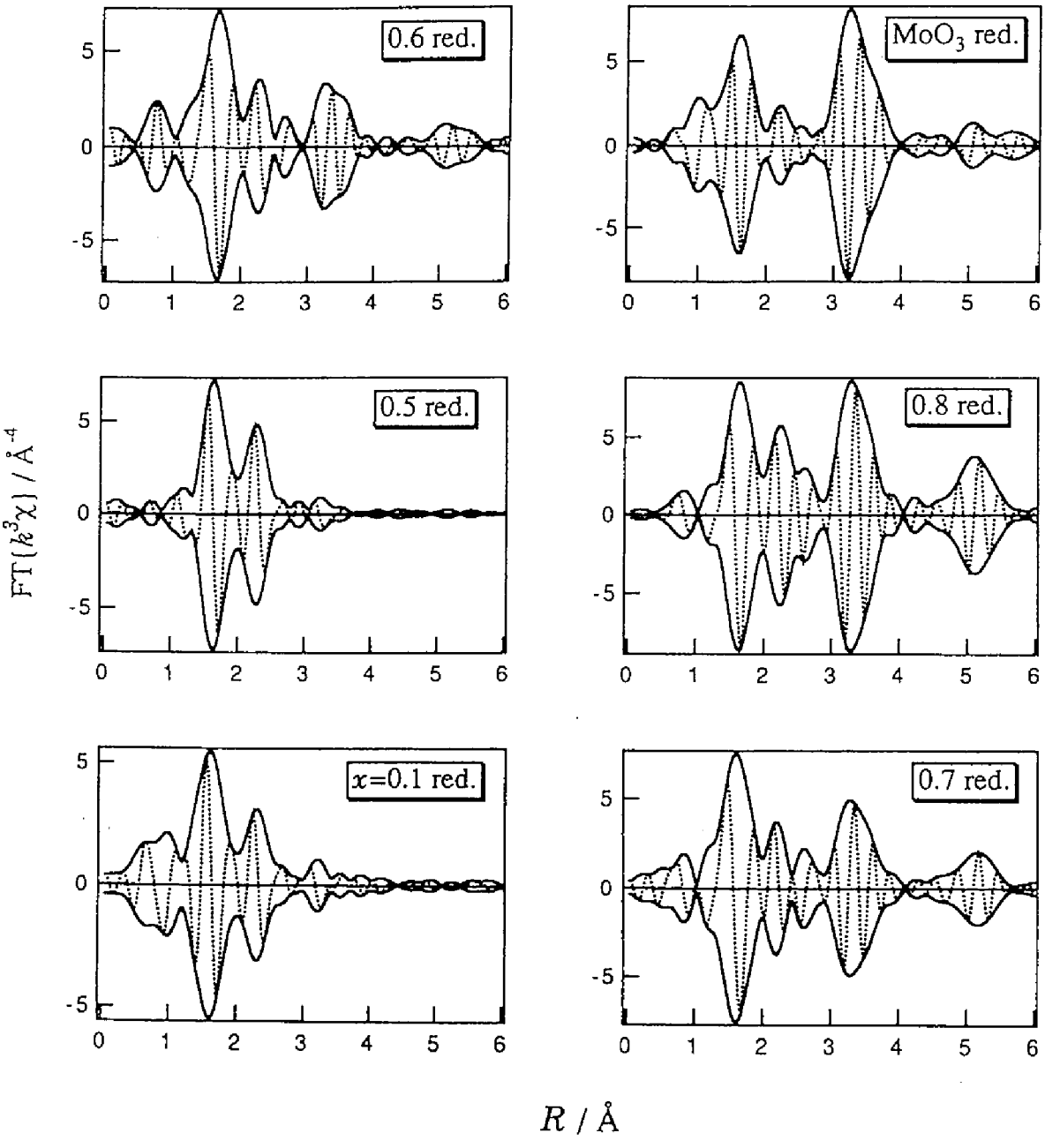

Fig. 12 Fourier transformed EXAFS of H_2-treated MoO_3-MgO at 773K.

range higher than 8 $Å^{-1}$, appreciable high frequency components are missing. This indicates that the ordering of the atomic array is generated by H_2 treatment, and that the atoms at longer distance are not heavy, and probably Mg. On the other hand, it is noted that the wave is similar to that of MoO_2 (Fig. 7) around x=0.7. It suggests that MoO_2-like local structure, having a slightly distorted MoO_6 unit, is formed in this region. Note that this information was not obtained by X-ray diffraction. MoO_3 is very difficult to reduce under these conditions. In fact, it is known that bulk MoO_3 is reduced to a MoO_2 phase above 823K,[25,26] while the reduction of MoO_3 by H_2 at 773K to a MoO_2 phase is very slow.[27] However, the result suggests that MoO_3-MgO of high x can be reduced easier than bulk MoO_3 to MoO_2 phase.

Fig. 12 shows the Fourier transformed EXAFS oscillations of the H_2-treated samples. In the case of $x \leqq 0.5$, peaks at 1.6 Å and 2.3 Å are observed. The peak at 1.6 Å is due to backscattering by O, and that at 2.3Å is assigned to Mg backscattering by inverse Fourier transformation within the range ΔR= 2.0-2.6 Å, followed by curve-fitting. These peaks are different from those in the unreduced samples, and it is concluded that a structural change in environment of the Mo atoms was brought about by H_2-treatment. This suggests that an ordered Mo-O-Mg bond structure is generated. On the other hand, at a higher Mo ratio, peaks around 3.3 and 3.6 Å are seen which become more intense with increasing Mo contents. Furthermore, the peaks which may be due to the scattering from the second and the third shells at 3.3-3.6 Å and 5.1 Å exhibit the same features as same as those of MoO_2 (Fig. 10), and metallic Mo structure is not observed. In addition, the spectrum is very similar to that of MoO_2 for the samples of x=0.8. Therefore, it is concluded that an ordered MoO_2 structure of almost symmetric MoO_6 octahedra is formed for these samples of x=0.6-0.8. These peaks were not observed for reduced MoO_3.

4. Discussion

The crystalline phases determined by the analyses of X-ray diffraction analysis and the local structure around the Mo ions obtained by the analyses of X-ray absorption

spectra over reduced and unreduced Mo-Mg binary oxides can be summarized as follows.

For the samples of MoO_3-MgO calcined at 873K, there are three different types of crystalline phases detected by XRD depending on x ; (a) For the samples of $x \leqq 0.5$, MgO and/or $MgMoO_4$ phases. (b) For x=0.6 and 0.7, MoO_3, $Mg_2Mo_3O_{11}$, and a trace amount of $MgMoO_4$ and/or $MgMo_2O_7$ phases. (c) For $x > 0.7$, $Mg_2Mo_3O_{11}$ and/or MoO_3 phases.

MoO_3 has an orthorhombic crystal structure where a Mo atom is stabilized in a distorted octahedral MoO_6 unit which is built up of double-layered $(MoO_6)_n$ sheets.[28] For molybdenum-rich samples with $x > 0.7$, the crystalline phases have an octahedral MoO_6 structure, because the lattice molybdenum ions of $Mg_2Mo_3O_{11}$ and MoO_3 occur only in distorted MoO_6 octahedra,[28,29] and these octahedral structures are similar to each other. For the samples of x=0.6 and 0.7, the $MgMo_2O_7$ phase was observed, which possesses both tetrahedral and octahedral molybdate units together in $(Mo_2O_7)^{2-}$ anion.[21,29] A trace amount of $MgMoO_4$ phase also remained for x=0.6. Thus, the main local structure around the Mo ion in the samples of of x=0.6 and 0.7 is the MoO_6 octahedron, but tetrahedral structures coexisted partly. At low contents of $x \leqq$ 0.5, $MgMoO_4$, with MoO_4 tetrahedra, prevails.

On the other hand, MoO_3-MgO which has been reduced with hydrogen at 773K has a different structure than the unreduced one. At low Mo contents ($x \leqq 0.5$), ordering of the structure around Mo ion is brought about, as indicated by the appearance of the peak which is due to a Mo-Mg shell in the Fourier transformed EXAFS spectra. This structural information was not detected by XRD, and therefore, it presumably suggests the formation of an ordered structure around Mo ion such as a rock solt-type structure with MgO in which a Mg ion is substituted by a Mo ion. At higher ratios ($x >$ 0.5), the molybdena is reduced to a MoO_2 phase, especially for the samples around x=0.7. In the case of reduction of MoO_3, the MoO_2 phase is not definitely observed. The reduction of MoO_3 does not proceed easily without MgO ingredient. For the samples with $x > 0.5$, however, the formation of MoO_2 was not observed by XRD but only by EXAFS, indicating that the MoO_2 phase is highly dispersed. This MoO_2 phase

is considered to be produced as a separate layer onto an ordered structure of reduced MoO_3-MgO.

It has been reported that reduced MoO_3-MgO at x=0.6-0.7 has a metathesis reactivity for propene.[12] It is known that Mo ions in a low oxidation state such as Mo^{4+} and/or Mo^{5+} ions act as the active species for metathesis. However, we have not been able to find any Mo^{5+} ions in the present work. The molybdenum species which acts as the metathesis active sites are still not well-defined, however, and it has been reported in some works that Mo^{4+} acts as an induced species for olefin metathesis. Tanaka *et al.*[4] concluded that well-dispersed Mo^{4+} and/or Mo^{5+} ions with some particular coordination of oxygen ions are the active centers. Kazansky and co-workers[30-32] proposed that the active sites for propene metathesis involve Mo^{4+} ions. Kadushin *et al.*[33] did not rule out this possibility completely, although they suggested that Mo^{5+} ion pairs could be active as well. Segawa *et al.* reported[34] that reduced MoO_x/TiO_2 has a metathesis reactivity for propene, which is maximized at x=1.9. In this manner, highly reduced Mo ions including Mo^{4+} species are believed to be the active sites. Bartlett and co-workers recently investigated[35] the activity of various kinds of molybdenum oxides grown on a molybdenum metal foil, and reported that MoO_2 is more active for propene metathesis than MoO_3 and/or Mo metal. This is consistent with the results in this work. We postulate here that MoO_3-MgO samples of x=0.6-0.7 are reduced to form a dispersed MoO_2 phase, which is possibly relevant for propene metathesis. For a reduced sample of x=0.8, the particle size of the formed MoO_2 would be too large for metathesis activity, because bulk MoO_2 is almost inactive.

Oganowski *et al.*[10] reported that the active species of a molybdena-rich Mo-Mg binary oxide is a surface octahedral phase on the $MgMoO_4$ phase. Our present work revealed that the bulk phase of Mo-rich samples mainly consists of octahedral molybdena after calcination at 873K. For H_2-treated samples at 773K, it is noted that the reduction to MoO_2 does not only take place in the surface layer, but also in the bulk. The examination of the possibility that metathesis takes place on dispersed MoO_2 is in progress.

Acknowledgment

The X-ray absorption experiments at the Mo *K*-edge were performed under the approval of the Photon Factory Program Advisory Committee (proposal No. 90-027 and 94G-002). The X-ray absorption experiments at the Mg *K*-edge were supported by the Joint Studies Program (proposal No. 6-841, 1994) of UVSOR of the Institute for Molecular Science.

References

(1) Engelhardt, J.; Goldwasser, J.; Hall, W. K. *J. Catal.* **1982**, *76*, 48.

(2) Shelimov, B. N.; Elev, I. V.; Kazansky, V. B. *J. Catal.* **1986**, *98*, 70.

(3) Tanaka, K.; Miyahara, K.; Tanaka, K. *J. Mol. Catal.* **1982**, *15*, 133.

(4) Tanaka, K.; Miyahara, K.; Tanaka, K. *Proc. 7th Int. Congr. Catal.*; Tokyo, 1981; pp 1318.

(5) Llorente, J. M. M.; Rives, V.; Malet, P.; Gil-Llanbias, F. J. *J. Catal.* **1992**, *135*, 1.

(6) Deo, G.; Wachs, I. E. *J. Phys. Chem.* **1991**, *95*, 5889.

(7) Shimada, H.; Matsubayashi, N.; Sato, T.; Yoshimura, Y.; Nishiyama, A.; Kosugi, N.; Kuroda, H. *J. Catal.* **1992**, 746.

(8) Stampfl, S. R.; Chen, Y.; Dumesic, J. A.; Niu, C.; Hill Jr., C. G. *J. Catal.* **1987**, *105*, 445.

(9) Tomenov, D. N.; Doroshenko, V. A.; Shapavolova, L. P.; Taranukha, O. M.; Lushnik, N. S. *Ukr. Khim. Zr.* **1981**, *74*, 93.

(10) Oganowski, W.; Hanuza, J.; Jerowska-Trzebiatowska, B.; Wrzyszcz, L. *J. Catal.* **1975**, *39*, 161.

(11) Haber, J. *Proc. 3rd Int. Conf. Chemistry and Uses of Molybdenum*; Climax Molybdenum Co.: London, 1979; pp 114.

(12) Hasegawa, S.; Tanaka, T.; Kudo, M.; Mamada, H.; Hattori, H.; Yoshida, S. *Catal. Lett.* **1992**, *12*, 255.

(13) Bare, S. R.; Mitchell, G. E.; Maj, J. J.; Vrieland, G. E.; Gland, J. L. *J. Phys. Chem.* **1993**, *97*, 6048.

(14) Chang, S.; Leugers, M. A.; Bare, S. R. *J. Phys. Chem.* **1992**, *96*, 10358.

(15) Che, M.; Figueras, F.; Forisser, M.; McAtter, J.; Perrin, M.; Portefaix, J. L.; Praliaud, H. *Proc. 6th Int. Congr. Catal.*; Elsevier: London, 1976; pp 261.

(16) Kim, D. S.; Segawa, K.; Soeya, T.; Wachs, I. E. *J. Catal.* **1992**, *136*, 539.

(17) Tanaka, T.; Yamashita, H.; Tsuchitani, R.; Funabiki, T.; Yoshida, S. *J. Chem. Soc. Faraday Trans. 1* **1988**, *84*, 2987.

(18) Cramer, S. P.; Hodgson, K. O.; Gillum, W. O.; Mortenson, L. E. *J. Am. Chem. Soc.* **1978**, *100*, 3398.

(19) Tullius, T. D.; Gillum, W. O.; Carlson, R. M. K.; Hodgson, K. O. *J. Am. Chem. Soc.* **1980**, *102*, 5670.

(20) Shulman, R. G.; Yafet, Y.; Eisenberger, P.; Kincaid, B. M. *Proc. Nat. Acad. Sci. USA*; 1976; pp 1384.

(21) Cotton, F.; Wilkinson, G. *Adv. Inorg. Chem. (4th ed.)*; Interscience: New York, 1980, pp 847.

(22) Yoshida, T.; Tanaka, T.; Yoshida, H.; Funabiki, T.; Yoshida, S.; Murata, T. *J. Phys. Chem.* **1995**, *99*, 10890.

(23) Wang, L. P.; Soto, C.; Tysoe, W. T. *J. Catal.* **1993**, *143*, 92.

(24) Boland, J. J.; Halaka, F. G.; Baldeschwieler, J. D. *Phys. Rev. B* **1983**, *28*, 2921.

(25) Sotani, N. *Bull. Chem. Soc. Jpn.* **1975**, *48*, 1820.

(26) Ueno, A.; Kotera, Y.; Okuda, S.; Bennett, C. O. *Proc. 4th Int. Conf. Chemistry and Uses of Molybdenum*; Climax Molybdenum Co.: London, 1982; pp 250.

(27) Carpenter, K. H.; Hallada, C. J. *Proc. 3rd Int. Conf. Chemistry and Uses of Molybdenum*; Climax Molybdenum Co.: London, 1979; pp 204.

(28) Ziolkowski, J. *J. Catal.* **1983**, *80*, 263.

(29) Fournier, M.; Louis, C.; Che, M.; Chaquin, P.; Masure, D. *J. Catal.* **1989**, *119*, 400.

(30) Kazansky, V. B.; Shelimov, B. N.; Vikulov, K. A. *Proc. 10th Int. Congr. Catal.*; Elsevier: Budapest, 1992; pp 515.

(31) Elev, I. V.; Shelimov, B. N.; Kazansky, V. A. *J. Catal.* **1988**, *113*, 229.

(32) Vikulov, K. A.; Elev, I. V.; Shelimov, B. N.; Kazansky, V. B. *J. Mol. Catal.* **1989**, *55*, 126.

(33) Kadushin, A. A.; Aliev, R. K.; Krylov, O. V.; Andreev, A. A.; Edreva-Kardjieva,

R. M.; Shopov, D. M. *Kinet. Katal.* **1982**, *23*, 276.

(34) Segawa, K.; Kim, D. S.; Kurusu, Y.; Wachs, I. E. *Proc. 9th Int. Congr. Catal.*; Elsevier: Calgary, 1988; pp 1960.

(35) Bartlett, B.; Soto, C.; Wu, R.; Tysoe, W. T. *Catal. Lett.* **1993**, *21*, 1.

Chapter 2

Study of the Local Structure in Near-Surface Region of Mo-Mg Binary Oxides by means of XANES and UV-VIS Spectroscopy

Abstract

Mo L_3-edge XANES and diffuse reflectance UV-VIS spectra have been recorded for structural studies of Mo-Mg binary oxides which catalyze metathesis reaction of olefins after pretreatment with H_2 at 773K. The XANES of reference compounds revealed that the local symmetry around Mo ion as well as the valence state affects the spectral feature. From the XANES of Mo-Mg binary oxides in oxidized/reduced states, it is concluded that the MoO_4 tetrahedra are the main component in near-surface region for the samples of x (Mo/(Mo+Mg)) ≤ 0.7 in the oxidized state. For the samples in the reduced state, the tetrahedral species remains but reduced Mo ions including MoO_2 species are also formed, while the MoO_2 phase is formed in the bulk phase at x = 0.5 - 0.8. In the latter samples, Mo ions are easily reduced by the treatment with H_2. The active species for metathesis reaction relates to the formation of MoO_2 phase not only in the bulk but also in near-surface region.

Introduction

It is well known that supported molybdenum oxides catalyze metathesis reaction of olefins. So far, a variety of mechanisms and intermediates in the reaction process have been proposed for olefin metathesis.[1] Of this, a mechanism involving metal-carbenes and metallo-cyclobutane has been generally accepted for the heterogeneous catalysis.[2,3] As the initial step, the formation of metal-carbene species from adsorbed olefins is proposed in several studies.[4-6] It is likely that dispersed low-valent molybdenum ions play a significant role in the reaction, in particular, at the initial stage. Kazansky *et al.* reported[7-9] that a MoO_x/SiO_2 including Mo^{4+} monoxo-species, which is formed by pretreatment of photo-reduction with CO or H_2, exhibited a high activity for olefin metathesis. Tanaka *et al.*[10] proposed that dispersed Mo^{4+} and/or Mo^{5+} ions participate as the active sites on MoO_x/TiO_2. However, what the active species is has been still unclear, although Zhang *et al.*[11] and Anpo *et al.*[12,13] concluded that photo-reduced Mo^{5+} dioxo-species is active for olefin metathesis.

As for MgO-supported MoO_3, it has been reported that the sample containing relatively low amount of molybdenum is inactive for a metathesis of alkenes even after prereduction.[10] This is in a marked contrast with the cases of other supports such as SiO_2, Al_2O_3 and TiO_2.[10] In the case of MgO-supported molybdena, most Mo ions are thought to be stabilized in a tetrahedral MoO_4 unit of magnesium molybdate ($MgMoO_4$) phase formed by calcination.[14-16] The MoO_4 unit is also formed by mechanical mixing of MoO_3 and MgO,[17] indicating that Mo ions are easily diffused in MgO. Therefore, Mo ions in MgO-supported MoO_3 catalysts are naturally expected to be similar to those in Mo-Mg binary oxide.

On the olefin metathesis by binary oxide catalysts including molybdenum, only a few works have been reported. In general, mixed molybdenum oxides are not active for metathesis but for oxidation of alkenes. For instance, Bi_2O_3-MoO_3 is known as a powerful catalyst for partial oxidation of olefins,[18] *e.g.*, to produce unsaturated aldehydes or dienes.[19] MoO_3-SnO_2 catalysts exhibit high activity and selectivity for oxidations,[20] such as the conversion of propene to acrolein,[21] and that to acetone in

the presence of H_2O.[22,23] A Mo-Mg binary oxide also exhibits catalytic activity for partial oxidation.[24,25] On the contrary, we found that propene metathesis takes place over MoO_3-MgO binary oxides with relatively higher Mo-loading when they are pretreated with hydrogen at 773K.[26] This seems to be noteworthy that dispersed molybdenum ions relate to the active species for olefin metathesis. In order to clarify the bulk structure of Mo-Mg binary oxides and structural change by reduction with hydrogen and generation of active species for metathesis, we have already carried out a Mo *K*-edge XANES/EXAFS study of MoO_3-MgO in oxidized and reduced states.[27] In the previous work, we concluded that MoO_3-MgO samples containing high amount of molybdenum (Mo / (Mo + Mg) = 0.6 - 0.7) are easily reduced to form a dispersed MoO_2 superfine particle in the matrix, and deduced that this bulk species relates to active center for metathesis.

Only a few works have been reported on the structure of Mo-Mg binary oxide so far. Mo L_3-edge XANES spectroscopy was applied to the system recently.[28] The prominent feature of Mo *L*-edge XANES spectrum is the white line(s) due to $2p$-$4d$ transition.[29] Therefore, the spectrum probes the orbitals of $4d$-character participating in Mo-O bond. The white lines of the XANES spectrum are split corresponding to the ligand field splitting of the *d*-orbitals.[30,31] The environmental condition of the Mo ion is sensitively reflected to the XANES spectrum.[32,33] In the study of Mo *L*-edge XANES spectra, Bare *et al.* presented that supported-molybdena at low Mo contents are stabilized in an octahedral MoO_6 structure on MgO, and tetrahedral one was formed at relatively higher contents.[28,34] This result is inconsistent with the results of the studies by UV-VIS and Raman spectroscopy.[14,35]

In this paper, we describe the local structure around Mo ions of MoO_3-MgO binary oxides deduced from Mo L_3-edge XANES recorded in a total electron yield mode and UV-VIS diffuse reflectance spectroscopy in order to clarify the structure in near-surface region and formation of active species for metathesis by the treatment with hydrogen.

Experimental

MoO_3-MgO samples were prepared as described previously.[27] In brief, the samples of Mo-Mg binary oxide, ranging in molybdenum content from 0.1 to 0.9 by atomic ratio, x (= Mo / (Mo + Mg)), were prepared by a solution-evaporation method from aqueous AHM (ammonium heptamolybdate : $(NH_4)_6Mo_7O_{24}\cdot 4H_2O$) and $MgCl_2\cdot 6H_2O$ mixed solution, followed by drying the mixture overnight and calcination at 873K for 3 h. Reduction of MoO_3-MgO samples was carried out by the treatment with H_2 gas (100 Torr) at 773K for 1 h, removing resultant water in a liquefied N_2 cold trap in a closed system.

The commercially available authentic samples, Na_2MoO_4, MoS_2 (Wako), PMA (phosphomolybdic acid : $H_3PMo_{12}O_{40}\cdot nH_2O$), AHM, Mo-metal (Nacalai), $MoO_2(acac)_2$, $MgMoO_4$ (Mitsuwa), MoO_2 (Rare-Metal) were used for the reference of XANES information. Other reference samples, MoO_3 and hydrogen molybdenum bronzes, were prepared in our laboratory. A MoO_3 sample is prepared by calcination of AHM at 873K for 3 h. It has not a hexagonal but a rhombic structure. The hydrogen molybdenum bronze (H_xMoO_3)[36] samples, type I ($0.21 < x < 0.40$)[37] and type II ($0.85 < x < 1.04$), were prepared by a method as reported by Sotani *et al.*[38] The bulk structure of these reference samples are analyzed by a powder X-ray diffraction.

The Mo L_3-edge XANES data were collected on a facility of BL-7A station of soft X-ray beam line at UVSOR, in the Institute for Molecular Science, Okazaki, Japan, with a ring energy of 750 MeV and stored current of 100 - 200 mA. The synchrotron radiation from the wiggler operated at 4 T in the bending magnet was used. Each sample was prepared for measurement by pasting with hexane, and then spread on a beryllium-copper dinode which was attached to the first stage of electron multiplier placed in a vacuum chamber. After the chamber had been evacuated ($< 1.0\times10^{-7}$ Torr), the spectrum was recorded in a total electron yield mode at room temperature, using a Ge(111) two-crystal monochromator. The beam size at the sample was 1.0×5.0 mm^2. At Mo L_3-edge (2.52 keV), energy resolution was about 0.3 eV. In the measurement, not only LMM Auger electrons but also low energy secondary electrons constitute a significant fraction of the spectra in total electron yield mode.[39] The

penetration range of the spectra is possibly several hundred Angstroms into the bulk. Thus, the spectra reflect the structure of the samples in "near-surface region". The photon energy was calibrated by the Mo L_3-edge of a Mo metal sample (2520.63 eV), and this energy is set as a standard reference energy. The TEY signal (I) of the samples was normalized to the signal (I_0) without Mo sample ($\mu = I / I_0$). μ was normalized to the post-edge intensity (at + 27 eV from the edge position) to adjust the height around the post-edge region for each spectrum.

UV-VIS spectra of powdered samples were recorded in a diffuse reflectance mode, with a Perkin-Elmer LAMBDA-19 spectrometer at room temperature, using an *in situ* cell for mounting the powdered samples.

Results and Discussion

(1) Mo L_3-edge XANES of reference compounds.

The origin of Mo L_3-edge XANES is mostly the electron transition from a core level, $2p_{3/2}$, to a vacant $4d$ state. Teo and Lee showed that the contribution of p-s transition to L_3-edge absorption spectra is about fifty times less than that of p-d transition.[29] Fig. 1 shows the Mo L_3-edge XANES spectra of reference compounds with Mo^{6+} (d^0) ion, except for MoO_2, MoS_2, and Mo-metal. In the case of $MgMoO_4$ and Na_2MoO_4 having tetrahedral (MoO_4) unit, the two white lines of each XANES spectrum are attributed to the electron transition from $2p_{3/2}$ to split $4d$ states, *i.e.*, t_2 (d_{xy}, d_{xz} and d_{yz}) and e ($d_{x^2-y^2}$ and d_{z^2}). For these samples, the white line in higher energy side is more intense (peak height) than that in lower one. On the other hand, for the XANES spectra of MoO_3, $MoO_2(acac)_2$, AHM and PMA having octahedral MoO_6 unit, the two white lines are due to the electron transition from $2p_{3/2}$ to t_{2g} (d_{xy}, d_{xz} and d_{yz}) and e_g ($d_{x^2-y^2}$ and d_{z^2}) of $4d$ state of atomic orbitals. In these samples, it is clear that the white line of higher energy side is less intense than that of lower one. It is quite different from the case of MoO_4 tetrahedra due to the difference of the transition cross sections in molecular orbital of Mo($4d$)-O($2p$)

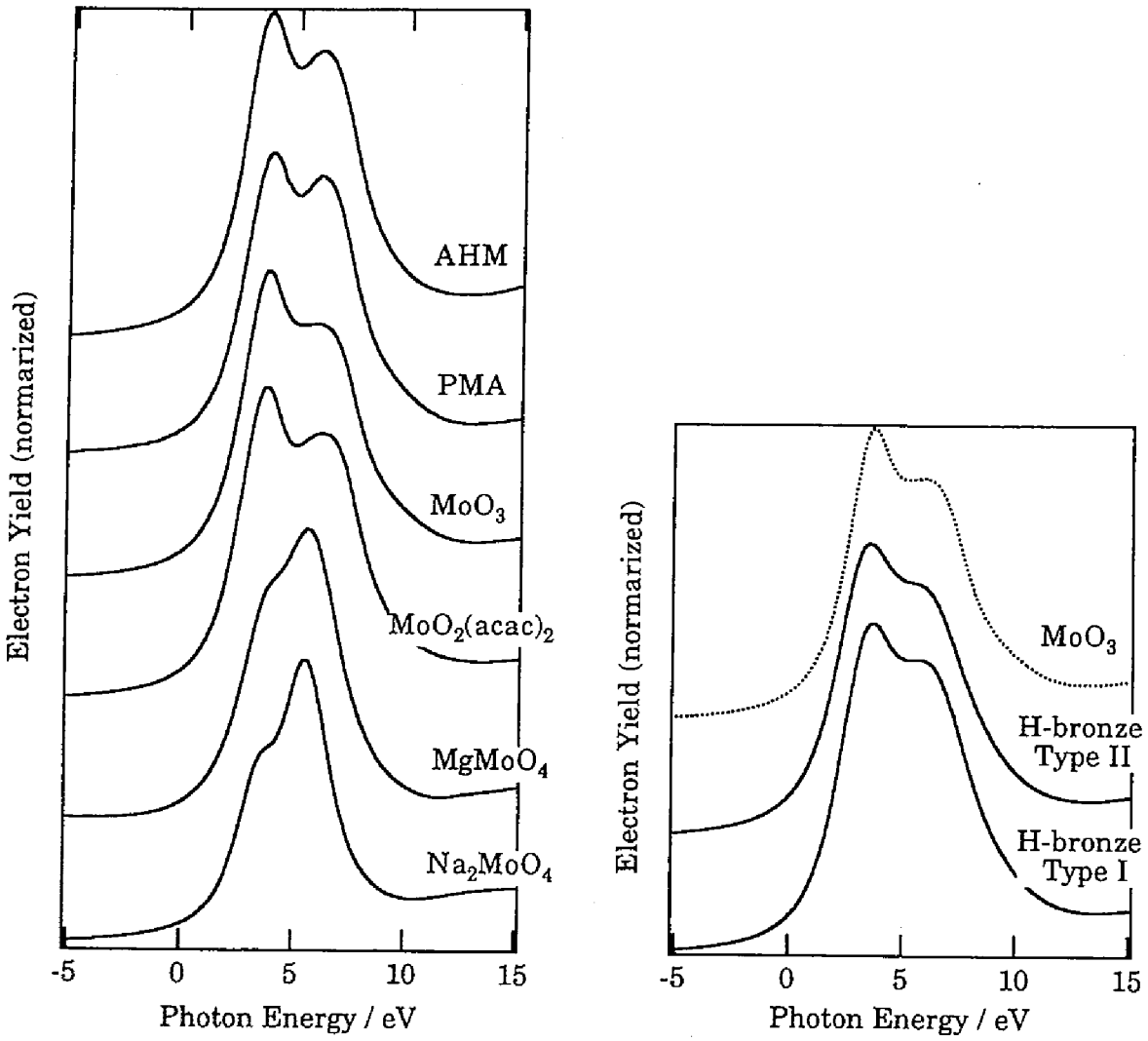

Fig. 1 Mo L_3-edge XANES spectra of reference compounds including Mo^{6+} ions.

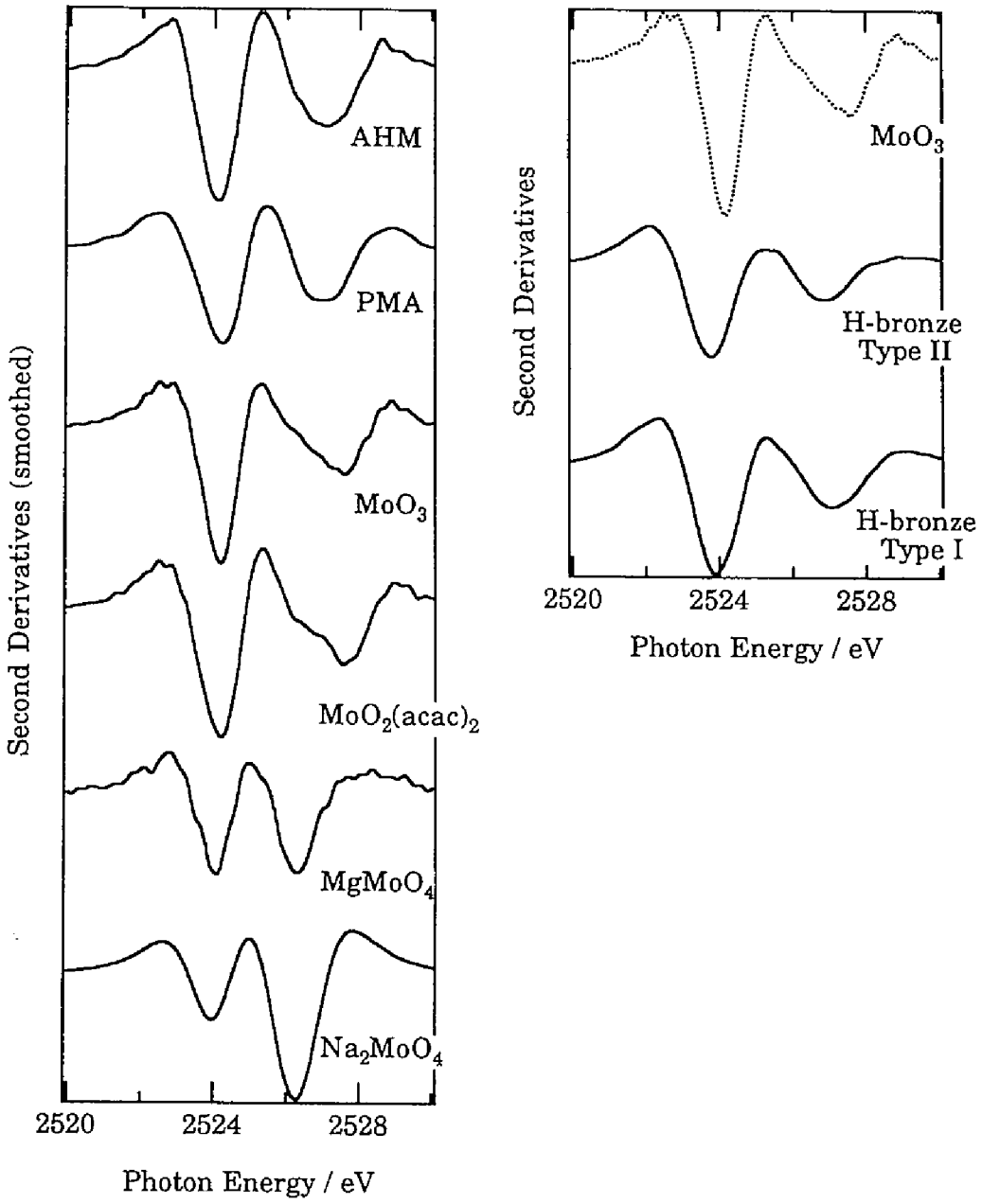

Fig. 2 Second derivatives of Mo L_3-edge XANES spectra of reference compounds including Mo^{6+} ions.

Table 1 The energy gap between two white lines (obtained by 2nd derivatives of XANES spectra).

Sample	Local structure	peak energy[a] / eV		*d*-orbital splitting / eV
Na_2MoO_4	T_d	3.5	5.7	2.4
$MgMoO_4$	T_d	3.6	5.8	2.2
AHM[b]	O_h (nearly C_{2v})	3.5	6.4	2.9
PMA[c]	O_h (nearly C_{2v})	3.6	6.4	2.8
MoO_3	O_h (distorted)	3.6	7.0	3.4
$MoO_2(acac)_2$	O_h (distorted)	3.6	6.9	3.3
type I[d]	O_h [e]	3.3	6.4	3.1
type II[d]	O_h [e]	3.2	6.3	3.1
MoO_2	O_h	1.4	3.8	2.4
MoS_2	D_{3h}	1.7		-
Mo (metal)	<*bcc*>	0.0		-

[a]energy offset is taken to be 2520.6 eV.

[b]Ammonium heptamolybdate : $(NH_4)_6Mo_7O_{24} \cdot 4H_2O$.

[c]Phosphomolybdic acid : $P_2O_5 \cdot 24MoO_3 \cdot xH_2O$.

[d]Hydrogen molybdenum bronze (H_xMoO_3) sample.

[e]axially symmmetric. (the distances of six Mo-O bonds are different from each other.)

between tetrahedral and octahedral molybdena, *i.e.*, the intensity is (t_{2g} : e_g)= 3 : 2 for octahedron, and (e : t_2)= 2 : 3 for tetrahedron.

In order to clarify the ligand field splitting of the final state 4*d* orbitals by splitting of *L*-edge XANES, a second derivative spectrum is often used.[28,30,31,33] The second derivatives of XANES spectra exhibit the splitting clearer, and the energy gap reflects the *d*-orbital splitting directly as shown in Fig. 2. The energy gaps between two white lines were evaluated and listed in Table 1. For these samples having MoO_4 tetrahedron, the energy gap is 2.2-2.3 eV, while, for MoO_3 having distorted MoO_6 octahedra, the gap was 3.3 eV. The values are the same as them reported by Bare *et al.*[28] who recorded the XANES spectra in a fluorescence yield mode. XANES spectra of $MoO_2(acac)_2$, AHM and PMA comprising of MoO_6 units are shown in Fig. 1. For MoO_3 and $MoO_2(acac)$ with a distorted O_h structure, the splitting gaps are 3.3 - 3.4 eV. While, for AHM and PMA having a Mo-polyanion structure with almost O_h but nearly C_{2v} symmetry, the energy gaps between two peaks are around 2.9 eV. In the former two compounds, oxygen ligands on an equatorial plane are located at apexes of an almost regular square. This effects the $d_{x^2-y^2}$ of e_g orbitals unstable to be lifted up, resulting in large energy gaps.

In case of polyanion structure such as $(Mo_7O_{24})^{6-}$ ion in AHM, distorting Mo ions interact with the neighboring Mo ions so that the bond strengths of Mo-O are weakened, resulting that the molecular orbitals corresponding to Mo-O_6 are more spread and the *d* band is tighter than that of completely O_h symmetric octahedra.[40] Therefore, the energy gap between t_{2g} and e_g is smaller than that for MoO_3 and/or $MoO_2(acac)_2$, which have a little distorted MoO_6 octahedra, but lengths of six Mo-O bonds are almost similar to those of MoO_3. This tendency of distortion effect is also reflected in the HOMO-LUMO gap, which relates to a UV-VIS spectroscopy directly,[40] as discussed in the later section. As long as the discussion is limited to the local symmetry, the local structure of $(PMo_{12}O_{40})^{3-}$ anion in PMA is almost similar to that $(Mo_7O_{24})^{6-}$ ion in AHM, reported by ^{95}Mo-NMR studies.[41,42] Thus, the splitting of PMA is assigned as same as that of AHM.

We investigated the L_3-edge XANES of Mo-Mg binary oxides in reduced state as described in the later section. Thus, the information of local structure of compounds including reduced Mo ions are necessary for the discussion of reduction effect. Hydrogen molybdenum bronze (H-bronze) and MoO_2 samples are available for reference ones to obtain a spectral information of MoO_6 octahedra with reduced Mo ions. In case of H-bronzes, MoO_6 octahedra of $(MoO_6)_n$ sheets cause minor rearrangements in Mo-O framework by insertion of hydrogen into MoO_3 interlayers.[43,44] As a result, the H-bronze samples have axially symmetric MoO_6 units and six Mo-O bonds whose distances are almost as same as those of MoO_3.[45] Hydrogen atoms are intercalated into the $(MoO_6)_n$ layers and stabilized by linking to oxygen atoms, resulting in OH or OH_2 groups located between the intra- and inter-layers.[45] In this manner, hydrogen atoms act as a structural change in MoO_6 octahedra, however, it is naturally accepted that formation of reduced Mo ions such as Mo^{5+} and/or Mo^{4+} are brought about by insertion of hydrogen atoms. The H-bronze shows distinct phases, called as type I - IV, depending on the amount of intercalated hydrogen atoms. We recorded the L_3-edge XANES spectra of the H-bronze samples of type I and II. For these samples, a $H_{0.21}MoO_3$ in type I and $H_{0.91}MoO_3$ in type II were observed in the bulk phase.[45,46] The L_3-edge XANES spectra of H-bronze samples and their second derivatives are shown in Fig. 1 and 2. For these samples, the amount of hydrogen atoms of type I is smaller than type II, as mentioned above.[45] The peak of XANES over H-bronzes are positioned at lower energy than those of other samples with Mo^{6+}-octahedra, *e.g.*, MoO_3, indicating that reduced Mo ions exist in H-bronzes. Thus, it is clearly shown that intercalated hydrogen atoms in H-bronzes bring about not only formation of axially symmetric MoO_6 octahedra but also reduction of Mo ions. For these spectra, the peak in the lower energy side is positioned at 3.2 - 3.3 eV, which is independent of hydrogen amount. Furthermore, the energy gap of the splitting is also similar to each other. These results show that intercalation of hydrogen atoms brings about formation of axially symmetric MoO_6 octahedra in $(MoO_6)_n$ sheets even in $x \geq 0.3$ (type I) as H_xMoO_3, and increasing of hydrogen

amount does not cause more reduction of surface Mo ions but affect the bulk Mo ions. The results of type II that hydrogen atoms intercalate into $(MoO_6)_n$ sheets as similarly as those of type I, and elongate the lattice spacings between these sheets.[45,47] When the bronzes are assumed to have only a Mo^{6+} ion, the energy gap between two white lines is expected to be larger than that of MoO_3 and white line at higher energy side should be narrower, because the MoO_6 unit in H-bronze is closer to the regular octahedron than that in MoO_3. However, the energy gaps of splitting of H-bronzes are smaller than that of MoO_3. This suggests that the reduction of Mo ions gives the decrease of the energy gap between t_{2g} and e_g in 4*d*-state of Mo. It is also discussed in the analysis of MoO_2 XANES, as below.

The Mo^{4+} (d^2) ions in MoO_2 exist in almost symmetric MoO_6 O_h structure. For the local structure of MoO_2 with an orthorhombic system, the threefold-degenerate t_{2g} manifold of MoO_6 octahedral symmetry is split into a more stable $d_{\parallel}$ (d_{xy}) orbital and two $d_{\perp}$ (d_{xz} and d_{yz}) orbitals. The $d_{\perp}$ orbitals overlap the p_{π} orbitals of O^{2-} ions, which have three coplanar Mo near neighbors, and form Mo($d_{\perp}$)-O(p_{π})-Mo($d_{\perp}$) bonding, whose interactions bring about a quasidegenerate pair of π^* bands.[36] By the studies of He-I photoelectron spectroscopy, it is concluded that the 4*d* electron of Mo^{4+} participates in the π^* bands.[48] Therefore, in MoO_2, a pair of Mo 4*d* electrons in t_{2g} state occupies molecular orbitals of Mo($d_{\perp}$)-O(p_{π}) and the orbitals in e_g state are vacant. The energy gap between t_{2g} and e_g in MoO_2 having Mo^{4+} ions should be smaller than that of the sample having Mo^{6+} ions, because of the less effect of perturbation by the ligand field of six O ions. In the XANES spectrum of MoO_2 shown in Fig. 3, a shoulder peak at 1.4 eV due to the electron transition to the π^* band is seen. The intensity of this peak is smaller than that of the samples including Mo^{6+} ions, because of the decrease in transition cross sections. The broad peak maximized at 3.8 eV is due to the transition to e_g state. The splitting of these peaks can be clearly seen in the second derivative spectrum. The 2.4 eV of energy gap is much smaller than that of MoO_3, although the Mo ions in MoO_2 exist in a symmetric MoO_6

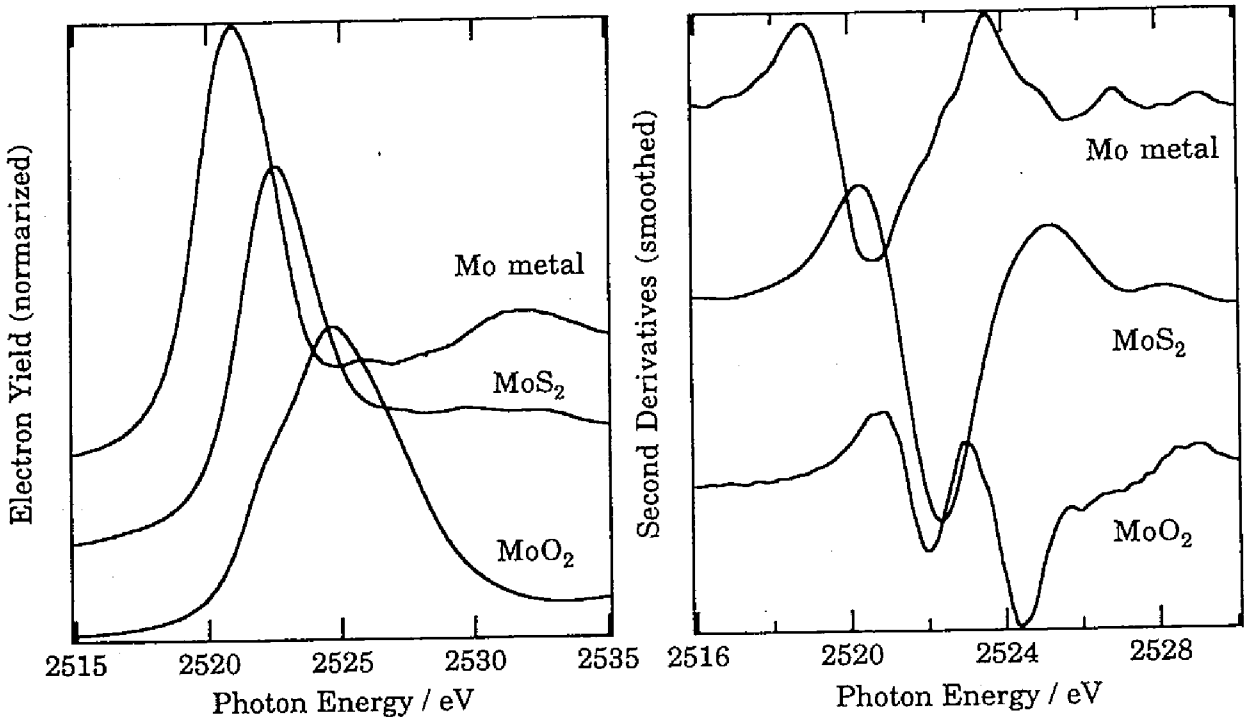

Fig. 3 Mo L_3-edge XANES spectra (left hand) and these second derivatives (right hand) of Mo, MoS_2 and MoO_2.

octahedra. This result strongly explains that the reduction of Mo ions brings about the condensation of a total 4*d*-state, and it reflects the L_3-edge XANES spectra directly. The reduction of Mo ions from Mo^{6+} gives the lower absorption edge, and narrower splitting of energy gap, regardless of the symmetry of MoO_6 octahedra.

In case of MoS_2 having a trigonal prismatic MoS_6 octahedra, the $Mo^{4+}(4d^2)$ configuration lies at the top of the $S^{2-}(3p^6)$ band. The Mo-Mo 4*d*-electron bonding is formed as zig-zag chains, and the octahedral site allows Mo-Mo bonding only with the three t_2 orbitals. These orbitals bring about the band of conduction electron, by the studies of a molecular orbital study by Hughbanks *et al.*[49] Therefore, the electron transition from 2*p* to 4*d* is assigned to an inter-atomic-like transition of a *d-d* band which is delocalized in Mo 4*d* state but not to an atomic-like transition like that of MoO_2. As shown in the XANES spectrum of MoS_2 (Fig. 3), the spectrum does not have split bands but shows only a single band. This feature of the spectrum is also seen in case of Mo metal. In MoS_2, the peak energy of XANES spectrum is 2.4 eV, which is located between two peaks of MoO_2. It is possibly supported that the XANES of MoS_2 at L_3-edge is due to the band of conduction electron formed in interatomic one, and the ligand field reflects to the XANES directly.

(2) Mo L_3-edge XANES of MoO_3-MgO.

We discussed the the bulk structure of Mo-Mg binary oxides on the basis of the XRD and Mo *K*-edge XAFS in a previous report.[27] In brief, it is concluded that α-$MgMoO_4$ and MgO phases exist in the samples of low Mo ratio less than $x \leq 0.5$, and the phases including Mo-polyanion such as $Mg_2Mo_3O_{11}$ are stabilized in the samples of higher ratio. It is important to investigate the local structure in near-surface and clarify the relationship between bulk and surface structures for the discussion of catalytic behavior.

In this study, we recorded the Mo L_3-edge XANES spectra in a total electron yield mode. These spectra reflect the state of Mo ions in near-surface region, as described in

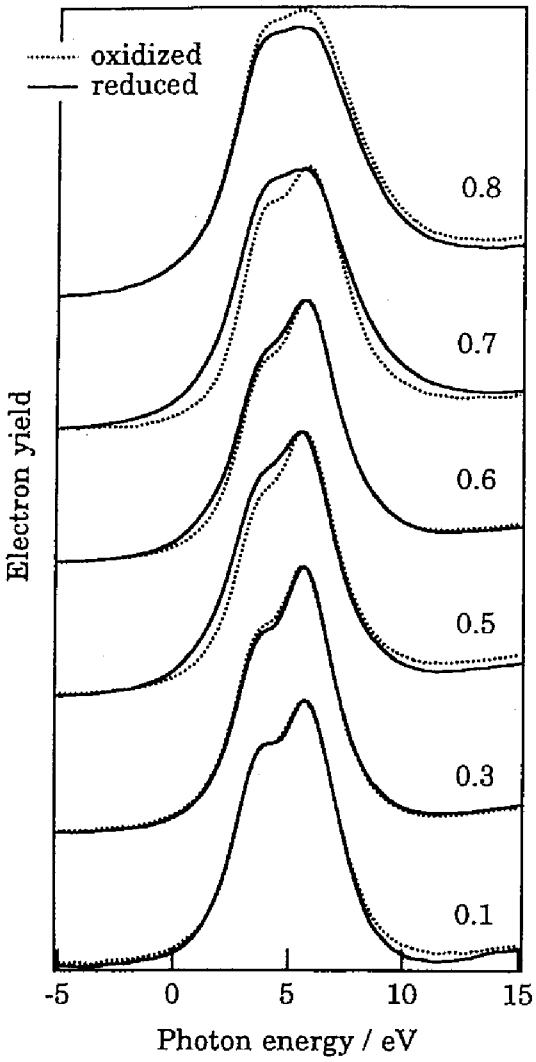

Fig. 4 Mo L_3-edge XANES spectra of MoO_3-MgO in oxidized (dotted line) and reduced (solid line) states.

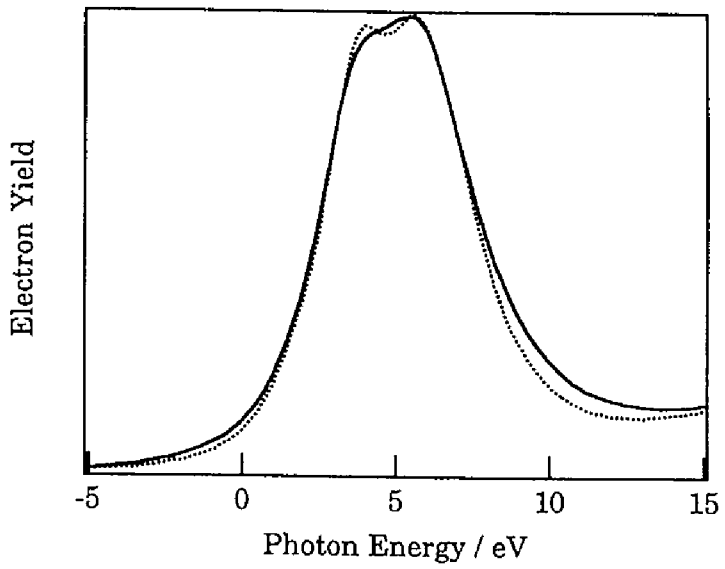

Fig. 5 Mo L_3-edge XANES spectrum of a reduced sample of x=0.7 (solid line) and a superposed spectra (dotted line) obtained by a mixture of MoO_2 (multiplied by 20%), $MgMoO_4$ (45%), and AHM (35%).

Table 2 The energy gap between two white lines over MoO_3-MgO.

Mo ratio	peak energy / eV		*d*-orbital splitting / eV
0.8	3.4	6.0	2.6
0.7	3.7	5.9	2.2
0.6	3.7	5.9	2.2
0.5	3.6	5.7	2.1
0.3	3.5	5.7	2.2
0.1	3.6	5.7	2.1

Table 3 The energy gap between two white lines over reduced MoO_3-MgO.

Mo ratio	peak energy / eV		*d*-orbital splitting / eV
MoO_3 red.	3.8	7.1	3.3
0.8 red.	3.7	5.9	2.2
0.7 red.	3.7	6.0	2.3
0.6 red.	3.6	5.9	2.3
0.5 red.	3.5	5.7	2.2
0.3 red.	3.6	5.7	2.1
0.1 red.	3.6	5.7	2.2

the experimental section. The spectra of MoO_3-MgO are shown in Fig. 4. The dotted lines are the spectra of the samples prior to the hydrogen treatment (oxidized state), and the solid lines are the spectra after the treatment at 773K (reduced state).

For the samples of low Mo ratio less than $x \leq 0.5$, each spectrum is similar to that of $MgMoO_4$ or Na_2MoO_4. The values of the energy gap between two white lines determined by the second derivatives of the XANES spectrum (Fig. 6) are shown in Table 2 (oxidized state) and Table 3 (reduced state). The values in these samples are 2.1-2.2 eV, and these are close to those of $MgMoO_4$ and Na_2MoO_4. These results indicate that the local structure around surface Mo ions are stabilized as MoO_4 tetrahedra, as in the bulk. However, the XANES spectra of these samples are partly different from that of $MgMoO_4$. For the samples of x = 0.1 and 0.3, the relative intensities (peak height) of two white lines are not the same as that of $MgMoO_4$, but the white line in lower energy side is more intense than that of $MgMoO_4$. This result suggests that MoO_6 octahedra exist in near-surface region. In x = 0.5, the XANES spectrum is quite similar to that of $MgMoO_4$, indicating that the Mo ions exist in a tetrahedra as that of $MgMoO_4$ not only in the bulk phase but also in near-surface.

For the samples of x = 0.1 and 0.3, the XANES spectra in oxidized state are almost same as those in reduced state. This result exhibits that no effect by H_2 treatment is brought about the surface Mo ions in these samples. On the other hand, changes of the XANES spectra were observed by the treatment with H_2 in the samples of $x \geq 0.5$. Thus, we will discuss the XANES spectra of the oxidized samples of $x \geq 0.5$ first.

The XANES spectra of x = 0.6 and 0.7 have a different feature from that of x = 0.8. For the samples of x = 0.6 and 0.7, the spectra have a similar feature to that of x = 0.5. The energy gaps between the white lines are 2.2 eV, and this value is the same as that of $MgMoO_4$. These results show that MoO_4 tetrahedra is a main component in near-surface region. However, in the case of the spectrum of x = 0.7, the white line at lower energy side is more intense than that of $MgMoO_4$, whose feature is the same as that of $x \leq 0.3$, indicating that MoO_6 octahedra is stabilized partly in near-surface region. For the sample of x = 0.8, a white line in higher energy side has a broad band, which is characteristic those of the reference samples with MoO_6 octahedra such as

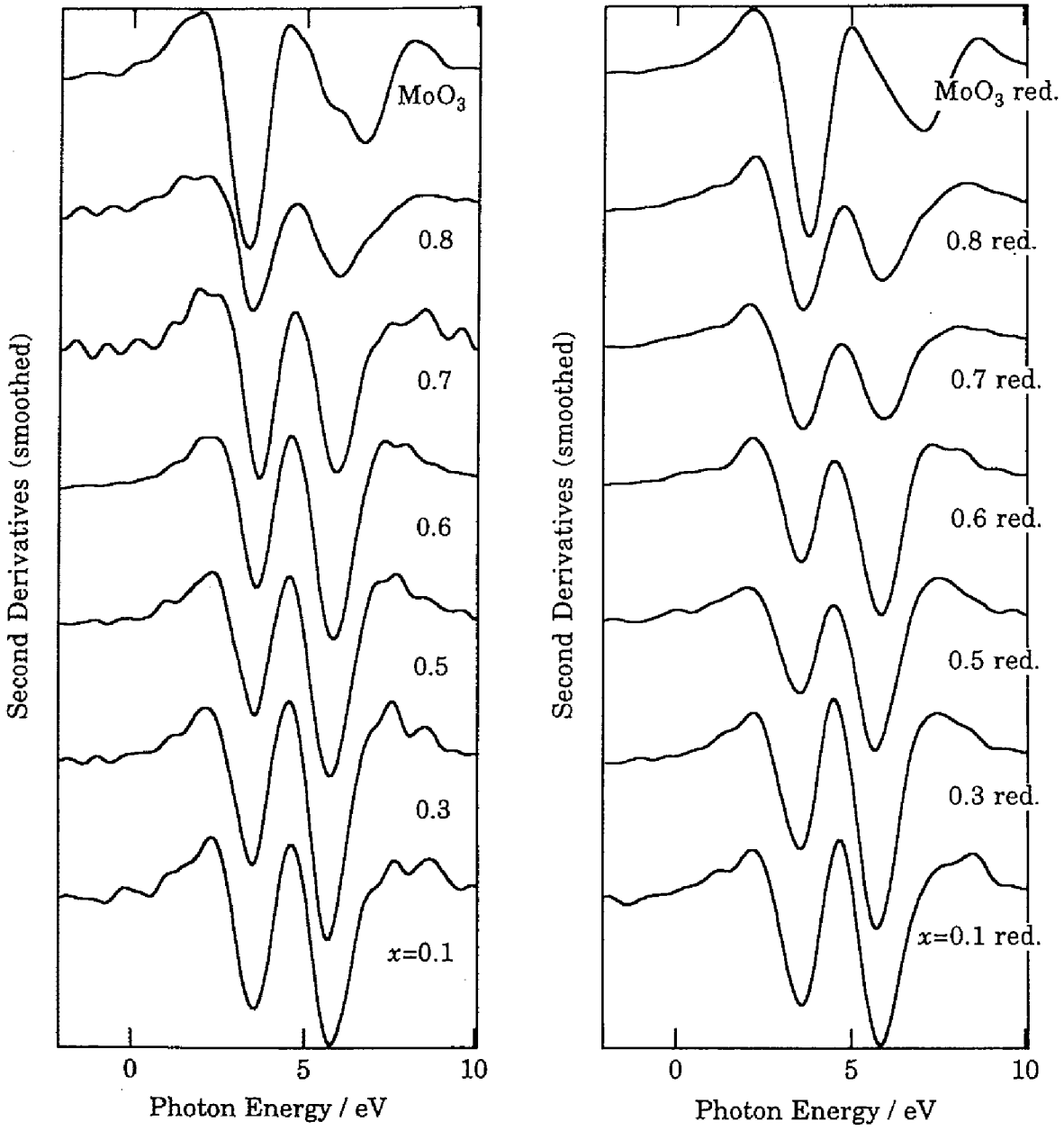

Fig. 6 Second derivatives of Mo L_3-edge XANES spectra of MoO_3-MgO in oxidized (left hand) and reduced (right hand) states.

AHM and MoO_3, indicating that the surface Mo species exist as octahedra mainly. The energy gap between the white lines is 2.6 eV. This value is close to rather AHM and PMA than MoO_3 and $MoO_2(acac)_2$. Thus, distorted octahedra having a polyanion-like structure are mainly exposed in near-surface region.

These results lead a conclusion that the local structure of Mo ions in near-surface is not necessarily the same as that in the bulk phase. Bare *et al.* reported the *L*-edge XANES study of MgO-supported MoO_3 measured in a fluorescence mode in a recently paper.[28] They concluded definitely by means of XANES spectra and their second derivatives that Mo-ion species on MgO are stabilized as octahedra in the samples of loading amount less than 15 wt% as MoO_3, and tetrahedra exists in the samples of higher loading. The present study reveals that the samples of lower Mo ratio less than $x = 0.3$ (51.7wt% as MoO_3) have an octahedral species. The previous study of these samples showed that MgO and $MgMoO_4$ phases coexist in the bulk, and Mo species are almost MoO_4 tetrahedra, as mentioned above.[27] From the results of Bare *et al.* and ours, it is proposed that octahedral species in the surface or near-surface are stabilized by existence of MgO phase and/or coexistence of $MgMoO_4$ and MgO phases in the bulk. In addition, it is concluded by the present study that the generation of octahedral species in near-surface region is brought in the samples of about higher Mo amount ($x \geq 0.7$) than that in the bulk phase ($x \geq 0.6$).

By the treatment with H_2, XANES spectra of $x \geq 0.5$ samples are changed. In these samples, the edge energy of each XANES spectrum becomes lower than that in oxidized ones. This strongly suggests that Mo ions are reduced by the treatment with H_2. It is noteworthy that the sample of $x = 0.5$ is also reduced partly by the treatment, and the spectrum becomes similar to those of H-bronze samples. The sample in the oxidized state has only $MgMoO_4$ phase in both bulk and surface layers as mentioned above. For the sample of $x = 0.6$, the change in the spectrum by the treatment is almost similar to that of $x = 0.5$.

On the other hand, the samples of $x = 0.7$ and 0.8 showed a different change in the XANES spectra from those of $x \leq 0.6$ by the H_2 treatment. In the XANES spectra of $x = 0.7$, the two white lines are not clearly split, and the edge of a white line at lower

energy side shifts more than that for the sample of $x = 0.6$. This phenomenon was not observed for MoO_3. From these results, it is concluded that surface Mo ions of $x = 0.7$-0.8 samples are easily reduced by the treatment to bring about reduced ones, *e.g.*, Mo^{5+} and/or Mo^{4+}. In fact, the XANES spectrum of $x = 0.7$ in reduced state is able to fit the superposition of the spectra of $MgMoO_4$ (multiplied by 45%), AHM (35%), and MoO_2 (20%), as shown in Fig. 5, indicating that the reduced ions including a MoO_2 phase are formed in near-surface region by H_2 treatment. In the XANES spectrum of these reduced samples, the values of the energy gap between the white lines are 2.2-2.3 eV, suggesting that Mo^{6+}-tetrahedral species still remains in the reduced state. The previous study on Mo *K*-edge XAFS revealed the formation of MoO_2 as a definite phase.[27] Therefore, it is concluded that the Mo ions of the samples at around $x = 0.7$ are easily reduced to form a MoO_2 phase by H_2 treatment more intense in the bulk than in near-surface region, and the surface Mo ions are stabilized as a coexistence of Mo^{6+}-tetrahedra, octahedra, and MoO_2. It should be mentioned that the reduced samples of around $x = 0.7$ exhibit catalytic activity for olefin metathesis.[26] The present results suggest the generation of the activity is related to the formation of reduced Mo ions in the MoO_2 phase.

(3) Diffuse Reflectance UV-VIS Spectroscopy

In order to obtain more information about the reduced state of surface Mo ion, UV-VIS spectroscopy was applied in a diffuse reflectance mode. The structural study by UV-VIS spectra has already been reported, and the assignment of the bands has been done.[50-52] In the present work, MoO_3, $MgMoO_4$, AHM and MoO_2 are used for reference compounds for the discussion about the local structure of Mo ions.

The energy of electron transitions depends on the ligand field symmetry surrounding the Mo center. For oxygen ligands, a more energetic transition is expected for a tetrahedral Mo^{6+} than for an octahedral one.[53] The spectra of the reference compounds with Mo^{6+} ions are shown in Fig. 7. The spectrum of $MgMoO_4$ shown an absorption maximum at 256 nm, which is due to the ligand-metal charge

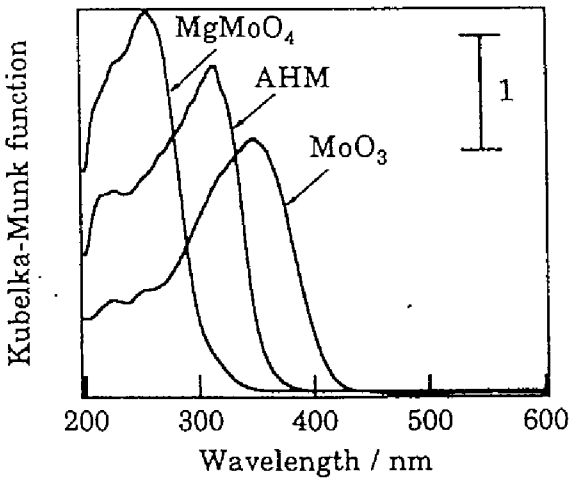

Fig. 7 UV-VIS reflectance spectra of Mo^{6+} reference compounds.

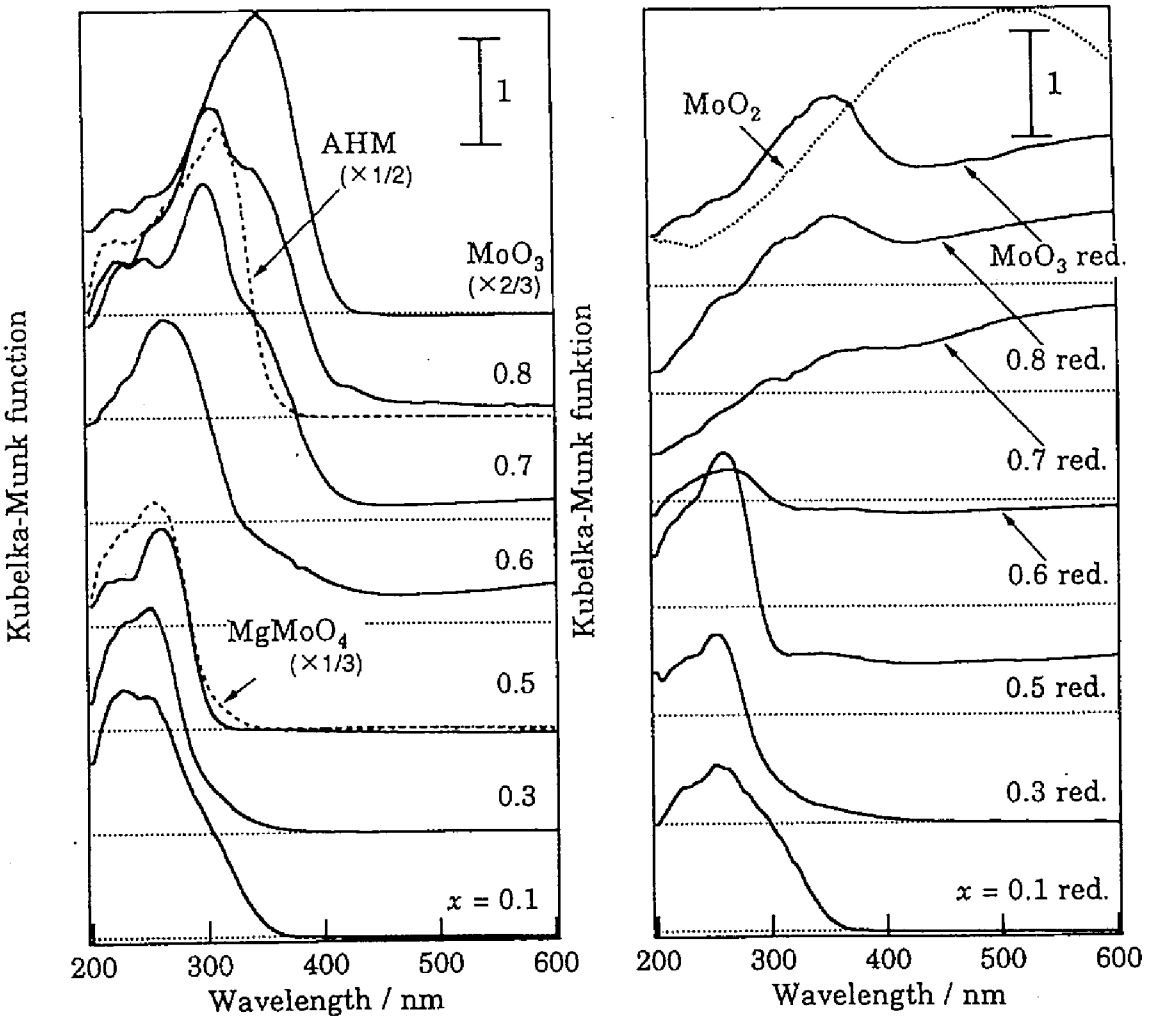

Fig. 8 UV-VIS reflectance spectra of MoO_3-MgO binary oxides in oxidized (left) and reduced (right) states.

transfer (LMCT) of $O^{2-} \rightarrow Mo^{6+}(d^0)$ of $(MoO_4)^{2-}$ in T_d-symmetry.[35,50,51] For the samples having Mo^{6+} octahedra, the band centered at 315 nm in AHM, and at 348 nm in MoO_3, which are also due to the LMCT of $O^{2-} \rightarrow Mo^{6+}$ of MoO_6 octahedra. By distortion of MoO_6 structure, the LMCT band shifts to a shorter wavelength. In addition, the threshold energy also reflects the local structure as reported by Weber *et al*,[54] *i.e.*, the energy of polymolybdate samples becomes lower with the aggregation of MoO_6 units. These are a good information for distinguishing the local structure.

The spectra of Mo-Mg binary oxides in the oxidized state are shown in Fig. 8 (left hand). In case of the oxidized samples of $x \leq 0.5$, each spectrum clearly exhibits an absorption band centered at around 250 nm, indicating that Mo ions exist as T_d structure with Mo^{6+}. For instance, the spectrum of $x = 0.5$ sample is similar to that of $MgMoO_4$ as a whole. Thus, Mo ions are stabilized as only Mo^{6+} tetrahedra. However, the spectra of the samples of $x \leq 0.3$ are different from that of $x = 0.5$. The threshold energy of $x \leq 0.3$ is higher than that of $x = 0.5$, indicating the coexistence of octahedral and tetrahedral species. This result is accordance with that of L_3-edge XAFS study but not with the studies of Mo *K*-edge XAFS and XRD.[27] Therefore, it is supported that MoO_4 tetrahedra is formed in the bulk phase, and octahedral species is present partly only in near-surface region. This implies that the information obtained by diffuse reflectance UV-VIS spectra is more sensitive to the surface structure than to that of Mo *K*-edge XAFS spectra.

In case of the sample of $x = 0.6$, the threshold energy of the spectrum is lower than that of $MgMoO_4$, and the absorption maximum is seen at 264 nm. These features are the same as those of $x \leq 0.3$, indicating that Mo ions are present as a mixture of octahedra and tetrahedra. With respect to the XAFS studies in the sample, octahedral structure of Mo ions are less observed in near-surface region but investigated in the bulk. Therefore, the octahedra analyzed by UV-VIS spectroscopy is formed in the bulk phase. It is explained that the diffuse reflectance UV-VIS spectra include the information of the bulk more than the L_3-edge XANES spectra in a total electron yield mode. Therefore, the surface sensitivity of these spectra, in the present case, are in this order; L_3-edge XANES in a total electron yield mode > diffuse reflectance UV-VIS

> *K*-edge XAFS in a transmission mode.

On the other hand, the spectra of $x \geq 0.7$ have a large and narrow band maximized at 290 nm, and a smaller band in a shoulder peak at around 345 nm. The wavelength of the absorption maximum at 290 nm is close to that of AHM having a distorted octahedra, indicating that the structure around Mo ions is distorted MoO_6 octahedra like a polyanion. In a similar manner, the smaller band at around 345 nm is due to the MoO_6 octahedra in a MoO_3 phase. This peak is more intense with increasing the Mo content. As for L_3-edge XANES spectroscopy, it is concluded that the sample of x = 0.7 has MoO_6 octahedra as a minor component, while, the result of UV-VIS spectrum shows that the octahedra as a polyanion structure are formed as a main component. Therefore, it exhibits that concentration of MoO_6 octahedra is lower in near-surface than in the bulk.

The spectra of reduced samples with H_2 at 773K are also shown in Fig. 8 (right hand). For the samples of $x \leq 0.3$, a band is seen at 260 nm, which corresponds to MoO_4 tetrahedra with Mo^{6+} ions. For the samples of $x = 0.1$, the spectrum is identical with unreduced one, *i.e.*, stabilized as a coexistence of tetrahedra mainly and octahedra partly. Thus, it is suggested that the structure of surface Mo ions are less changed by H_2-treatment. While, at relatively higher Mo ratio of $x \geq 0.5$, a broad band at the wavelength longer than 320 nm is exhibited, and the absorption becomes more intense with an increase in Mo ratio. The absorption of wavelength between 400 and 800 nm is due to reduced Mo ions such as $Mo^{5+}(d^1)$ and/or $Mo^{4+}(d^2)$.[51] It indicates that reduced Mo ions are formed by the treatment with H_2. The band at around 250 nm is less intense in x = 0.6 than in $x \leq 0.5$, and this band is almost disappeared for the higher Mo content in $x \leq 0.7$. The relative intensity of the absorption at 350 nm, which is due to the Mo^{6+}-octahedra in MoO_3, increases with an increase of Mo content, and it is also seen clearly for the sample of H_2-treated MoO_3. While, in the reduced samples at around x = 0.7, this band can be seen indefinitely. Thus, the Mo^{6+}-octahedra in oxidized samples are reduced by H_2-treatment at 773K to form other structures having reduced Mo ions. It results that the treatment is more effective for octahedra in MoO_3 than that of polyanion structure in coexistence of tetrahedra. For

the broad band at the longer wavelength than 450 nm, deeply reduced Mo ions such as MoO_2 species is likely. For MoO_2, which have slightly distorted O_h-symmetry around Mo^{4+} ion, the absorption is maximized at 480 nm due to $T_{1g} \rightarrow T_{2g}$ of $Mo^{4+}(d^2)$.[51] On the other hand, the absorption band due to MoO_2 is less seen in the spectrum of H_2-treated MoO_3. Thus, bulk MoO_3 is not reduced enough to produce MoO_2 species. As discussed above, the formation of MoO_2 phase by the treatment with H_2 at 773K is clearly shown in the bulk phase for the samples at around $x = 0.7$ by the studies of Mo *K*-edge XAFS.[27] Furthermore, the formation of MoO_2 phase is also seen by means of UV-VIS spectroscopy. With respect to these studies and L_3-edge XANES one, the intensity of MoO_2 phase is less observed in near-surface region than in the bulk. It is concluded that the reduction of Mo ions to form a MoO_2 phase is more effective in the bulk than in near-surface region. This feature of the effect of reduction over Mo-Mg binary oxides is much similar to that over Mo-Sn binary oxides, as reported by Okamoto *et al.*[20]

In previous report,[26] the metathesis reactivity for olefins is brought about for the reduced samples at around $x = 0.7$. These samples have small particles of MoO_2 phase in the bulk.[27] As discussed above, the active species for metathesis reaction relates to the reduced Mo ions including MoO_2 phase not only in the bulk but also in near-surface region. The Mo ions in near-surface are reduced more hardly than those in the bulk. However, the MoO_2 phase is stabilized in near-surface region as a minor component. We suppose that that these species act as an active center for metathesis, and the correlation between bulk and surface Mo ions relate to the stabilization of active species with low valent Mo ions.

Acknowledgment

The X-ray absorption experiments at Mo *L*-edge were supported by the Joint Studies Program (proposal No. 6-841, 1994 and 7-542, 1995) of UVSOR in the Institute for Molecular Science. We thank Mr. Osamu Matsudo and Dr. Toyohiko Kinoshita (Institute for Molecular Science, Japan) for the assistance of XANES

spectra-measurements and helpful discussion. We acknowledge the invaluable indication of the reviewer about the penetration range of XANES spectra.

References and Notes

(1) Mol, J. C.; Moulijn, J. A. *Adv. Catal.* **1975**, *24*, 131.

(2) Gardin, D. J.; Lappert, M. F. *J. Chem. Soc. Chem. Commun.* **1972**, *927*, 927.

(3) Mol, J. C.; Moulijn, J. A. *Catal. Sci. Technol.* **1988**, *8*, 69.

(4) Rappe, A. K.; Goddard, W. A. *J. Am. Chem. Soc.* **1980**, *102*, 5114.

(5) Lombardo, E. A.; Houalla, M.; Hall, W. K. *J. Catal.* **1978**, *51*, 256.

(6) Gassman, P. G.; Johnson, T. H. *J. Am. Chem. Soc.* **1976**, *28*, 6055.

(7) Kazansky, V. B.; Shelimov, B. N.; Vikulov, K. A. In *Proc. 10th Int. Congr. Catal.*; Elsevier: Budapest, 1992; pp 515.

(8) Vikulov, K. A.; Elev, I. V.; Shelimov, B. N.; Kazansky, V. B. *J. Mol. Catal.* **1989**, *55*, 126.

(9) Elev, I. V.; Shelimov, B. N.; Kazansky, V. A. *J. Catal.* **1988**, *113*, 229.

(10) Tanaka, K.; Miyahara, K.; Tanaka, K. In *Proc. 7th Int. Congr. Catal.*; Elsevier: Tokyo, 1981; pp 1318.

(11) Zhang, B.; Li, Y.; Lin, Q.; Jin, D. *J. Mol. Catal.* **1988**, *46*, 229.

(12) Anpo, M.; Kubokawa, Y. *J. Catal.* **1982**, *75*, 204.

(13) Anpo, M.; Kondo, M.; Kubokawa, Y.; Louis, C.; Che, M. *J. Chem. Soc. Faraday Trans. 1* **1988**, *84(8)*, 2771.

(14) Llorente, J. M. M.; Rives, V.; Malet, P.; Gil-Llanbias, F. J. *J. Catal.* **1992**, *135*, 1.

(15) Deo, G.; Wachs, I. E. *J. Phys. Chem.* **1991**, *95*, 5889.

(16) Shimada, H.; Matsubayashi, N.; Sato, T.; Yoshimura, Y.; Nishiyama, A.; Kosugi, N.; Kuroda, H. *J. Catal.* **1992**, 746.

(17) Stampfl, S. R.; Chen, Y.; Dumesic, J. A.; Niu, C.; Hill Jr., C. G. *J. Catal.* **1987**, *105*, 445.

(18) Moro-oka, Y.; Ueda, W. *Adv. Catal.* **1994**, *40*, 233.

(19) Glaeser, L. C.; Brazdil, J. F.; Hazle, M. A.; Mehicic, M.; Grasselli, R. K. *J. Chem. Soc. Faraday Trans. 1* **1985**, *81*, 2903.

(20) Okamoto, Y.; Oh-hiraki, K.; Imanaka, T.; Teranishi, S. *J. Catal.* **1981**, *71*, 99.

(21) Margolis, L. Y. *J. Catal.* **1971**, *21*, 93.

(22) Takita, Y.; Ozaki, A.; Morooka, Y. *J. Catal.* **1972**, *27*, 185.

(23) Morooka, Y.; Takita, Y.; Ozaki, A. *J. Catal.* **1971**, *23*, 183.

(24) Yun, Y.; Ueda, W.; Moro-oka, M. The 72nd Annual Meeting of the Catalysis Society of Japan, Nishinomiya, 1993.

(25) Tomenov, D. N.; Doroshenko, V. A.; Shapavolova, L. P.; Taranukha, O. M.; Lushnik, N. S. *Ukr. Khim. Zr.* **1981**, *74*, 93.

(26) Hasegawa, S.; Tanaka, T.; Kudo, M.; Mamada, H.; Hattori, H.; Yoshida, S. *Catal. Lett.* **1992**, *12*, 255.

(27) Aritani, H.; Tanaka, T.; Funabiki, T.; Yoshida, S.; Kudo, M.; Hasegawa, S. *J. Phys. Chem.* **1996**, *100*, 5440.

(28) Bare, S. R.; Mitchell, G. E.; Maj, J. J.; Vrieland, G. E.; Gland, J. L. *J. Phys. Chem.* **1993**, *97*, 6048.

(29) Teo, B. K.; Lee, P. A. *J. Am. Chem. Soc.* **1979**, *101*, 2815.

(30) Evans, J.; Frederick, W.; Mosselmans, W. *J. Phys. Chem.* **1991**, *95*, 9673.

(31) George, G. N.; Cleland Jr., W. E.; Enemark, J. H.; Smith, B. E.; Kipke, C. A.; Roberts, S. A.; Cramer, S. P. *J. Am. Chem. Soc.* **1990**, *112*, 2541.

(32) Hedman, H.; Frank, P.; Gheller, S. F.; Roe, A. L.; Newton, W. E.; O., H. K. *J. Am. Chem. Soc.* **1988**, *110*, 3798.

(33) Hu, H.; Wachs, I. E.; Bare, S. R. *J. Phys. Chem.* **1995**, *99*, 10897.

(34) Chang, S.-C.; Leugers, M. A.; Bare, S. R. *J. Phys. Chem.* **1992**, *96*, 10358.

(35) Che, M.; Figueras, F.; Forisser, M.; McAtter, J.; Perrin, M.; Portefaix, J. L.; Praliaud, H. In *Proc. 6th Int. Congr. Catal.*; Elsevier: London, 1976; pp 261.

(36) Goodenough, J. B. In *4th Int. Conf. Chemistry and Uses of Molybdenum*; Climax Molybdenum Co.: London, 1982; pp 1.

(37) Sotani, N.; Kawamoto, Y.; Inui, M. *Mater. Res. Bull.* **1983**, *18*, 797.

(38) Sotani, N.; Eda, K.; Sadamatsu, M.; Takagi, S. *Bull. Chem. Soc. Jpn.* **1989**, *62*, 903.

(39) Erbil, A.; Cargill III, G. S.; Frahm, R.; Boehme, R. F. *Phys. Rev. B* **1988**, *37*, 2450.

(40) Masure, D.; Chaquin, P.; Louis, C.; Che, M.; Fournier, M. *J. Catal.* **1989**, *119*,

415.

(41) Maksimovskaya, R. I.; Chumachenko, N. N. *Polyhed.* **1987**, *6*, 1813.

(42) Fedotov, M. A. *Bull. Acad. Sci. USSR, Div. Chem. Sci.* **1984**, 1070.

(43) Kihlborg, L. *Ark. Kemi.* **1963**, *21*, 357.

(44) Hibble, S. J.; Dickens, P. G. *Ber. Bunsengers. Phys. Chem.* **1986**, *90*, 702.

(45) Sotani, N.; Eda, K.; Kunitomo, M. *J. Chem. Soc. Faraday Trans.* **1990**, *86(9)*, 1583.

(46) Sotani, N.; Yoshida, N.; Yoshioka, Y.; Kishimoto, S. *Bull. Chem. Soc. Jpn.* **1985**, *58*, 1626.

(47) Thomas, D. M.; McCarron III, E. M. *Mater. Res. Bull.* **1986**, *21*, 945.

(48) Beatham, N.; Orchard, A. F. *J. Electron. Spectr. and Related Phenom.* **1979**, *16*, 77.

(49) Hughbanks, T.; Hoffmann, R. *J. Am. Chem. Soc.* **1983**, *105*, 1150.

(50) Fournier, M.; Louis, C.; Che, M.; Chaquin, P.; Masure, D. *J. Catal.* **1989**, *119*, 400.

(51) Prialiaud, H. In *2nd Int. Conf. Chemistry and Uses of Molybdenum*; Climax Molybdenum Co.: London, 1976; pp 195.

(52) Massoth, F. E. *Adv. Catal.* **1978**, 265.

(53) Cotton, F.; Wilkinson, G. *Adv. Inorg. Chem. (4th ed.)*; Interscience: New York, 1980, pp 847.

(54) Weber, R. S. *J. Catal.* **1995**, *151*, 470.

Part II

Characterization of Active Copper Species in Supported Cu Catalysts for *de*NO_x Reactions

Introduction of Part 2

Cu has a single 4*s* electron in the atomic state, and thus, Cu^+ is in a stable state in the oxide. However, Cu^{2+} is also stable because the second ionization enthalpy is much lower than that of alkalies.[1] In fact, Cu metal is burnt in red heat with oxygen to give CuO and Cu_2O. The change of copper valence, *i.e.*, $Cu^0(d^{10}) \leftrightarrow Cu^+(d^{10}) \leftrightarrow Cu^{2+}(d^9)$, relates to the catalytic performance. In the local structure around Cu, linear $Cu\text{-}O_2$ dioxo-structure exists in Cu_2O, and square planer $Cu\text{-}O_4$ are present in CuO. In the model calculations by means of INDO/S MO for CuO and Cu_2O clusters, the bands near below Fermi level are composed mostly of Cu 3*d* orbitals, and the bottom of the valence bands have strong O 2*p* character in both CuO and Cu_2O.[2]

1. Copper and copper-oxide as catalysts

Both Cu metal and Cu-oxides are useful as a catalyst for many reaction systems. In particular, Cu-oxides, Cu_2O and CuO, are semiconductors and effective for redox-type reactions. For supported and ion-exchanged copper catalysts, it is well known that the activity of Cu ions relates to the redox performance of Cu ions directly. Classifying the reactions by Cu catalysts, the typical reactions are pointed out as oxidation, hydrogenation, and reduction. In particular, Cu-supported or ion-exchanged oxides are well-known for a *de*NO_x catalyst such as Cu ion-exchanged zeolites. The outlines of the studies are described as follows.

(1) Oxidation

Cu_2O is known as an industrial catalyst for propene oxidation to acrolein.[3] The kinetics study showed that the reaction is of the first order with respect to oxygen and independent of propene pressure.[4] By IR spectroscopy, π-allyl species are confirmed to be formed on Cu_2O, which has a high affinity for oxygen.[5] Thus, it is summarized that oxygen adsorption appears to be a rate-determining step and an allylic species formed by abstraction of hydrogen atom from propene by adsorbed oxygen is an intermediate in oxidation. Although, in the actual and industrial process, the development of Sohio-

method using MoO_3-Bi_2O_3 binary oxide catalysts, as described at part 1, brings about the less role for Cu_2O catalyst, the catalyst including Cu^+ (*e.g.*, Cu_2O) has an activity for partial oxidation of olefins, and CO oxidation, as reported.[6]

Copper-based catalysts have been proved to be highly useful for steam reforming of methanol ($CH_3OH + H_2O \rightarrow CO_2 + 3\ H_2$) with high activity and selectivity.[7,8] For the various Cu-containing catalysts, the reaction mechanisms of steam reforming reaction was reported by Takezawa *et al.* They concluded in Cu/ZrO_2 and Cu/Al_2O_3 catalysts that micro particles of Cu-metal, which is formed during the reaction, is the most active species by the spectroscopic study of XPS, AES, and IR.[7] It is concluded that formation of formaldehyde from methanol is the rate-determing step in the reaction, and formic acid is formed by addition of H_2O to formaldehyde in the path way of producing CO_2 and H_2 over Cu catalysts.[9]

Other reported oxidation reactions catalyzed by Cu-based catalysts are oxidation of formaldehyde over Cu-Zn-O,[10], water-gas shift ($CO + H_2O \rightarrow CO_2 + H_2$) over Cu/ZnO,[11] ethylene oxidation over Cu/Al_2O_3,[12], CO oxidation over Cu/SiO_2[13] benzyl alcohol oxidation in gas phase over alkaline-promoted Cu/SiO_2,[14] dehydrogenation of methanol over Cu ion-exchanged TSM (fluorotetrasilicic mica),[15] and so on. Several reactions are used industrially.

(2) Hydrogenation

Cu catalysts are also utilized for hydrogenation reactions. As for Cu-oxide type catalysts, Cu-Cr-O binary oxide is active for hydrogenation of aliphatic ketones to alcohols[16] Cu/ZnO is industrially used for the methanation of CO with H_2.[17] Cu-including binary metal alloys are also widely utilized. In particular, amorphous metal alloys exhibit high activity for hydrogenation reactions.[18] It is accepted that the reaction rate strongly depends on the crystal structure of the catalyst. In this viewpoint, the use of amorphous alloys in catalytic syntheses has received considerable attention because amorphous alloys have a high concentration of coordinatively unsaturated sites which are expected to act as catalytically active sites.[18]

Cu-Zr alloys have been reported as catalysts in the reactions such as the

hydrogenation of CO,[19,20] CO_2,[20,21] ethene,[22] and 1,3-butadiene.[23] In the study of ethene hydrogenation reported by Yamashita *et al*,[22] it is found that an amorphous pulverized $Cu_{62}Zr_{38}$ alloy, pretreated with a dilute HF solution exhibits much higher activity for olefin hydrogenation than a crystalline one. The change of the activity by the pretreatment is due to the increase in the surface concentration of Cu as well as increase in surface area while keeping the highly scattered active sites derived from the structure of the amorphous alloy. In addition, they proposed that Cu^+ is the active species for hydrogenation.[22] They also reported that Cu-Ti amorphous alloys revealed high turnover frequencies in dehydration of methanol to methyl formate.[24]

Recently, Yoshida[25] and Katona[26] reported the structural analyses of active Cu and another metal sites over Cu-Zr and Cu-Ti alloys. Yoshida *et al.* found the treatment of alloys with hydrogen and oxygen under mild conditions were effective to obtain alloys with higher surface area and catalytic activity.[25] They also reported that both Cu-Ti and Cu-Zr amorphous alloys treated with an HF solution exhibit a high activity for liquid-phase hydration of acrlonitrile, and concluded that the activity closely related with the highly homogeneous structure of amorphous alloys with skeletal Cu.[27] On the other hand, Katona *et al.* studied on the state of Cu ions in the surface by Auger electron spectroscopy. They concluded that the HF treatment of the alloys brought about Cu enrichment definitely in the surface region, and Cu^{2+} ions are mostly detected on Cu-Ti whereas Cu^0 and Cu^{2+} coexist on Cu-Zr.[26]

The alloy catalysts composed of Cu are utilized for many reactions, such as dehydrogenation of alcohols to methyl formate over Cu-Zr alloys,[28,29] and decomposition of N_2O over Cu-Ni alloys.[30]

(2) Reductive decomposition of NO_x

Since NO is thermodynamically unstable in comparison with N_2 and O_2 at low temperatures, its catalytic decomposition is expected for NO removal, which is very important in environmental catalysis science. So far, many catalysts including Cu are reported for NO decomposition. However, no suitable one of consistently high activity has been found. For the *de*NO_x catalyst containing Cu, removal of the surface oxygen and regeneration of the catalytic activity by high temperatures and/or gaseous

reductants are required.

It is known that Cu ion-exchanged zeolite catalyst, such as Cu/NaY, has a high activity for selective decomposition (or reduction) of NO,[31] because of easier regeneration of active Cu species than that of other transition-metals by thermal reduction. Iwamoto *et al.*[32] showed that Cu ion-exchanged MFI (ZSM-5) zeolites show high and steady activity for the catalytic decomposition of NO even in the presence of N_2 and O_2 in the reaction above 673K. For Cu/MFI catalyst, NO conversion is maximized at 80 - 85 % of Cu ion-exchange level, while selectivities of N_2 and O_2 are increased with an increase in Cu amount.[33,34] In addition, deactivation of Cu/MFI catalyst with 85 % ion-exchange is less seen even in the reaction at 723K than that of the samples in other exchanging levels.[33] At the same time, the studies of the NO reduction and structural analysis of active Cu sites over Cu/MFI with a reductant such as CO,[35] H_2,[36] hydrocarbons,[37,38] and NH_3[39] were reported. In this manner, many workers studied the activity relating mainly to "redox property" of Cu ions, and reported that the property strongly relates to the local structure around Cu ions in over-exchanged MFI catalysts.

As for the active species of NO reduction over Cu/MFI catalysts, some conclusions are conflicted, and more study is called for. Liu *et al.*[38] presented by Cu K-edge XANES study that the intensity of Cu^+ is strongly correlated with the activity for NO reduction. Anpo *et al.*[40] also concluded that photo-reduced Cu^+ ion is the active center for NO decomposition by the study of NO photo-reduction. On the other hand, Sachtler *et al.*[41,42] reported the existence of dispersed Cu^{2+} ions in calcined Cu/MFI with 113 % of ion-exchange level on the basis of ESR study. Cu^+ is formed during the selective NO reduction in the samples with 55 - 113 % of the ion-exchange level, and a FT-IR study revealed founding of a new species comprizing of $(Cu\text{-}O\text{-}Cu)^{2+}$ in 'over-exchanged' region. These species seems to be the active species.[42] The divalent Cu-dimer species, $(Cu\text{-}O\text{-}Cu)^{2+}$, was also postulated by Masai *et al.* on the basis of absorption band at 440 nm in the UV-VIS spectrum, which is seen for high ion-exchanged Cu/MFI treated with oxygen at 773K.[43] Thus, it is proposed that Cu^+ and $(Cu\text{-}O\text{-}Cu)^{2+}$ species are the active species for NO reduction. However, many discussions about the active species have been continued. The study of deactivation of

Cu/MFI has been reported recently. For example, Yan *et al.*[44] proposed that no gross destruction of the zeolite framework is detected by XRD and BET surface area measurements even for a catalyst which was 50% deactivated, but redistribution of isolated Cu^{2+} ions, $(Cu\text{-}O\text{-}Cu)^{2+}$ oxocations, and CuO particles is detected. These Cu^{2+} species are also seen in Cu/Al_2O_3 and dealuminated Cu/MFI after deactivation. These results may be helpful for the discussion of active Cu species, but more detailed study is called for.

Binary oxides including Cu ions also exhibit an activity for *de*NO_x reaction. Yoshida *et al.*[45] reported that copper orthovanadate ($Cu_3V_2O_8$) has a unique catalytic activity for NO reduction with NH_3. TPD and IR studies indicate that the NO reduction proceeds by a mechanism involving $(NO)_{ads}$ and $(NH_3)_{ads}$, where $(NH_4)^+$ is not present, and surface oxygen plays a role in activation of $(NO)_{ads}$.[46] This process is possibly a rare one for Cu catalysts because oxidative decomposition of NO is brought about in this process even in a low temperature.

Cu/TiO_2 and Cu/ZrO_2 has been recently reported as NO reduction catalysts by a few groups. These catalysts are also applied to other reactions such as combustion of soot particles.[47] It is expected that TiO_2 or ZrO_2-support affects the unique performance for Cu ions such as SMSI as reported by Haller *et al*,[48] and thus, redox of Cu ions is different from that on other supports. The author presents the study of the activity for NO reduction over TiO_2- and ZrO_2-supported Cu catalysts and the structural analysis of Cu active species in this thesis.

2. Cu K-edge XAFS for characterizing copper compounds

Cu K-edge XAFS study has been utilized since 1980s. In particular, XANES study is widely used as a direct method for investigating the electronic and structural nature. An empirical correlation between the valence of Cu ions and the characteristics of Cu K-edge XANES has been used to detect the presence of Cu^+. It is accepted that a post-edge peak at 8984 eV is due to electron transition in Cu^+ compounds but not to that of Cu^{2+}.[49] It is recently reported that a small degree of non-

stoichimetry affects an additional part in modifying post-edge intensity of Cu^+ as well as the coordination number and geometry.[50,51]

The assignment of XANES peaks has been discussed by many groups. Kosugi *et al.*[52] discussed the core-hole screening effect to the XANES on the basis of *ab initio* molecular orbital theory in the case of the Cu-K-edge XANES spectra of monovalent or divalent Cu oxides and chrolide. They proposed that split $4p\sigma$ and $4p\pi$ orbitals exist in Cu $4p$ orbital, and $1s$-$4p\pi$ transition gives the post-edge peaks in the XANES when $1s$-$4p\sigma$ transition is seen in higher energy as resonance peaks than $1s$-$4p\pi$.[52-54] Recently, this assignment is followed by many workers. They also discussed using the XANES spectra of divalent Cu samples that the strong core-hole (final-state) effect strongly reflects on the intensity of XANES peaks due to $1s$-$4p\sigma$ and $1s$-$4p\pi$ transitions, and the effect is negligible to the pre-peak due to $1s$-$3d$ transition.[53]

Thus, XANES spectra can be applied to characterizing Cu species in the catalysts by analyzing the spectral feature of pre-peak and post-edge peak being on the mentioned assignment. Cu K-edge XAFS studies have been carried out to clarify the structure of active Cu species for various reactions. In case of Cu/ZnO catalysts for methanol synthesis, *in situ* EXAFS study was carried out by Neils *et al.*[55] Their study revealed a gradual disappearance of a Cu-O interaction in the H_2-reduced catalyst in the course of methanol synthesis from CO, CO_2, and H_2, and indicated that highly dispersed Cu^0 is the active species. This results are the same as that reported by Vliaic *et al*,[56] who studied the *in situ* EXAFS of $Cu/ZnO/Al_2O_3$ catalyst. In this study, it was concluded that Cu exists as a metallic species at a higher temperature, while at a lower one, it forms some oxide species of two-dimentional raft-like structure.

For Cu/MFI catalysts, Liu *et al.*[57] studied the state of Cu ions during the NO decomposition by *in situ* XANES. They found that integrated intensity of post-edge peak due to Cu^+ correlates with the NO decomposition rate, suggesting the existence of Cu^+ as an active site. They also suggested that Cu^{2+} ion can be partially reduced by propene to form Cu^+ even in a strongly oxidizing environment.[38] On the other hand, the divalent oxo-species, $(Cu\text{-}O\text{-}Cu)^{2+}$, has been reported as the active species by other groups. Kuroda *et al.*[58] demonstrated the generation of Cu^+ dioxo-species by

evacuation of Cu over-exchanged mordenites at high temperatures by application of XANES and EXAFS as well as ESR and IR spectroscopies. In recent years, the structural study by XAFS has become much popular, and more detailed structural information of active Cu sites is expected.

3. UV-VIS spectroscopy for characterizing copper compounds

There are a few studies applying diffuse reflectance UV-VIS spectroscopy to the analysis of Cu species. The absorption band due to *d-d* transition of Cu^{2+} ion is observed at 600 - 820 nm in wavelength. The *d-d* transition can be observed only for $Cu^{2+}(d^9)$ ions, and the absorption band relates to the local structure of Cu^{2+} ion sensitively.[59] Cu metal fine particles of 100Å size can be characterized by UV-VIS spectroscopy, while non fine-powdered one such as Cu-foil can not be characterized because of complete reflection.[60] Curtis *et al.*[61] reported that copper particles with diameter in the range of 30 to 300 Å show an optical spectrum with a peak maximum at 560 - 640 nm.

For Cu/MFI catalysts, UV-VIS spectroscopic study was carried out by Masai *et al.*[43] In the samples of higher Cu-exchange level, the absorption bands were observed at 320, 440, and 600 nm, and the peaks at 320 and 600 nm became more intense while that at 400 nm disappeared. They pointed out that the peak at 600 nm is due to Cu^{2+} species, and other peaks at 320 and 440 nm are assigned to charge transfer band of Cu^{2+}-O and $(Cu\text{-}O\text{-}Cu)^{2+}$, respectively. The species are suggested to relate to the formation of active sites in Cu/MFI samples with 75-100 % of ion-exchange level.

4. Survey of Part 2

The characterization of active Cu species is a very important study for the elucidation of catalytic mechanisms. The studies by XAFS and UV-VIS spectroscopy give a useful information about the electronic states and local structures of Cu species. The structural analysis of finr Cu-metal species is generally difficult, but it can be done by UV-VIS spectroscopy. However, in the viewpoint of catalysis, characterization of Cu-metal species by UV-VIS spectroscopy has been scarcely

reported. It is expected that this method can be used for the analysis of active Cu-metallic species in relation to a unique effect such as SMSI, spillover, *etc.* In this thesis, the author describes the structure of active Cu species on TiO_2 and ZrO_2 as NO reduction catalysts. By means of Cu K-edge XAFS and UV-VIS spectroscopy, the local structure of active Cu species and the structural changes of the active species during the reaction are discussed. In chapter 4, the activity for NO reduction with H_2 over Cu (2 wt%) supported on TiO_2 is discussed mainly, and the structure of active Cu species is suggested tentatively. The structural study of Cu/TiO_2 with various Cu loadings by means of Cu K-edge XAFS and UV-VIS spectroscopy is presented in chapter 5, in which the local structure of active Cu species and redox performance of Cu ions are mainly discussed. Chapter 6 is concerned with the activity of Cu/ZrO_2 for NO reduction with CO under a low contact time condition in a flow reaction system as well as the structure of active Cu ions.

References

(1) Cotton, F.; Wilkinson, G. In *Adv. Inorg. Chem. (4th ed.)*; Interscience: New York, 1980, p 847.

(2) Rodriguez, J. A.; Campbell, C. T. *J. Phys. Chem.* **1987**, *91*, 6648.

(3) Satterfield, C. N. In *Heterogeneous Catalysis in Practice*; McGraw-Hill Book: New York, 1980, p 191.

(4) Belousov, V. M.; Grakhovskii, Y. B.; Rubanik, M. Y. *Kinet. Katal.* **1962**, *3*, 221.

(5) Mikhal'chenko, V. G.; Sokolovskii, V. D.; Filippova, A. A.; Davydov, A. A. *Kinet. Katal.* **1973**, *14*, 1253.

(6) Hertle, W.; Farrauto, R. J. *J. Catal.* **1973**, *29*, 352.

(7) Kobayashi, H.; Takezawa, N.; Minochi, C. *J. Catal.* **1981**, *69*, 487.

(8) Minochi, C.; Kobayashi, H.; Takezawa, N. *Chem. Lett.* **1979**, 705.

(9) Takahashi, K.; Takahashi, H.; Akazawa, T.; Takezawa, N.; Kobayashi, H. *Shokubai (Catalyst)* **1984**, *26*, 339 (in Japanese).

(10) Goto, S.; Smith, J. M. *AIChE J.* **1975**, *21*, 714.

(11) Newsome, D. S. *Catal. Rev.-Sci. Eng.* **1980**, *21*, 275.

(12) Caretto, L. S.; Nobe, K. *AIChE J.* **1969**, *15*, 18.

(13) Kakuta, N.; Kazusaka, A.; Yamazaki, A.; Miyahara, K. *J. Chem. Soc., Faraday Trans. 1* **1984**, *80*, 3245.

(14) Arai, M.; Nishiyama, S.; Tsuruya, S.; Masai, M. *J. Chem. Soc., Faraday Trans.* **1996**, *92(14)*, 2631.

(15) Morikawa, Y. *Adv. Catal.* **1993**, *39*, 303.

(16) Jenck, J.; Germain, J. E. *J. Catal.* **1980**, *65*, 141.

(17) Klier, K. *Adv. Catal.* **1982**, *31*, 243.

(18) Molnár, Á.; Smith, G. V.; Bartók, M. *Adv. Catal.* **1989**, *36*, 329.

(19) Shibata, M.; Kawata, N.; Matsumoto, T.; Kimura, H. M. *J. Catal.* **1987**, *108*, 263.

(20) Schild, C.; Woukan, A.; Baiker, A. *J. Mol. Catal.* **1990**, *63*, 243.

(21) Gasser, D.; Baiker, A. *Appl. Catal.* **1989**, *48*, 279.

(22) Yamashita, H.; Yoshikawa, M.; Kaminade, T.; Funabiki, T.; Yoshida, S. *J. Chem. Soc., Faraday Trans. 1* **1986**, *82*, 707.

(23) Baiker, A.; Baris, H.; Guntherodt, H. J. *Appl. Catal.* **1986**, *48*, 279.

(24) Yamashita, H.; Kaminade, T.; Yoshikawa, M.; Funabiki, T.; Yoshida, S. *C1 Mol. Chem.* **1986**, *1*, 491.

(25) Yoshida, S.; Kakehi, T.; Matsumoto, S.; Tanaka, T.; Kanai, H.; Funabiki, T. In *Proc. 10th Int. Congr. Catal.*, Budapest, 1992: (L. Guzzi, F. Solymosi and P. Tétényi, Eds.; Elsevier-Akadémiai Kiadó, 1992), vol. B, p 981.

(26) Katona, T.; Molnár, Á. *J. Catal.* **1995**, *153*, 333.

(27) Funabiki, T.; Yamashita, H.; Yase, M.; Omatsu, T.; Yoshida, S. *Bull. Chem. Soc. Jpn.* **1993**, *66*, 2133.

(28) Molnár, Á.; Katona, T.; Bartók, M.; Varga, K. *J. Mol. Catal.* **1991**, *64*, 41.

(29) Molnár, Á.; Katona, T.; Kopasz, C.; Hegedüs, Z. In *Proc. 10th Int. Congr. Catal.*, Budapest, 1992: (L. Guzzi, F. Solymosi and P. Tétényi, Eds.; Elsevier-Akadémiai Kiadó, 1992), vol. C, p 1759.

(30) Chen, M. I.; Cheng, C. T.; Yen, C. T. *J. Catal.* **1985**, *95*, 346.

(31) Iwamoto, M.; Yokoo, S.; Sakai, K.; Kagawa, S. *J. Chem. Soc., Faraday Trans. 1* **1981**, *77*, 1629.

(32) Iwamoto, M.; Furukawa, H.; Uemura, F.; Mikuriya, S.; Kagawa, S. *J. Chem. Soc. Chem. Commun.* **1986**, 1272.

(33) Iwamoto, M.; Yahiro, H.; Mine, Y.; Kagawa, S. *Chem. Lett.* **1989**, 213.

(34) Iwamoto, M.; Yahiro, H.; Torikai, Y.; Yoshioka, T.; Mizuno, N. *Chem. Lett.* **1990**, 1967.

(35) Jang, H. J.; Hall, W. K.; d'Itri, J. L. *J. Phys. Chem.* **1996**, *100*, 9416.

(36) Burch, R.; Scire, S. *Catal. Lett.* **1994**, *27*, 177.

(37) Bethke, K. A.; Kung, C. L.; Yang, B.; Kung, H. H. *Catal. Lett.* **1995**, *31*, 287.

(38) Liu, D.-J.; Robota, H. J. *Appl. Catal. B* **1994**, *4*, 155.

(39) Komatsu, T.; Ogawa, T.; Yashima, T. *J. Phys. Chem.* **1995**, *99*, 13053.

(40) Anpo, M.; Matsuoka, M.; Shioya, Y.; Yamashita, H.; Giamello, E.; Morterra, C.; Che, M.; Patterson, H. H.; Webber, S.; Ouellette, S.; Fox, M. A. *J. Phys. Chem.* **1994**, *98*, 5744.

(41) Lei, G. D.; Adelman, B. J.; Sárkány, J.; Sachtler, W. M. H. *Appl. Catal. B* **1995**, *5*, 245.

(42) Beutel, T.; Sárkány, J.; Lei, G.-D.; Yan, J. Y.; Sachtler, W. M. H. *J. Phys. Chem.* **1996**, *100*, 845.

(43) Itho, Y.; Nishiyama, S.; Tsuruya, S.; Masai, M. *J. Phys. Chem.* **1994**, *98*, 960.

(44) Yan, J. Y.; Lei, G. D.; Sachtler, W. M. H.; Kung, H. H. *J. Catal.* **1996**, *161*, 43.

(45) Yoshida, S.; Ueda, A.; Tarama, K. *Stud. Surf. Sci. Catal.* **1981**, *7*, 1377.

(46) Yoshida, S.; Ueda, A.; Tarama, K. *Ind. Eng. Chem. Prod. Res. Dev.* **1979**, *18*, 283.

(47) Yuan, S.; Mériaudeau, P.; Perrichon, V. *Appl. Catal. B* **1994**, *3*, 319.

(48) Haller, G. L.; Resasco, D. E. *Adv. Catal.* **1989**, *36*, 173.

(49) Kau, L. S.; Spira-Solomon, D. J.; Penner-Halm, J. E.; Hodgson, K. O.; Solomon, E. I. *J. Am. Chem. Soc.* **1987**, *111*, 6433.

(50) Lamble, G.; Moen, A.; Nicholson, D. G. *J. Chem. Soc., Faraday Trans.* **1994**, *90(15)*, 2211.

(51) Moen, A.; Nicholson, D. G.; Rønning, M. *J. Chem. Soc., Faraday Trans.* **1995**, *91(18)*, 3189.

(52) Kosugi, N.; Tokura, Y.; Takagi, H.; Uchida, S. *Phys. Rev. B* **1990**, *41*, 131.

(53) Kosugi, N.; Yokoyama, T.; Asakura, K.; Kuroda, H. *Chem. Phys.* **1984**, *91*, 249.

(54) Kosugi, N.; Kondoh, H.; Tajima, H.; Kuroda, H. *Chem. Phys.* **1989**, *135*, 149.

(55) Neils, T. L.; Burlitch, J. A. *J. Catal.* **1989**, *118*, 79.

(56) Vliaic, G.; Bart, J. C. J.; Cavigiolo, W.; Mobilio, S. *Chem. Phys. Lett.* **1980**, *76*, 453.

(57) Liu, D.-J.; Robota, H. J. *Catal. Lett.* **1993**, *21*, 291.

(58) Kuroda, Y.; Yoshikawa, Y.; Kon-no, S.; Hamano, H.; Maeda, H.; Kumashiro, R.; Nagao, M. *J. Phys. Chem.* **1995**, *99*, 10621.

(59) Schoonheydt, R. A. *Catal. Rev.-Sci. Eng.* **1993**, *35(1)*, 129.

(60) Crelghton, J. A.; Alvarez, M. S.; Weltz, D. A.; Kim, M. W. *J. Phys. Chem.* **1983**, *87*, 4793.

(61) Curtis, A. C.; Duff, D. G.; Edwards, G. D.; Jefferson, D. A.; Johnson, B. F. G.; Kirkland, A. I.; Wallace, A. S. *J. Phys. Chem.* **1988**, *92*, 2270.

Chapter 3

Reduction of NO over TiO_2 Supported Cu Catalysts

Abstract

TiO_2-supported Cu catalyst pretreated with H_2 at 473K exhibits higher activity for the conversion of NO at low temperatures than Cu supported on other supports. In the reaction at 303K, NO is reduced to N_2O. For the reaction above 323K, the conversion to N_2 is accelerated. In the process of the reduction, the NO is converted to N_2 directly, and the conversion to N_2 *via* N_2O is partly.

The samples were characterized by XANES, UV/VIS and ESR spectroscopy. The treatment of the sample with hydrogen at 473K brings about the formation of Cu metal particles and promotes the reduction of Ti ions. The extent of the reduction of TiO_2 supporting Cu is much higher than that of TiO_2 itself. NO has a role for oxidizing both Cu and Ti ion even at room temperature. On the other hand, H_2 has a role for reducing both ions. The active Cu-species is CuO particle with a Cu metal core.

Introduction

The catalytic decomposition/reduction of nitrogen monoxide (NO) is of current interest because of the significance of the removal of NO_x compounds included in exhaust gases of automobiles, power stations, *etc.* It is recognized recently that copper is one of the most effective materials to catalyze a *de*NO_x reaction. Cu-encapsulated zeolite such as ion-exchanged Cu/ZSM-5 catalyzes NO reduction at relatively low temperatures.[1,2] In addition, Cu/ZSM-5 and Cu/SiO_2 have been found to decompose NO to N_2 and O_2 by photo-exitation of the Cu by Anpo *et al.*[3,4] The characterization of the Cu/ZSM-5 catalyst has been carried out by means of ESR,[5,6] FT-IR,[5-7] STEM,[8] XANES,[9] EXAFS[10] and so on. For these catalysts, it is possibly concluded that a cuprous ion, Cu^+, plays a significant role in the catalytic decomposition and/or reduction of NO. It has been known that Cu and its oxide is fairly active for N_2O decomposition.[11] In these examples, the redox performance of Cu may be highlighted. Such activity of Cu also relates to the kind of support. In this study, we choose TiO_2 as a support, because TiO_2 is a material which is reduced easily to form Ti^{3+} even by thermal treatment *in vacuo*[12,13] and it is expected that TiO_2 has a great effect on supported metals as found in the SMSI systems.

In fact, there have been some reports that *de*NO_x reaction takes place on TiO_2-supported transition metal ion. Thampi *et al.*[14] reported that Ru/TiO_2 has an activity for NO-CO reaction to produce CO_2, N_2O and N_2 at low temperatures above 423K, and N_2O decomposition is enhanced by addition of Rh and Cu. In this report, they proposed that a copper ion possibly acts as an active center for N_2O decomposition. However, the role of Cu ions on TiO_2 for decomposition of NO and/or N_2O is still left unclear.

In the present paper, we report the NO reduction with H_2 over Cu/TiO_2 at fairly low temperatures and discussed the active sites of the catalysts by ESR, UV/VIS and Cu *K*-edge XANES spectroscopies.

Experimental

Preparation of the Catalyst Samples. Supported copper catalysts were prepared by impregnation of powdery metal oxide supports with an aqueous solution of $Cu(NO_3)_2 \cdot 3H_2O$ (Nacalai Tesque, GR). The used supports were TiO_2 (P25, Degussa), SiO_2 synthesized from $Si(OC_2H_5)_4$[15], Al_2O_3 (JRC-ALO-4), ZnO (synthesized from $Zn(NO_3)_2 \cdot 6H_2O$) and MgO (Merck). These supports had been calcined at 773K prior to impregnation. The amount of loading Cu is 2 wt% (321 μmol/g-support) for each sample. The impregnating solution was stirring at 353K for about 8 h to evaporate water and dried for overnight, followed by calcination at 773K for 3 h. Before the reactions and measurements, each catalyst sample was evacuated at 473K for 1 h. Reduction of the samples was carried out by the treatment with 100 Torr of hydrogen at the given temperatures for 1 h, removing the produced water in a liquefied N_2 cold trap. After the reduction, the samples were heated at the same temperature *in vacuo* for 1 h.

Reaction of NO with Cu-Catalysts. The 100 mg of the catalyst sample was placed in reaction vessels (44.1 or 129.6 cm^3), and then the reactant gas including ^{15}NO (or $^{15}N_2O$) was introduced. After 1 h passed, the composition of product was analyzed with a quadrupole-type mass spectrometer (ULVAC Massmate-100). The fragment and sensitivity of the ion signals were estimated by analyses of authentic compounds. Through all the analyses, $^{15}NO_2$ or $^{15}NH_3$ were not detected as products and only $^{15}N_2$ and $^{15}N_2O$ were detected.

X-ray Absorption Spectra at Cu K-edge. The measurement of Cu *K*-edge XANES and EXAFS spectra were carried out by a facility of BL-7A station with a Si(111) double crystal (d = 3.1355Å) monochromator at Photon Factory in the National Laboratory for High Energy Physics (KEK-PF) with 2.5 GeV of a ring energy and 150-190 mA of stored current in a fluorescence mode at room temperature. The samples after the treatment were transferred to a film for packing into a dry nitrogen purged globebox, and set for the measurement.

Diffuse Reflectance UV/VIS Spectroscopy. The UV/VIS spectra for the powdery samples were recorded in a diffuse reflectance mode at room temperature with a Perkin-Elmer LAMBDA-19 spectrometer, using an *in situ* cell.

Table 1 Results of NO reduction with H_2 at 303K for 1 h.[a)]

Sample	Treatment	Conversion[b)] /%	Selectivity / %	
			N_2O	N_2
Cu/TiO_2	473K evac.[c)]	28	100	0
	473K red.[d)]	58	100	0
Cu/Al_2O_3	473K evac.	7	100	0
	473K red.	19	84	16
Cu/SiO_2	473K red.	0	-	-
TiO_2	473K red.	4	0	100

a) Reactant is ^{15}NO (28 μmol) and H_2 (28 μmol).

Reaction vessel is 44.1 cm^3.

b) Based on NO.

c) Pretreated *in vacuo* for 1 h.

d) Pretreated with H_2 (100 Torr) for 1 h, and evacuated for 1 h.

ESR Spectroscopy. The ESR spectra (X-band) were recorded at 123 K with a JEOL JES-SRE2X spectrometer. The reference of Mn^{2+}-MgO was used for the determination of *g*-values. The sample after the treatment was placed on an *in situ* cell made of quartz, and put the sample cavity for the measurement.

Results and Discussion

(1) Reduction of NO with Cu-Catalysts

Table 1 shows the results of the reaction of NO and H_2 (28mmol, respectively) over Cu-catalysts at 303K for 1 h. Evidently, the Cu/TiO_2 exhibited the highest activity amongst the supported Cu samples. In case of TiO_2-supported Cu catalyst pretreated *in vacuo* at 473 K, the conversion of NO was 28 %. The activity of this sample was raised to 58 % conversion of NO by pretreatment with H_2 at 473K. The main product was N_2O.

Fig. 1 shows the conversion of NO at 303 K over the Cu/TiO_2 sample pretreated at various temperatures with H_2. NO conversion activity increased with an increase with the pretreatment temperature up to 473K. Pretreatment at more than 473K, the activity decreased. The optimum pretreatment temperature was found to be around 473K.

The results of the reaction at 473K are given in Table 2. Non-supported copper oxide samples, Cu_2O and CuO, were almost inactive for NO reduction. For the Cu/TiO_2 pretreated with H_2 at 473K, conversion of NO reaches 100% and N_2 is selectively produced without N_2O opposite to the reaction at 303 K. The other supported Cu-samples, Cu/SiO_2, Cu/ZnO and Cu/MgO, exhibit low activity for the NO reduction, even under pretreatment with H_2 at 473K. Only a Cu/Al_2O_3 exhibits a relatively higher reactivity than the other supported-Cu samples, except for Cu/TiO_2. However, the selectivity of N_2 is still 87% and N_2O remains. Therefore, it is concluded that TiO_2-supported Cu pretreated with H_2 at 473K shows the highest activity for NO reduction. In fact, in this reaction condition, NO conversion reaches 100% at 15 min

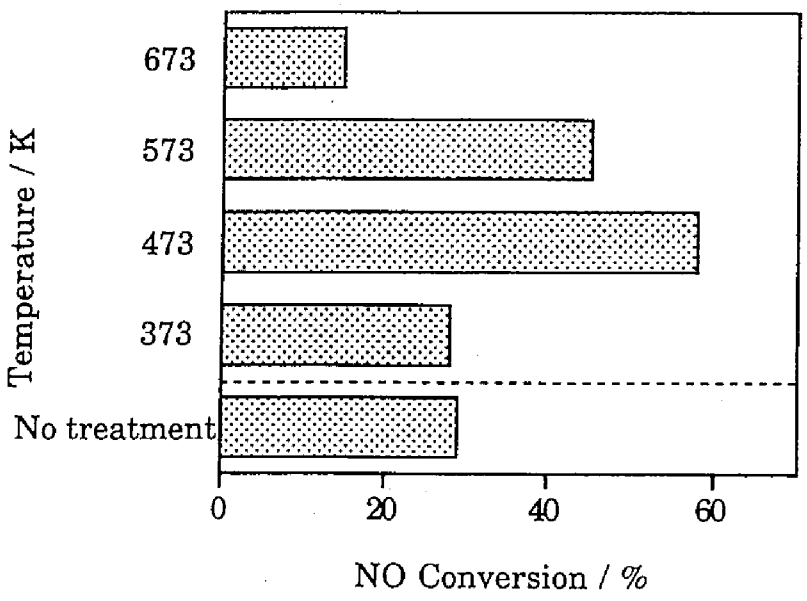

Fig. 1 Effect of H_2 pretreatment temperature upon activity of NO reduction with H_2 at 303K.

Table 2 Results of NO reduction with H_2 at 473K for 1 h.

Sample[b]	Treatment	Conversion[c] /%	Selectivity / mol%	
			N_2O	N_2
CuO		0	-	-
Cu_2O		2	50	50
Cu		15	17	83
Cu/SiO_2	473K red.[d]	30	15	85
Cu/Al_2O_3	473K evac.[e]	74	80	20
	473K red.	99	13	87
Cu/MgO	473K evac.	2	100	0
	473K red.	9	41	59
Cu/ZnO	473K evac.	1	100	0
	473K red.	6	16	84
Cu/TiO_2	473K evac.	71	58	42
	473K red.	100	0	100
TiO_2	473K red.	11	0	100

a) Reactant : NO 28 μmol, H_2 28 μmol.
Reaction vessel 41.1 cm^3.
b) Catalyst : 0.1 g.
c) Based on NO.
d) Pretreated with H_2 (100 Torr) for 1 h, and evacuated for 1 h.
e) Pretreated *in vacuo* for 1 h.

Table 3 Successive reactions of NO with H_2 over Cu/TiO_2 (pretreated with H_2 at 473K) reacted at 373K.[a]

Run	Conversion / %	TN[b] mol/mol
1st	100.0	1.8
2nd	85.0	1.6
3rd	68.4	1.3

a) Catalyst 0.1 g. Reacted at 373K for 1 h.
NO 58 μmol, H_2 58 μmol. ; Reaction vessel 85.5 cm^3.
The reactor was evacuated (not treatedwith H_2) between each reaction.
b) Turnover number; number of converted NO molecules per a Cu atom.

from the start of the reaction, as mentioned below.

The successive reaction of NO and H_2 (58 mmol, respectively) was carried out at 373K over Cu/TiO_2 pretreated with H_2 at 473K, to examine whether or not the reaction catalytically takes place. The result is shown in Table 3. Turnover number (TN, the ratio of converted NO molecules to Cu atom/ions included) is 1.8 at the first run, and the TN is kept to be 1.3 at the third run. The result indicates that the reaction takes place catalytically at above 373K.

(2) Effect of the Reaction Temperature upon Activity and Selectivity

Fig. 2 shows the conversion of NO and selectivity of N_2O and N_2 in the reaction of NO with H_2 at various temperatures for 1 h over Cu/TiO_2 pretreated with H_2 at 473K. The NO conversion is almost 100 % at the reaction temperatures above 323K. On the other hand, the selectivity of reduced products, N_2O and N_2, varied with reaction temperature. At 303K, the product is only N_2O and N_2 is not detected at all. In case of the reactions at the temperature up to 323K, the formation of N_2 was observed. At 473K, N_2O was not formed and only N_2 is produced. These results suggest that NO is completely reduced to N_2 at the higher reaction temperature. The N_2O is likely to be an intermediate toward N_2 and it requires high temperature to reduce N_2O.

(3) Time Course of the Reaction at 473K

To clarify the reaction process of NO reduction with H_2, time course of the reaction was investigated. The reaction profile at 473K over Cu/TiO_2 is shown in Fig. 3. After 60 min from the start of the reaction, NO completely disappeared and only N_2 was detected as shown in Table 2. In the initial stage of the reaction, however, the formation of N_2O was observed. The composition of N_2O increased during the first 5 min and decreased after 10 min. This result suggests that N_2O is produced as an intermediate in the path way to N_2. On the other hand, at the time when N_2O decreased, NO was consumed almost completely and more than 70 % of consumed NO

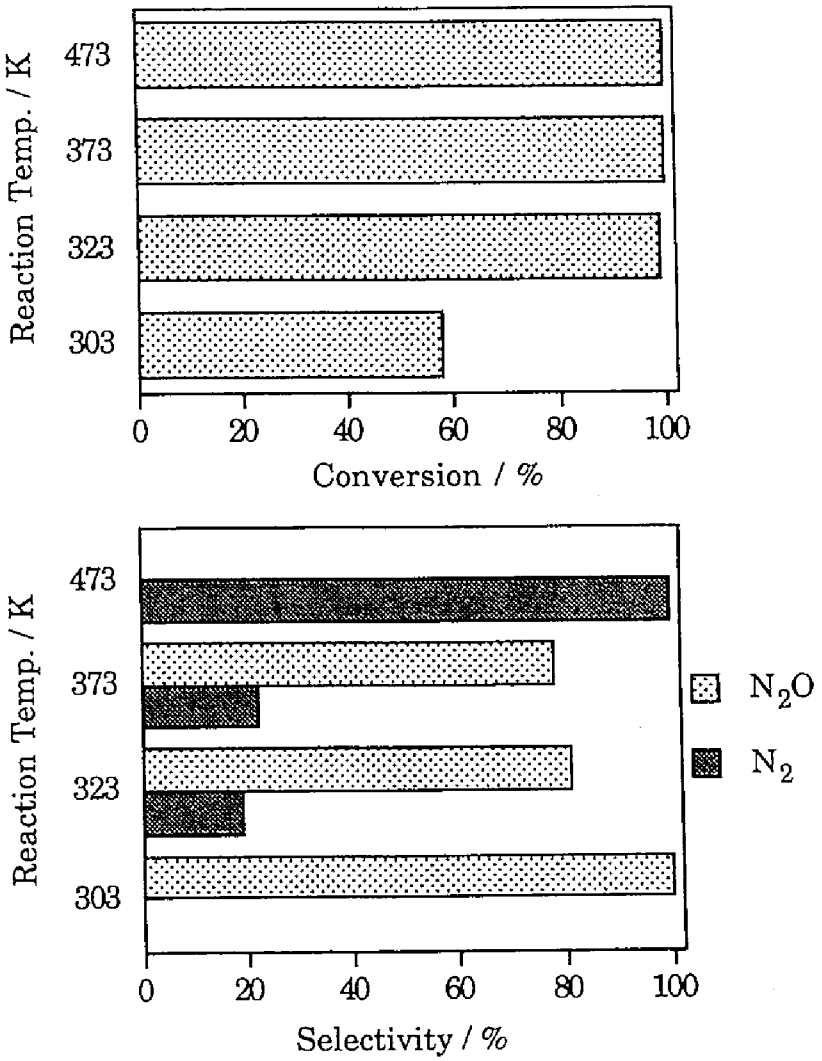

Fig. 2 Effect of the reaction temperature upon activity and selectivity over Cu/TiO_2.
Catalyst 0.1 g; pretreated with 100 Torr H_2 at 473K.
Reactant NO (28 μmol) + H_2 (28 μmol).
Reacted for 1 h.

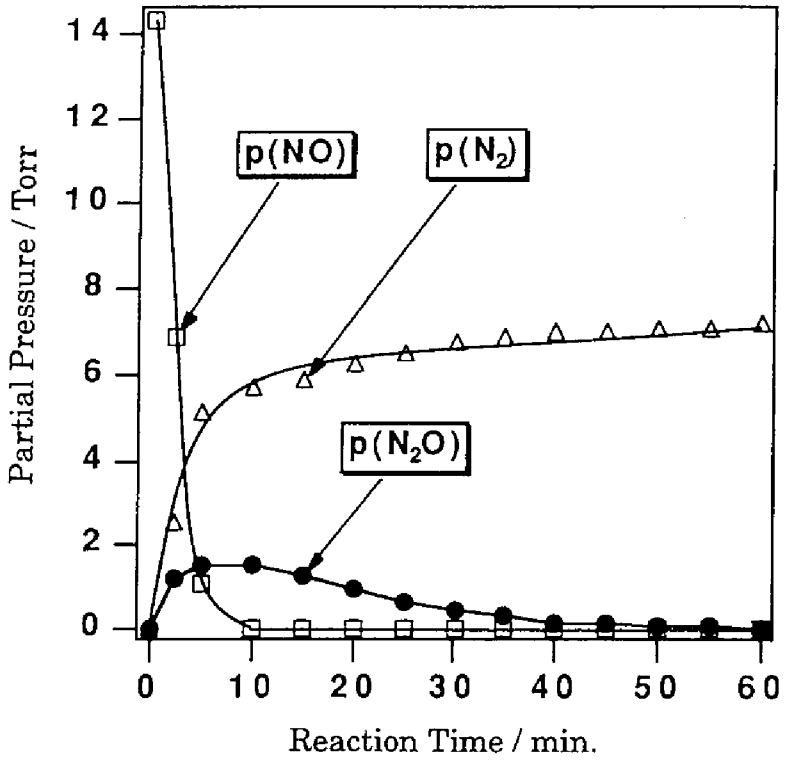

Fig. 3 Time course of the reaction of NO with H_2 over Cu/TiO_2 (pretreated with H_2 at 473K) reacted at 473K. Catalyst 0.1 g; Reactant NO (28μmol) + H_2 (28μmol).

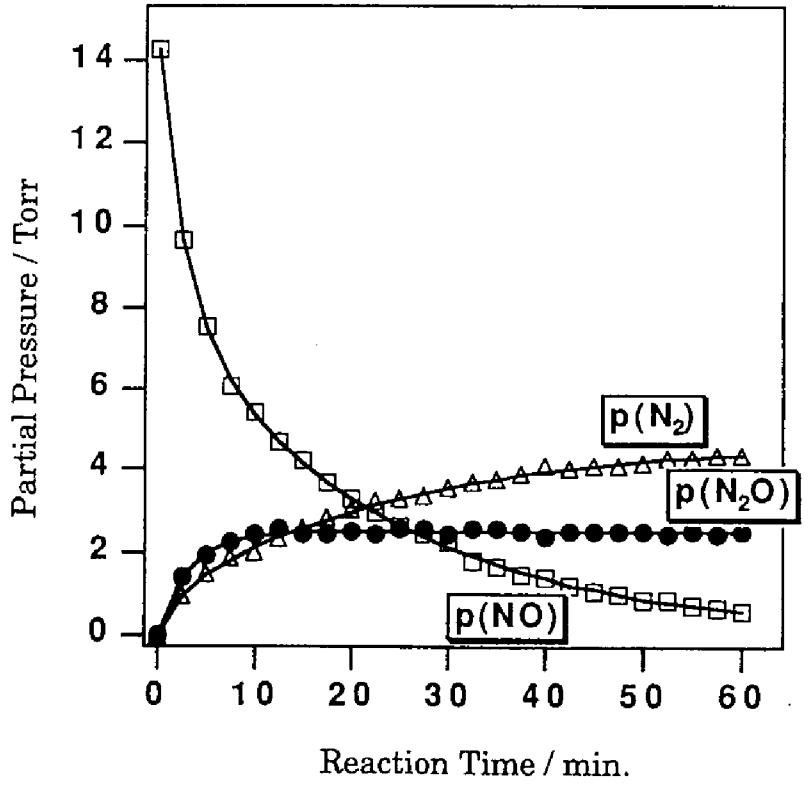

Fig. 4 Time course of the reaction of NO with H_2 over Cu/TiO_2 (pretreated with H_2 at 473K) reacted at 473K. Catalyst 0.02 g; Reactant NO (28μmol) + H_2 (28μmol).

was converted to N_2. This strongly suggest that there is another direct path from NO toward N_2 and this reaction path is faster than that including N_2O as an intermediate.

In order to examine the initial stage of the reaction more in detail, we carried out the reaction under another condition. Fig. 4 shows the time course of the reaction carried out using much less amount of the catalyst sample (0.02 g), one fifth of the amount of the catalyst in Fig. 3. In this profile, it is found that the formation rate of N_2O was not so sluggish as that of N_2 in the initial period of the reaction. N_2 was formed in paralell with the formation of N_2O. The composition of N_2O was apparently constant after 10 min from the start of the reaction. During through this period, the rate of decrease of NO is twice of the rate of the formation of N_2. This shows that whether that the formation rate and anihilation rate of N_2O are the same or that NO is directly and stoichiometrically converted to N_2 in the coexistence of N_2O in the gas phase. At 60 min, NO almost disappeared in the gas phase but still the amount of N_2O in the gas phase kept constant. It is unlikely that steady state lasts very long in the closed system. Therefore, in order to examine the behavior of N_2O contacting with Cu/TiO_2, the reaction of N_2O with H_2 was carried out.

The activity of N_2O reduction to N_2 over pretreated Cu/TiO_2 with H_2 at 473 K is shown in Fig. 5. When the reaction temperature was 303K, no formation of N_2 was observed. At 373K, an induction period for the conversion of N_2O into N_2 is seen, and the conversion level of N_2O reached 31 % after 1 h contact. In case of the reaction at 473 K, N_2O was completely converted to N_2 within 5 min. This result shows that N_2O is converted to N_2 very fast at 473 K and this may relate to the selectivity of N_2O and N_2 shown in Fig. 2. However, in the coexistence of N_2O and NO, the first step should be competing adsorption of both gas molecules and the behavior of N_2O may be different. As shown in Fig. 6, we carried out the reaction of N_2O in the presence of NO with H_2. Evidently, decrease rate of NO is much faster. After disappearance of N_2, the decrease rate of N_2O is slow despite the sufficient H_2 reductant still remained. This clearly shows that NO is converted not mainly via. N_2O intermediate but directly to

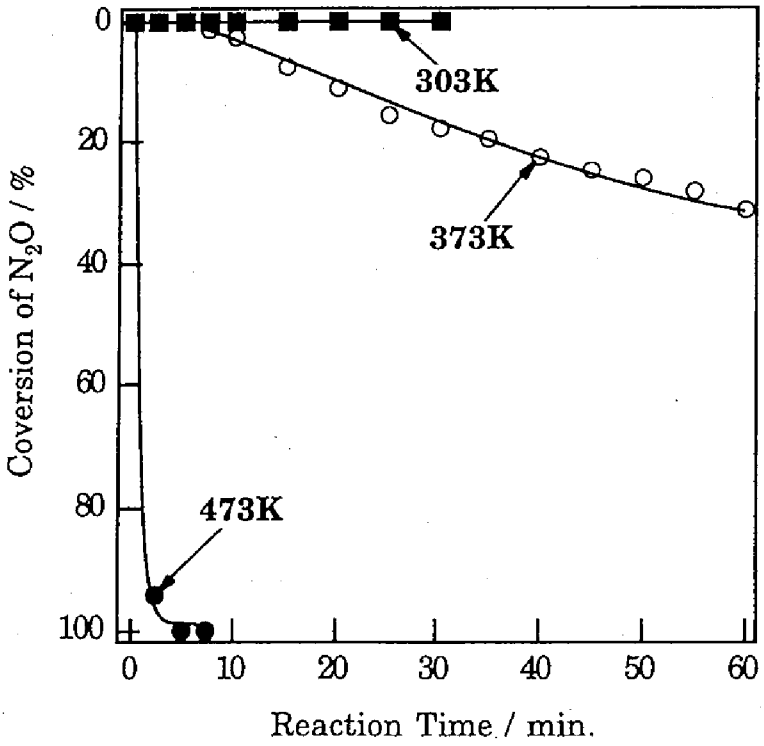

Fig. 5 Time course of the conversion of N_2O at various reaction temperatures over Cu/TiO_2 pretreated with H_2 at 473K.
Catalyst 0.1 g; Reactant N_2O (28μmol) + H_2 (28μmol).

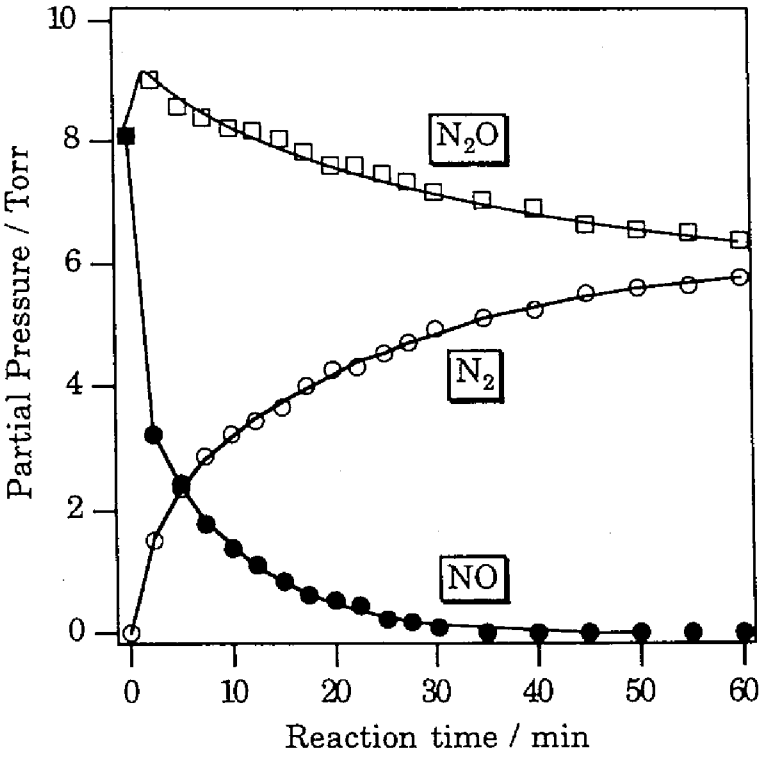

Fig. 6 Time course of the reduction of ($NO+N_2O$) mixed gases with H_2 over Cu/TiO_2 (pretreated with H_2 at 473K) reacted at 473K.
Catalyst 0.02 g;
Reactant NO (14μmol)+N_2O (14μmol)+H_2 (28μmol).

N_2. In the presence of NO, adsorption of N_2O is interfered and even after disapearance of N_2, the reduction rate of N_2O is slow possibly due to the formation of water molecules during the reduction of NO. We can conclude that the dominant reaction of NO in contact with Cu/TiO_2 in the presence of H_2 is direct conversion to N_2 and the path *via.* N_2O intermediate is minor.

(4) XANES Spectra at Cu K-edge

Cu K-edge XANES spectra of authentic Cu-samples are shown in Fig. 7, and those of Cu/TiO_2 samples are shown in Fig. 8. In the case of Cu metal, the shoulder peak in edge absorption is seen at 8980.0 eV and in the case of Cu_2O, a sharp shoulder-peak is found at 8981.7 eV, a larger energy position than that for Cu metal. For the samples of CuO, $Cu(OH)_2$ and $Cu(CH_3COO)_2$ which have Cu^{2+} ions, each shoulder peak has relatively small intensity, and the these peaks exist at larger energy positions than that found for Cu and Cu_2O. But the peaks at post edge positions of these samples including Cu^{2+} are different from each other.

For the samples of non-treated Cu/TiO_2 with H_2, a feature of the spectrum is similar to $Cu(OH)_2$ or $Cu(CH_3COO)_2$, indicating that Cu^{2+} ions mainly exists. By the treatment with H_2 at 473K, the XANES profiles are evidently changed to similar one to that of Cu metal. Thus, it is noteworthy that Cu ion on TiO_2 is easily reduced to form a structure of Cu-metal particle. After admission of NO at 303K, the spectral feature is still similar to that for Cu-metal. However, the shoulder peak shifted to high energy side and the peak just beyond the edge absorption became more prominent. This suggests Cu species are partially oxidized. The spectral feature characteristic to that for the Cu-metal almost disappeared by NO admission at 473K and the spectrum got similar to that for CuO. Thus, the NO admission at 473K brings about the oxidation of supported Cu completely. On the other hand, for the sample in contact with NO and H_2 at 473K, the XANES spectrum has a few components. The two shoulder peaks are present at the absorption edge. The one of the peaks suggests the presence of Cu-metal and the other is possibly due to the presence of the oxidized

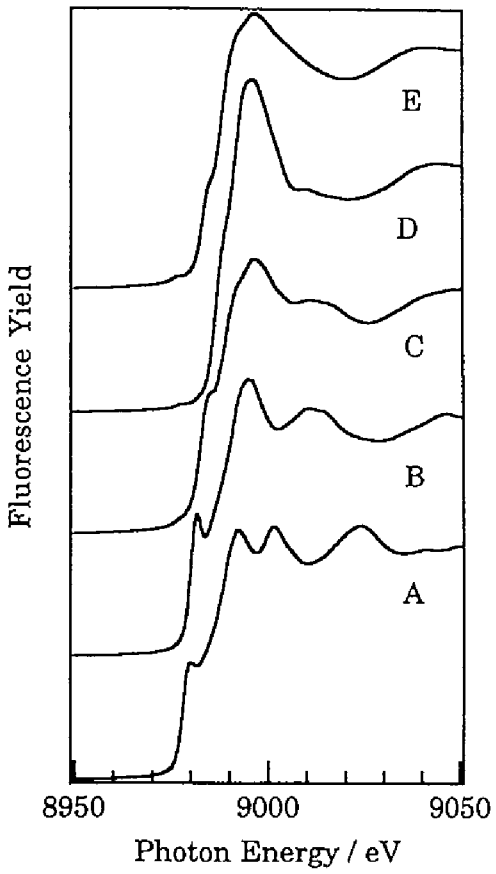

Fig. 7 Cu K-edge XANES spectra of authentic samples;
(A) Cu metal, (B) Cu_2O, (C) CuO,
(D) $Cu(OH)_2$ and (E) $Cu(CH_3COO)_2$.

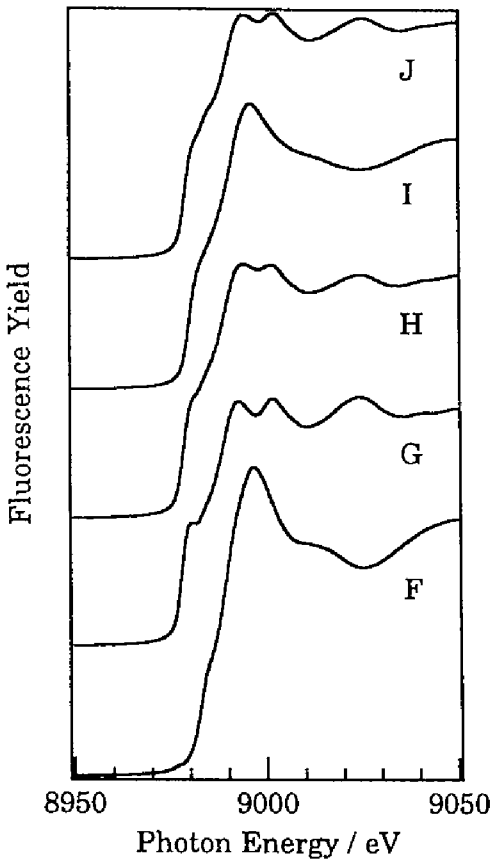

Fig. 8 Cu K-edge XANES spectra of Cu/TiO_2 (2wt% as Cu). The treatment is as follows;
(F) 473K evacuated.
(G) Treated with H_2 at 473K prior to admittion.
(H) NO admitted to sample (G) at 303K.
(I) NO admitted to sample (G) at 473K.
(J) NO+H_2 admitted to sample (G) at 473K.

Cu-species. It is noteworthy that a small peak is observed just before the edge absorption and is so called a pre-peak due to 1*s* - 3*d* electron transition, indicating that the Cu has a *d*-hole. This strongly suggests that oxidized Cu-species is divalent and the Cu ions are located at a center of a rectangular of four oxygen atoms like the cations in CuO.[16-18] The sample in this condition catalyzes the reduction of NO with H_2. Although monovalent Cu ions are often postulated to be active species in NO reduction/decomposition, divalent Cu cations are the one in the present case. It is concluded that Cu-metal is present prior to admission of NO and H_2 and after admission of NO at 473K, the Cu is oxidized to Cu^{2+}-species to some extent. However, Cu-metal species still remains in a working state.

(5) Diffuse Reflectance UV/VIS Spectra

The UV/VIS spectra were recorded in a diffuse reflectance mode. Fig. 9 shows the spectra of Cu/TiO_2 samples pretreated with H_2 at 473K. In the range of the wavelength between 200 and 400 nm, the absorption bands mainly due to ligand to metal charge transfer (LMCT) of Ti-O are seen. For the sample prior to admission of NO, the narrow peak centered at 582 nm is observed. This absorption is due to the presence of a fine particle of Cu metals particle sizing 100 - 300 Å, as reported by Crelghton *et al.*[19] and Curtis *et al.*[20] in the study of copper colloids. This is consistent with the results of XANES, *i.e.*, Cu metal particles are formed by reduction with H_2 at 473K. After admission of NO over the sample at room temperature, the absorption at 582 nm disappeared and a broad band centered at 702 nm is exhibited. This absorption is not observed for metal microclusters but observed for $Cu(CH_3COO)_2$ and $Cu(OH)_2$ due to *d-d* transition of octahedrally coordinated Cu^{2+}-ions. This indicates that Cu-metal is easily oxidized in the surface layer by admission of NO and H_2 at room temperature, and formed a Cu^{2+}-species. After admission of NO and H_2 at 473K, the absorption band due to Cu^{2+}-species is also seen similarly to the case at room temperature. Therefore after admission of NO and H_2, Cu-species is not metallic in the surface layer but oxidized Cu^{2+}-species formed. This is inconsistent with the

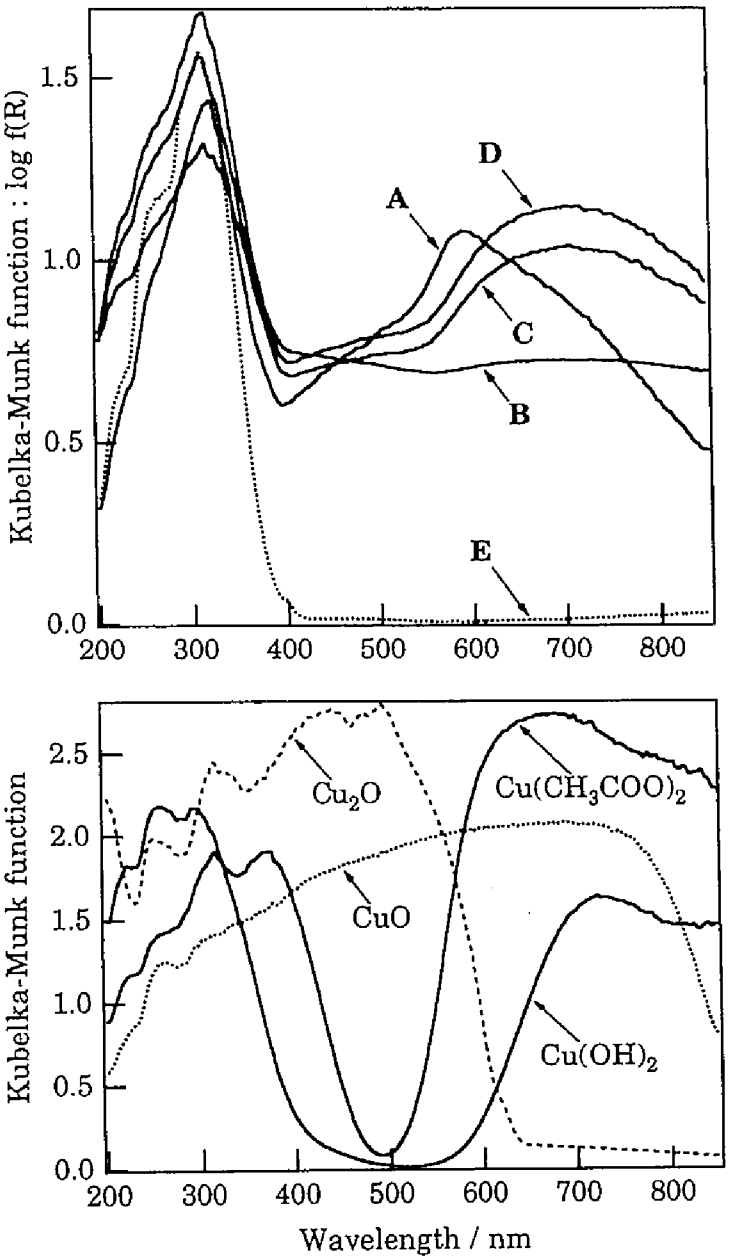

Fig. 9 Diffuse reflectance UV/VIS spectra of Cu/TiO_2 (upper side) and authentic Cu-samples (lower side). The Cu/TiO_2 samples after the each treatments are as follows;

(A) Treated with H_2 at 473K prior to admission.
(B) NO admitted to sample (A) at room temperature.
(C) $NO+H_2$ admitted to sample (A) at room temperature.
(D) $NO+H_2$ admitted to sample (A) at 473K.
(E) TiO_2 treated with H_2 at 473K.

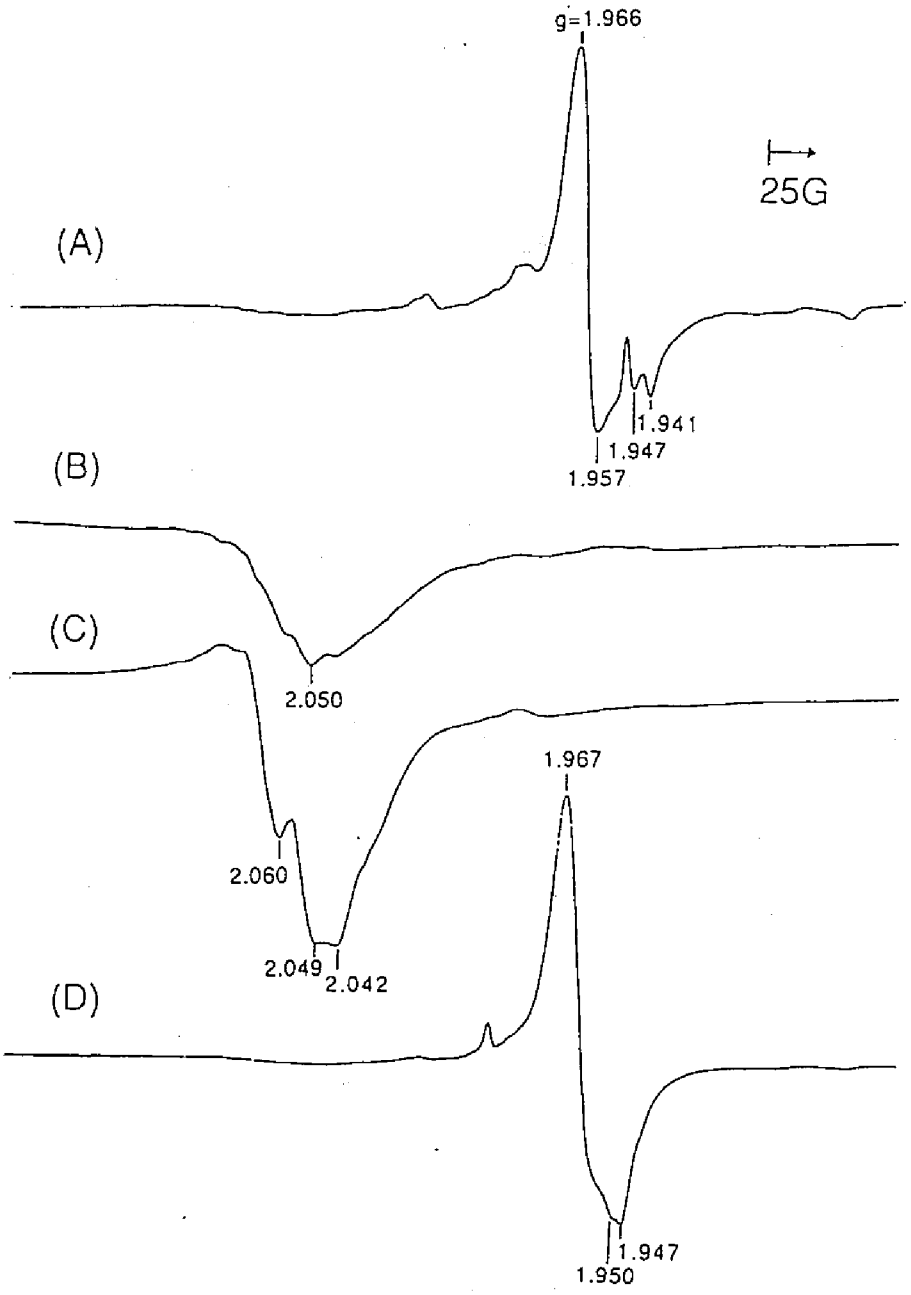

Fig. 10 ESR spectra of Cu/TiO_2 (2wt% Cu) recorded at 123K.
(A) Treated with H_2 at 473K prior to admission.
(B) After admission of sample (A) with $NO+H_2$ at room temperature.
(C) After admission of sample (A) with $NO+H_2$ at 473K.
(D) Re-treated of sample (C) with H_2 at 473K.

result from XANES. If UV/VIS spectra afford the information of the surface layer, Cu metal is covered with a fairly thick CuO layers. Therefore, active Cu species is possibly CuO particle with a Cu-metal core.

(6) ESR Spectra

The ESR spectra of Cu/TiO_2 pretreated samples are shown in Fig. 10. In the case of the samples pretreated with H_2 at 473K, no signals due to Cu-species were recorded, but Ti^{3+} signal is seen with g=1.966 on top[21]. It is concluded that Cu ion of these samples exists mainly as an ESR silent species like Cu^0 and/or Cu^+ ions and Ti ions included TiO_2-support are partly reduced to Ti^{3+} ions. The signal intensity of Ti^{3+} ions is obtained *ca.* 20 times that of TiO_2 reduced with H_2 at 473K, indicating that Ti ions of TiO_2 is reduced much easier with H_2 by loading Cu. For the sample in contact with NO and H_2, the Ti^{3+} signal disappeared and a signal due to Cu^{2+} appeared. This result shows that the admission of NO brings about oxidation of both Ti and Cu ions. This supports the results of XANES and UV/VIS spectra. In the case of the sample in contact with NO and H_2 at 473K, the Cu^{2+} signal became more intense, and the hyperfine structure by Cu^{2+} ion became clear. After treatment of the latter sample with H_2 at 473K, the Ti^{3+} signal restored. From these results, it is concluded that Cu and Ti ions are easily oxidized and reduced by NO and H_2. We expect that this redox performance of these ions plays a significant role in the NO reduction.

Acknowledgment

This work is partially supported by a grant-in-aid (No. 07242103) from the Japan Ministry of Education, Science, Sports and Culture. The X-ray absorption measurements were performed under the approval of the Photon Factory (KEK-PF) Program Advisory Committee (Proposal No. 94G205).

References

(1) Iwamoto, M.; Yahiro, H.; Mine, Y.; Kagawa, S. *Chem. Lett.* **1989**, 213.

(2) Iwamoto, M.; Furukawa, H.; Uemura, F.; Mikuriya, S.; Kagawa, S. *J. Chem. Soc. Chem. Commun.* **1986**, 1272.

(3) Negishi, N.; Matsuoka, M.; Yamashita, H.; Anpo, M. *J. Phys. Chem.* **1993**, *97*, 5211.

(4) Anpo, M.; Matsuoka, M.; Shioya, Y.; Yamashita, H.; Giamello, E.; Morterra, C.; Che, M.; Patterson, H. H.; Webber, S.; Ouellette, S.; Fox, M. A. *J. Phys. Chem.* **1994**, *98*, 5744.

(5) Giamello, E.; Murphy, D.; Magnacca, G.; Morterra, C.; Shioya, Y.; Nomura, T.; Anpo, M. *J. Catal.* **1992**, *136*, 510.

(6) Lei, G. D.; Adelman, B. J.; Sárkány, J.; Sachtler, W. M. H. *Appl. Catal. B* **1995**, *5*, 245.

(7) Iwamoto, M.; Yahiro, H.; Mizuno, N.; Zhang, W.; Mine, Y.; Furukawa, H.; Kagawa, S. *J. Phys. Chem.* **1992**, *96*, 9360.

(8) Zhang, Y.; Leo, K. M.; Sarofim, A. F.; Hu, Z.; Flytzani-Stephanopoulos, M. *Catal. Lett.* **1995**, *31*, 75.

(9) Liu, D.-J.; Robota, H. J. *Appl. Catal. B* **1994**, *4*, 155.

(10) Hamada, H.; Matsubayashi, N.; Shimada, H.; Kintaichi, Y.; Ito, T.; Nishijima, A. *Catal. Lett.* **1990**, *5*, 189.

(11) Hugo, P. In *Proc. 4th Europ. Symp. on Chem. React. Eng.*; Brussels, 1968; pp 459.

(12) Hattori, H.; Itoh, M.; Tanabe, K. *J. Catal.* **1975**, *38*, 172.

(13) Tanaka, T.; Kumagai, H.; Hattori, H.; Kudo, M.; Hasegawa, S. *J. Catal.* **1991**, *127*, 221.

(14) Thampi, K. R.; Ruterana, P.; Grätzel, M. *J. Catal.* **1990**, *126*, 572.

(15) Yoshida, S.; Matsuzaki, T.; Kashiwazaki, T.; Mori, K.; Tarama, K. *Bull. Chem. Soc. Jpn.* **1974**, *47*, 1564.

(16) Kau, L. S.; Spira-Solomon, D. J.; Penner-Halm, J. E.; Hodgson, K. O.; Solomon, E. I. *J. Am. Chem. Soc.* **1987**, *111*, 6433.

(17) Kau, L. S.; Hodgson, K. O.; Solomon, E. I. *J. Am. Chem. Soc.* **1989**, *111*, 7103.

(18) Kosugi, N.; Kondoh, H.; Tajima, H.; Kuroda, H. *Chem. Phys.* **1989**, *135*, 149.

(19) Crelghton, J. A.; Alvarez, M. S.; Weltz, D. A.; Kim, M. W. *J. Phys. Chem.* **1983**, *87*, 4793.

(20) Curtis, A. C.; Duff, D. G.; Edwards, G. D.; Jefferson, D. A.; Johnson, B. F. G.; Kirkland, A. I.; Wallace, A. S. *J. Phys. Chem.* **1988**, *92*, 2270.

(21) Qin, D.; Chang, W.; Chen, Y.; Zhou, J.; Chen, Y.; Gong, M. *J. Catal.* **1993**, *142*, 719.

Chapter 4

Study of Active Cu Species of Cu/TiO_2 for NO reduction by means of Cu K-edge XAFS and UV-VIS Spectroscopy

Abstract

The active species of Cu supported on TiO_2, which were prepared by impregnation method with cupric nitrate and acetate, is investigated by means of Cu *K*-edge XAFS. The XAFS and UV-VIS spectra showed that the H_2 pretreatment of the samples at 473K brings about the formation of Cu^0 micro particles with several hundred Angstroms of particle size, and the particle on TiO_2 prepared from cupric acetate is more stable than that from cupric nitrate. It is concluded that the Cu^0 particle with pertinent size, which coexists with cations such as Cu^{2+}, is the active species for NO reduction.

Introduction

Development of a catalytic system for removing nitrogen oxides, NO_x, is an important problem in environmental catalysis. It is well known that supported and ion-exchanged Cu catalysts are active for *de*NO_x reaction. For instance, Cu-ion-exchanged ZSM-5 is one of the most reactive catalysts as reported by many workers. The active species for the reaction have been characterized recently by FT-IR,[1-6] ESR,[2-4] STEM,[7] XAFS[8-10], *etc.* Although, the reaction mechanism and mobility of Cu ions in the reaction are proposed in these studies, they are conflicting with each other. The reaction mechanism of *de*NO_x reaction and the structure of reactive Cu-species have been studied so far, and more detailed study is called for. It is widely accepted that Cu^+ ions stabilized strongly in the cation hole of ZSM-5 play a major role in selective decomposition of NO through Cu^+-dinitrosyl species as a pathway,[1,6] whereas the Cu-dimer species, $(Cu\text{-}O\text{-}Cu)^{2+}$, also plays a role for the active species, as reported by several groups.[2,10,11] Thus, the characterization of active Cu species for *de*NO_x reaction has been in progress.

However, it is generally accepted that redox performance of Cu ions relates to the catalytic activity. In case of supported Cu catalysts, the redox of Cu ions correlates strongly to the support. If the oxide-support is easily affected by the redox treatment, it is expected that the redox mobility of Cu ions is more enhanced. In the present study, TiO_2-supported Cu (Cu/TiO_2) catalysts are chosen, because Ti ions in TiO_2 are easily reduced to Ti^{3+} even by thermal treatment *in vacuo* at more than 573K.[12] In fact, it is reported that the Cu/TiO_2 catalyst has high reactivities for selective oxidation of ammonia,[13] and combustion of soot particles.[14] In this manner, TiO_2 has a peculiar effect on supported Cu ions, and this effect is expected to bring about the high reactivity for the *de*NO_x reaction.

We have studied the catalytic reactivity for reduction of NO with H_2 over supported Cu catalysts reacted in a closed system. In the previous report,[15] it is found that Cu/TiO_2 has a higher reactivity for reduction of NO at 473K than Cu supported on other oxides. For the characterization of Cu/TiO_2 by ESR, XANES, and UV-VIS spectroscopy, it is also found that both Cu and Ti ions are reduced easily by the

treatment with hydrogen at 473K to form reduced ions, and Cu ions on TiO_2 is stabilized as a small metal particles after the treatment.[15] However, the correlation between the local structure and/or valence of Cu ions and catalytic reactivity is still unclear. In order to clarify the structure of Cu ions which act as an active species for NO reduction, Cu *K*-edge XAFS study is presented in this paper. By obtaining an information of local structure around Cu ions, we discuss about the effect of TiO_2 support and structural changes of Cu ions on TiO_2 during the reaction.

Experimental

Preparation of the Samples. Supported Cu samples are prepared by the method as follows. The samples were obtained by impregnation of TiO_2 (P25, Degussa) with an aqueous solution of cupric nitrate ($Cu(NO_3)_2 \cdot 3H_2O$) or cupric acetate ($Cu(CH_3CO_2)_2 \cdot 4H_2O$), and followed by drying at 353K and calcination at 773K for 3 h. The TiO_2 support was calcined at 773K prior to impregnation. The loading amount is 1 - 8 wt% as Cu for each sample. Reduced samples were carried out by the treatment with 100 Torr of H_2 at 473K for 1 h after evacuation at the same temperature. As pretreatment before each reaction or measurement, the sample was evacuated at 473K for 1 h. The reaction of NO with supported Cu-catalysts was carried out in a closed system as described in the previous paper.[15]

Measurement of X-ray Absorption Spectra at Cu K-edge. The Cu *K*-edge XANES / EXAFS spectra were collected by a facility of BL-7C station at Photon Factory in the National Laboratory for High Energy Physics (KEK-PF), with 2.5 GeV of ring energy and 250 - 360 mA of stored current, in a fluorescence mode at room temperature. The measurements, Si(111) double crystal monochromator (d = 3.13551Å) was used. Incident X-ray flux and fluorescent emission were measured with ionization chambers in which 100 % nitrogen and 100 % argon gases, respectively, are flowing at 1 atm. The reduced and/or used samples were moved to the polyethylene bag and the bag was sealed in the golve box filled with Ar gas to prevent the sample from exposing to air.

Computational analyses for the spectra were performed with the FACOM M1800 computer system at the Data Processing Center of Kyoto University. Each spectrum

Table 1 Effect of pretreatment temperature on activity of NO reduction with H_2 over 2 wt% Cu/TiO_2.[a]

Sample	H_2 pretreatment temperature / K	NO conversion / %	
		reacted at 303K[a]	reacted at 473K[b]
Cu/TiO_2 from nitrate	none	28	57
	373	44	70
	473	91	76
	573	78	75
	673	15	72
Cu/TiO_2 from acetate	none	8	44
	373	47	77
	473	75	75
	573	36	76
	673	12	76

[a] Catalyst 0.1 g. Reacted for 1 h.
[b] Reactant : NO and H_2 (28 μmol, each).
[c] Reactant : NO and H_2 (88 μmol, each).

Table 2 Effect of Cu-loading on activity and selectivity for NO reduction over Cu/TiO_2 (pretreated with H_2 at 473K).[a]

Sample (Cu loading)	NO conversion / %	N_2 selectivity / %
Cu/TiO_2 from nitrate		
1 wt%	34	76
2 wt%	76	89
4 wt%	82	94
6 wt%	81	94
8 wt%	83	95
Cu/TiO_2 from acetate		
1 wt%	51	78
2 wt%	75	93
4 wt%	78	92
6 wt%	83	98
8 wt%	82	98

[a] Catalyst : 0.1 g. ; Reactant : NO and H_2 (88 μmol, each). Reacted at 473 K for 1 h.

was normalized to the height of the McMaster curve which is an approximation of absorption by a free atom after removal of the contribution from absorptions other than the *K*-edge absorption, as described elsewhere.[16] The k^3-weighted EXAFS spectra were obtained from normalized EXAFS spectra, and Fourier-transformations were performed within the range Δk = 3 - 12 $Å^{-1}$ without any phase shift correction. Curve-fitting analyses were performed with the empirical parameters extracted from Cu foil for Cu-Cu shells and from Cu_2O for Cu-O shells.

Measurement of UV-VIS spectroscopy. UV-VIS spectra were recorded in a diffuse reflectance mode at room temperature with a Perkin-Elmer LAMBDA-19, using an *in situ* cell.

Results and Discussion

(1) Comparison between Cu/TiO_2 prepared from nitrate and acetate on reactivity for NO reduction.

In our previous report,[15] it is shown that TiO_2-supported Cu (2 wt% as Cu) catalyst prepared from nitrate and pretreated with H_2 at 473K exhibits higher activity for the NO reduction than Cu supported on other supports, such as Al_2O_3, SiO_2, MgO, and ZnO. As for the pretreatment temperature with H_2, it has been found that 473K is the optimum temperature for NO reduction at 303 K.[15]

The relation between reactivity for NO reduction and H_2 treatment temperature over the Cu/TiO_2 samples prepared from cupric nitrate and acetate was investigated. The result is shown in Table 1. In case of the reaction at 303K, NO conversion is maximized when H_2 pretreatment temperature is 473K in the samples prepared from nitrate and acetate. It suggests that 473K is also the optimum temperature for NO reduction over the samples from acetate, and reactivity is similar to that over the samples from nitrate. However, in the reaction at 473K, NO conversion (88 μmol of NO) is kept 70 - 76 % over both samples from nitrate and acetate in the H_2 pretreatment temperature range 373 - 673K.

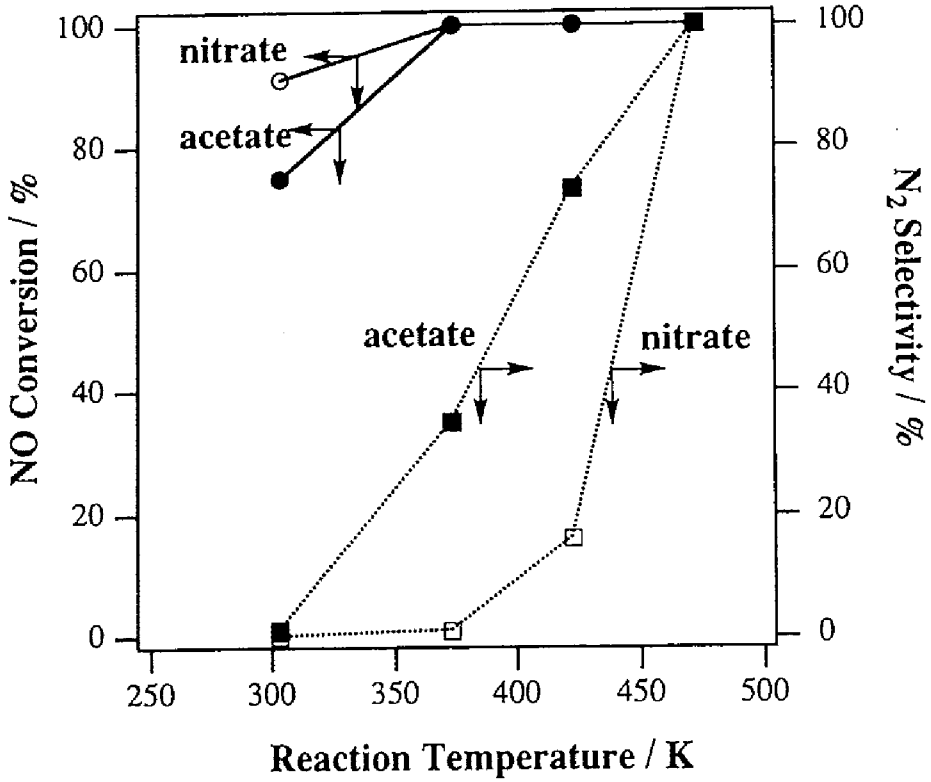

Fig. 1 Relationship between reaction temperature and the activity on NO reduction over 2 wt% Cu/TiO_2 prepared from cupric nitrate and acetate.

Catalyst 0.1 g. Pretreated with H_2 at 473K.
Reactant NO and H_2 (28 μmol, each). Reacted for 1 h.

and acetate with 2 wt% Cu loading (315 μmol•(g-sample)$^{-1}$ as Cu) is shown in Table 4. The reactions take place catalytically. It is deduced that the decrease of activation for the sample from acetate is less than that for the sample from nitrate by successive reaction. It also suggests that the sample from acetate possess more appropriate reactivity for NO reduction than that from nitrate, and the active species for NO reduction is different between these samples.

(2) Cu K-edge XAFS Study of Cu / TiO_2

In our previous report,[15] it is concluded in 2 wt% Cu/TiO_2 samples prepared from nitrate that the treatment with hydrogen at 473K brings about the formation of Cu metal particles and promotes the reduction of Ti ions studied by XANES, UV-VIS and ESR spectroscopies. The extent of the reduction of TiO_2 supporting Cu is much higher than that of TiO_2 itself. NO has a role for oxidizing both Cu and Ti ions even at room temperature, and H_2 has a role for reducing both ions. It is revealed that the active Cu-species of Cu/TiO_2 from nitrate is CuO particle with a Cu metal core.

To compare the structure of Cu species between the samples prepared from nitrate and acetate, local structure around Cu ions and/or metals are investigated by means of Cu *K*-edge XANES/EXAFS. The XANES spectra of 2 wt% Cu/TiO_2 samples from nitrate are shown in Fig. 3. For the sample before the pretreatment with H_2, the spectrum is almost similar to that of $Cu(OH)_2$, indicating that Cu species on TiO_2 exist as Cu^{2+} ions centered in oxygen octahedra. After the treatment with H_2 at 473K, the spectrum can be attributed to Cu metal.[15] In comparison with the spectra of 4 wt% Cu/TiO_2 sample from nitrate, they are similar to those for 2 wt% sample before and after the pretreatment. After pretreatment with H_2, total spectral feature for both the samples is of that for Cu metals. However, the careful observation of the peaks at the absorption edge tells the presence of oxide. The peaks are not so well resolved as those for Cu metal due to overlapping the peaks due to oxide phase. These peaks for 4 wt% sample are unclearer than those for 2 wt% sample, indicating that the spectrum of 4 wt% sample has a smaller intensity of Cu metal than that of 2 wt% sample. This is rationallized by the difference spectrum as shown in Fig. 3. The spectrum was obtained by subtration of the spectrum for 2 wt% sample multiplied by 0.8 from the

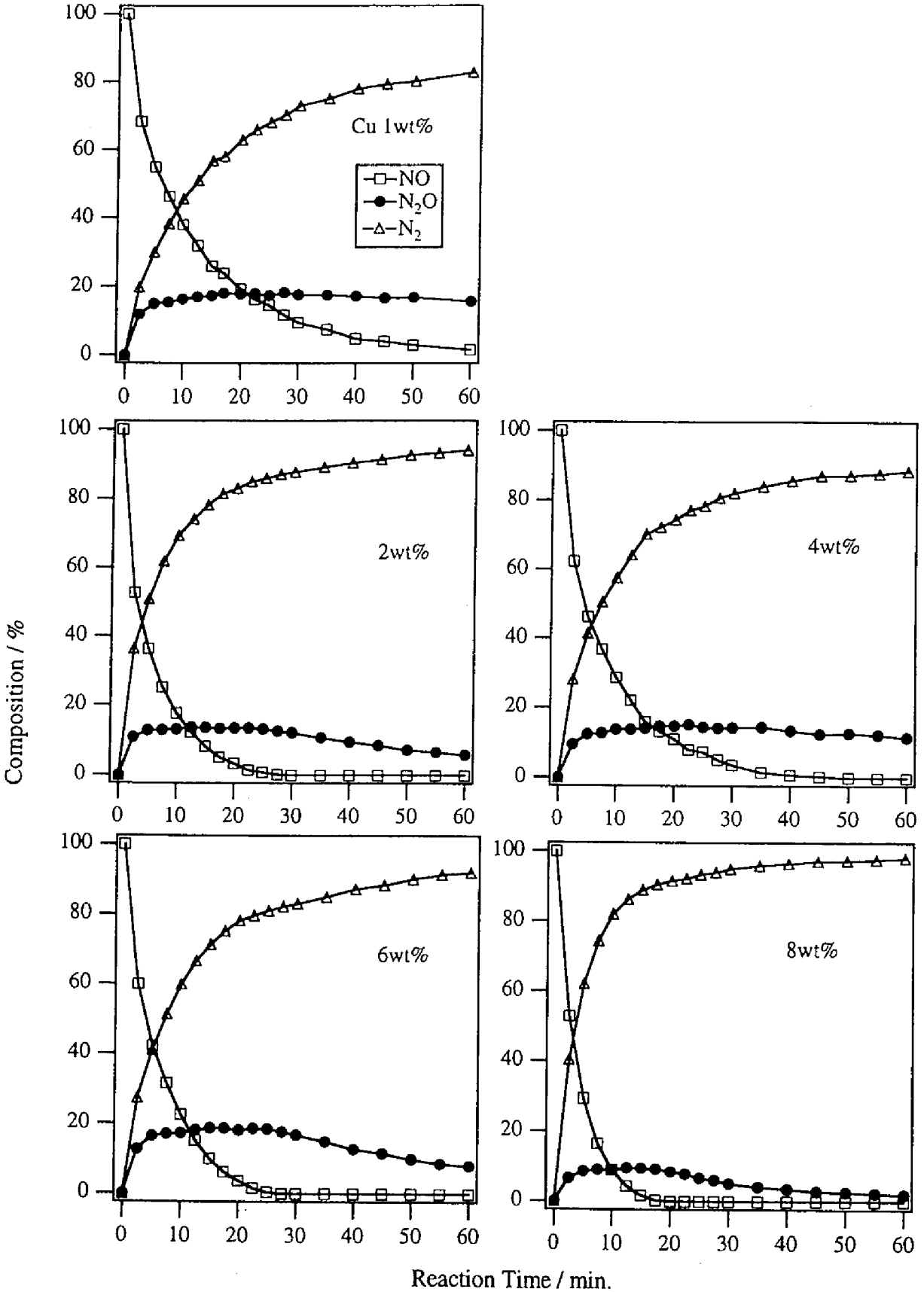

Fig. 2a Time courses of NO reduction with H_2 over Cu/TiO_2 prepared from nitrate with various Cu loading.

Reactant NO and H_2 (65 μmol, each). Reacted at 473K.

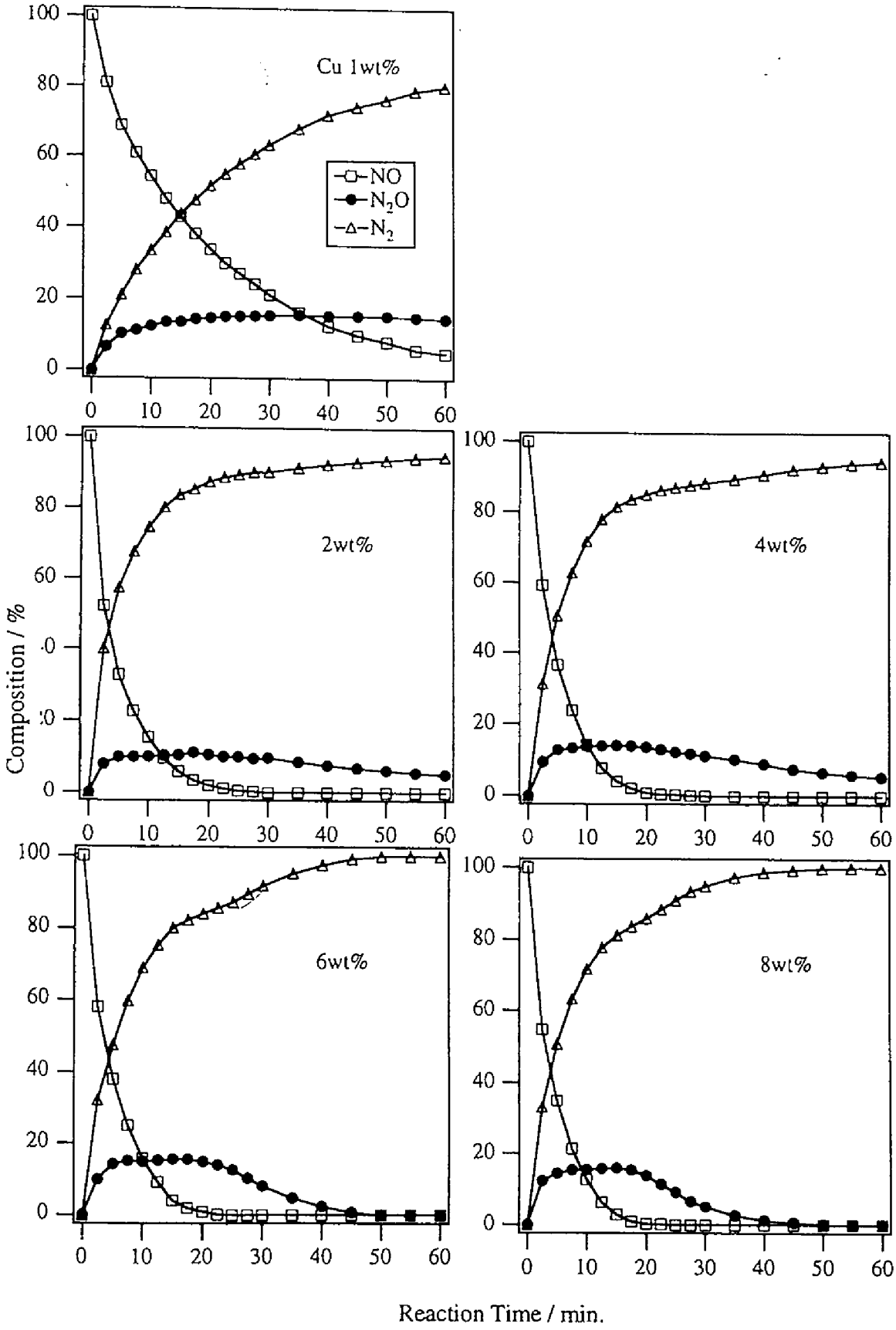

Fig. 2b Time courses of NO reduction with H_2 over Cu/TiO_2 prepared from acetate with various Cu loading.

Reactant NO and H_2 (65 μmol, each). Reacted at 473K.

Table 3 Effect of Cu-loading on activity and selectivity for NO reduction over Cu/TiO_2 (pretreated with H_2 at 473K) in the initial stage.[a]

Sample (Cu loading)	NO conversion / %	N_2 selectivity / %
Cu/TiO_2 from nitrate		
1 wt%	29	43
2 wt%	47	77
4 wt%	34	61
6 wt%	40	68
8 wt%	47	86
Cu/TiO_2 from acetate		
1 wt%	32	62
2 wt%	48	84
4 wt%	41	77
6 wt%	42	76
8 wt%	45	73

[a] Catalyst : 0.1 g. ; Reactant : NO and H_2 (55 μmol, each). Reacted at 473K for 2.5 min.

Table 4 Successive reactions of NO with H_2 over 2 wt% Cu/TiO_2 from nitrate and acetate (pretreated with H_2 at 473K).[a]

run[b]	NO conversion / %	
	from nitrate	from acetate
1st	76	75
2nd	62	70
3rd	50	61

[a] Catalyst 0.1 g. Reacted at 473K for 1 h. Reactant NO and H_2 (88μmol, each).

[b] The reactor was evacuated (not treated with H_2) at 473K between each reactions.

formation and the reaction path *via.* N_2O intermediate is minor.

For the samples from nitrate as shown in Fig. 2-1, the NO consumption rate at the initial stage decreased with an increase in Cu loading amount less than 8 wt%. The results of reactivity in the initial stage (reacted for 2.5 min.) are shown in Table 1. In comparison between various Cu loading samples in 1 - 6 wt%, 2 wt% Cu-loading sample exhibits the highest activity for both NO conversion and N_2 selectivity. In case of 8 wt% sample, the rate of NO conversion is the same as that for 2 wt% one. However, it can be considered that the reaction in 8 wt% sample includes a non-catalytic one. Thus, it suggests that the sample with 2 wt% Cu is relatively the most active for NO reduction to produce N_2. On the other hand, for the samples from acetate, the NO consumption rates at the initial stage are higher those that of the samples from nitrate in the whole range of Cu loading amounts. In addition, composition of N_2O at the initial stage is smaller than that of the samples from nitrate, as shown in Table 3. These results indicate that the samples from acetate are more active for NO reduction to N_2 than those from nitrate. In comparison between the samples from acetate with various Cu-loading, 2 wt% sample exhibits the highest activity for both NO conversion and N_2 selectivity. This result is similar to that for the samples from nitrate. In case of the samples from acetate with 6 and 8 wt% Cu, selectivity to N_2 reached 100 % after 50 min from starting the reaction. For these samples, NO is perfectly consumed within 20 min from starting the reaction. After disappearance of NO, converting N_2O to N_2 is significantly faster than in case of other samples from acetate with lower Cu content, while it is not clear whether or not N_2 is produced catalytically. In case of the samples from acetate with higher Cu loadings, the formation of N_2O is larger and the reduction of N_2O is faster after disappearance of NO. From these results, it is summarized that the samples prepared from acetate exhibit more appropriate reactivity for NO reduction to produce N_2 than those from nitrate. Higher amount of Cu loading (6 - 8 wt%) shows lower activity for NO reduction to N_2 and/or N_2O but higher activity for N_2O reduction to N_2 than lower amount of Cu loading (1 - 4 wt%). 2 wt% sample exhibits a highest activity in the initial stage of the reaction.

The result of the successive reaction of NO and H_2 over the samples from nitrate

and acetate with 2 wt% Cu loading (315 μmol·(g-sample)$^{-1}$ as Cu) is shown in Table 4. The reactions take place catalytically. It is deduced that the decrease of activation for the sample from acetate is less than that for the sample from nitrate by successive reaction. It also suggests that the sample from acetate possess more appropriate reactivity for NO reduction than that from nitrate, and the active species for NO reduction is different between these samples.

(2) Cu K-edge XAFS Study of Cu / TiO_2

In our previous report,[15] it is concluded in 2 wt% Cu/TiO_2 samples prepared from nitrate that the treatment with hydrogen at 473K brings about the formation of Cu metal particles and promotes the reduction of Ti ions studied by XANES, UV-VIS and ESR spectroscopies. The extent of the reduction of TiO_2 supporting Cu is much higher than that of TiO_2 itself. NO has a role for oxidizing both Cu and Ti ions even at room temperature, and H_2 has a role for reducing both ions. It is revealed that the active Cu-species of Cu/TiO_2 from nitrate is CuO particle with a Cu metal core.

To compare the structure of Cu species between the samples prepared from nitrate and acetate, local structure around Cu ions and/or metals are investigated by means of Cu *K*-edge XANES/EXAFS. The XANES spectra of 2 wt% Cu/TiO_2 samples from nitrate are shown in Fig. 3. For the sample before the pretreatment with H_2, the spectrum is almost similar to that of $Cu(OH)_2$, indicating that Cu species on TiO_2 exist as Cu^{2+} ions centered in oxygen octahedra. After the treatment with H_2 at 473K, the spectrum can be attributed to Cu metal.[15] In comparison with the spectra of 4 wt% Cu/TiO_2 sample from nitrate, they are similar to those for 2 wt% sample before and after the pretreatment. After pretreatment with H_2, total spectral feature for both the samples is of that for Cu metals. However, the careful observation of the peaks at the absorption edge tells the presence of oxide. The peaks are not so well resolved as those for Cu metal due to overlapping the peaks due to oxide phase. These peaks for 4 wt% sample are unclearer than those for 2 wt% sample, indicating that the spectrum of 4 wt% sample has a smaller intensity of Cu metal than that of 2 wt% sample. This is rationallized by the difference spectrum as shown in Fig. 3. The spectrum was

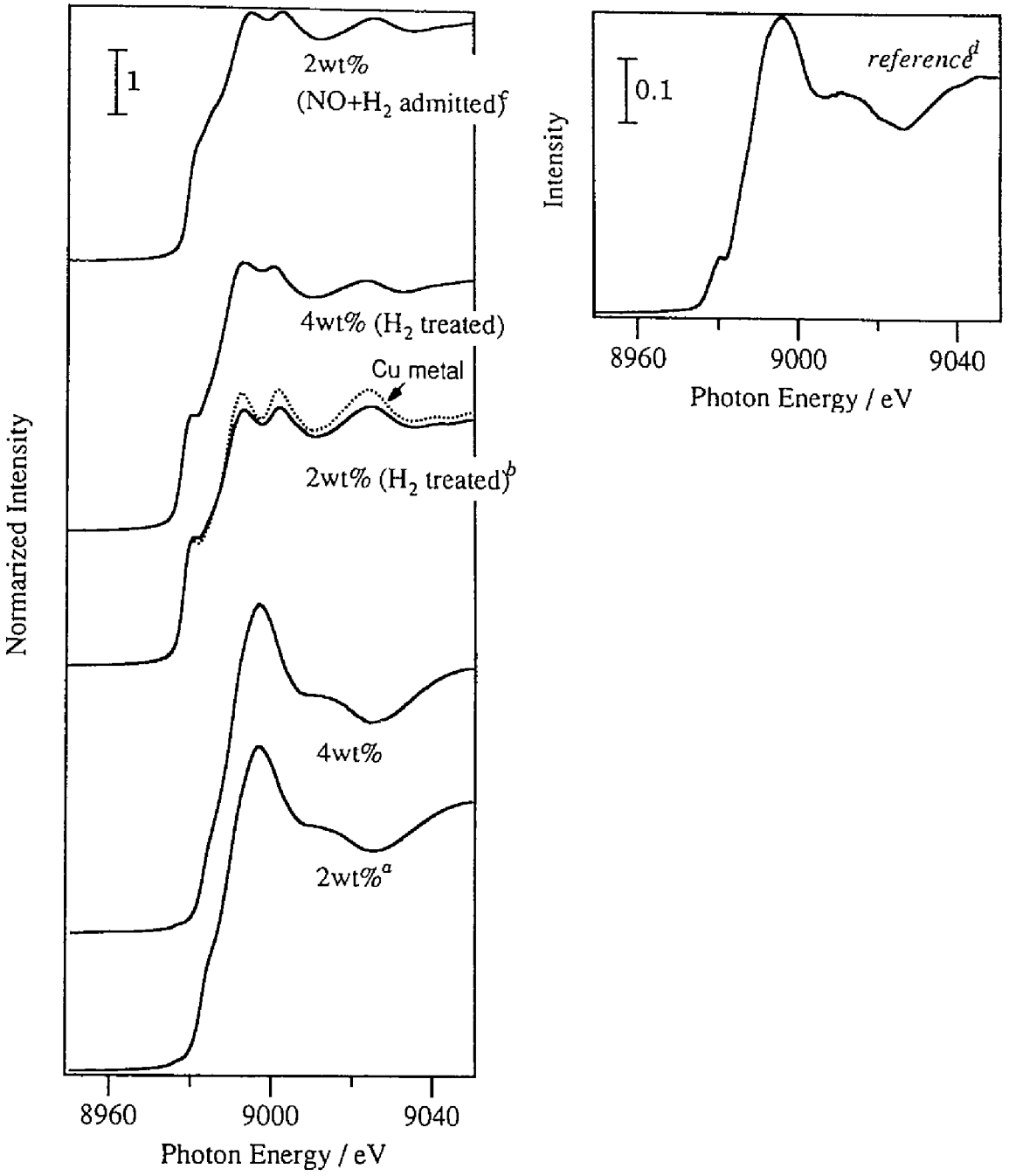

Fig. 3 Cu K-edge XANES spectra of Cu/TiO_2 samples prepared from nitrate.

a calcined at 773K.

b treated with H_2 at 473K for 1 h.

c after admission of ($NO+H_2$) to sample *b* at 473K for 1 h.

d reference spectrum : {(4wt% H_2 treated) - (2wt% H_2 treated) x 0.8}.

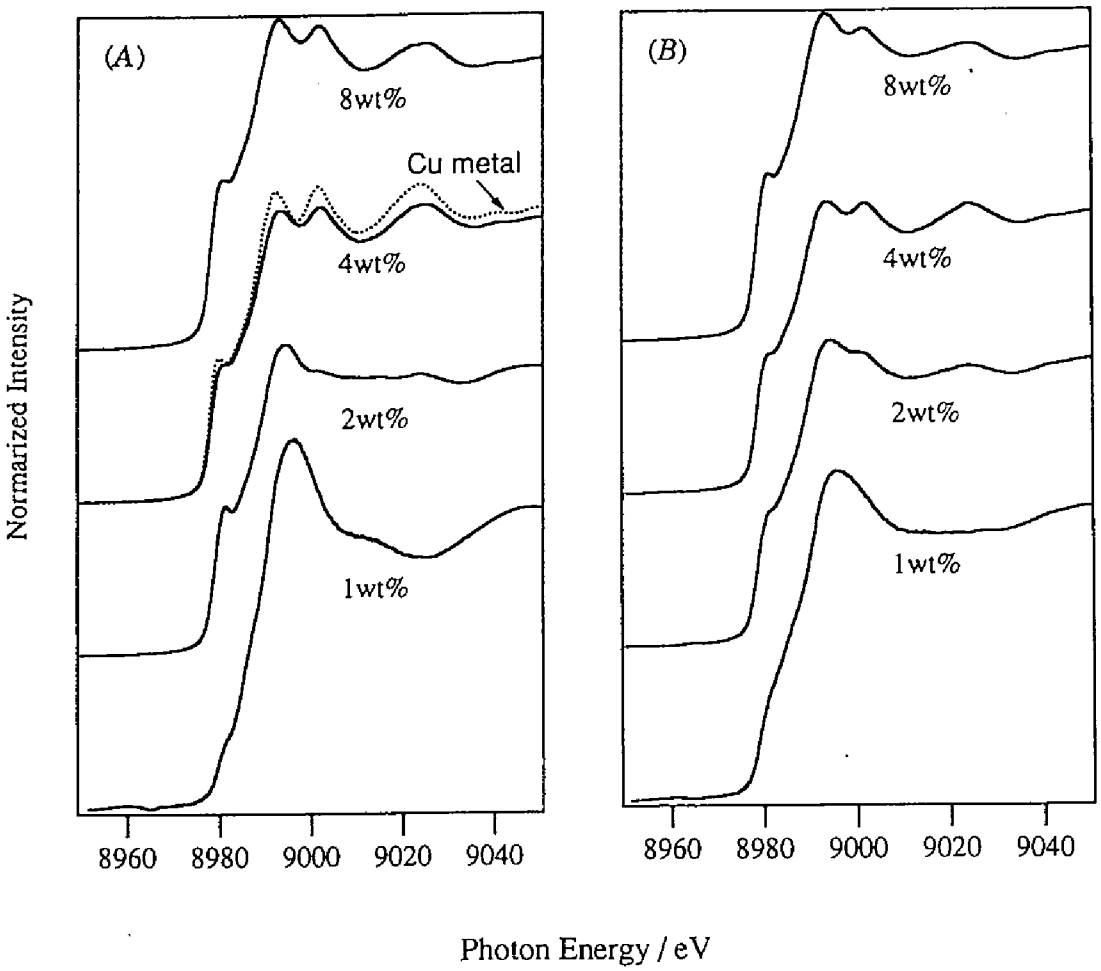

Fig. 4 Cu K-edge XANES spectra of Cu/TiO_2 samples from acetate treated with H_2 at 473K (*A*) and after admission of ($NO+H_2$) to sample *A* at 473K (*B*).

obtained by subtration of the spectrum for 2 wt% sample multiplied by 0.8 from the spectrum for 4 wt%. The feature of the difference spectrum is that of oxide phase, indicating that the fraction of Cu^0 in the spectrum of pretreated 2 wt% sample is higher than that of pretreated 4 wt% sample. It suggests that the Cu ions in 2 wt% sample is reduced to Cu^0 more easily than those in 4 wt% sample in this condition of H_2 treatment. In our previous paper,[15] it was proposed by XANES study that Cu metal species are oxidized by admission of NO even at room temperature to form octahedrally coordinated Cu^{2+} species by admission of NO at 473K. In case of the samples after admission of (NO + H_2) mixed gases, the spectrum in Fig. 3 suggests the coexistence of Cu metal and its oxidized ions, indicating that Cu metal species are partially oxidized by the admission.

The spectra for the samples from acetate pretreated with H_2 at 473K are shown in Fig. 4. For 1 - 2 wt% of Cu loading, the spectra can be attributed to a mixture of Cu^{2+} ions and Cu^+ and/or Cu^0. The spectral feature around post-edge peak (due to electron transition of 1*s* - 4*p*π[17]) is very similar to $Cu(OH)_2$ but position of adsorption threshold is lower than that for Cu^{2+}, resulting the lack of pre-edge peak (due to 1*s* - 3*d* transition[18]). However, for the spectrum of 2 wt% Cu sample, the energy position of post-edge peak is the same as that for Cu metal, suggesting that Cu^0 and Cu^{2+} ions coexist. In comparison between the samples prepared from nitrate and acetate in 2 wt% of Cu loading, although, the H_2 treatment brings about the reduction of Cu ions in both samples, Cu metals are not definitely formed in the sample from acetate but in the sample from nitrate. It is directed that Cu ions in the sample from nitrate is reduced easier than those in the sample from acetate. The spectra of 4 - 8 wt% Cu show the formation of Cu metal species clearly. In comparison with these samples, it may suggest that intensity of Cu metal in 4 wt% Cu is relatively higher than that in 8 wt%.

The changes of Cu species on TiO_2 before and after the reaction were investigated by means of EXAFS in 2 wt% Cu samples, which have a high reactivity at the initial stage. The k^3-weighted EXAFS oscillations and Fourier-transformed EXAFS (FT-EXAFS) of the samples from both nitrate and acetate are shown in Fig. 5. In the whole cases, the oscillations strongly reflect the scattering of Cu-Cu in the local

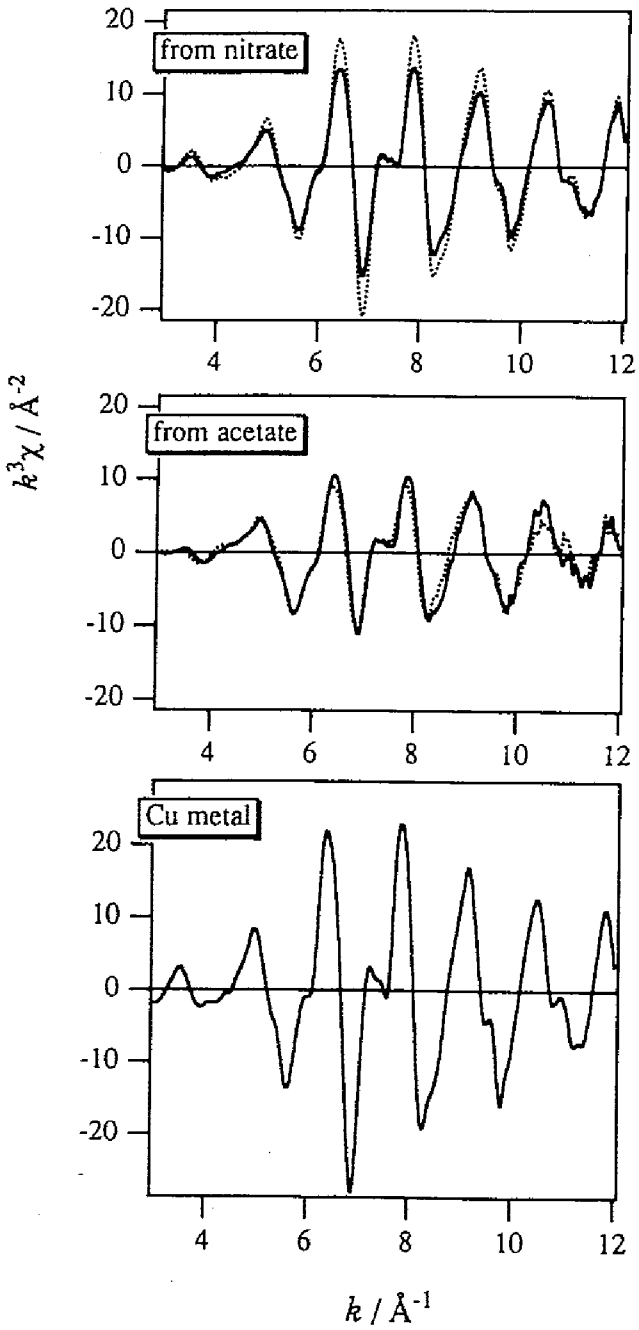

Fig. 5 EXAFS oscillations of 2wt% Cu/TiO_2 prepared from nitrate and acetate before and after the reaction.
dotted lines : after pretreatment with H_2 at 473K prior to admission.
solid lines : after admission of ($NO+H_2$) at 473K for 1 h.

structure of Cu^0 metal species, which gives a peak at 2.3 Å in FT-EXAFS (shown in Fig. 6). In case of a sample from nitrate after H_2 treatment at 473K, the intensity of the oscillation due to the scattering of Cu-Cu metal is smaller than that of Cu metal, exhibiting that micro particles of Cu metal are stabilized. For the sample from acetate after H_2 treatment, the Cu-Cu scattering is also observed, while Cu metal is less observed by XANES spectrum. It is remarkably shown that the intensity of Cu-Cu scattering in the sample from nitrate is larger than that in the sample from acetate before and after ($NO+H_2$) admission at 473K. This suggests that Cu^0 metal species formed after pretreatment with H_2 have a larger particle size for the nitrate sample than those for acetate sample. For the samples from nitrate, the Cu-Cu scattering becomes less intense by admission of ($NO+H_2$), indicating that Cu metal particles become smaller size. On the other hand, the Cu-Cu intensity for the samples from acetate is less changed by the admission. It is a definite difference between the samples prepared from nitrate and acetate. In these results, it can be considered that the Cu metal particles in the sample from nitrate are oxidized in near-surface region, but remained a Cu metal core which has a smaller particle size. In case of the sample from acetate, the metal species are more stable for ($NO+H_2$) admission than those of the sample from nitrate.

For FT-EXAFS shown in Fig. 6, a peak at 2.3 Å due to Cu-Cu scattering and a small peak at around 1.8 Å possibly due to Cu-O scattering are observed for each sample. The intensity of Cu-Cu peak relates to that of oscillation wave as mentioned above. For the samples from nitrate, the Cu-Cu peak at 2.3 Å becomes less intense by ($NO+H_2$) admission at 473K. On the other hand, for the samples from acetate, the Cu-O peak at around 1.8 Å are investigated definitely even after H_2 pretreatment. It supports the coexistence of Cu metallic species and oxidized ones in this sample. After admission of ($NO+H_2$) at 473K, the Cu-Cu peak is less intense and the Cu-O peak is more intense. It is deduced that the effect of admission for Cu species on TiO_2 is different between the samples prepared from nitrate and acetate, *i.e.*, Cu-metal particle size is reduced by admission for the nitrate sample, but it is a little enlarged for the acetate sample.

To estimate the particle size of Cu metallic species, we performed curve fitting of

Cu-O and Cu-Cu shells by inverse-FT after FT-filtered EXAFS in the range of ΔR = 1.1 - 2.7 Å. The results are shown in Table 5. In Fig. 7, the best fits for 2 wt% Cu/TiO_2 samples from nitrate and acetate are shown as examples. For all the samples, two-shell-fitting of both Cu-O and Cu-Cu bonds gave the satisfactory result. For 2 wt% Cu/TiO_2 sample from nitrate, coordination number (CN) of Cu is estimated to be 10.6 before ($NO+H_2$) admission, supporting that Cu metal species exist as a small metal particle because of smaller number than that of Cu metal sample. The CN decreased evidently to 7.5 by ($NO+H_2$) admitting. It substantiates that the metal particle becomes smaller. The CNs for oxygen as well as the Debye-Waller factors include large errors and we can not discuss the size of oxidized layer on the basis of CN. But the bond distance between Cu and oxygen shows that Cu ions are divalent. For the 2 wt% sample from acetate, the CNs before and after admission are almost similar to each other, supporting that Cu metal particle is stable for ($NO+H_2$) mixed gases. In these results, the active Cu species in 2 wt% Cu/TiO_2 samples consists of Cu-metal particles and oxidized species. Again, we can not discuss the CN of oxygen but the shorter bond distances than those found in the case of 2 wt% Cu/TiO_2 sample from nitrate suggests that Cu ions are monovalent. Thus, it is deduced that the admission of ($NO+H_2$) at 473K brings about the formation of Cu metal species having a suitable particle size for reduction of NO.

As a reference, the curve fitting results of EXAFS spectra for the samples from acetate with higher Cu loading are shown in Table 5. Before the admission of ($NO+H_2$), the CNs are 10.2 and 10.6 in 4 and 8 wt% of Cu loading, respectively. It suggests that the particle size is larger than that in 2 wt% sample, and the particle size for 4 and 8 wt% Cu samples is almost the same as each other. After admission of ($NO+H_2$), the size becomes smaller in both samples, but the reduction of the size is smaller in 4 wt% than in 8 wt%. This evidence is similar to that of the sample from nitrate. It strongly suggests that admission of ($NO+H_2$) gives the oxidation of Cu metal particles in the surface region to form smaller particles, but the degree of oxidation depends on the particle size. Suitable particle size for NO reduction is formed by the admission. Therefore, this species exists as an active one for NO reduction. If it is justified, the acetate sample is more stable than the nitrate sample

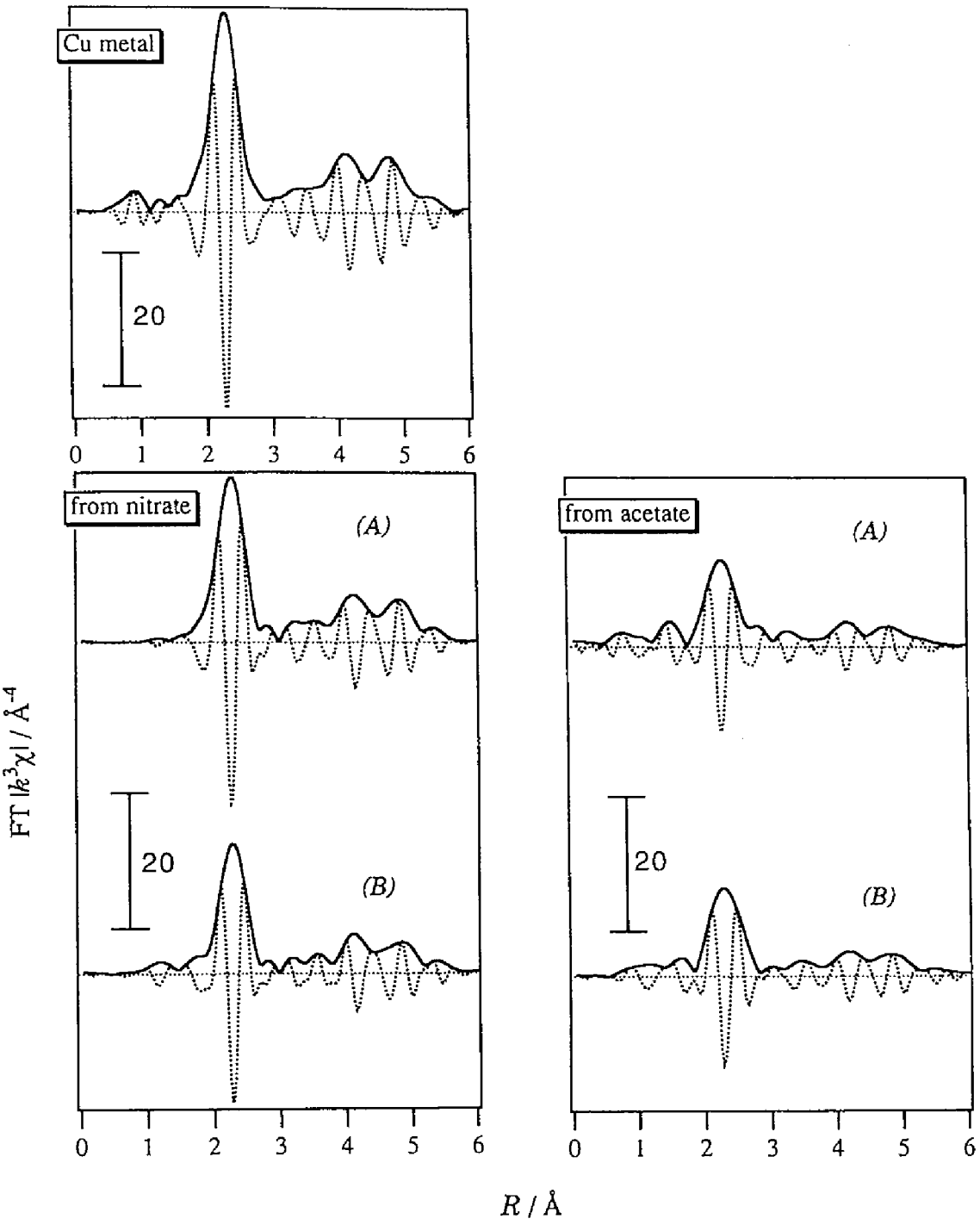

Fig. 6 Fourier-transformed EXAFS of 2wt% Cu/TiO_2 prepared from nitrate and acetate before and after reaction.
(A) after pretreatment with H_2 at 473K prior to admission.
(B) after admission of ($NO+H_2$) at 473K for 1 h.

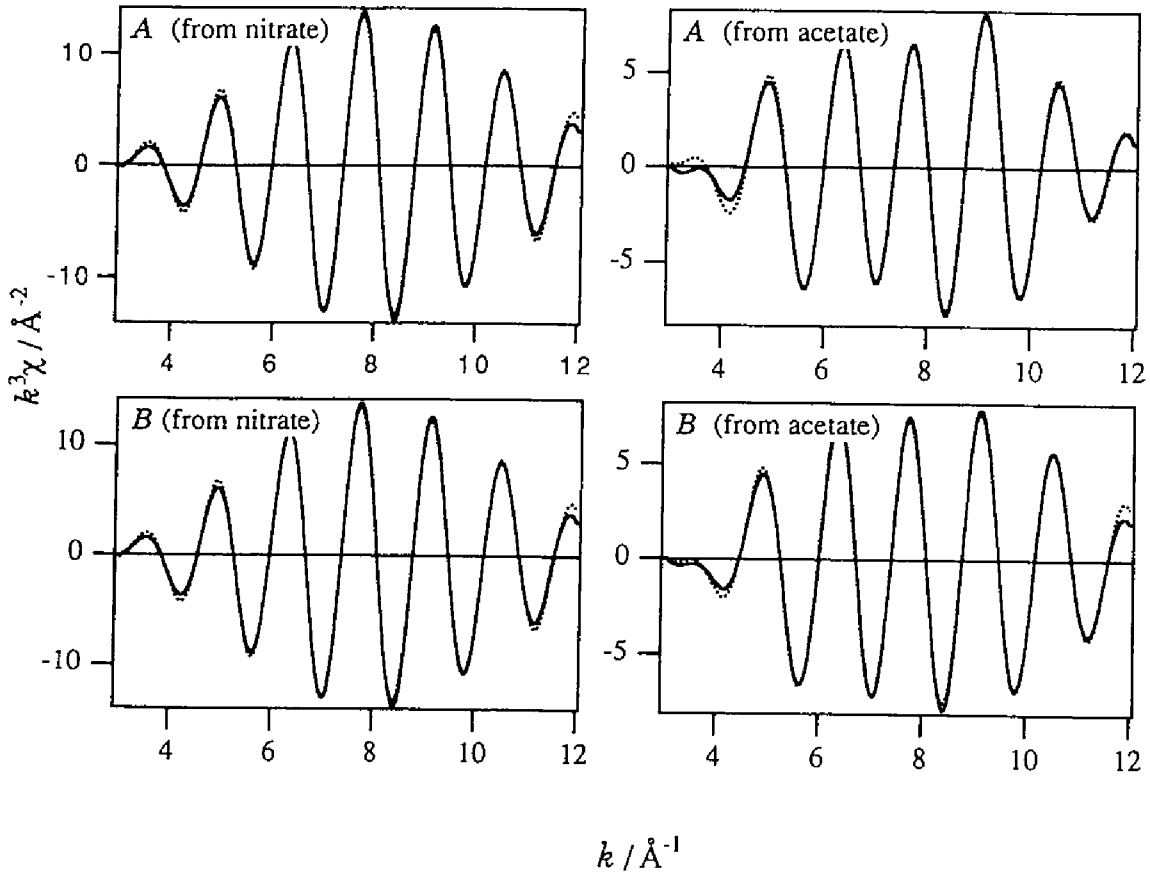

Fig. 7 The best fitting of Fourier back-filtered EXAFS oscillations in the range ΔR=1.1-2.7 Å.
solid lines : isolated EXAFS, dotted lines : model EXAFS obtained by 2-shell fitting of Cu-O and Cu-Cu.
A Treated with H_2 at 473K for 1 h prior to admission.
B After admission of ($NO+H_2$) at 473K for 1 h.

Table 5 Results of EXAFS analysis by curve-fitting of 2-shells (Cu-O and Cu-Cu) at ΔR = 1.7-2.7 Å.*

Sample	shell	N(NC)	R / Å	$\Delta\sigma^2$ / 10^{-3}Å^2	R-factor / %
Cu metal	Cu-Cu	12	2.56		
2 wt% Cu/TiO_2 from nitrate					
A	Cu-O	2.7 (1.6)	2.00(0.03)	8.5 (16.5)	3.9
	Cu-Cu	10.6 (0.9)	2.55(0.01)	0.7 (1.3)	
B	Cu-O	2.5 (1.1)	1.96(0.02)	5.2 (6.0)	4.8
	Cu-Cu	7.5 (0.7)	2.56(0.01)	0.0 (5.7)	
2 wt% Cu/TiO_2 from acetate					
A	Cu-O	1.7 (0.5)	1.85(0.01)	-1.6 (1.3)	6.6
	Cu-Cu	6.3 (0.5)	2.56(0.01)	1.1 (0.5)	
B	Cu-O	3.4 (0.8)	1.89(0.01)	8.3 (4.4)	6.0
	Cu-Cu	6.2 (0.5)	2.55(0.01)	0.4 (0.6)	
4 wt% Cu/TiO_2 from acetate					
A	Cu-O	2.8 (1.3)	1.98(0.05)	8.4 (7.5)	2.4
	Cu-Cu	10.2 (1.0)	2.55(0.01)	0.1 (0.7)	
B	Cu-O	4.6 (1.2)	1.94(0.03)	19.1 (11.0)	4.8
	Cu-Cu	8.6 (0.5)	2.55(0.01)	0.1 (0.7)	
8 wt% Cu/TiO_2 from acetate					
A	Cu-O	2.5 (1.2)	2.00(0.02)	4.5 (7.5)	4.0
	Cu-Cu	10.6 (1.0)	2.55(0.01)	0.8 (0.7)	
B	Cu-O	3.9 (1.0)	1.91(0.01)	17.5 (14.0)	5.2
	Cu-Cu	8.0 (0.7)	2.55(0.01)	0.8 (0.7)	

*The values in parentheses are the standard deviations.

A After H_2 pretreatment at 473K for 1 h prior to admission.

B After admission of ($NO+H_2$) at 473K for 1 h.

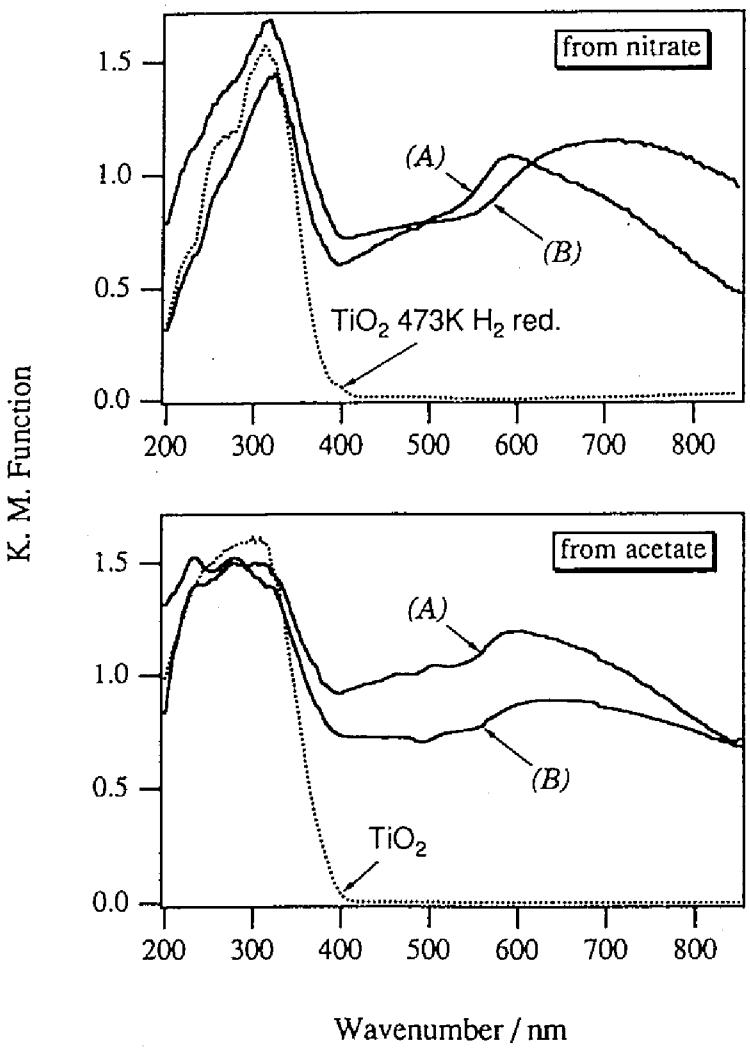

Fig. 8 Diffuse reflectance UV-VIS spectra of 2wt% Cu/TiO_2 prepared from nitrate and acetate before and after reaction.
(A) after pretreatment with H_2 at 473K prior to admission.
(B) after admission of $(NO+H_2)$ at 473K for 1 h.

for the reaction in 2 wt% Cu. By means of UV-VIS spectroscopy in a diffuse reflectance mode shown in Fig. 8, the spectra in both the nitrate and acetate samples with 2 wt% Cu have a peak cantered at around 580 nm is observed. This absorption is due to the existence of Cu-metal micro particles with 100 - 300 Å of particle size, as reported in the study of Cu metal colloids.[19,20] After admission of ($NO+H_2$), the absorption band becomes less intense in the samples from acetate although it still remains. For the sample from nitrate, the band is almost disappeared and a new band is seen centered at 700 nm, which is attributed octahedrally coordinated Cu^{2+} as found in case of $Cu(OH)_2$.[21,22] It is to be noted that the absorption bands in the region of 200 - 300 nm are different between the samples prepared from nitrate and acetate. In case of the sample from nitrate, both (A) and (B) exhibit the similar feature to the reduced TiO_2. On the contrary, in case of the sample from acetate, both (A) and (B) exhibit the similar one and to TiO_2 in oxidized state. The presence of Cu in the nitrate samples urged the reduction of TiO_2, but that in the acetate sample does not affect the TiO_2 at all. Feasibility of TiO_2 reduction may dominate the stability of Cu particles. These evidences relate to that of EXAFS. However, Cu-Cu CN for the 2 wt% sample from acetate is 6.2 - 6.3 which corresponds to 8 - 20 Å diameter of the Cu cluster provided that Cu cluster is spherical.[23] This is inconsistent with the size predicted by UV-VIS spectrum. If the spherical cluster was so small, then the peaks due to the presence of Cu atoms in the third and fourth shells at longer distances in FT-EXAFS in Fig. 6 should have been invisible. The small CN and the clear peaks at long distances show that the Cu cluster in the 2 wt% sample from acetate are not spherical. It is likely that the cluster is raft-like with a few atomic layers. If monolayer cluster of Cu(110) is assumed, CN is always less than 6 and number of Cu atoms in the thrid shell becomes extremely small. If the two-layer cluster is assumed, the CN, 6.2-6.3, corresponds to 20 - 100 Å particle size, which depends on the shape of the cluster. In any case, the Cu cluster presumably has the thin-layered raft-like structure. The spectral feature of XANES proves that electronic band structure is very similar to that of bulk Cu. In such case, behavior of free electrons in Cu cluster is expected to be similar to that of bulk Cu that the narrow VIS absorption peak at 580 nm is due to the presence of fairly large Cu raft-like cluster.

The suitable Cu metal particle for NO reduction has *ca.* 100 Angstroms of particle

size.

Conclusion

From the results mentioned above, it is concluded that the Cu metal species with suitable metal particle size for NO reduction and oxidized Cu ions partly exist as active ones. In this species, Cu ions exist as Cu^0 in a core and Cu^{2+} (and Cu^+, partly) in near-surface region. By means of UV-VIS spectroscopy, the presence of octahedrally coordinated Cu^{2+} is observed and Cu^+ is not found definitely in 2 wt% Cu/TiO_2 sample from nitrate, and the sample from acetate exhibited a similar phenomenon. Thus, it possibly deduced that coexistence of Cu^0 and Cu^{2+} relates to generate the active species. By means of EXAFS studies, suitable particle size of Cu metal leads to the active center.

In case of TiO_2-supported with Cu metal particle, it can be considered that the redox performance is enhanced by other effect, such as SMSI. In fact, it is shown that both Cu and Ti ions show a redox behavior easier than TiO_2 only by means of ESR study.[15] However, how metal species (and oxidized Cu^{2+}) play a role for an active center for NO reduction is still unclear, and it is now in progress.

Acknowledgement

The X-ray absorption experiments at the Cu *K*-edge were performed under the approval of the Photon Factory (KEK-PF) Program Advisory Committee (proposal No. 94G205). This work was partially supported by a grant-in-aid (No. 07242103 and 8405052) from Japan Ministry of Education, Science, Sports, and Culture.

References

(1) Cheung, T.; Bhargava, S. K.; Hobday, M.; Foger, K. *J. Catal.* **1996**, *158*, 301.

(2) Lei, G. D.; Adelman, B. J.; Sárkány, J.; Sachtler, W. M. H. *Appl. Catal. B* **1995**, *5*, 245.

(3) Giamello, E.; Murphy, D.; Magnacca, G.; Morterra, C.; Shioya, Y.; Nomura, T.; Anpo, M. *J. Catal.* **1992**, *136*, 510.

(4) Anpo, M.; Matsuoka, M.; Shioya, Y.; Yamashita, H.; Giamello, E.; Morterra, C.; Che, M.; Patterson, H. H.; Webber, S.; Ouellette, S.; Fox, M. A. *J. Phys. Chem.* **1994**, *98*, 5744.

(5) Beutel, T.; Adelman, B. J.; Lei, G.-D.; Sachtler, W. M. H. *Catal. Lett.* **1995**, *32*, 83.

(6) Iwamoto, M.; Yahiro, H.; Mizuno, N.; Zhang, W.; Mine, Y.; Furukawa, H.; Kagawa, S. *J. Phys. Chem.* **1992**, *96*, 9360.

(7) Zhang, Y.; Leo, K. M.; Sarofim, A. F.; Hu, Z.; Flytzani-Stephanopoulos, M. *Catal. Lett.* **1995**, *31*, 75.

(8) Liu, D.-J.; Robota, H. J. *Appl. Catal. B* **1994**, *4*, 155.

(9) Yamashita, H.; Matsuoka, M.; Tsuji, K.; Shioya, Y.; Anpo, M.; Che, M. *J. Phys. Chem.* **1996**, *100*, 397.

(10) Beutel, T.; Sárkány, J.; Lei, G.-D.; Yan, J. Y.; Sachtler, W. M. H. *J. Phys. Chem.* **1996**, *100*, 845.

(11) Itho, Y.; Nishiyama, S.; Tsuruya, S.; Masai, M. *J. Phys. Chem.* **1994**, *98*, 960.

(12) Hattori, H.; Itoh, M.; Tanabe, K. *J. Catal.* **1975**, *38*, 172.

(13) Wöllner, A.; Lange, F.; Schmelz, H.; Knözinger, H. *Appl. Catal. A* **1993**, *94*, 181.

(14) Yuan, S.; Mériaudeau, P.; Perrichon, V. *Appl. Catal. B* **1994**, *3*, 319.

(15) Aritani, H.; Akasaka, N.; Tanaka, T.; Funabiki, T.; Yoshida, S.; Gotoh, H.; Okamoto, Y. *J. Chem. Soc., Faraday Trans.* **1996**, *92(14)*, 2625.

(16) Tanaka, T.; Yamashita, H.; Tsuchitani, R.; Funabiki, T.; Yoshida, S. *J. Chem. Soc. Faraday Trans. 1* **1988**, *84*, 2987.

(17) Kosugi, N.; Tokura, Y.; Takagi, H.; Uchida, S. *Phys. Rev. B* **1990**, *41*, 131.

(18) Bart, J. C. *Adv. Catal.* **1986**, *34*, 203.

(19) Crelghton, J. A.; Alvarez, M. S.; Weltz, D. A.; Kim, M. W. *J. Phys. Chem.* **1983**, *87*, 4793.

(20) Curtis, A. C.; Duff, D. G.; Edwards, G. D.; Jefferson, D. A.; Johnson, B. F. G.; Kirkland, A. I.; Wallace, A. S. *J. Phys. Chem.* **1988**, *92*, 2270.

(21) Bjerrum, J.; Ballhausen, C. J.; Jørgensen, C. K. *Acta. Chem. Scand.* **1954**, *8*, 1275.

(22) Tominaga, H.; Ono, Y.; Keii, T. *J. Catal.* **1975**, *40*, 197.

(23) Greegor, R. B.; Lytle, F. W. *J. Catal.* **1980**, *63*, 476.

Chapter 5

Surface Copper-TiO_2 Interaction Species for NO-CO Reactions

Abstract

The catalytic properties of Cu/TiO_2 have been studied for an NO-CO reaction as a function of the calcination temperature, Cu content, and origin of TiO_2. It was found that Cu-TiO_2 interaction species were responsible for a catalytic activity at a low temperature (413 K). It is suggested by means of XAFS and TPR that a rutile phase of TiO_2 is very effective for the formation of the catalytically active Cu-TiO_2 interaction species in an octahedral symmetry.

Introduction

Recently, supported copper catalysts have been extensively investigated for the abatement of NO_x from effluent gases: Cu-exchanged zeolites for a direct decomposition of NO into N_2 and O_2 and for selective reduction of NO by hydrocarbons in the presence of O_2[1-3] and Cu-containing perovskite catalysts for the direct decomposition of NO and for NO reduction by CO[4-7]. Copper catalysts supported on metal oxides have also been studied for NO reduction. Bauerle *et al.*[8] showed that Al_2O_3-supported Cu catalysts exhibited activities for an NO-CO reaction at a lower temperature than 593 K in an excess of CO. We have recently demonstrated that ZrO_2[9,10] and TiO_2-supported Cu catalysts[11] show significantly high catalytic activities at low temperatures for NO reduction by CO or H_2. Very recently, on the basis of an FTIR study of NO and CO adsorptions, Boccuzzi *et al.*[12] also suggested a low temperature activity of Cu/TiO_2 for NO reduction by CO. With Cu/ZrO_2 catalysts, it was revealed on the basis of FTIR[10] Cu K-edge XAFS and TPR (temperature programmed reduction) studies [13] that interactions between Cu and ZrO_2 produced highly dispersed Cu species in an octahedral symmetry and thereby highly active Cu^0 species for a low temperature NO-CO reaction. In the case of Cu/TiO_2 catalysts, it has been reported that metallic Cu species are readily oxidized by NO even at room temperature[11].

Metal and/or metal oxide-support interactions are considered to modify the catalytic behaviors of Cu species for NO abatement reactions. In the present study, the catalytic behaviors of TiO_2-supported Cu catalysts were studied for NO-CO reactions. It was found by means of XAFS and TPR that Cu-TiO_2 surface interactions cause the generation of highly active Cu species at a low temperature.

Experimental Section

Cu/TiO_2 catalysts were prepared by impregnating TiO_2 powder with aqueous solutions of $Cu(CH_3COO)_2$. After drying at 383 K for 20 h, the catalyst was calcined in

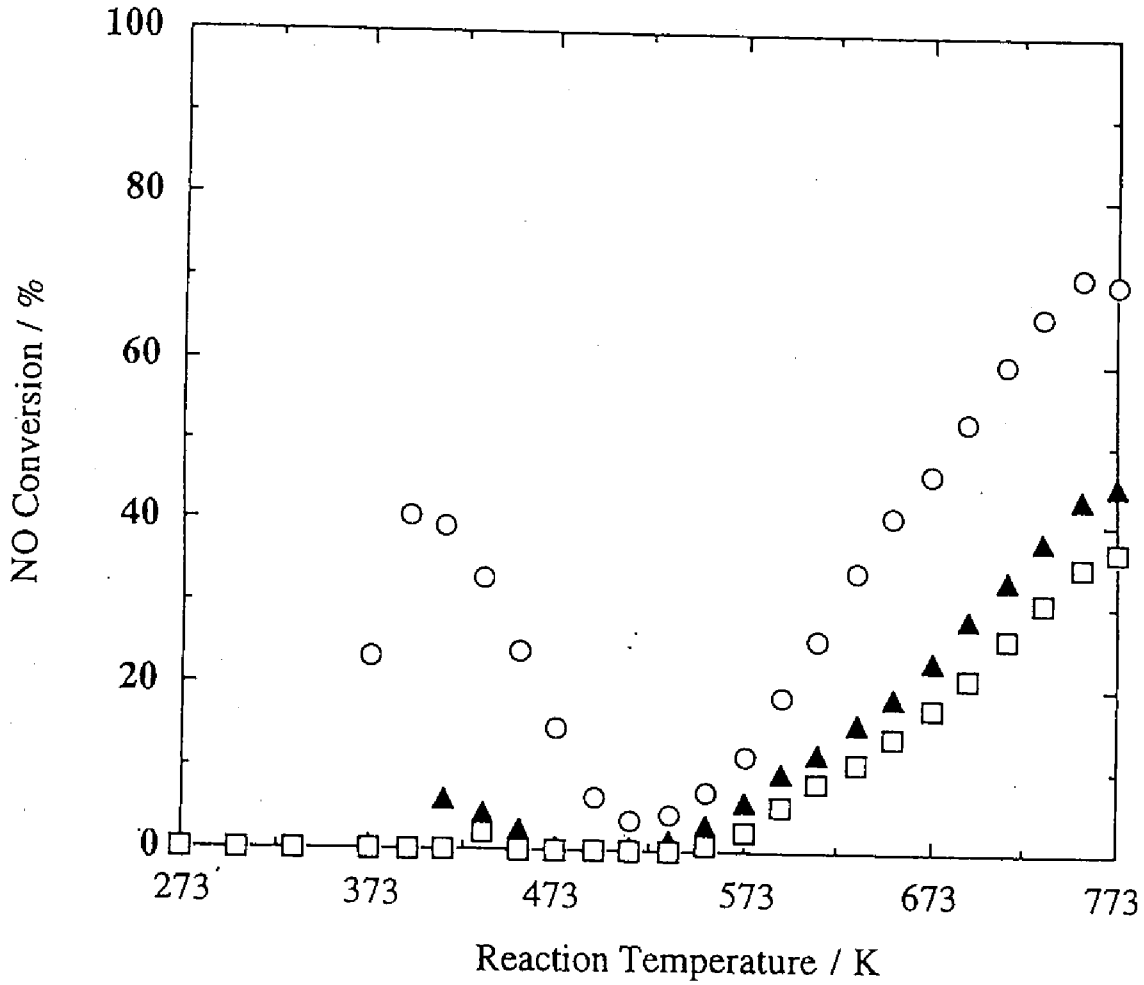

Fig. 1 Catalytic Activity of 1 wt% Cu/TiO_2(TIO-4) calcined at 573K(▲), 773K(□), and 973K(○) for NO-CO reaction.

air at 573, 773, 973 or 1173 K for 1 h. Three kinds of TiO_2 were provided by the Catalysis Society of Japan as reference catalysts (JRC-TIO-2, -3, and -4)[14]. The specific surface areas were 14.3, 49.2, and 47.6 $m^2\ g^{-1}$ for TIO-2, -3, and -4, respectively, and the crystal structures determined by an X-ray powder diffraction technique were anatase, rutile, and a mixture of anatase (73%) and rutile (27%), respectively.

NO-CO reactions were conducted using a fixed bed flow reactor. The concentrations of CO and NO in a He stream were 2500 ppm (12000 h^{-1}). The catalyst was treated at 673 K for 1 h in a stream of 5% O_2 before the reaction. The reaction temperature was increased at a rate of 3 K min^{-1} from room temperature to a desired temperature. The reaction gas was analyzed by means of an on-line gas chromatography.

In the TPR experiments, the catalyst sample was reduced in a stream of 1% CO/He. The reduction temperature was ramped at a rate of 3 K min^{-1} from room temperature to 673 K. The amount of CO_2 formed was periodically analyzed using an on-line gas chromatography.

The Cu K-edge XANES spectra of Cu/TiO_2 were measured using a Si(111) double crystal monochromator at the BL-7C station at the Photon Factory in the National Laboratory for High Energy Physics with 2.5 GeV ring energy in a fluorescence mode. The spectra of the catalyst samples were obtained at room temperature.

Results and Discussion

Figure 1 shows the catalytic activity of 1 wt% Cu/TiO_2 (TIO-4) for an NO-CO reaction as a function of a calcination temperature. It is evident that the calcination temperature strongly affects the activity of the catalyst. The catalyst calcined at 973 K shows activities in two temperature regions, that is, a low temperature activity at around 413 K and a high temperature activity at > 523 K. At < 473 K, N_2O was selectively produced. On the other hand, Cu/TiO_2 calcined at 573 K showed only a moderate activity at 413 K and Cu/TiO_2 calcined at 773 K showed no activity at the low temperature. A calcination at 1173 K completely lost the activity (not shown).

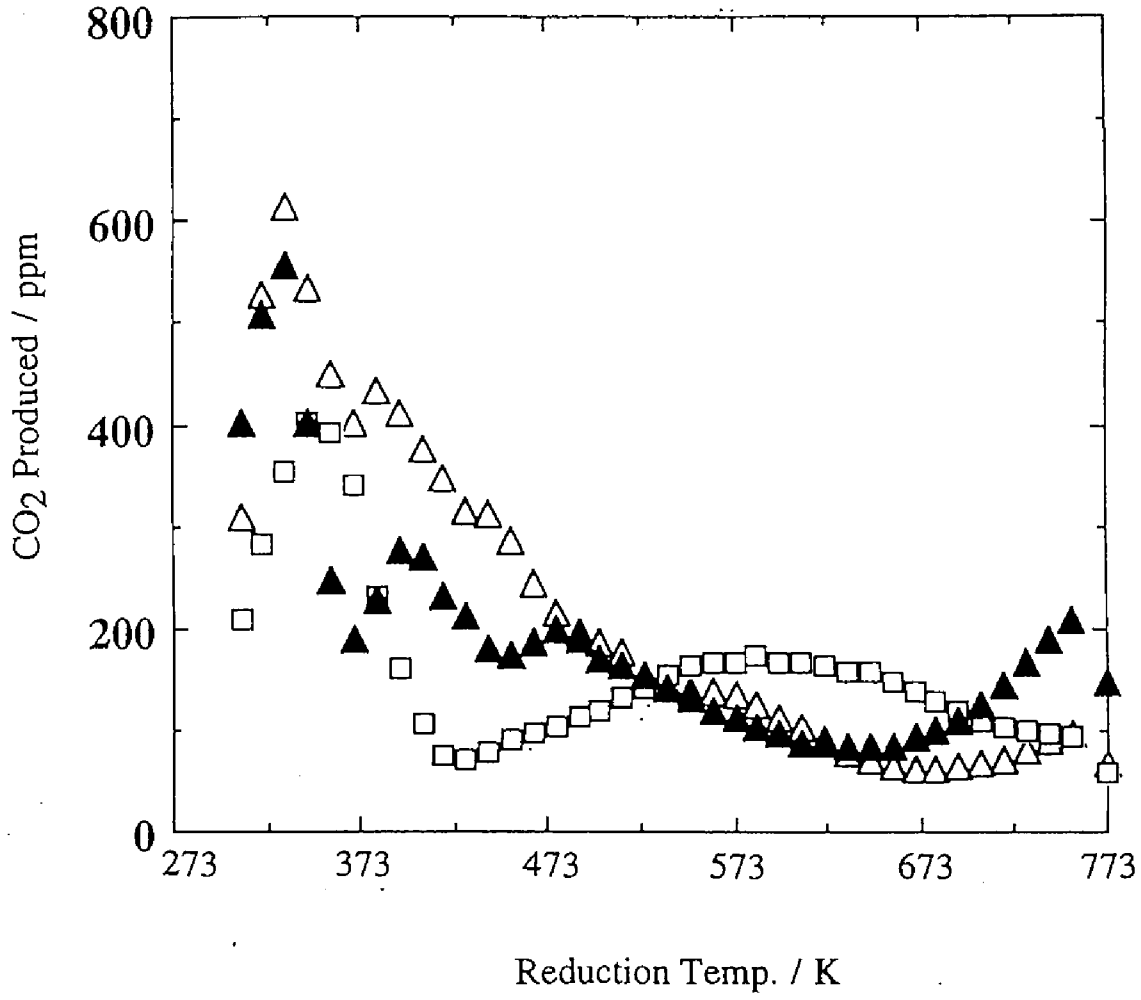

Fig. 2 TPR profiles of 1 wt% Cu/TiO_2(TIO-4) calcined at 573K(▲), 773K(□), 973K(△).

Taking into account the specific surface area of the catalysts (17 and 50 $m^2 g^{-1}$ for Cu/TiO_2 calcined at 973 K and 573 or 773 K), the results in Fig. 1 strongly suggest that with Cu/TiO_2 (TIO-4), catalytically active $Cu\text{-}TiO_2$ interaction species are formed by the high temperature treatment.

TPR experiments were conducted to examine if $Cu\text{-}TiO_2$ interaction species are formed in the calcined Cu/TiO_2 catalysts. The TPR profiles are presented in Fig. 2 for 1 wt% Cu/TiO_2 (TIO-4) calcined at 573, 773, and 973 K. The reduction of crystalline CuO was found to take place at 523 K under the present TPR conditions. The reduction peaks at 333 K and *ca.* 373 K apparently indicate the formation of Cu species reducible at much lower temperature than CuO, showing the formation of $Cu\text{-}TiO_2$ interaction species. The TPR peak at 353 K observed for Cu/TiO_2 calcined at 773 K is considered to be due to a convolution of the two reduction peaks. It is speculated on the basis of the reduction temperature that a weak TPR peak observed at 483 K for Cu/TiO_2 calcined at 573 K is due to surface CuO clusters and that a broad CO_2 evolution peak at around 573 K for the 773 K-calcined catalyst to subsurface $Cu\text{-}TiO_2$ interaction species. A weak feature observed at > 723 K for Cu/TiO_2 calcined at 573 K may be ascribed to disproportion of CO to CO_2 on metallic Cu species[13]. It is concluded from Fig. 2 that various $Cu\text{-}TiO_2$ interaction species are formed. A comparison of the activity to the TPR profile suggests that the Cu species reduced at 333 K are not responsible for the generation of the low temperature activity for the NO-CO reaction but that the TPR peak at around 373 K is correlated to the activity.

The XANES spectra of Cu K-edge are shown in Fig. 3 for 1 wt% Cu/TiO_2 (TIO-4) calcined at 573, 973, and 1173 K. The Cu K-edge XANES spectra for reference compounds are also presented in Fig. 3 for comparison. The XANES features of the Cu/TiO_2 calcined at 573 and 973 K are very close to that for $Cu(OH)_2$, suggesting that the $Cu\text{-}TiO_2$ interaction species are in an octahedral symmetry as reported previously.[11] Unfortunately, the XANES spectra cannot discriminate the highly active and less active Cu species at the low temperature. With 1 wt% Cu/TiO_2 calcined at 1173 K, the XANES spectrum indicates a clear sign of a formation of CuO, that is, a post-edge peak at 8986 eV and a hump at 9013 eV. The transformation of the $Cu\text{-}TiO_2$

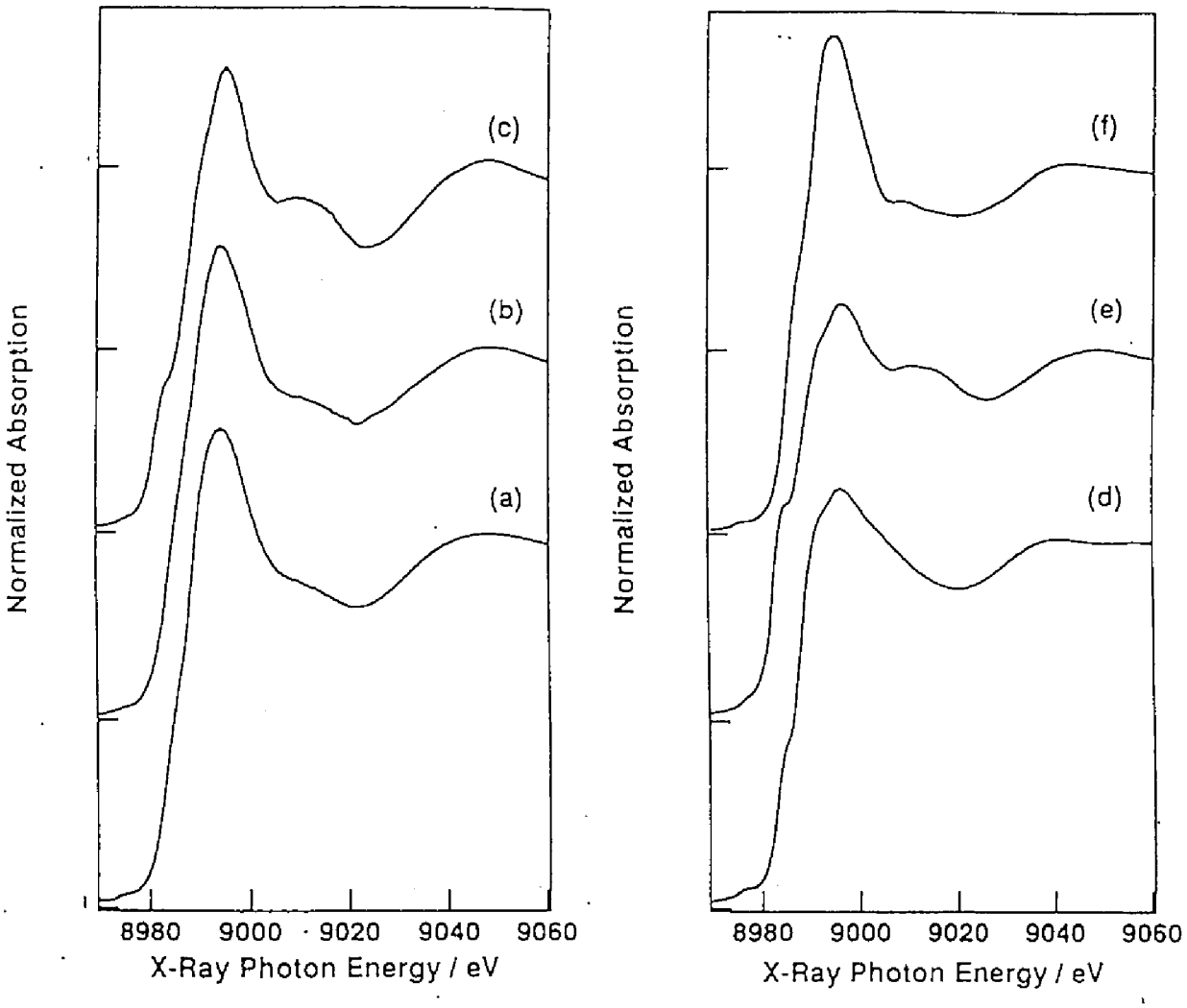

Fig. 3 Cu K-edge XANES spectra of 1 wt% Cu/TiO_2 calcined at (a) 573, (b) 973, and (c) 1173 K, and for reference compounds, (d) $Cu(CH_3COO)_2 \cdot H_2O$, (e) CuO, and (f) $Cu(OH)_2$.

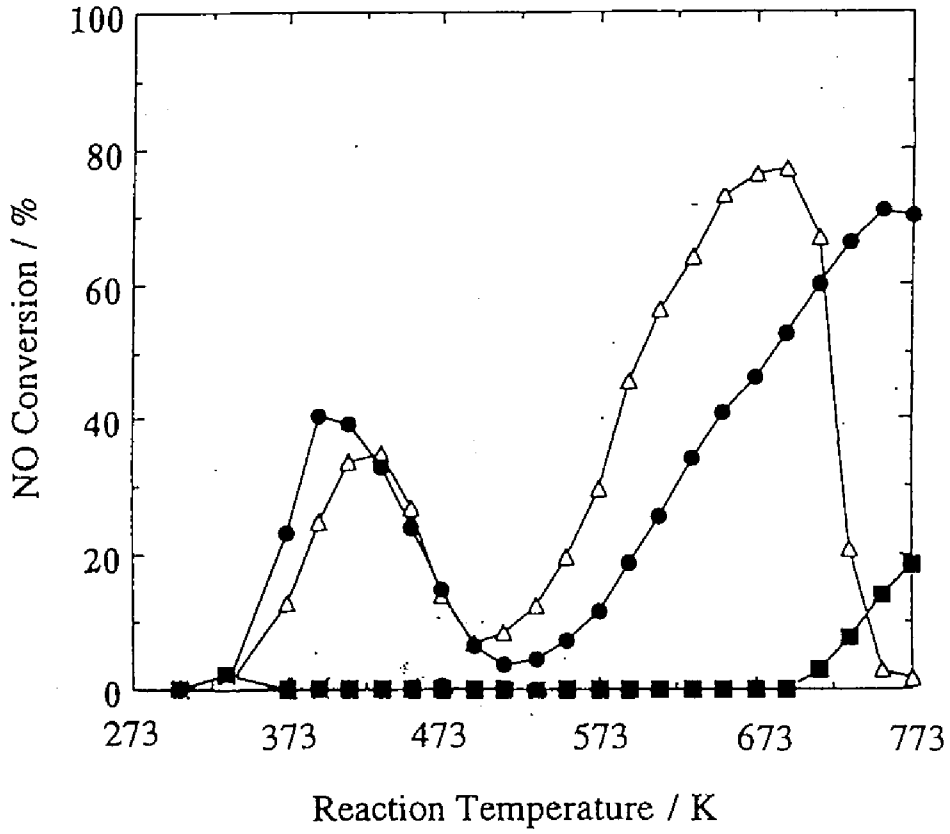

Fig. 4 Catalytic Activity of 1 wt% Cu/TiO_2 using various TiO_2-support calcined at 973 K.
TIO-4(●), TIO-3(△), TIO-2(■).

interaction species into CuO is responsible for the significant loss of the activity of the catalyst.

The dependence of the catalytic activity of Cu/TiO_2 on the Cu content was examined for the NO-CO reaction. It was found that the NO conversion of Cu/TiO_2 at 413 K linearly increased up to 1 wt% Cu and leveled off at 3 wt% Cu, followed by a slight decrease at 5 wt%. The activity at a higher temperature than 523 K showed a different tendency, in which 3 wt% Cu/TiO_2 showed the maximum activity. The TPR profiles for 3 wt% and 5 wt% Cu/TiO_2 (TIO-4) showed a strong reduction peak at 473-523 K, which is ascribed to the reduction of CuO, in addition to the TPR peaks due to the Cu-TiO_2 interaction species. In accordance with the TPR results, the XANES spectra for 3 and 5 wt% Cu/TiO_2 calcined at 973 K indicated a formation of CuO (8986 and 9013 eV-peaks). These results indicate that the amount of the interaction species is limited and saturated at 1 wt% Cu for Cu/TiO_2 (TIO-4).

The effect of TiO_2 on the catalytic behaviors of 1 wt% Cu/TiO_2 for the NO-CO reaction is presented in Fig. 4. The low temperature activity of Cu/TiO_2 (TIO-3) is almost the same as that of Cu/TiO_2 (TIO-4), while at a higher temperature than 523 K, the activity of the TIO-3 derived catalyst prevailed that of TIO-4-supported catalyst. The activity of Cu/TiO_2 (TIO-3) was steeply lost at 673 K, probably due to SMSI effects,[15] whereas Cu/TiO_2 (TIO-4) showed an increasing activity with increasing reaction temperature. On the other hand, Cu/TiO_2 (TIO-2) showed only a marginal activity over the whole reaction temperature region studied here. It is revealed that the kind of the TiO_2 support strongly affects the catalytic behaviors of Cu species for the NO-CO reaction. Figure 5 shows the TPR profiles for 1 wt% Cu/TiO_2 prepared using different TiO_2 supports and calcined at 973 K. The profiles were considerably different between the Cu/TiO_2 catalysts. The TPR peak at 333 K is prominent for TIO-2 and TIO-4, while the TPR peak at 383 K is characteristic to TIO-3 and TIO-4. In addition to these low temperature TPR features, Cu/TiO_2 (TIO-3) showed a strong peak at 543 K ascribed to subsurface Cu-TiO_2 compounds. TIO-2 and TIO-3 are pure anatase and rutile by the XRD analysis, respectively, while TIO-4 contains both phases. Accordingly, it is proposed that the formations of Cu-TiO_2

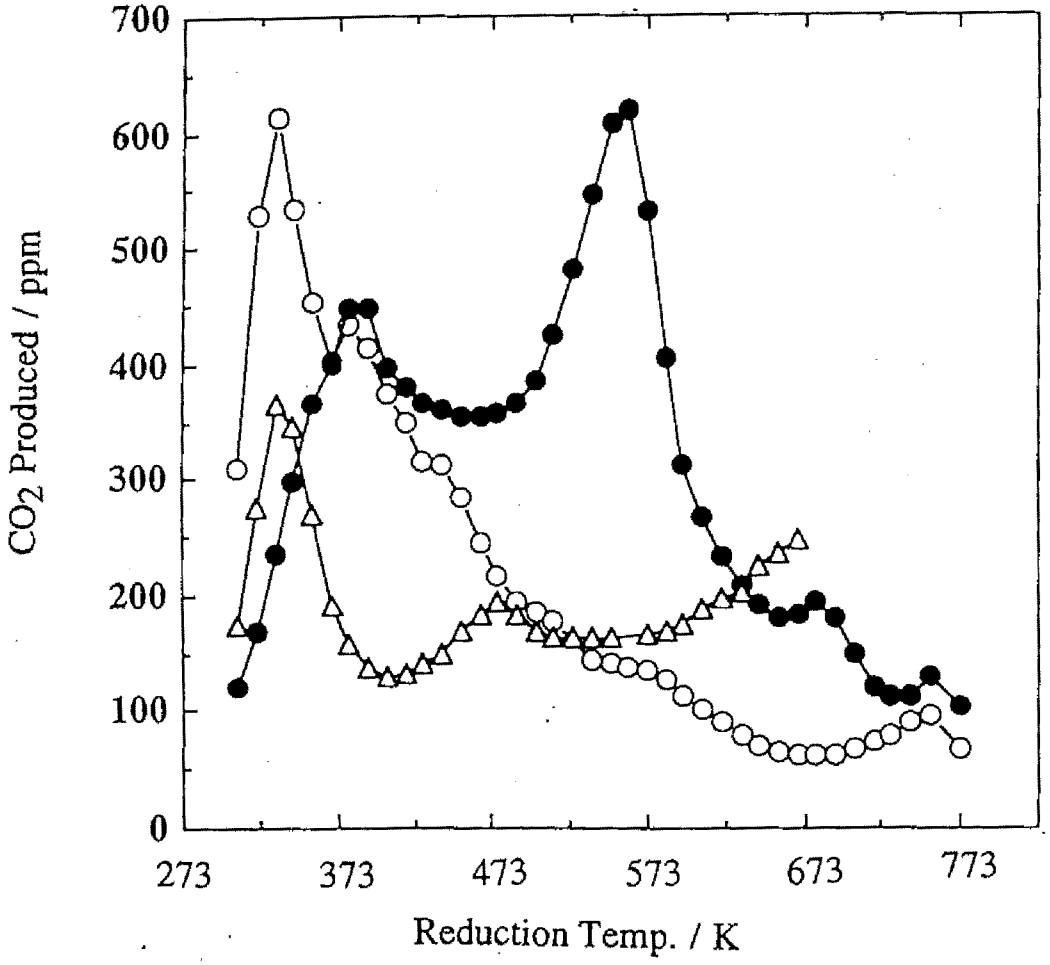

Fig. 5 TPR profiles of 1 wt% Cu/TiO_2 calcined at 973 K. TIO-4(○), TIO-3(●), TIO-2(△).

interaction species are strongly affected by the crystal structure of TiO_2 and that the Cu species reduced at 333 K is produced on the anatase phase, whereas the Cu species reduced at 383 K on the rutile phase. Comparing the NO conversion in Fig. 4 and the TPR profiles in Fig. 5, it is conceivable that the Cu species reduced at 383 K are responsible for the low temperature activity of Cu/TiO_2, in conformity with the above suggestions for the effect of the calcination temperature of 1 wt% Cu/TiO_2 (TIO-4). It is concluded that catalytically active Cu-TiO_2 interaction species are formed only on the rutile surface of TiO_2. The rutile surface may produce the subsurface Cu species, for instance a $CuTiO_3$ like phase with an illuminate structure. In line with the conclusions, 1 wt% Cu/TiO_2 (TIO-3) calcined at 573 K showed a high activity at a low temperature as presented in Fig. 4.

Irrespective of TiO_2 used, the XANES features indicate the formation of Cu^{2+} species in an octahedral symmetry when 1 wt% Cu/TiO_2 was calcined at 973 K. A more detailed XAFS study is under way to define exact nature of several kinds of Cu-TiO_2 interaction species.

Acknowledgment

We express our sincere thanks to Mr. Makoto Kaneko for a part of experimental works. The X-ray absorption measurements were performed under the approval of the Photon Factory (KEK-PF) Program Advisory Committee (Proposal No. 94G205). This work was partially supported by a grant-in-aid (No. 07242103) from the Japan Ministry of Education, Science, Sports, and Culture.

References

(1) Iwamoto, M., Hamada, H., *Catal. Today*, 1991, **10**, 57.
(2) Iwamoto, M., Yahiro, H., *Catal. Today*, 1994, **22**, 5.
(3) Li, Y., Hall, W. K., *J. Phys. Chem.*, 1990, **94**, 6145.
(4) Tabata, K., Mater, J., *Sci. Lett.*, 1988, **7**, 147.
(5) Shimada, H., Miyama, S., Kuroda, H., *Chem. Lett.*, 1988, 1797.

(6) Mizuno, N., Toyama, H., Tanaka, M., Yamamoto, M., Misono, M., *Bull. Chem. Soc. Jpn.*, 1991, **64**, 1383.

(7) Mizuno, N., Yamamoto, M., Tanaka, M., Misono, M., *J. Catal.*, 1991, **132**, 560.

(8) Bauerle, G. L., Service, G. R., Nobe, K., *Ind. Eng. Chem. Prod. Res. Devel.*, 1992, **11**, 54.

(9) Okamoto, Y., Ohto, K., Imanaka, T., *Kagaku Kogaku Ronbunshu*, 1993, 19, 863.

(10) Okamoto, Y. Gotoh, H., *Catal. Today*, in press.

(11) Aritani, H., Akasaka, N., Tanaka, T., Funabiki, T., Yoshida, S., Gotoh, H., Okamoto, Y., *J. Chem. Soc. Faraday Trans.*, 1996, **92**, 2625.

(12) Boccuzzi, F., Gulielminotti, E., Martra, G., Cerrato, G., *J. Catal.*, 1994, **146**. 449.

(13) Okamoto, Y., Gotoh, H., Aritani, H., Tanaka, T., Yoshida, S., in preparation.

(14) Murakami, Y., *"Preparation of Catalysts III"* (Poncelet, G., Grange, P., and Jacobs, P. A., *eds.*) Elsevier, Amsterdam, 1993, p775.

(15) Tauster, S. J., Fung, S. C., Garten, R. L., *J. Am. Chem. Soc.*, 1978, **100**, 170.

Chapter 6

Catalysis and Physicochemical Characterization of Zirconia-Supported Copper Catalysts for NO-CO Reactions: Surface Copper Species on Zirconia

Abstract

The structure and reduction behaviors of ZrO_2-supported Cu species have been characterized by means of XANES, EXAFS, and TPR. It was found that highly dispersed Cu^{2+} species, interacting with a ZrO_2 surface and in an octahedral symmetry, dominated at a lower Cu content than 1 wt% and that the amount of formation of the Cu^{2+} species, 2.9×10^{14} Cu atoms cm^{-1}, was saturated at a Cu loading of 1 wt%. On the other hand, CuO was exclusively formed at a Cu content exceeding 1 wt%. The highly dispersed Cu^{2+} species were reduced by CO at a much lower temperature than CuO, producing highly dispersed Cu^{+} species at 373 K and subsequently highly dispersed Cu^{0} species at 443-453 K. It is concluded that a high catalytic activity of Cu/ZrO_2 for NO-CO reactions at a low temperature is brought about by the highly dispersed Cu^{0} species generated by a low-temperature reduction of the Cu^{2+} species interacting with the ZrO_2 surface.

Introduction

Supported copper catalysts have recently attracted much attention because of their high catalytic activities for NO_x abatement reactions. Cu-exchanged zeolites, in particular, Cu-ZSM-5, show prominent catalytic activities for selective reductions of NO by hydrocarbons in the presence of O_2 and for a direct decomposition of NO into N_2 and O_2.[1-3] Perovskite catalysts[4-7] containing Cu exhibit high activities for the direct decomposition of NO and for NO reduction by CO. The latter reaction is also catalyzed by Cu catalysts supported on metal oxides. Although the reduction of NO using CO is one of the most fundamental reactions in the abatement of NO_x in exhaust gases, NO-CO reactions over Cu catalysts have never been fully developed nor understood yet. Bauerle *et al.*[8] showed that Al_2O_3-supported CuO and $CuCr_2O_4$ exhibited catalytic activities for an NO-CO reaction at a lower temperature than 593 K in an excess of CO. In our previous studies, TiO_2-supported Cu catalysts were found to show significantly high catalytic activities at low temperatures for NO reduction by CO[9,10] and, in particular, by H_2.[11] However, the activity of Cu/TiO_2 was lost at 523 K for NO-CO reactions.[9] Very recently, on the basis of an FTIR study of NO and CO adsorptions, Boccuzzi *et al.*[12] also suggested a low temperature activity of Cu/TiO_2 for NO reduction by CO. It was revealed in our previous study[9,10] that Cu/ZrO_2 catalysts were active as highly as Cu/TiO_2 catalysts for NO-CO reactions at 373-423 K and much more active than the TiO_2-supported catalysts at a higher temperature than 473 K. It has been suggested with Cu/ZrO_2 catalysts[10] that Cu species highly active for NO-CO reactions are formed on a ZrO_2 surface together with less active species and that the amount of the former Cu species is limited and saturated within 1 wt% Cu.

In the present study, to obtain more detailed information on the catalytically active Cu species on ZrO_2, the structure and reduction behaviors of the Cu species supported on ZrO_2 were characterized by means of X-ray absorption near edge structure (XANES), extended X-ray absorption fine structure (EXAFS), and temperature programmed reduction (TPR) techniques. The deactivation, regeneration, and stabilization of the highly active Cu species will be presented

elsewhere.[13]

Experimental

Catalyst Preparation. Cu/ZrO_2 catalysts were prepared by impregnating ZrO_2 with aqueous solutions of $Cu(CH_3COO)_2$. After drying at 383 K for 20 h, the catalyst was calcined in air at 973 K for 1 h using an electric furnace. Zirconia was provided by Dai-ichi Kigenso Ltd. (EP, 1.38wt%; Hf, 25 m^2/g).

Reaction Procedures. NO-CO reactions were carried out using a fixed bed flow reactor (0.1 g cat). The flow rates of the reaction gases were controlled by means of mass flow meters (Ueshima-Brooks, 5850E). The concentrations of CO and NO in a He stream were 2500 ppm (20 cm^3 min^{-1} or GHSV; 12000 h^{-1}), unless otherwise noted. The catalyst was treated at 673 K for 1 h in a stream of 5% O_2 before the reaction. The reaction temperature was increased at a rate of 3 K min^{-1} from room temperature to a desired temperature. The reaction gas was analyzed by means of an on-line gas chromatography.

Temperature Programmed Reduction (TPR). The catalyst sample was reduced in a stream of 1% CO/He (10 cm^3 min^{-1}). The reduction temperature was ramped at a rate of 3 K min^{-1} from room temperature to 673 K. The amount of CO_2 formed was periodically analyzed using an on-line gas chromatography.

Measurements of Cu K-edge Absorption Spectra. The Cu K-edge XANES and EXAFS spectra of Cu/ZrO_2 were measured using a Si(111) double crystal (d = 0.31366 nm) monochromator at the BL-7C station at the Photon Factory in the National Laboratory for High Energy Physics with 2.5 GeV ring energy in a fluorescence mode. The spectra of the catalyst samples were obtained at room temperature using an *in situ* EXAFS cell with Kapton windows.

Results and Discussion

Figure 1 presents the catalytic activities of the Cu/ZrO_2 catalysts as a function of Cu content and reaction temperature. The activity expressed by an NO conversion appeared at a higher temperature than 373 K and reached a maximum

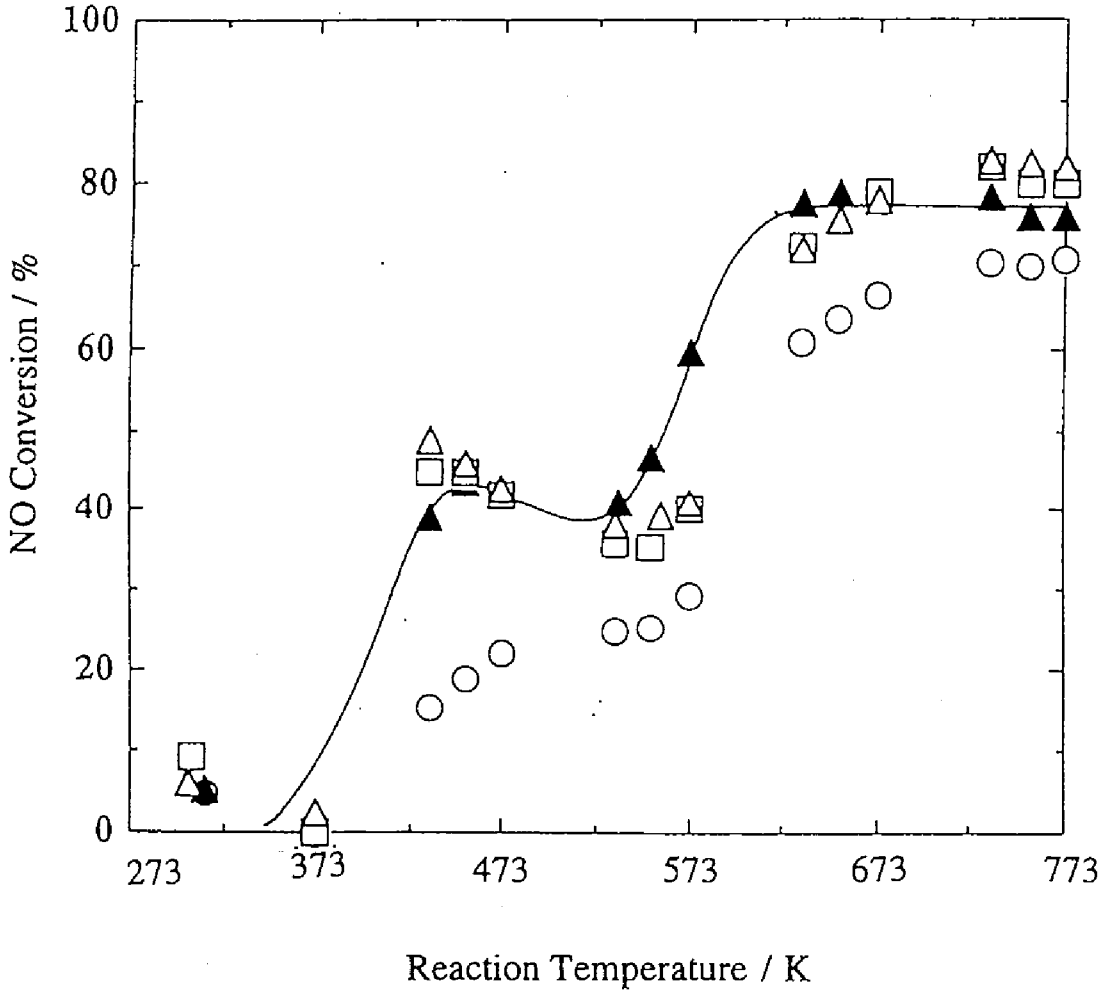

Fig. 1 Catalytic activities of Cu/ZrO_2 catalysts as expressed by the NO conversion for NO-CO reaction (CO 2000 ppm and NO 2000 ppm) as a function of the reaction temperature and Cu content.
○; 0.5 wt%, ▲; 1 wt%, □; 3 wt%, and △; 5 wt%.

at about 443 K, followed by a second activity increase at a further increase in the temperature (> 523 K). Since the CO and NO compositions were 2000 and 2500 ppm, respectively, in these experiments, it should be noted that so long as a direct decomposition of NO does not take place, the maximum conversion of NO is limited to 80% in Fig. 1. Nitrous oxide was exclusively produced at a lower temperature than 443 K. The selectivity to N_2O decreased as the reaction temperature increased further and became negligible at a higher temperature than 523 K, selectively producing N_2.

As shown in Fig. 2 (CO; 2500ppm and NO; 2500ppm), the NO conversion at 473 K increased with the Cu content and was maximized at 1 wt% Cu, followed by a gradual decrease at a further increase in the Cu loading. It is suggested from Fig. 2 that the amount of the Cu species which show a low temperature activity for the reduction of NO by CO is limited and saturated at 1 wt% Cu. Figure 2 also presents the turnover frequency (TOF; s^{-1}) of the reaction at 473 K calculated on the basis of the total Cu content. It is evident that the TOF decreases as the Cu content increases, clearly indicating an increase in the fraction of less active Cu species with increasing Cu content.

It was found that the activity peak observed at 443 K disappeared when the temperature programmed reaction was conducted again after the reaction temperature had been raised up to 573 K and cooled down to room temperature in the stream of the reaction gas. On the other hand, an almost identical catalytic activity was observed at a higher temperature than 573 K in the second reaction cycle. Therefore, it is conceivable that catalytically active Cu species are different in the region of the reaction temperature, that is, < 473 K and > 523 K and that the Cu species active at < 473 K are readily deactivated during the reaction, in particular, at a higher temperature.

For deeper understandings of the catalytic behaviors of Cu/ZrO_2 catalysts for NO-CO reactions, it is of a great importance to elucidate the structure and electronic state of the Cu species catalytically active, in particular, at the low temperature and to clarify deactivation mechanisms on a molecular level. The X-ray absorption spectra of the Cu K-edge[14-16] of Cu/ZrO_2 catalysts were measured to unveil the structure and electronic state of the Cu species in oxidized state and in reduced states. The reduction behaviors of the Cu species in Cu/ZrO_2 were also

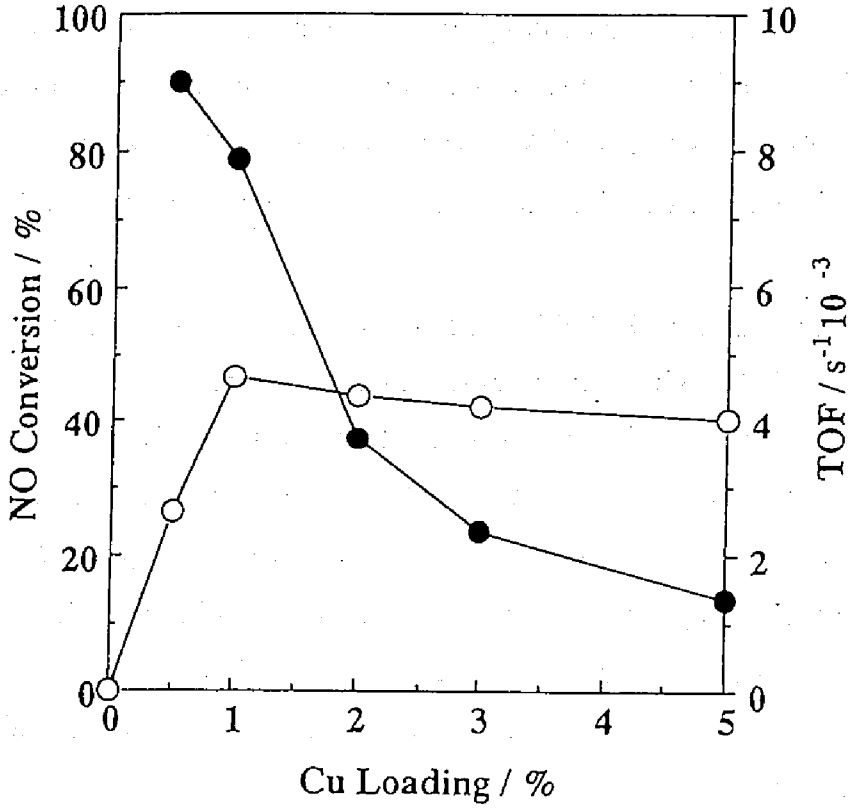

Fig. 2 NO conversion (○) and turnover frequency (●) of Cu/ZrO_2 at 473 K as a function of Cu content. CO and NOconcentrations are 2500 ppm.

examined by means of TPR.

Figure 3 shows the Cu K-edge XANES spectra of the Cu/ZrO_2 catalysts possessing 0.5, 1, 3, and 5 wt% Cu, after calcination at 973 K. The sample was treated at 673 K for 1 h in a stream of 5% O_2/He prior to the measurements. The XANES spectra of reference compounds, CuO (Cu^{2+} in a square symmetry), $Cu(OH)_2$ (Cu^{2+} in an octahedral symmetry), and $Cu(CH_3COO)_2 \cdot 2H_2O$ (Cu^{2+} in an octahedral symmetry), are shown in Fig. 4 for comparison. The 0.5 and 1 wt% Cu/ZrO_2 catalysts showed XANES spectra very close to that for $Cu(OH)_2$, indicating that major Cu^{2+} species in the catalysts are surrounded by six O^{2-} anions in the oxidized state. On the other hand, clear humps appeared at 8986 and 9013 eV at 3 wt% Cu and increased in intensity as the Cu content increased up to 5 wt%. Since CuO shows similar characteristic peaks in the XANES spectrum as presented in Fig. 4, it is suggested that CuO is formed at the higher Cu content than 1 wt%, in addition to the Cu^{2+} species in an octahedral coordination and that the fraction of CuO increases with increasing Cu content.

Figure 5 shows the background subtracted k^3-weighted EXAFS oscillations, $k^3\chi(k)$, for the calcined Cu/ZrO_2 catalysts having various Cu contents together with those for CuO and $Cu(OH)_2$ for comparison. With Cu/ZrO_2 having 3 and 5 wt% Cu, there appeared oscillations at 8.0 and 8.5 $Å^{-1}$ characteristic to CuO, in agreement with the suggestions by XANES in Fig. 3. The Fourier transforms of $k^3\chi(k)$ are shown in Fig. 6 for the calcined catalysts (Δk = 2.8 - 11.8$Å^{-1}$). The Fourier transform for 0.5 wt% Cu/ZrO_2 is significantly different from that of CuO or $Cu(OH)_2$, suggesting a formation of Cu species in a distinct local structure. The absence of Cu-Cu bondings for 0.5 wt% Cu/ZrO_2 suggests that the Cu^{2+} species in an octahedral symmetry are highly, possibly atomically, dispersed on the ZrO_2 surface.

On the other hand, with Cu/ZrO_2 having a larger Cu content than 1 wt%, a weak peak due to Cu-Cu bondings appeared at 0.28 - 0.29 nm (not corrected for phase shifts) in addition to Cu-O bondings at *ca.* 0.15 nm. Structural parameters as derived from an EXAFS analysis are summarized in Table 1. The Cu-Cu bond distance in Table 1 is close to that for CuO, suggesting the formation of small CuO

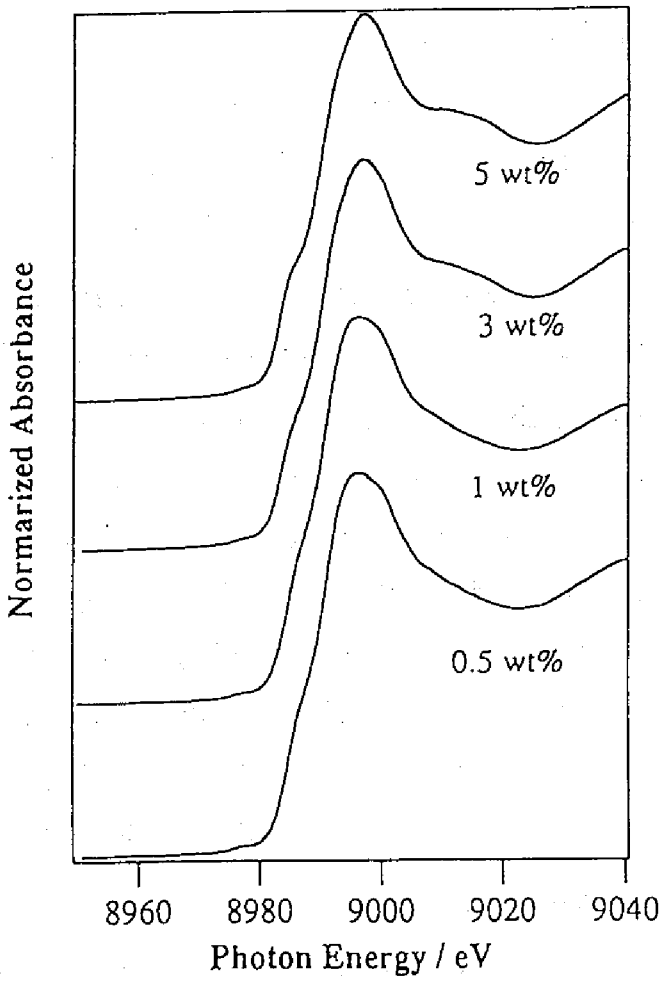

Fig. 3 Cu K-edge XANES spectra for calcined Cu/ZrO_2 catalysts with 0.5, 1, 3, and 5 wt% Cu.

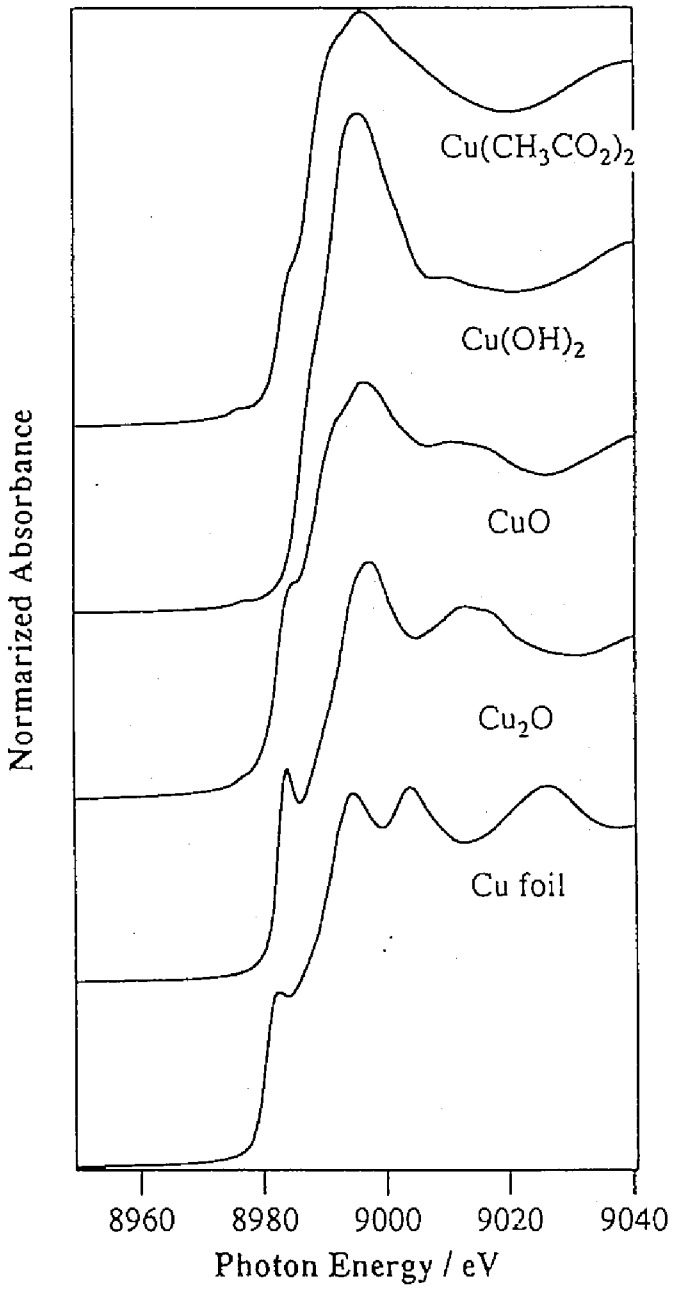

Fig. 4 Cu K-edge XANES spectra of reference compounds.

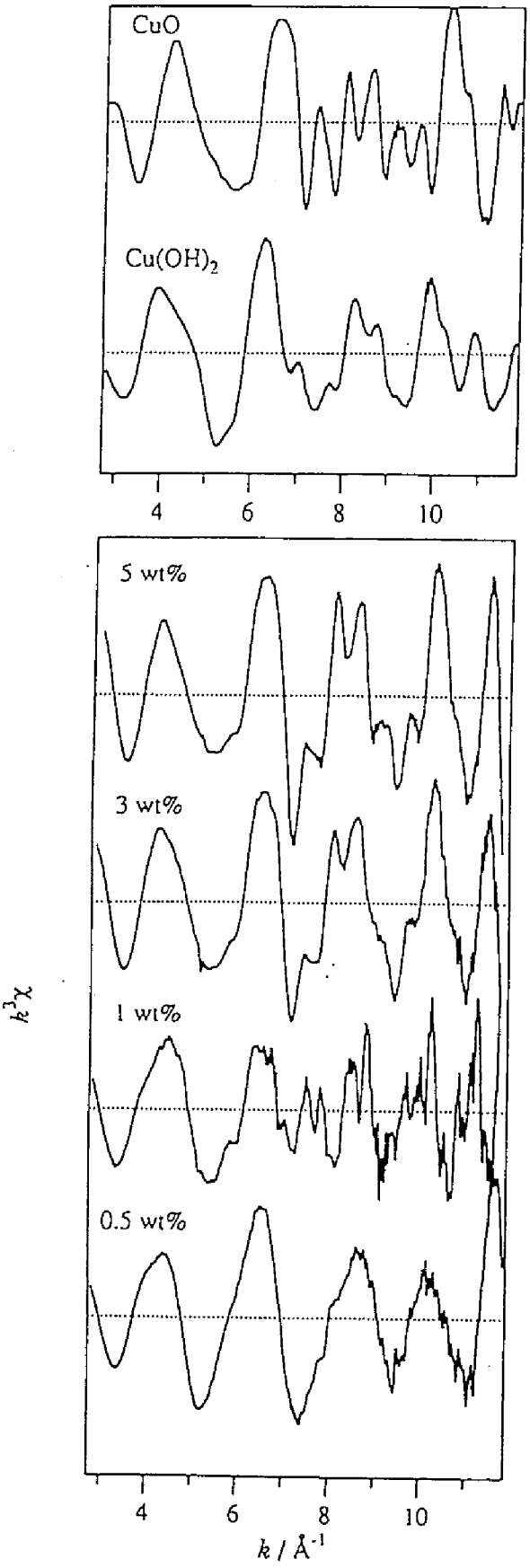

Fig. 5 k^3-weighted EXAFS oscillations, $k^3\chi(k)$, for calcined Cu/ZrO_2 catalysts with 0.5, 1, 3, and 5 wt% Cu.

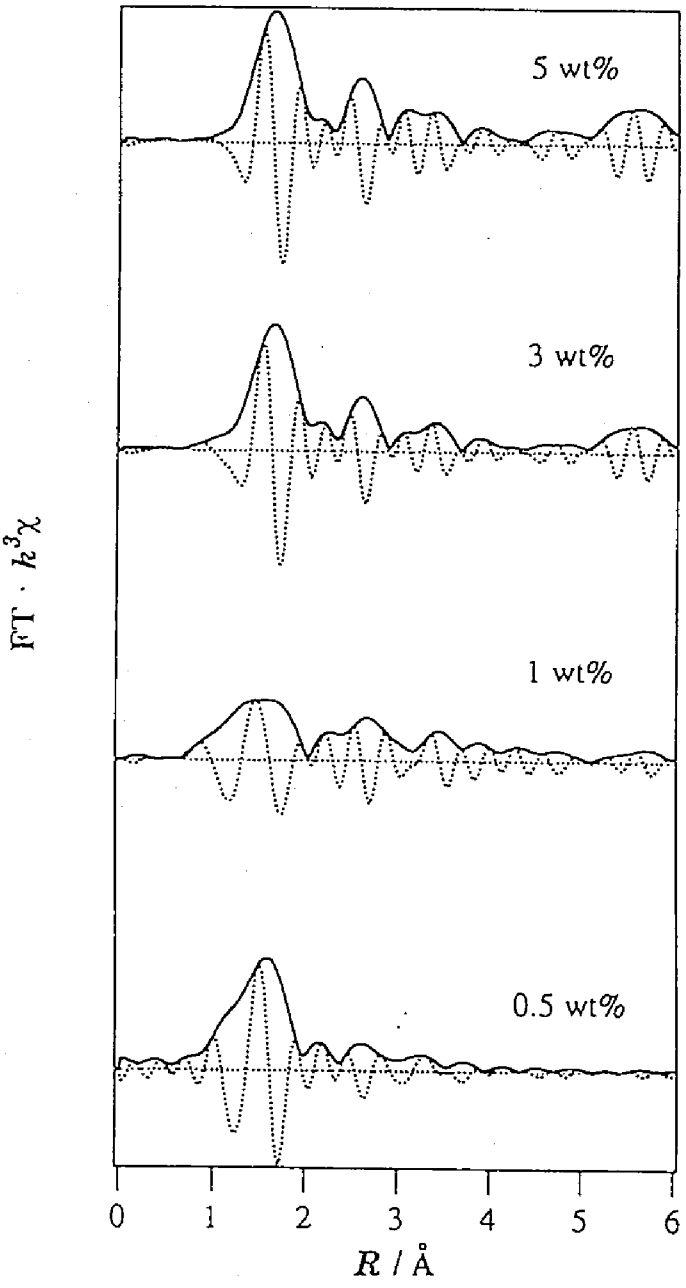

Fig. 6 Fourier transforms of $k^3\chi(k)$ for calcined Cu/ZrO_2 catalysts possessing 0.5, 1, 3, and 5 wt% Cu.

clusters. The coordination number of the Cu-Cu bondings increases with increasing Cu content. Combined with the XANES and EXAFS results in Fig. 3 and Fig. 6, respectively, it is likely that a stable Cu oxide phase, CuO, is formed on the ZrO_2 surface at a higher Cu content than 1 wt% in addition to the highly dispersed Cu species in an octahedral symmetry and that the fraction of CuO increases with the Cu content, especially at a higher Cu content than 1 wt%. Taking into account an FT-IR study of hydroxyl groups of ZrO_2,[10] it is proposed that the Cu^{2+} species in an octahedral symmetry form at the expense of terminal OH groups on the ZrO_2 surface and that an exclusive formation of CuO particles starts after the terminal surface OH groups are consumed.

A TPR study of the Cu/ZrO_2 catalysts having 0.5, 1 and 5 wt% Cu was conducted in a 1% CO stream. TPR profiles expressed by a CO_2 formation are shown in Fig. 7. No significant formation of CO_2 was detected for ZrO_2. With 1 wt% Cu/ZrO_2, three CO_2 evolution peaks were observed at 373, 443, and 643 K when the reduction temperature was raised up to 673 K. The amount of CO_2 formation was estimated on the basis of the peak area intensity of the profile. The total amount of CO_2 evolved up to 673 K was calculated to be 2.8×10^{-4} mol/g for 1 wt% Cu/ZrO_2. It exceeded the amount of CO_2 evolution expected from the Cu content in the sample, 1.6×10^{-4} mol Cu/g and a reduction stoichiometry of reaction (1).

$$CuO + CO \text{ ---> } Cu^0 + CO_2 \quad (1)$$

If the TPR peak observed at a higher temperature than 523 K was removed, the total amount of CO_2 evolved was calculated to be 1.6×10^{-4} mol g^{-1} and consistent with the Cu content used. Accordingly, it is deduced that the TPR peak extending over a higher temperature than 523 K and maximized at 643 K is ascribed to a CO_2 formation due to a disproportion reaction of CO, reaction (2), on metallic Cu surface, since similar and more extensive CO_2 formations were detected for 5wt% Cu/ZrO_2 and CuO (not shown for brevity), while no significant evolution of CO_2 was observed for ZrO_2 alone.

$$2CO \text{ ---> } C + CO_2 \quad (2)$$

The intensity ratio of the reduction peak at 443 K to that at 373 K was 1.60 for 1

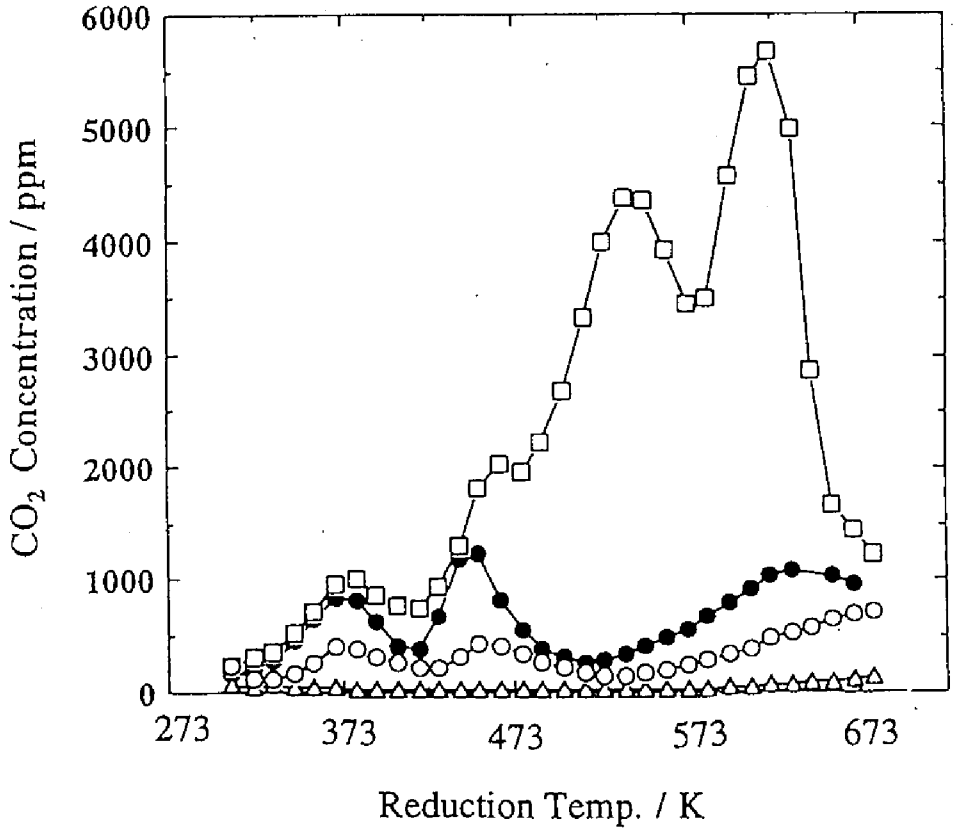

Fig. 7 Temperature programmed reduction (TPR) profiles of calcined ZrO_2 and Cu/ZrO_2 catalysts in a steam of 1 % CO/He. Cu content; △:0 wt%, ○:0.5 wt%, ●:1 wt%, and □:5 wt%.

wt% Cu/ZrO_2.

The TPR profile for 0.5 wt% Cu/ZrO_2 is presented in Fig. 7. Two peaks were observed at 373 and 453 K together with the peak due to the disproportion of CO. The total area intensity of the former two peaks observed at < 523 K corresponded to 0.80×10^{-4} mol Cu/g, in agreement with the composition of the sample (0.79×10^{-4} mol Cu g^{-1}). The peak intensity ratio, higher temperature peak per lower temperature peak, was calculated to be 1.15 for 0.5 wt% Cu/ZrO_2.

With the TPR profile of 5 wt% Cu/ZrO_2, a very strong reduction peak was observed at 543 K in addition to the peaks at 373 and 463 K. The latter two reduction peaks obviously correspond to those observed for 0.5 and 1 wt% Cu/ZrO_2. The area intensity of the reduction peak at 373 K for 5 wt% Cu/ZrO_2 was approximately identical with that for 1 wt% Cu/ZrO_2. A strong and broad CO_2 evolution at 543 K is assigned to a reduction of CuO to Cu metal on the basis of the reduction temperature of crystalline CuO at 523 K. It seems that the TPR profile of CuO in 5 wt% Cu/ZrO_2 is such broad that it extends down to 473 K or a lower temperature, distorting the TPR profile at 443 - 453 K. It has been reported with supported Co oxides[17] that the reduction temperature depends on the particle size and decreases with decreasing particle size. A strong TPR peak at 613 K is ascribed to the CO_2 formation by reaction (2).

The TPR profiles indicate that there are two reduction peaks of Cu in Cu/ZrO_2 which are not assigned to CuO, leading to a conclusion that Cu^{2+} species interacting with the ZrO_2 surface are formed. This is in conformity with the FT-IR,[10] XANES, and EXAFS results that the Cu^{2+} species in an octahedral coordination are formed at a lower Cu content than 1 wt% at the expense of surface OH groups. It is suggested from the TPR profile that two kinds of Cu^{2+} species having different reducibility to Cu metal or two consecutive reduction steps of one kind of Cu^{2+} species, that is, Cu^{2+} to Cu^{+} and Cu^{+} to Cu^{0}. It is difficult to discriminate two possibilities on the basis of the TPR profiles alone. The reduction behaviors of the Cu^{2+} species were investigated by means of XANES and EXAFS.

Figure 8 shows the XANES spectra of 1 wt% Cu/ZrO_2 treated in a 1 % CO at

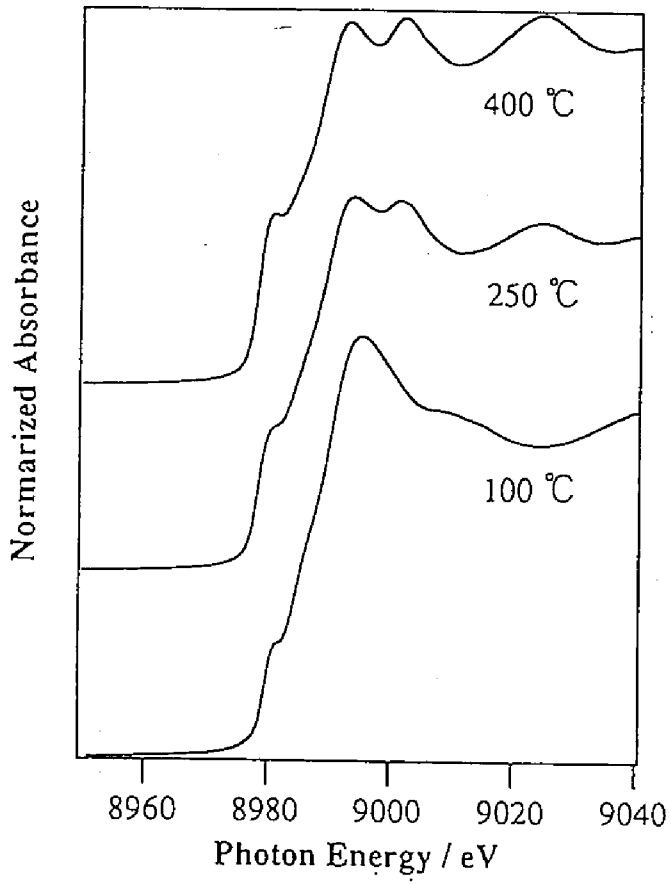

Fig. 8 Cu K-edge XANES spectra of 1 wt% Cu/ZrO_2 reduced at 373, 523, and 673K in a steam of 1 % CO/He for 14 h.

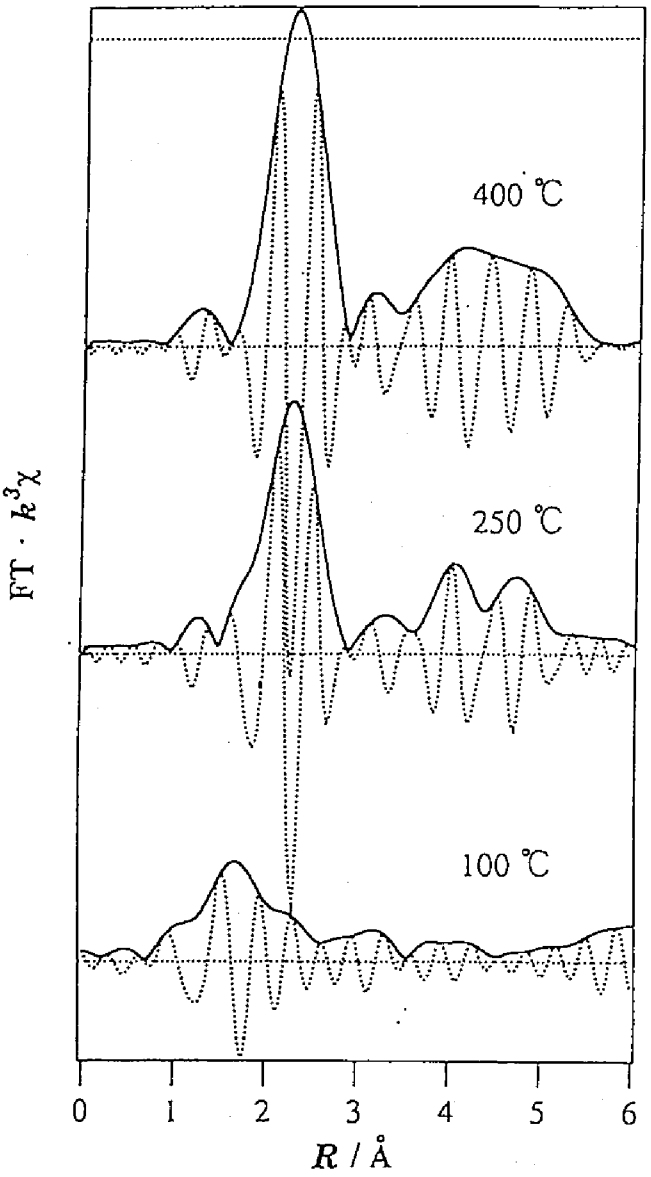

Fig. 9 Fourier transforms of $k^3\chi(k)$ for 1 wt% Cu/ZrO_2 reduced at 373, 523, and 673K in a steam of 1 % CO/He for 14 h.

various temperatures for 14 h. After the treatment at 373 K, the reduction process at the lowest temperature in the TPR profile is considered to be completed. A shoulder peak at 8981 eV and a weak hump at 9013 eV appeared, accompanying a disappearance of the $1s \rightarrow 3d$ pre-peak[18,19] observed at 8977 eV characteristic to Cu^{2+} species in the oxidized states (Fig. 3). Furthermore, a post-edge peak at 9002 eV characteristic to Cu^0 was not observed in the XANES spectrum. These spectral features are attributed to the formation of Cu^+ species.[18,19] Consequently, it is concluded that a majority of Cu^{2+} species in 1 wt% Cu/ZrO_2 is reduced to Cu^+ species at 373 K. The relatively weak intensity of the post-edge peak at 8981 eV may be due partly to a formation of tetrahedrally coordinated Cu^+ species[18] and partly to a superposition of the XANES spectra of the Cu^+ and Cu^{2+} species. As stated below, 23% of the Cu species is expected to remain in a Cu^{2+} state as CuO. Very recently, on the basis of an FT-IR study of CO adsorption, Centi *et al.*[20] reported a formation of Cu^+ species on a 1 wt% Cu/ZrO_2 sample evacuated at a high temperature.

After the reduction at 523 K, the XANES of 1 wt% Cu/ZrO_2 turned into that characteristic to Cu metal (Fig. 4). No further change in the spectrum of Cu K-edge was observed by the reduction at 673 K. It is concluded that the Cu^{2+} species in 1wt% Cu/ZrO_2 are reduced at a lower temperature than 523 K to Cu metal particles. This is consistent with the estimation from the TPR results in Fig. 7 that the reduction of Cu^{2+} to Cu^0 is completed up to 523 K.

Figure 9 shows the Fourier transforms of k^3-weighted EXAFS functions for 1wt% Cu/ZrO_2 reduced at various temperatures for 14 h, corresponding to the XANES spectra in Fig. 8. After the reduction at 373 K, no Cu-Cu bondings due to Cu metal appeared in agreement with the conclusion of a partial reduction of Cu^{2+} to Cu^+. It is considered that the resultant Cu^+ species are highly dispersed. The Fourier transform in Fig. 9 for Cu/ZrO_2 reduced at 523 or 673 K shows a peak at 0.22 nm ascribed to Cu-Cu bondings. The Cu-Cu bond distance was calculated to be 0.255 - 0.256 nm (Table 1), obviously indicating the formation of metallic Cu species (Cu-Cu bond distance: 0.256 nm) in agreement with the XANES results in Fig. 8. The presence of the Cu-Cu bondings of the second and third coordination spheres in

the Fourier transforms for Cu/ZrO_2 reduced at 523 or 673 K indicates a formation of Cu metal particles. The fact that the coordination number of the Cu-Cu bondings at 0.256 nm for 1 wt% Cu/ZrO_2 reduced at 673 K is larger than that reduced at 523 K suggests an increase in the Cu metal particle size with the increase in the reduction temperature.

On the basis of the XANES and EXAFS results, it is concluded that with 1 wt% Cu/ZrO_2 the TPR peak at 373 K is ascribed to the reduction of the Cu^{2+} species in an octahedral symmetry to highly dispersed Cu^+ species and that the peak at 443 K is attributed to a subsequent reduction of the resultant Cu^+ species to Cu^0 species. The size of the metallic Cu particles increases with increasing reduction temperature.

In the case of 1wt% Cu/ZrO_2, the TPR peak at 443 K is larger by 60 % than that at 373 K. This is considered to be a result of a superposition of the reduction peak of CuO extending at 473 - 523 K and that of the Cu^+ species at 443 K, in conformity with an asymmetry of the reduction peak toward a higher temperature. The 60% higher intensity of the TPR peak at 443 K than that at 373 K indicates that 77% of the Cu^{2+} species in 1 wt% Cu/ZrO_2 is the interaction species in an octahedral symmetry and the rest is present in a form of CuO. As clearly revealed by the TPR results in Fig. 7, the amount of octahedral Cu^{2+} species is not increased at 5 wt% Cu/ZrO_2, suggesting that the maximum amount of the octahedral Cu^{2+} species is 1.2×10^{-4} mol Cu g^{-1} or 2.9×10^{14} Cu atoms cm^{-2}. The TPR peak intensity ratio for 0.5wt% Cu/ZrO_2 indicates that 93% of Cu^{2+} (0.74×10^{-4} mol Cu g^{-1}) is in an octahedral symmetry. The high reducibility of the octahedral Cu^{2+} species is considered to be caused by interactions with the ZrO_2 surface and resultant extremely high dispersions of the species. The consumption of surface OH groups on the formation of the Cu^{2+} species[10] indicates the formations of Cu^{2+}-O-Zr^{4+} bondings. The low temperature reduction of the Cu^{2+} species may result from a high reactivity of Cu^{2+}-O-Zr^{4+} bondings toward CO due to a high polarizability of the bondings. The relatively high thermal stability of Cu^+ species may be induced by the interactions with ZrO_2 surface oxygens.

Taking into consideration the TOF (Fig. 2) of the Cu/ZrO_2 catalyst for the NO-CO reaction at 473 K, it is considered that highly dispersed Cu^{2+} species in an octahedral symmetry show the high catalytic activity for the reaction. In addition, the temperature at which the activity generates for the NO-CO reaction is in accordance with the temperature at which Cu^0 species are formed at the expense of the Cu^+ species. The TOF of the reaction was evaluated on the basis of the amount of the Cu^{2+} interaction species for 0.5 and 1 wt% Cu/ZrO_2, resulting in essentially the same TOF values, 9.7×10^{-3} s^{-1} and 10.2×10^{-3} s^{-1}, respectively. Consequently, it is concluded that highly dispersed Cu^0 species derived from the interaction species on Cu/ZrO_2 exhibits a high catalytic activity for the NO-CO reaction at a low temperature and that the limited number of active Cu^0 species (2.9×10^{14} Cu atoms cm^{-2}) results in the decrease of the TOF, calculated on the basis of the total Cu content, with increasing Cu loading. The lack of the low temperature activity of CuO species is well rationalized by the difficulty in the reduction by CO at the low reaction temperature, since the NO-CO reaction proceeds *via* a redox mechanism.[10] The gradual activity decrease in Fig. 2 at a Cu content exceeding 1 wt% may be due to a formation of CuO overlayers on the Cu^{2+} species interacting with the ZrO_2 surface.

Conclusions

The structure and reduction behaviors of ZrO_2-supported Cu species were characterized by XANES, EXAFS, and TPR techniques. The salient findings in the present study are as follows.

[1] Highly dispersed Cu^{2+} species, interacting with a ZrO_2 surface and in an octahedral symmetry, dominate at a lower Cu content than 1 wt% and the amount of the Cu^{2+} species, 2.9×10^{14} Cu atoms/cm^2, is saturated at 1 wt% Cu. On the other hand, CuO is exclusively formed at a Cu content exceeding 1 wt%.

[2] The highly dispersed Cu^{2+} species are reduced by CO at a much lower temperature than CuO, producing highly dispersed Cu^+ species at 373 K and

subsequently forming highly dispersed Cu^0 species at 443 - 453 K.

[3] A high catalytic activity of Cu/ZrO_2 for NO-CO reactions at a low temperature is brought about by the highly dispersed Cu^0 species generated by a low-temperature reduction of the Cu^{2+} species interacting with the ZrO_2 surface.

Acknowledgment

We express our sincere thanks to Mr. Makoto Kaneko (Osaka University) for a part of experimental works. The X-ray absorption measurements were performed under the approval of the Photon Factory (KEK-PF) Program Advisory Committee (Proposal No. 94G205). This work was partially supported by a grant-in-aid (No. 07242103) from the Japan Ministry of Education, Science, Sports, and Culture.

References

(1) Iwamoto, M., Hamada, H., *Catal. Today*, 1991, **10**, 57.

(2) Iwamoto, M., Yahiro, H., *Catal. Today*, 1994, **22**, 5.

(3) Li, Y., Hall, W. K., *J. Phys. Chem.*, 1990, **94**, 6145.

(4) Tabata, K., Mater, J., *Sci. Lett.*, 1988, **7**, 147.

(5) Shimada, H., Miyama, S., Kuroda, H., *Chem. Lett.*, 1988, 1797.

(6) Mizuno, N., Toyama, H., Tanaka, M., Yamamoto, M., Misono, M., *Bull. Chem. Soc. Jpn.*, 1991, **64**, 1383.

(7) Mizuno, N., Yamamoto, M., Tanaka, M., Misono, M., *J. Catal.*, 1991, **132**, 560.

(8) Bauerle, G. L., Service, G. R., Nobe, K., *Ind. Eng. Chem. Prod. Res. Devel.*, 1992, **11**, 54.

(9) Okamoto, Y., Ohto, K., Imanaka, T., *Kagaku Kogaku Ronbunshu*, 1993, 19, 863.

(10) Okamoto, Y. Gotoh, H., *Catal. Today*, in press.

(11) Aritani, H., Akasaka, N., Tanaka, T., Funabiki, T., Yoshida, S., Gotoh, H., Okamoto, Y., *J. Chem. Soc. Faraday Trans.*, 1996, **92**, 2625.

(12) Boccuzzi, F., Gulielminotti, E., Martra, G., Cerrato, G., *J. Catal.*, 1994, **146**. 449.

(13) Okamoto, Y., Gotoh, H., Aritani, H., Tanaka, T., Yoshida, S., in preparation.

(14) Clausen, B. S., Lengeler, B., Rasmussen, B. S., *J. Phys. Chem.*, 1985, **89**, 2319.

(15) Tohji, K., Udagawa, Y., Mizushima, T., Ueno, A., *J. Phys. Chem.*, 1985, **89**, 5671.

(16) Tzou, M. S., Kusunoki, M., Asakura, K., Kuroda, H., Moretti, G., Sachtler, W. H. M., *J. Phys. Chem.*, 1991, **95**, 5210.

(17) Okamoto, Y., Nagata, K., Adachi, T., Imanaka, T., Inamura, K., Takyu, T., *J. Phys. Chem.*, 1991, **95**, 310.

(18) Kau, L. S., Spira-Solomon, D. J., Penner-Hahn, J. E., Hodgson, K. O., Solomon, E. I., *J. Am. Chem. Soc.*, 1987, **109**, 6433.

(19) Hedman, B., Hodgson, K. O., Solomon, E. I., *J. Am. Chem. Soc.*, 1990, **112**, 1643.

(20) Centi, G., Perathoner, S., Cerrato, G., Giamello, E., Morterra, C., *Proc. 11th Int. Congr. Catal.*, Baltimore, 1996, Po-135.

Appendix

Chapter 7

Structural Study of Molybdenum Bronzes: XAFS Study for Analysis of Local Structure around Mo ions

Abstract

Hydrogen molybdenum bronzes, $H_{0.21}MoO_3$ (type I) and $H_{0.91}MoO_3$ (type II) were characterized by means of Mo K-edge XAFS spectroscopy. XANES specetra showed that type I has an axially symmetric MoO_6 unit which is mainly conncted to each other with vertices sharing and a MoO_6 unit in type II are similar to that in MoO_2. EXAFS spectra suggested that the MoO_x sheet in type I is similar to MoO_3 while in type II, a MoO_x sheet is similar to that in rutile MoO_2 in which MoO_6 is conneced to form a chain by sharing the edges of opposite sides. The curve fitting analysis of Mo-O bonds for type I supported the earlier results obtained from diffraction and IR methods; MoO_6 unit has C_{4v} symmetry. In case of type II, D_{4h} structure is possible and hydrogen is captured by Mo=O bonds resulting in the formation of Mo-OH bonds.

1. Introduction

Hydrogen molybdenum bronze, H_xMoO_3, is classified to four phases depending on included hydrogen[1]; type I (orthorhombic) $0.21 < x < 0.4$[2], type II (monoclinic) $0.85 < x < 1.04$, type III (monoclinic) $1.55 < x < 1.72$ and type IV (monoclinic) $x = 2$. Type I has a layered structure in which a layer consists of two MoO_x sheets. The MoO_6 units connecting to each other with vertices (corner) sharing in the sheet have been proposed to be in an axially symmetric moiety deduced from the result of infrared absorption (IR)[3,4] and ^1H NMR[5] studies. The other monoclinic phases are not fully characterized. The present paper is devoted to analysis of the local structure of hydrogen molybdenum bronzes types I and II by means of Mo K-edge XAFS spectroscopy.

2. Experimental

Types I and II were prepared by reduction of MoO_3 in an acidic media according to the Glemser's method.[1] The formation of types I and II are confirmed by XRD[1] and the hydrogen contents were $x = 0.21$ and $x = 0.91$, respectively.[3]

XAFS spectra were taken by EXAFS facility installed on BL-10B at Photon Factory (ring energy 2.5 GeV and stored current 360-270 mA) in National Laboratory for High Energy Physics, Tsukuba (Proposal No. 94G002) with a Si (311) channel cut monochromator. The data reduction was performed[6] at the Data Processing Center of Kyoto University.

3. Results and Discussion

3.1 XANES spectra

Figure 1 shows normalized XANES spectra of the samples and some reference complexes. For XANES spectrum of type I, the pre-edge peak due to 1*s* to 4*d* transition is seen and the intensity is almost the same as that of $MoO_2(acac)_2$ with D_{4h} symmetry, in which four O atoms from acetylacetonato groups are located at

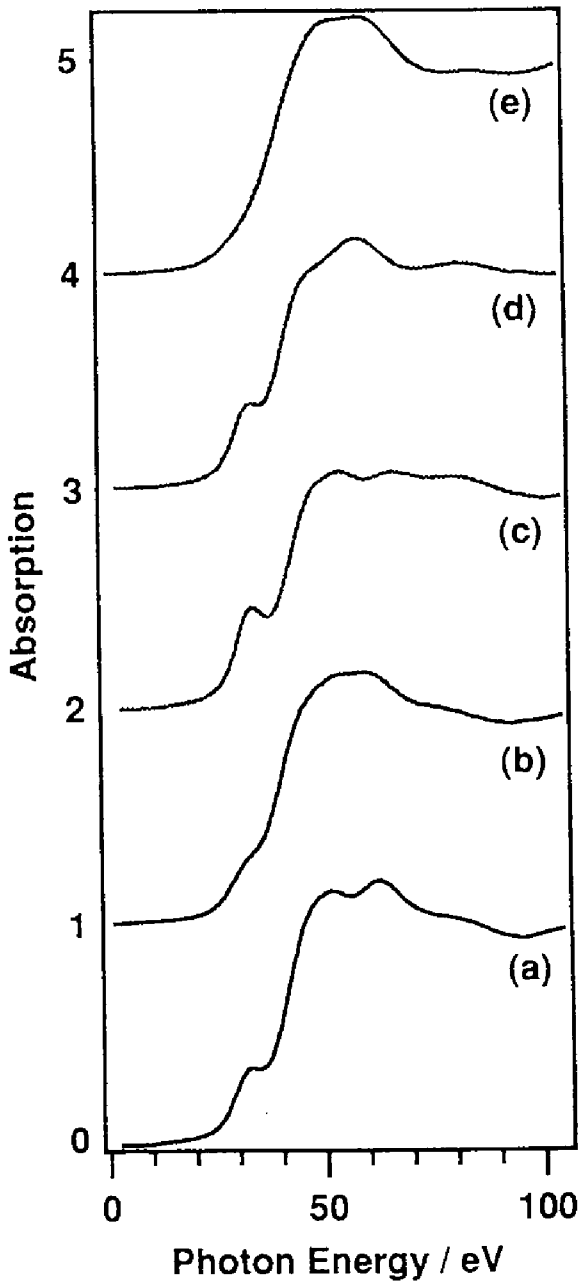

Fig. 1 Normalized Mo K-edge XANES spectra of (a) type I, (b) type II, (c) MoO_3, (d) $MoO_2(acac)_2$, and (e) MoO_2. Energy offset is taken to be 1996.0eV.

Table 1 Curve-fitting results of Mo-O in the samples.*

Sample	CN	R / Å	$\Delta\sigma^2$ / Å^2	Refinement
Type I	0.6(5)	1.64(1)	0.0019(6)	3.6 %
	4.1(4)	1.97(2)	0.0027(4)	
	1.0(5)	2.40(2)	0.0027(4)	
Type II	1.5(5)	1.84(1)	0.0021(8)	8.6 %
	3.9(5)	2.01(1)	0.0055(7)	

*The empirical parameters from K_2MoO_4 were used.
The values in parentheses are standard deviation.
$\Delta\sigma^2$ is the relative Debye-Waller factor.

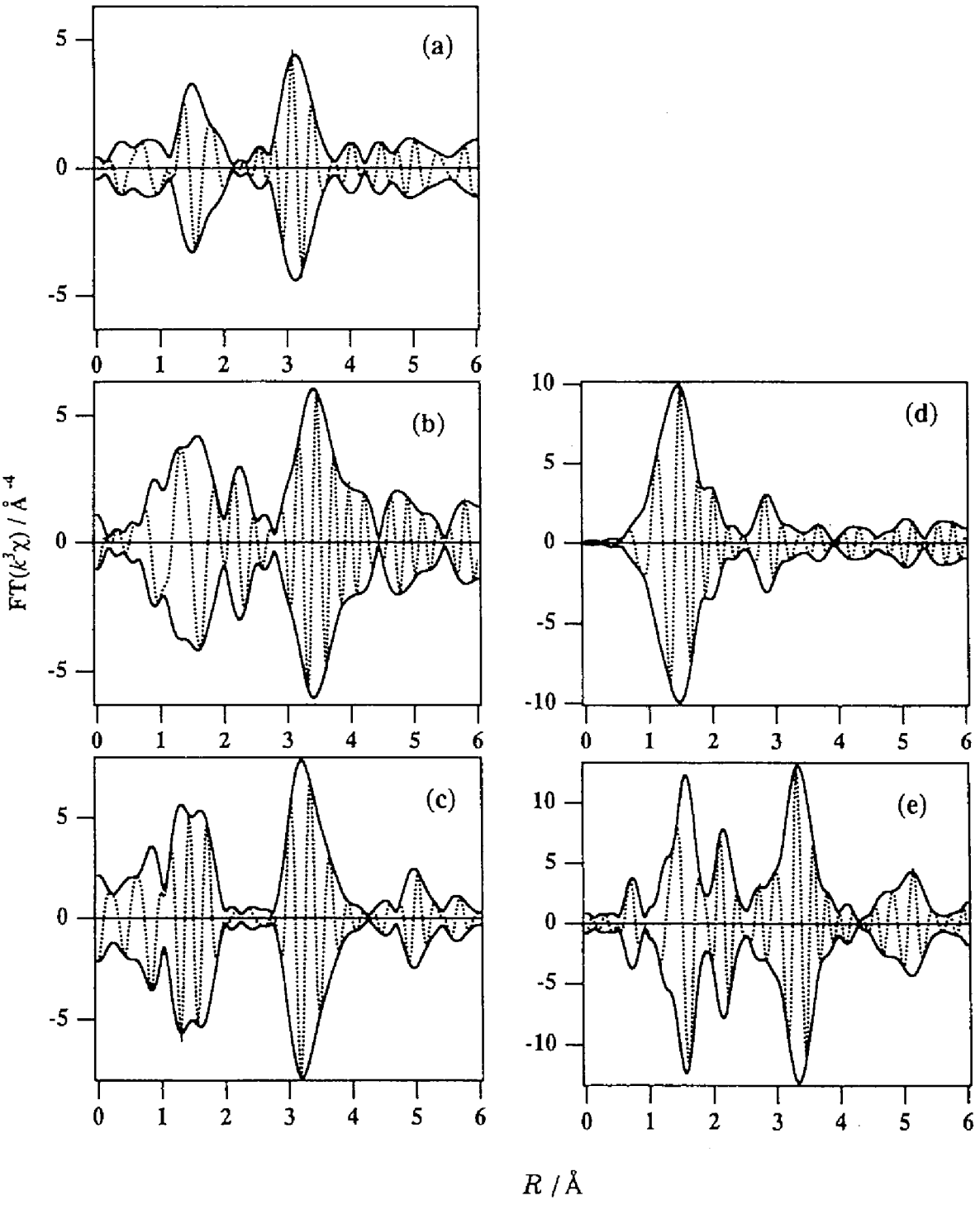

Fig. 2 Fourier transformed EXAFS of Mo compounds. (a)-(e), see captions to Fig. 1.

square apexes and two O atoms of molybdenyl are at the vertical axis. The pre-edge peak intensity is lower than that of MoO_3 in which a Mo ion is located at the center of a much distorted oxygen octahedron, indicating that Mo ions in type I is located at the center of highly symmetric moiety. Twin peaks at post-edge regions are found at the similar positions to that found in the case of $MoO_2(acac)_2$ although the intensities are slightly different. This is possibly due to the positions of axial O atoms as Sotani *et al.* reported[2,3]; *i.e.*, in type I with C_{4v} symmetry, one O at an axial position is of a Mo=O bond and the other is a bridging oxygen. On the other hand, the spectrum of type II is totally similar to that of MoO_2 of rutile structure. The pre-edge peak for MoO_2 was almost missing this is mainly due to the valence of Mo in an axial symmetry. The weak shoulder peak due to 1*s* to 4*d* transition for type II reveals that Mo is located at a more symmetric center than that of type I and/or Mo is partly reduced from hexavalence. Type II, $H_{0.91}MoO_3$, has a molybdenum ions the formal charge of which is almost 5+.

3.2 EXAFS Spectra

Figure 2 shows Fourier transforms of k^3-weighted EXAFS spectra. The peaks found in a region 1-2 Å are due to the scattering from adjacent O atoms in all spectra. As found in the cases of MoO_2 and $MoO_2(acac)_2$, the complex with small divergency of Mo-O bonds exhibits intense peaks. From this point of view, Mo-O divergency is high in the cases of types I and II. The peaks found at 2 - 4 Å are due to the scattering from adjacent Mo atoms. In case of MoO_3, MoO_6 units are linked with edges and vertices sharing and the nearest Mo-Mo distances are diverging resulting in the weak intensities in the region 2- 3 Å. Therefore contribution of Mo-Mo scattering is mainly due to the adjacent Mo ions in MoO_6 unit connecting with vertices sharing. This type of MoO_x sheet is similar to that of type I. On the other hand, MoO_2 of a rutile structure has a regular Mo-Mo atomic distances 2.51 and 3.51 Å, which is reflected to twin Mo-Mo peaks in the region 2 - 4 Å. The same feature can be seen for the case of type II, suggesting that MoO_6 unit in type II is connected to each other with not only vertices sharing but also edge sharing as found in the rutile structure.

The curve fitting analysis was carried out[6] for the Mo-O bonds and the result are given in Table 1. In case of type I, the presence of three kinds Mo-O was concluded. The shortest is possibly due to Mo=O which faces to the interlayer and four O atoms are located in the sheet. The longest is due to the O atoms at the opposite vertex of Mo=O. The result is well consistent with that deduced from IR analysis.[2,3] In case of type 1, two shell fitting gave the satisfactory result. The longer Mo-O bonds are equatorical. The shorter were axial corresponding to Mo=O in type I. The elongation of this bond is caused by the H intercalations resulting in the formation of Mo-OH. Therefore, D_{4h} structure for a MoO_6 unit as in the case of $MoO_2(acac)_2$ is very likely. The strucure is basically the same as that found in MoO_2.

From the results mentioned above we concluded the structure of type I and type II as follows. Type I has a layered structure in which MoO_x sheet similar to that in MoO_3 and the MoO_6 unit is more regular symmetric (C_{4v}). This is well consistent with the earlier result from diffraction technics[1,7,8] and IR.[2,3] In type II, MoO_x sheet is similar to that in MoO_2 in which MoO_6 is conneced to form a chain by sharing the edges of opposite sides.

References

(1) Birtill, J. J., Dickens, P. C., *Mater. Res. Bull.* **13** (1978) 311.

(2) Sotani, N., Kawamoto, Y., Inui, M., *Mater. Res. Bull.* **18** (1983) 797 .

(3) Sotani, N., Eda, K., Sadamatsu, M., Takagi, S., *Bull. Chem. Soc. Jpn.* **62** (1989) 903.

(4) Sotani, N., Yoshida, N., Yoshioka, N., Kishimoto, S., *Bull. Chem. Soc. Jpn.* **58** (1985) 1626.

(5) Sotani, N., Eda, K., Kunimoto, M., *J. Chem. Soc. Faraday Trans.* **86** (1990) 1583.

(6) Tanaka, T., Yamashita, H., Tsuchitani, R., Funabiki, T., Yoshida, S., *J .Chem. Soc., Faraday Trans.* 1 **84** (1988) 2987.

(7) Dickens, P. G., Birtill, J. J., Wright, C. J., *J. Solid State. Chem.* **28** (1979) 185.

(8) Hibble, S. J., Dickens, P. G., *Ber. Bunsen-Ges. Phys. Chem.* **90** (1986) 702.

Summary

The author applied XAFS and UV-VIS spectroscopy to the characterization of catalysis systems, *i.e.*, Mo-Mg binary oxides for metathesis of olefins (described in "part I") and TiO_2-supported Cu for reduction of NO (described in "part II"). The main results are summarized as follows.

In chapter 1, the local structure around Mo ions including Mo-Mg binary oxides in oxidized and reduced states has been clarified by XAFS of Mo *K*- and Mg *K*- edges, and the relationship between the structural change in the bulk phase and generation of active species for propene metathesis is discussed. XANES and EXAFS spectra show that the binary oxides have a tetrahedral MoO_4 unit in the oxidized state with a lower Mo ratio than 0.5, and an octahedral MoO_6 unit exists mainly in the oxidized state with a higher ratio. By H_2 treatment at 773K, Mo ions in a molybdena-rich samples, which exhibit a metathesis activity, are easily reduced to form MoO_2 phase. This MoO_2 phase can not be detected by XRD but be observed by EXAFS, indicating that the MoO_2 phase is highly dispersed. It is concluded that a dispersed MoO_2 phase, which exists as a small particle in the bulk, strongly relates to the active species for metathesis.

In chapter 2, the characterization of molybdena species in near-surface region is carried out by means of Mo L_3-edge XANES and diffuse reflectance UV-VIS spectroscopy. It is revealed by L_3-XANES spectra of reference compounds that the local symmetry around Mo ions as well as the valence state affects the spectral feature of XANES. In addition, a molybdenum bronze sample is suitable for reference because it has an axially symmetric MoO_6 octahedron. And thus, detailed structural analysis of molybdenum bronzes is proposed, as described in appendix section. The L_3-XANES is applied for characterizing surface molybdena species of oxidized / reduced Mo-Mg binary oxides. For the samples in the oxidized state, the MoO_4 tetrahedra exists in the whole Mo ratio, and MoO_6 octahedra is present partly in molybdena-rich samples. In case of molybdena-rich samples in the reduced state, the tetrahedral species remains but reduced Mo ions including MoO_2 species are also formed. These

results are supported to those by UV-VIS spectra. The formation of MoO_2 species by H_2 treatment more definitely in the bulk than in near-surface. It is concluded that the active species for metathesis reaction relates to the formation of MoO_2 phase not only in the bulk but also in near-surface region.

In part I, it is summarized that dispersed MoO_2 species is formed by H_2 treatment in both the surface region and the bulk phase, and this species acts as an active species. In the viewpoint of characterizing the binary oxide catalysts, it is important to compare the informations between in the bulk and in the surface region, because not only surface property but also crystalline phases in the bulk affect the catalytic activity. The structural analyses of Mo-Mg binary oxides by using XAFS and UV-VIS spectroscopy give a direct information in bulk or surface region, which is necessary to clarify the catalysis systems. More detailed characterization about the catalytic mechanisms of metathesis reaction is called for.

In chapter 3, the reactivity of NO reduction with H_2 over TiO_2-supported Cu catalysts (calcined at 773K) are proposed using a closed reaction system, and the active species are characterized. It is found at first that Cu/TiO_2 pretreated with H_2 at 473K exhibits higher activity for the conversion of NO at low temperatures than Cu supported on other supports. NO is reduced to N_2O in the reaction at 303K, and the conversion to N_2 is accelerated above 323K. In the process of the reduction, the NO is converted to N_2 directly, and the conversion to N_2 *via* N_2O is partly. The catalytically active species are characterized by means of Cu *K*-edge XANES, UV/VIS and ESR spectroscopies. It is summarized; (*1*) The treatment of the sample with H_2 at 473K brings about the formation of Cu metal particles and promotes the reduction of Ti ions. (2) The extent of the reduction of TiO_2 supporting Cu is much higher than that of TiO_2 itself. (3) NO has a role for oxidizing both Cu and Ti ion even at room temperature. On the other hand, H_2 has a role for reducing both ions. The active Cu-species is CuO particle with a Cu metal core. In these results, it is suggested that the catalytically active Cu species for NO reduction is stabilized as a dispersed metal particles. The detailed characterization is described in the next chapter.

In chapter 4, the active species of Cu supported on TiO_2, which were prepared by

impregnation with cupric nitrate and acetate, is investigated by means of Cu *K*-edge XAFS. It is found that the Cu/TiO_2 prepared from acetate exhibits a longer catalytic lifetime than that from nitrate. The results of structural analyses by means of XAFS and UV-VIS spectroscopy are summarized; (*1*) the H_2 pretreatment of the Cu/TiO_2 samples at 473K brings about the formation of Cu^0 micro particles with several hundred Angstroms of particle size. (2) From the results of coordination numbers obtained by EXAFS analysis, the Cu particle on TiO_2 prepared from cupric acetate is more stable than that from cupric nitrate for the reaction. (3) By means of UV-VIS spectroscopy, the presence of octahedrally coordinated Cu^{2+} is observed and Cu^+ is not found definitely in Cu/TiO_2 after the reaction. Thus, it possibly deduced that coexistence of Cu^0 and Cu^{2+} relates to generate the active species. By means of EXAFS studies, suitable particle size of Cu metal leads to the active center. It suggests that the redox performance is enhanced by other effect (such as SMSI) in the catalytic system of Cu^0/TiO_2. However, how metal species (and oxidized Cu^{2+}) play a role for an active center for NO reduction is now in progress.

In chapter 5, the catalytic activities of Cu/TiO_2 is studied for NO-CO reaction using a fixed bed flow reaction system as a function of the calcination temperature, Cu content, and origin of TiO_2. It was found that Cu-TiO_2 interaction species were responsible for a catalytic activity at a low temperature (413K). It is noted in 1 wt% Cu/TiO_2 that higher calcination temperature gives the higher activity for NO-CO reaction. In addition, the sample prepared from cupric acetate exhibits the higher activity for the reaction than that from other precursors. It is suggested by means of XAFS and TPR that a rutile phase of TiO_2 is very effective for the formation of the catalytically active Cu-TiO_2 interaction species in an octahedral symmetry. From the results in chapter 4, 5, and 6, the active species for NO reduction is not also Cu metal species but also other Cu species which is strongly interacted with TiO_2 support. In addition, many *de*NOx catalysts containing a Cu^+ ion exhibit a high activity, as described in introduction of part II. It suggests that a few effects bring about the stabilization of active Cu species by interaction between Cu and TiO_2-support. Therefore, the characterization must has been continued in order to clarify the role of

Cu in Cu/TiO_2 for NO reduction.

In chapter 6, the structure and reduction behaviors of ZrO_2-supported Cu species were characterized by XANES, EXAFS, and TPR techniques. The salient findings are summarized; (*1*) Highly dispersed Cu^{2+} species interacting with ZrO_2 exist as an octahedrally coordinated. (*2*) The dispersed Cu^{2+} species are easily reduced by CO at a much lower temperature than CuO. The reduced Cu on ZrO_2 is formed highly dispersed Cu^{+} species at 373K and subsequently formed highly dispersed Cu^0 species at *ca.* 350K. (*3*) A high activity for NO-CO reactions at a low temperature is brought about by the highly dispersed Cu^0 species formed by a low-temperature reduction of the Cu^{2+} species interacting with the ZrO_2 surface. These phenomenoma is similar to that in Cu/TiO_2. However, the interaction between Cu and ZrO_2-support is still unclear as well as that of Cu/TiO_2. In the study of this section, the enhancement of redox performance of Cu ions is proposed by the effect of ZrO_2 support. To clarify this effect, the structural analysis has been studying now by XAFS and other spectroscopy.

In part II, the XAFS and UV-VIS spectroscopy is applied to characterizing catalytically active Cu species. The EXAFS analysis at Cu K-edge is relatively difficult to obtain a definite parameters such as coordination numbers and bond lengths, because several types of Cu-O and Cu-Cu bonds exist generally. However, the XANES can be used for determination of the valence of Cu ions, because post-edge peak strongly reflects to the valence. In addition, XANES is more appropriate technique to detect a Cu^{+} ion than using other spectroscopy. UV-VIS can be detected the bands due to *d-d* transition of Cu^{2+} and the vibration of free electrons in Cu-metal micro-particle. Thus, UV-VIS is one of the useful technique for characterizing Cu-based samples widely. Both XAFS and UV-VIS techniques gives the definite structural information of Cu species. By characterization of catalytically active Cu species during the reaction, the redox performance of Cu ions can be clarified. In Cu/TiO_2 and Cu/ZrO_2 catalysts, more detailed study is called for in order to clarify the effect of support.

List of Publication

Part I

Chapter 1

1 Structure of Mo-Mg Binary Oxides in Oxidized/Reduced States Studied by X-Ray Absorption Spectroscopy at Mo K edge and Mg K edge
H. Aritani, T. Tanaka, T. Funabiki, S. Yoshida, M. Kudo, S. Hasegawa,
J. Phys. Chem., **100** (1996) pp. 5440-5446.

Chapter 2

2 Study of the Local Structure in the Surface Layers of Mo-Mg Binary Oxides by means of Mo L_3-edge XANES and UV-VIS Spectroscopy
H. Aritani, T. Tanaka, T. Funabiki, S. Yoshida, K. Eda, N. Sotani, M. Kudo, S. Hasegawa,
J. Phys. Chem., **100** (1996) pp. 19495-19501.

Part II

Chapter 3

3 Reduction of NO over TiO_2-Supported Cu Catalysts
H. Aritani, N. Akasaka, T. Tanaka, T. Funabiki, S. Yoshida, H. Gotoh, Y. Okamoto,
J. Chem. Soc. Faraday Trans., **92** (1996) pp. 2625-2630.

Chapter 4

4 Reduction of NO over TiO_2 Supported Cu Catalysts (2) : Structure of Active Cu Species Studied by Cu K-edge XAFS
H. Aritani, T. Tanaka, N. Akasaka, T. Funabiki, S. Yoshida, H. Gotoh, Y. Okamoto,
J. Catal., in press.

Chapter 5

5 Surface Copper-TiO_2 Interaction Species for NO-CO Reaction
Y. Okamoto, H. Gotoh, K. Hishida, H. Aritani, T. Tanaka, S. Yoshida
Appl. Surf. Sci. submitted.

Chapter 6

6 An X-ray Absorption Fine Structure Study of Zirconia-Supported Copper Catalysts for NO-CO Reactions : Surface Copper Species on Zirconia
Y. Okamoto, H. Gotoh, H. Aritani, T. Tanaka, S. Yoshida,
Catal. Today, in press.

Appendix

Chapter 7

7 Structural Analysis of Molybdenum Bronzes
T. Tanaka, H. Aritani, S. Yoshida, K. Eda, N. Sotani, S. Hasegawa,
J. Phys. (colloque), in press.

In this thesis, the following papers are not contained.

8 XAFS study of niobium oxide on alumina
T. Tanaka, T. Yoshida, H. Yoshida, H. Aritani, T. Funabiki, S. Yoshida, J.-M. Jehng, I. E. Wachs,
Catal. Today, **28** (1996) pp. 71-78.

9 Na K-edge XAFS Study of Sodium Loaded on Alumina
S. Hasegawa, M. Morooka, H. Aritani, H. Yoshida, T. Tanaka,
Jpn. J. Appl. Phys., **32**-2 (1993) pp. 508-510.

10 Structures and catalytic behavior of some niobium oxides
S. Hasegawa, H. Aritani, M. Kudo,
Catal. Today, **16** (1993) pp. 371-377.